

**Assessment of a novel high-throughput process development
platform for biopharmaceutical protein production**

(Einschätzung einer neuen Hochdurchsatz-Prozessentwicklungs-
plattform für die biopharmazeutische Proteinproduktion)

Von der Fakultät für Mathematik, Informatik und Naturwissenschaften der RWTH
Aachen University zur Erlangung des akademischen Grades eines Doktors der
Naturwissenschaften genehmigte Dissertation

vorgelegt von

Patrick Opdensteinen, M.Sc.

aus Nettetal

Berichter:

Prof. Dr. rer. nat. Dr.-Ing. Johannes F. Buyel

Prof. Dr. rer. nat. Stefan Schillberg

Tag der mündlichen Prüfung:

11. April 2023

Acknowledgements

I would first like to thank my principal examiner and mentor Prof. Buyel, who I could count on for excellent scientific feedback and advice regardless of the time and day. Thank you for supporting my many endeavors beyond the thesis, for always staying open-minded and for providing me with a high degree of freedom during my work. I hope I get the chance to work with you again in the future.

I am grateful to Prof. Schillberg for the possibility to conduct my research at such an excellent institution as the Fraunhofer IME and for his scientific input and advice as second supervisor for my thesis. I appreciate your critical, yet constructive feedback during the outline discussions and PhD seminars.

I also want to thank Prof. Blank for his support during my doctoral studies and for stepping in as a temporary supervisor, which was crucial for the completion of this project.

I am grateful to the RWTH Aachen University for granting me a scholarship for my doctoral studies, which provided me with great flexibility during my research. In this context I also want to acknowledge the support from the Research Training Group Tumor-Targeted Drug Delivery, which provided the framework for exciting cooperations.

A big thank you goes to Birgit, who has dedicated herself to establishing a supporting foundation for PhD students at the Fraunhofer IME.

I'd like to give special thanks to the students Steffen, Lisa, Svenja and Aleks who completed their master theses under my supervision. None of the master projects would have been such a great success without your hard work and I would be happy to work with you again.

My fellow PhD candidates in the department and institute deserve my gratitude for their team spirit and support over the years, inside and outside of the laboratory. I wish to especially thank Matthias, Ben, Cath, Vera, Ron and Patty. It was a blast working with you all and I hope we get the chance to work together again in the future.

Additionally, I would like to thank Holger Spiegel for his advice in the context of SPR experiments and Michael Kupper for his support with mass spectrometry.

I also want to thank my colleagues Nicole, Dirk and Andreas for maintaining our plants and plant cell culture. Thank you, Jörg and Sandor for maintaining our equipment and keeping the laboratory up and running. Thank you, Heinz for your support with all kinds of rebellious equipment.

Finally, I want to thank my friends and family for their support throughout the years.

This thesis would not have been possible without you.

EIDESSTATTLICHE ERKLÄRUNG

Ich versichere ehrenwörtlich, dass ich die vorliegende Arbeit selbst verfasst habe, dass ich außer den angegebenen Quellen keine anderen benutzt habe, dass jede Quelle gekennzeichnet ist, und dass ich diese Arbeit an keiner anderen Stelle eingereicht habe.

Teile der in Abschnitt (III.2.3.3) gezeigten Ergebnisse wurden als Fachartikel unter folgendem Titel publiziert: Opdensteinen, P., Buyel, J.F. (2022), Reducing water uptake into BY-2 cells by systematically optimizing the cultivation parameters increases product yields achieved by transient expression in plant cell packs. *Biotechnology Journal*, 17(10), 2200134. Die Mitautoren haben in folgender Weise zu der oben genannten Publikation beigetragen: Johannes Felix Buyel hat Forschungsgelder akquiriert, die Datenanalyse unterstützt und das Manuskript revidiert.

Die in Abschnitt (III.2.4.1) gezeigten Ergebnisse wurden als Fachartikel unter folgendem Titel publiziert: Opdensteinen, P., Sperl, L.E., Mohamadi, M., Kündgen-Redding, N., Hagn, F. and Buyel, J.F. (2022), The transient expression of recombinant proteins in plant cell packs facilitates stable isotope labeling for NMR spectroscopy. *Plant Biotechnology Journal*, 20(10), 1928-1939. Die Mitautoren haben in folgender Weise zu der oben genannten Publikation beigetragen: Laura Sperl und Mariam Mohamadi haben Kontroll-Konstrukte für die GB1 Expression in *E. coli* kloniert, GB1 in *E. coli* exprimiert, und NMR Messungen durchgeführt. Nicole Kündgen-Redding hat BY-2 Zellen kultiviert. Johannes Felix Buyel und Franz Hagn haben Forschungsgelder akquiriert, die Datenanalyse unterstützt und das Manuskript revidiert.

Teile der in Abschnitt (III.4.2.2) gezeigten Ergebnisse wurden als Fachartikel unter folgendem Titel publiziert: Opdensteinen, P., Meyer, S., Buyel, J.F (2021). *Nicotiana* spp. for the expression and purification of functional IgG3 antibodies directed against the *Staphylococcus aureus* alpha toxin. *Frontiers in Chemical Engineering*, 3, 737010. Die Mitautoren haben in folgender Weise zu der oben genannten Publikation beigetragen: Svenja Meyer hat IgG3 Antikörper Konstrukte (nativ und Domänen austausch) in die hier erstellten modularen Vektoren kloniert, ~80% der Expressionsversuche in PCPs und ~60% der Chromatographie durchgeführt. Johannes Felix Buyel hat Forschungsgelder akquiriert, die Datenanalyse unterstützt und das Manuskript revidiert.

Die nachfolgenden Analysen wurden als Auftragsarbeiten durchgeführt: Michael Kupper hat die massenspektrometrische Analyse von gereinigten Wirtsproteinen durchgeführt.

Unterschrift des Verfassers: Patrick Opdensteinen

Ort, Datum: _____

A. Table of contents

I.	Introduction	1
I.1	Infectious diseases	1
I.1.1	Methicillin-resistant <i>Staphylococcus aureus</i>	1
I.1.1.1	Adaptability of <i>S. aureus</i> to antibiotics	1
I.1.1.2	<i>S. aureus</i> biofilms	2
I.1.1.3	<i>S. aureus</i> virulence factors and anti-virulence therapies	2
I.1.2	Challenges during development and supply of new drugs	3
I.1.2.1	Challenges during biopharmaceutical development	3
I.1.2.2	Challenges during biopharmaceutical supply	5
I.2	Plant-based production of biopharmaceuticals	6
I.2.1	Unique features of plants compared to dominant hosts	6
I.2.2	Plant molecular farming	7
I.2.3	Mitigation of constraints in plant molecular farming	9
I.3	High-throughput screening in plants	11
I.3.1	Automated cloning of vector libraries	11
I.3.2	High-throughput expression in plant cell packs	13
I.3.3	Quantification with surface plasmon resonance spectroscopy	13
I.4	Aim of the thesis and workflow	15
I.4.1	Model protein classes and molecular targets	15
I.4.2	State of completion	17
II.	Materials and Methods	18
II.1	Equipment and chemicals	18
II.2	Expression vectors and cloning	18
II.2.1	Gene synthesis and codon optimization	18
II.2.2	PCR amplification	18
II.2.3	Restriction digest	19
II.2.4	Agarose gel electrophoresis	19
II.2.5	Ligation	19
II.2.6	Gibson assembly	19
II.2.7	Assembly of modular expression vectors	19
II.2.8	Cloning of multi-subunit constructs for antibody expression	20
II.2.9	Cloning automation	21
II.2.9.1	PCR cleanup with ultrafiltration plates	21

II.2.9.2	Separation of DNA fragments with ultrafiltration plates.....	22
II.2.9.3	Optimization of size-dependent DNA precipitation	22
II.2.9.4	Automation on a liquid handling station.....	22
II.3	Bacterial cultivation and recombinant expression	23
II.3.1	<i>Escherichia coli</i>	23
II.3.1.1	Preparation of chemically competent <i>E. coli</i>	23
II.3.1.2	Transformation of <i>E. coli</i>	24
II.3.1.3	Preparation of <i>E. coli</i> glycerol stocks	24
II.3.1.4	SacB negative selection with <i>E. coli</i>	24
II.3.1.5	Recombinant protein expression in <i>E. coli</i>	24
II.3.2	<i>Agrobacterium tumefaciens</i> (<i>Rhizobium radiobacter</i>).....	25
II.3.2.1	Preparation of competent <i>A. tumefaciens</i>	25
II.3.2.2	Transformation of <i>A. tumefaciens</i>	25
II.3.2.3	Preparation of <i>A. tumefaciens</i> glycerol stocks	26
II.3.2.4	SacB negative selection with <i>A. tumefaciens</i>	26
II.3.2.5	Limiting dilution cloning with <i>A. tumefaciens</i>	26
II.3.2.6	Small scale <i>A. tumefaciens</i> cultures for infiltration of PCPs	27
II.3.2.7	Large scale <i>A. tumefaciens</i> cultures for infiltration of whole plants.....	27
II.3.3	<i>Staphylococcus aureus</i>	27
II.4	Plant cultivation and recombinant expression	28
II.4.1	BY-2 cells	28
II.4.1.1	Cultivation of BY-2 cells in shake flasks.....	28
II.4.1.2	Cultivation of BY-2 cells in stirred tank bioreactors	28
II.4.1.3	Characterization of BY-2 cell cultures.....	29
II.4.1.4	Transient expression in BY-2 PCPs.....	30
II.4.2	Differentiated plants.....	30
II.4.2.1	Cultivation of differentiated plants in a phytotron.....	30
II.4.2.2	Transient expression in differentiated plants	31
II.5	Downstream processing	31
II.5.1	Extraction of <i>E. coli</i>	31
II.5.2	Extraction of BY-2 PCPs	32
II.5.2.1	Bead mill.....	32
II.5.2.2	Infiltration-centrifugation.....	32
II.5.3	Extraction of differentiated plants.....	32

II.5.4	Ultrafiltration/diafiltration	33
II.5.5	Chromatography	33
II.5.5.1	Immobilized metal affinity chromatography	33
II.5.5.2	Protein G chromatography.....	34
II.6	Protein quantification and characterization	34
II.6.1	Bradford assay	34
II.6.2	Fluorescence spectroscopy	35
II.6.2.1	DsRed extract concentration.....	35
II.6.2.2	DsRed surface fluorescence.....	35
II.6.3	Surface plasmon resonance spectroscopy.....	35
II.6.3.1	Quantification of His-tagged proteins	35
II.6.3.2	Quantification of IgG1 and IgG3 antibodies	36
II.6.3.3	Binding kinetics of IgG3 antibodies.....	37
II.6.4	Polyacrylamide gel electrophoresis	37
II.6.4.1	Coomassie staining.....	37
II.6.4.2	Silver staining.....	38
II.6.4.3	Western blotting	38
II.6.5	Dot blot analysis	39
II.6.6	PPK activity assay	39
II.6.7	Biofilm degradation assay	39
II.7	Data evaluation and visualization.....	40
II.7.1	Design of experiments	40
II.7.1.1	Expression models.....	40
II.7.1.2	Harvest time model.....	41
II.7.1.3	Light exposure model	41
II.7.1.4	IgG integrity model	42
II.7.2	Statistical methods.....	42
III.	Results and discussion.....	43
III.1	High-throughput cloning	43
III.1.1	Modular expression vectors.....	43
III.1.1.1	Selection of target proteins	44
III.1.1.2	Selection of vector elements for screening studies.....	46
III.1.1.3	Assembly of modular vectors	46
III.1.2	Negative selection with SacB	49

III.1.3	Automated cloning of expression vectors	52
III.1.3.1	High-throughput DNA purification of cloning intermediates.....	52
III.1.3.2	Automated separation of DNA fragments	53
III.1.3.3	Automation workflow	55
III.1.3.4	High-throughput transformation of <i>A. tumefaciens</i>	57
III.2	High-throughput expression in BY-2 PCPs	60
III.2.1	Prediction of ideal expression cassettes	61
III.2.2	Effect of intrinsic protein properties on accumulation levels	63
III.2.3	Transferability between PCPs and differentiated plants	65
III.2.3.1	Correlation factors.....	65
III.2.3.2	Physiological origin of correlation factors.....	67
III.2.3.3	Origin of variation in BY-2 PCPs	68
III.2.3.4	Origin of variation in differentiated plants	76
III.2.4	Novel applications for PCPs	80
III.2.4.1	Isotope labeling in PCPs	81
III.2.4.2	High throughput infiltration-centrifugation in BY-2 PCPs.....	83
III.3	Purification of target proteins from plant extracts	85
III.3.1	High-throughput screening of chromatography conditions	86
III.3.2	Laboratory scale target protein purification.....	88
III.3.2.1	Clarification of plant extracts in the laboratory scale	88
III.3.2.2	Transferability between liquid handling station and laboratory scale	89
III.3.2.3	Combined UF/DF and IMAC purification process.....	89
III.4	High-throughput target protein quantification and characterization.....	94
III.4.1	High-throughput quantification of His-tagged proteins by SPR.....	94
III.4.1.1	Sensor functionalization.....	94
III.4.1.2	Sensor characterization	95
III.4.2	Assessment of target protein functionality.....	98
III.4.2.1	Functionality of plant-made polyphosphate kinases	98
III.4.2.2	Functionality of plant-made IgG3 antibodies	99
III.4.2.3	Functionality of plant-made biofilm degrading enzymes	101
IV.	Conclusion and outlook	103
IV.1	High-throughput screening in plants.....	103
IV.2	Smart candidate and strategy selection	104
IV.3	Plant-made proteins for controlling MRSA.....	105

V. Summary.....	106
VI. References	108
VII. Appendix	136
VII.1 Publications	136
VII.2 Publications in preparation	137
VII.3 Conference contributions.....	137
VII.4 Register of equipment.....	138
VII.5 List of chemicals.....	140
VII.6 List of buffers	142
VII.7 List of cultivation media.....	145
VII.8 Expression vectors and primers.....	147
VII.9 Supplementary data	156
VII.9.1 SacB negative selection	156
VII.9.2 Cloning automation	159
VII.9.3 Prediction of ideal expression cassettes	160
VII.9.4 Effect of intrinsic protein properties on accumulation	164
VII.9.5 Origin of variability in BY-2 PCPs	167
VII.9.6 Origin of variability in differentiated plants.....	173
VII.9.7 Isotope labeling in BY-2 PCPs.....	174
VII.9.8 Target protein purification.....	176
VII.9.9 SPR quantification of His-tagged target proteins	178
VII.9.10 Target protein functionality	182
VII.10 Curriculum vitae	184

B. Abbreviations

(m v ⁻¹)	Mass per volume
(v v ⁻¹)	Volume per volume
(vvm)	Volume gas per volume of liquid per minute
ADP	Adenosine diphosphate
Agr	<i>Staphylococcus aureus</i> quorum sensing system
Amp	Ampicillin
ANOVA	Analysis of variance
AP	Alkaline phosphatase
AU	Arbitrary unit
AT	Alpha toxin
BAP	Biofilm associated protein
BB	Backbone
BCIP	5-bromo-4-chloro-3-indolyl phosphate
BSA	Bovine serum albumin
BY-2	Bright Yellow 2
CFCA	Calibration-free concentration analysis
CaMV	<i>Cauliflower mosaic virus</i>
CDR	Complementarity-determining region
CFU	Colony forming unit
CHAPS	3-[(3-cholamidopropyl)dimethyl ammonio]-1-propane sulphonate
CHO	Chinese hamster ovary
CHS	Chalcone synthase
CV	Coefficient of variation
cv.	Cultivated variety
d	Days
Da	Dalton
DNA	Deoxyribonucleic acid
dNTP	Deoxynucleoside triphosphate
DoE	Design of experiments
DOT	Dissolved oxygen tension
dpi	Days post infiltration
DspB	Dispersin B
EDC	1-ethyl-3-(3-dimethylaminopropyl)carbodiimide
EDTA	Ethylenediaminetetraacetic acid
ELISA	Enzyme-linked immunosorbent assay
EP	Polysorbate-20 (Tween-20)
EPS	Exopolysaccharides
ER	Endoplasmic reticulum
Fab	Fragment antigen binding
Fc	Fragment crystallisable
FPLC	Fast protein liquid chromatography
g	Gravitational force equivalent
GA	Gibson assembly

GB1.....	Protein G B1 domain
GF	Glass fiber
h	Hours
HCl	Hydrochloric acid
HBS	HEPES-buffered saline
HEPES	4-(2-hydroxyethyl)-1-piperazineethanesulfonic acid
His.....	Histidine
IC50	Half-maximal inhibitory concentration
IgG.....	Immunoglobulin G
IL	Interleukin
IMAC.....	Immobilized metal affinity chromatography
kb	Kilobase
KDEL	ER retention signal from the chaperone protein grp78
KISIA	Vacuolar targeting signal
LB	Lysogeny broth
LDS.....	Lithium dodecylsulfate
LPH.....	Leader peptide sequence of heavy chain from murine mAb24
LSD.....	Least significant difference
LysK-L	Fusion protein of LysK and lysostaphin
mAb	Monoclonal antibody
MOPS	3-(N-morpholino) propane sulphonic acid
MES.....	2-(N-morpholino)ethanesulfonic acid
MERS	Middle East respiratory syndrome coronavirus
mRNA.....	Messenger ribonucleic acid
MRSA.....	Methicillin-resistant <i>Staphylococcus aureus</i>
MS	Murashige & Skoog salts
MWCO	Molecular weight cut-off
MVA.....	Multivariate data analysis
n.a.	Not applicable/not available
NaOH.....	Sodium hydroxide
n.s.....	Not significant
NBT	Nitroblue tetrazolium
NHS	N-hydroxysuccinimide
NTU	Nephelometric turbidity units
OD _{600nm}	Optical density at 600 nm
omega	<i>Tobacco mosaic virus</i> omega prime sequence
Pa	Pascal
PAGE.....	Polyacrylamide gel electrophoresis
PAM4	Plant peptone Agrobacterium medium 4
PBS	Phosphate buffered saline
PBS-T	PBS with Tween-20
PCP	Plant cell pack
PCR.....	Polymerase chain reaction
PEG.....	Polyethylene glycol
PNAG	Poly- β -1,6-N-acetyl-d-glucosamine

PPK	Polyphosphate kinase
PRSA.....	Penicillin-resistant <i>Staphylococcus aureus</i>
pH.....	Negative decadic logarithm of H ⁺ concentration
pI	Isoelectric point
PID	Proportional, Integral, Derivative
PTM	Post-translational modification
QbD.....	Quality by design
rbcS	Transit peptide from <i>Solanum tuberosum</i> RuBisCO small subunit
RC	Regenerated cellulose
RE.....	Restriction endonuclease
rfp.....	Red fluorescent protein (DsRed)
rpm	Revolutions per minute
RU	Response units
RuBisCO	Ribulose-1,5-bisphosphate carboxylase/oxygenase
s	Second
SAR.....	Scaffold attachment region
SARS.....	Severe acute respiratory syndrome
SacB ⁺	Clones that contain a SacB cassette
SCC <i>mec</i>	Staphylococcal Cassette Chromosome <i>mec</i>
SD.....	Standard deviation
SEC	Size exclusion chromatography
SpA.....	<i>Staphylococcus aureus</i> protein A
SPR.....	Surface plasmon resonance
TB.....	Terrific broth
T-DNA	Transfer DNA
TFF.....	Tangential flow rate
Ti	Tumor-inducing
TMP	Transmembrane pressure
TL.....	TEV leader sequence
TRIS	Tris(hydroxymethyl)aminomethane
TSP.....	Total soluble protein
U	Enzyme unit
UF/DF	Ultrafiltration/Diafiltration
UTR.....	Untranslated region
V _H	Heavy chain variable domain
vir	virulence
V _L	Light chain variable domain
VRSA.....	Vancomycin-resistant <i>Staphylococcus aureus</i>
YEB.....	Yeast extract broth

I. Introduction

I.1 Infectious diseases

Emerging and re-emerging infectious diseases represent a major threat to human health and recent examples include the outbreak of severe acute respiratory syndrome coronavirus (SARS-CoV) in 2003, H1N1 influenza virus in 2009, Ebola virus in 2013, Zika virus in 2015 and Middle East respiratory syndrome coronavirus (MERS-CoV) in 2018 [1]. Many of these diseases have the potential to cause an epidemic or even a pandemic [2]. The latest example is the SARS-CoV-2 pandemic, accounting for > 6 million reported deaths worldwide (August 2021 [3]) and an estimated global death toll of 18.2 million (as measured by excess mortality [4]). Because of demographic changes [1], evolving resistance mechanisms [5] and stagnating innovation during pharmaceutical development [6], infectious diseases will likely pose an even bigger threat to human health in the foreseeable future. Antimicrobial resistance is one of the greatest future threats to human health and has been estimated to hit a global death toll of 10 million and a global economic loss of \$60 trillion in 2050 [7, 8]. One of the most prevalent antibiotic-resistant pathogens is methicillin-resistant *Staphylococcus aureus* (MRSA), causing tenfold more infections than all multidrug-resistant gram-negative pathogens combined [9].

I.1.1 Methicillin-resistant *Staphylococcus aureus*

I.1.1.1 Adaptability of *S. aureus* to antibiotics

S. aureus is a Gram-positive, nonmotile, coagulase-positive bacterium that colonizes ~30% of the human population persistently and ~60% transiently [9]. Whereas most individuals are asymptomatic carriers [10], *S. aureus* can cause severe infections when host immunity is impaired or when the skin epithelium is breached, for example through wounds [11, 12]. Antibiotic resistance in *S. aureus* was first described in the 1940s, when penicillin-resistant *S. aureus* (PRSA) emerged [13]. Since then, *S. aureus* has acquired resistance to nearly all antibiotics used to control it [14]. MRSA was first reported in 1961, only two years after methicillin had been introduced to treat infections with PRSA [15]. Resistance of *S. aureus* to the glycopeptide antibiotic vancomycin (VRSA) was first reported in 1996 in Japan, only 5 years after vancomycin had been introduced there [16]. The mechanisms that confer resistance to the above antibiotics are diverse. For example, resistance to penicillins is conferred by the β -lactamase BlaZ, which can be encoded either chromosomally or on a plasmid [17, 18]. Broad spectrum resistance to β -lactam antibiotics other than penicillins is conferred by the transpeptidase PBP2' encoded by the *mecA* gene, which is located on a mobile genetic element known as Staphylococcal Cassette Chromosome *mec* (SCC*mec* [19]). At least 11 SCC*mec* types

have been identified to date, all carrying different repertoires of resistance genes [19, 20]. In addition to resistance to β -lactam antibiotics, some SCCmec types also carry resistance genes for non- β -lactam antibiotics [21]. Deviating from resistance to β -lactam antibiotics, resistance to vancomycin is conferred by a thickened peptidoglycan layer, which prevents vancomycin molecules from reaching the cytoplasmic membrane [22]. In addition to specific antibiotic resistance, non-specific antibiotic resistance also plays a role in *S. aureus* infections and is facilitated by the formation of biofilms [23].

I.1.1.2 *S. aureus* biofilms

Biofilms are immobile microbial communities that are embedded in an extracellular matrix [24]. The extracellular matrix represents a diffusion barrier for anti-microbials [25] and provides additional resistance to host immune effector mechanisms such as phagocyte attacks as well as external threats such as UV light [26, 27]. Major building blocks of *S. aureus* biofilms are exopolysaccharides (EPS), proteins and nucleic acids [28]. The main EPS in *S. aureus* biofilms is poly- β -1,6-*N*-acetyl-d-glucosamine (PNAG). PNAG plays a crucial role during establishment and persistence of biofilms [29, 30] and > 90% of *S. aureus* strains produce PNAG [31]. Important protein components in *S. aureus* biofilms are fibronectin binding protein and biofilm associated protein (BAP), which facilitate intracellular adhesion and attachment to biotic and abiotic surfaces [32, 33], as well as amyloid fibers, which provide resistance to surfactants [29]. External DNA stabilizes biofilms, but can also act as a gene pool for horizontal gene transfer in biofilms [34].

I.1.1.3 *S. aureus* virulence factors and anti-virulence therapies

Pathogenicity of *S. aureus* is facilitated by a vast arsenal of virulence factors, including toxins, immune-evasion factors as well as protein and non-protein factors that facilitate host colonialization [26]. Expression of virulence factors is tightly regulated, for example through the quorum sensing system Agr, which delays expression of virulence factors during early infection to prevent an immune response and upregulates expression upon reaching a certain cell density threshold [26].

A major virulence factor in the context of immune evasion is Staphylococcal protein A (SpA), which binds to conserved fragment crystallizable regions (F_c regions) of immunoglobulin G (IgG), thereby producing a camouflage coat of Igs on the cell surface and impeding phagocytosis by macrophages [26, 35–37]. Additionally, SpA acts as a B-cell superantigen through binding to the fragment antigen-binding region (F_{ab} region) of IgG, causing B-cell apoptosis [26, 36].

The most important *S. aureus* toxin is probably alpha toxin, also termed alpha hemolysin or Hla [26, 38]. Alpha toxin forms heptameric membrane-spanning pores upon insertion into eukaryotic cell membranes, thereby inducing cell lysis through leakage and influx of ions (e.g. calcium) and macromolecules [39, 40]. Targets for alpha toxin in the human body include endothelial cells, monocytes and platelets [41].

Host invasion and colonialization by *S. aureus* is facilitated by a group of surface-anchored proteins referred to as microbial surface components recognizing adhesive matrix molecules, which specifically bind to extracellular components of host tissues [42]. Prominent targets for these proteins include fibrinogen, fibronectin and collagen [43].

Because antibiotics become less and less effective, novel approaches for treatment of *S. aureus* infections have begun to target the virulence factors as well as the quorum sensing system discussed above [26]. A recent example are monoclonal antibodies directed against *S. aureus* alpha toxin, which is highly conserved in many *S. aureus* strains and toxic to a broad range of mammalian cells [44]. However, despite these advances no effective vaccine that protects against *S. aureus* is available to date [45]. Similarly, only two new classes of antibiotics, namely oxazolidinone and lipopeptides have reached the clinic in the last 50 years [46], which has been frequently cited as an example for a stagnating innovation during the development of new pharmaceuticals [6]. Stagnating innovation is diametrical to the emerging challenges discussed above, thus emphasizing the need to improve the current situation during development of new biopharmaceuticals.

I.1.2 Challenges during development and supply of new drugs

I.1.2.1 Challenges during biopharmaceutical development

The development of new pharmaceuticals requires high investments (> \$2.6 billion) as well long development times (~10 years) until approval of a new drug [47]. Despite improvements through the implementation of quality by design (QbD) strategies [48], the success rate during pharmaceutical development (defined as moving a drug from phase 1 to approval) is still low in the clinical stage, i.e. 6.2% for orphan drugs (treatment of rare diseases) and 13.8% overall [49]. In the preclinical stage, the failure rate is even higher, i.e. ~99% [6, 50]. The low success rate in combination with high investments and long development times have recently been named among the leading causes for a currently observed stagnation of innovation throughout the entire pharmaceutical sector [51].

In the preclinical stage, the low success chance during development of new biopharmaceuticals has conventionally been addressed by employing high-throughput techniques [52]. For example, advances in automation, miniaturization and data handling gave rise to high-

throughput screening techniques that can process 50,000 – 100,000 samples per day, as well as ultra-high throughput screening techniques that can process up to 1,000,000 samples per day (small molecules tested against biological targets [52, 53]). However, a paradigm shift from a pure numbers game to a smart selection, i.e. the early elimination of drug candidates that are likely to fail during development has begun [54–56]. This approach offers multiple advantages: First, costs and development times can be reduced by narrowing down the number of potential candidates that have to be screened [57]. Second, resources can be saved by sorting out product candidates that fail late in the development process, considering that late phases (i.e. clinical phases II and III) have the greatest impact on per launch costs [58]. Third, research times can be reduced, considering that the clinical phases II and III are the longest phases (~2.5 years each) in the drug development process [58].

Statistical data analysis techniques that accelerate the development of biopharmaceuticals include multivariate data analysis (MVA) and statistical design of experiments (DoE), as well as combinations thereof [59]. The central concept of MVA is to simplify the extraction of useful information (e.g. trends or extreme values) from collected data, considering that researchers are confronted with increasingly large and complex datasets [59]. Examples for MVA tools used during the development of biopharmaceuticals include principal component analysis, principle least square regression or decision trees [59, 60].

The central concept of DoE is to identify causal effects by investigating multiple potential causes simultaneously, rather than investigating potential causes separately by varying only one variable at a time, which is the conventional approach [61]. DoE can thereby reduce the costs and time required for experiments up to 75% compared to the conventional approach [62]. The statistical methods used to analyze experimental data generated with a DoE approach are linear regression and analysis of variance (ANOVA) [63].

The relationship between the experimental response and multiple independent variables is modeled as multiple linear regression (Equation 1). Regression coefficients in the model are estimated by the least squares method, i.e. regression coefficients are fit to minimize the distance between the model and experimental data.

$$y = \beta_0 + \beta_1 x_1 + \beta_2 x_2 + \beta_{1,2} x_1 x_2 + \varepsilon \quad \text{Equation 1 [64]}$$

Where y represents the response (dependent variable), β represents the expected change of the response per unit change of the input variable (regression coefficient), x represents an input variable and ε accounts for all effects not included in the model, including noise. The term $\beta_{1,2} x_1 x_2$ represents a two-factor interaction.

The value of a regression coefficient does not allow to draw a conclusion about the significance of the relationship between input variable and response. Instead, ANOVA is used to test whether a variable has a significant influence on the response by comparing the variation resulting from changes in that variable to changes resulting from noise. Based on the identified significant influence factors, the value of the response can be estimated from input variables (Equation 2).

$$y \approx \hat{y} = b_0 + b_1x_1 + b_2x_1 + b_{1,2}x_1x_2 \quad \text{Equation 2}$$

Where y represents the observed value, \hat{y} represents the value predicted by the model, b_0 represents the intercept ($x = 0$), b_I represents the slope and x represents an input variable. The term $b_{I,2}x_1x_2$ represents a two-factor interaction.

Different design types are used depending on the experimental purpose: Screening designs are used to identify the main influence factors out of many potential influence factors as well as their interactions [65]. Response surface methodology is used to make an accurate estimate of the quantitative impact of identified influence factors on the response, provided a sufficient number of experiments [65]. Both design types have been successfully applied to various challenges during pharmaceutical development, including medium optimization, formulation development or drug release [60, 66]

I.1.2.2 Challenges during biopharmaceutical supply

In addition to the development of new pharmaceuticals, production capacities must exist to supply the latter, ideally on a global scale to efficiently fight emerging diseases. For example, increasing the global production capacity of SARS-CoV-2 vaccines from ~3 billion to ~4 billion courses per year has been estimated to reduce the time required to achieve a global vaccination rate of ~70% by more than 4 months, thereby preventing financial losses of ~\$1 trillion [67]. However, the rapidly spreading SARS-CoV-2 pandemic has demonstrated that production capacity for recombinant proteins become scarce in emergency scenarios because manufacturing of other drugs and diagnostics cannot be stopped or delayed [66, 68, 69], resulting in unequal vaccine distribution at the expense of developing countries [70]. Even though novel nucleic acid-based vaccination strategies allow a rapid response to emerging diseases, maintaining cold-chains (e.g. -70°C) is a major challenge for the global distribution of nucleic acid-based vaccines [71]. In contrast, protein-based vaccines require less stringent cold chains and are therefore important especially in resource-limited countries [72]. Aside from the pandemic, capacity bottlenecks for manufacturing of biopharmaceuticals

become more likely in the future, considering that market size and product range are growing faster than the production capacity [73], and that existing production capacity is often bound by existing products that cannot be discontinued [74]. Similarly, production capacity controlled by contract manufacturing organizations, who can react more quickly to new demands due to a flexible business model is often booked out years in advance [74]. Therefore, to sustain the growing demand for biopharmaceuticals in the future, flexible production capacity is desirable [73]. Plant-based production platforms can complement established platforms, for example with emergency response production capacity in the context emerging diseases [74]. This additional capacity would be particularly useful in developing countries by eliminating the requirement for cold chains [69, 70].

I.2 Plant-based production of biopharmaceuticals

The global market for biopharmaceuticals was about \$240 billion in 2019 and showed an expected compound annual growth rate of 14.2% [75]. The majority of biopharmaceuticals are recombinant proteins, predominantly antibodies corresponding to 65.6% of total sales (2018, [75, 76]) and vaccines corresponding to ~14.5% of sales (2015, [77]). To date, recombinant proteins are mainly produced in prokaryotes and mammalian cells [78, 79]. Specifically, *E. coli* is favored for the production of simple proteins that do not require complex post translational modifications, whereas mammalian cells such as Chinese hamster ovary (CHO) or murine myeloma cells are preferentially used for the production of glycoproteins such as antibodies [78, 79]. Plant-based expression systems do not yet hold a significant share of the global protein production capacity (< 1% of the capacity of mammalian cell bioreactors [78]), but offer several unique features compared to prokaryotes and mammalian cells that make them attractive in market niches such as animal-free production or rapid response to emerging diseases [74, 78, 80, 81].

I.2.1 Unique features of plants compared to dominant hosts

The dominant prokaryotic host for recombinant protein expression, *E. coli* cannot naturally carry out complex post translational modifications (PTMs) such as glycosylation or the formation of disulfide bonds [82, 83], which are often crucial for biological activity and suitable pharmacokinetics of recombinant therapeutic proteins [83, 84]. In contrast, plant-based expression systems are able to perform the PTMs required for recombinant pharmaceutical proteins [82–84] and offer additional flexibility because target proteins can be directed to different cell compartments, which differ in their ability to carry out PTMs [85, 86]. For example, chloroplasts have a bacterial origin and are not capable of glycosylation or the

formation of disulfide bonds [87], whereas glycosylation is enabled when directing a target protein to the secretory pathway [84]. Moreover, plant-based expression systems can be used to produce anti-microbials, which can be problematic for prokaryotic hosts due to their toxicity. In addition to targeting with signal sequences the use of compartment-specific promoters can further help to avoid toxicity in the plant host [88]. A potential concern in prokaryotic expression systems are endotoxins. However, this concern can also apply to transient expression in plants, when relying on prokaryotes to deliver a transgene into plants.

Compared to mammalian cell culture, which requires expensive ($\geq \$100 \text{ L}^{-1}$) media [89], upstream production costs are low in plant-based expression systems, because they only require light, water and inexpensive ($< \$0.01 \text{ L}^{-1}$ [90]) fertilizer for cultivation [86]. Specifically, the cultivation costs of plants account for only 2 – 10% of the costs of microbial fermentations and $< 0.01\%$ of the cost of mammalian cell cultures depending on target protein and yield [89–91]. Moreover, plant-based expression systems can react more flexible towards changing demands than mammalian cell culture, because no new infrastructure has to be constructed [74]. Additionally, plant-based expression systems can be used for the expression of toxic products such as immunotoxins (i.e. antibody fragments linked to a toxin), which are emerging as new tools for cancer therapy, but can be problematic in mammalian hosts due to the toxin component [81, 92–94]. Unlike mammalian cells, plant-based expression systems neither support the replication of human pathogens, nor do they require animal-derived components such as serum [95, 96], and are thus thought to offer a better safety profile [97, 98].

I.2.2 Plant molecular farming

The production of recombinant proteins in plants is referred to as molecular farming and aims to utilize the protein itself instead of traits the recombinant protein confers to the plant host [99]. Plants are interesting platforms for recombinant protein production, because high biomass yields of $\sim 500,000 \text{ kg ha}^{-1}\text{y}^{-1}$ (tobacco [100]) can be combined with high product yields of up to $\sim 6 \text{ g kg}^{-1}$ [101]. Different plant hosts are available for recombinant protein production, for example *N. benthamiana*, *N. tabacum*, cereal crops as well as cell lines derived thereof [87, 102]. Cereal crop such as maize (*Zea mays*), rice (*Oryza sativa*) and barley (*Hordeum vulgare*) are widely used production hosts, because their seeds can act as self-contained bioreactors that protect the product [87]. *N. benthamiana* can provide high biomass yields ($\sim 30\%$ of tobacco [103]) in a scalable manner and is susceptible to plant viruses due to a defective form of RNA-dependent RNA polymerase [104, 105], thus facilitating the use of viral expression vectors. *N. tabacum* (tobacco) is an excellent production host, because it is well characterized, easy to manipulate with established transformation procedures [106, 107] and scalable through

conventional agricultural practices [108]. Additionally, *N. benthamiana* and *N. tabacum* are non-food and non-feed crops, thus minimizing the risk to contaminate food or feed chains by spreading a transgene [109].

The two main expression strategies for production of recombinant proteins in plants are transient expression and stably transformed transgenic plants. Stable transformed plants can be established in approximately 4 – 6 months [105], whereas transient production processes can be established in only 3 weeks, as demonstrated for an influenza vaccine [110]. For generation of transgenic plants, a transgene has to be integrated into the plant genome, followed by time consuming selection of transformed cells [111, 112]. In contrast, during transient expression a transgene is not integrated into the plant genome and remains as episomal DNA in the plant cell nucleus [113]. Transient expression is thus unaffected by chromosomal position effects [114], which contributes to variability in stable plants [115]. Because transgene expression declines after 2 – 3 days [114], the transient setup is best suited for short-term high-level expression strategies.

Transient expression in plants has been mediated by (i) infiltration with the plant pathogen *Agrobacterium tumefaciens*, (ii) with plant virus-based vectors and (iii) by combining plant viruses with DNA delivery through *Agrobacterium* [116]. The first approach exploits the ability of the tumor-inducing (Ti) plasmid (~200 kbp) of *A. tumefaciens* to transfer a part of the Ti plasmid termed transfer DNA (T-DNA) into plant cells [117, 118]. This mechanism was refined into a binary vector system by placing the virulence (vir) genes required for T-DNA transfer onto one plasmid (the helper plasmid) and the T-DNA onto a separate plasmid, so that the latter can be easily modified in *E. coli* [116]. Oncogenes were deleted from the Ti plasmid to prevent the undesired formation of tumors (crown gall disease) in transformed plants. The *Agrobacterium* system does not confer systemic expression of the foreign gene, but is compatible with T-DNAs of ~150 kbp [119], and can be used to simultaneously deliver multiple transgenes into the same cell (co-transformation), for example antibody heavy and light chains [114].

Plant virus-based expression vectors exploit the ability of a viral sequence to spread from an initially infected cell, allowing systemic expression of a transgene [120, 121]. Depending on the strategy used for their engineering, plant virus-based vectors can be differentiated into full virus vectors, and more recently developed deconstructed vectors [122]. In the former strategy, a wildtype virus is modified to carry a heterologous sequence, which is then expressed in the plant host. Safety concerns and instability of large (> 2.0 kbp) inserts led to the development of deconstructed virus vectors [121, 123], where undesired or limiting functions are either deleted

from a wildtype virus or they are moved to the plant host through genetic engineering [122]. In this context also the viral movement proteins and coat proteins have been replaced with a gene of interest, thereby relying on *A. tumefaciens* for delivering deconstructed viral vectors into plant cells [121]. The utilization of *A. tumefaciens* to deliver virus-based vectors to plants is termed agroinfiltration and allows high recombinant protein yields (up to $\sim 0.7 \text{ mg g}^{-1}$ fresh mass [124]) due to efficient transcription and/or replication in plant cells [116, 124]. Prominent examples for deconstructed viral vectors are the MagnICON system or the geminiviral DNA replicon system [124].

Table 1: Overview of plant-made biopharmaceuticals that were approved for use in humans.

Product and year	Host	Expression strategy	Company
Elelyso (taliglucerase alfa) for treatment of Gaucher's disease, 2012	<i>Daucus carota</i> (carrot)	Transgenic cells in suspension culture	Protalix Biotherapeutics
CaroRx for prevention of dental caries, discontinued ^a	<i>N. tabacum</i> (tobacco)	Expression in transgenic plants	Plant Biotechnology
ZMapp for treatment of Ebola virus, 2015 ^b	<i>N. benthamiana</i>	Transient expression in plants	Mapp Biopharmaceutical
iBio-CFB03 for treatment of systemic sclerosis, 2016 ^c	<i>N. benthamiana</i>	Transient expression in plants	iBio Biotherapeutics
Palforzia (AR101) for oral immunotherapy of peanut allergy, 2020	<i>Arachis hypogaea</i>	Peanut flour produced using Good Manufacturing Practices	Aimmune Therapeutics
CoVLP for COVID-19 vaccination, 2022	<i>N. benthamiana</i>	Transient expression in plants	Medicago

^a approved as medical device, ^b emergency compassionate approval for human use, ^c received orphan drug designation.

Despite the flexibility of plant-based expression systems, only a small number of biopharmaceuticals derived from plants has so far gained regulatory approval for the use in humans (Table 1). Economic constraints are probably the foremost cause currently limiting a broader application of plant molecular farming, considering that companies are unlikely to risk a large investment when regulatory approved alternatives are already established [86, 125].

I.2.3 Mitigation of constraints in plant molecular farming

To make plant expression platforms more economically competitive compared to established hosts outside of market niches, low product yields, downstream processing costs and the lack of regulatory approval need to be addressed in particular [68, 80, 86]. However, significant progress has been made to overcome these limitations and plant molecular farming continues to mature as a technology [80, 87].

In the context of lacking regulatory approval, success stories such as taliglucerase alfa (Table 1) have cleared the way for novel plant-made biopharmaceuticals. More regulatory harmony can be expected in the future, because plant molecular farming has begun to consolidate around transient expression in *N. benthamiana* as well as stable expression in *N. tabacum*, crops and cell lines derived thereof [87, 102]. The lack of operational large-scale production facilities (< 5 in the range of ~250 tons biomass per year [69, 74]) is currently being addressed through ongoing construction processes worldwide [74, 87].

Whereas upstream production is already cost efficient in plants (I.2.1), downstream processing can be further optimized to reduce production cost in plant-based production platforms [78, 80]. Downstream processing is challenging in differentiated plants, because plant tissue has to be disrupted, thereby releasing particulate and soluble contaminants as well as host cell proteins (HCPs) alongside the product [68, 126]. Particulate impurities can be efficiently removed with depth filters, but filters have previously accounted for $\geq 20\%$ of the total production costs [127]. The combination of flocculants and cellulose-based filter aids has reduced these costs to $< 5\%$ [127]. Several strategies have been developed that facilitate the removal of HCPs and/or bulk water from plant extracts. One example is blanching of plant tissue, i.e. the incubation of intact leaves in a $\sim 60^\circ\text{C}$ water bath, which allows to remove $\sim 80\%$ of HCPs before chromatography [128]. The method has recently been refined to allow purification of a broader range of target proteins [129]. Another example is the implementation of ultrafiltration/diafiltration, which relies on membranes with a defined pore size to separate the target protein from HCPs and remove bulk water before chromatographic purification [130]. Additional strategies that omit the need to disrupt plant tissue are product secretion in plant cell suspension cultures [131] or extraction of recombinant proteins from the apoplast by infiltration centrifugation [132].

A concern frequently raised in the context of plant-made recombinant proteins is non-human glycosylation [133]. However, multiple glyco-engineered plant lines and plant cell cultures have been engineered to address this problem [133–135]. This development has been further accelerated by the release of CRISPR/Cas9 [133]. In some applications a non-human glycosylation can also be advantageous [78]. A prominent example for a beneficial effect of non-human glycosylation is the improved uptake of recombinant taliglucerase alfa (Elelyso) by macrophages through vacuole-specific glycans [136]. In the context of vaccines, plant-specific *N*-glycans can act as adjuvants and facilitate the uptake by antigen presenting cells [110].

A major limitation of plant-based expression systems is the often low (1 – 2% TSP) target protein accumulation [137]. Product yields in plant cells are limited by the high vacuolar volume (predominantly water) taking up the majority of the cellular space ($> 95\%$ in BY-2 cells

[78, 138]). Reducing the cell's water content, for example by increasing the medium osmolality has therefore allowed to increase product yields (~20-fold [139]). In cell-free systems the vacuole can even be entirely removed, which in combination with the removal of translation-inhibiting substances, contributed to high productivities (~3 g L⁻¹ cell lysate [140, 141]). Post-transcriptional gene silencing was proposed as another productivity-limiting factor, but has been addressed in *N. benthamiana* through silencing suppression, which allowed a ~50-fold enhanced target protein accumulation, corresponding to ~7% TSP [114]. Silencing can be countered with different strategies, for example with the tombusvirus p19 protein, which sequesters small RNA duplexes and prevents initiation of the RNA silencing pathway [142]. However, silencing suppression with p19 is not yet possible in *N. tabacum* [143]. Beyond cultivation and epigenetic, productivities in plant-based expression platforms can be further increased by optimizing the transgene construct through screening for ideal combinations of e.g. promoters, untranslated regions and signal sequences [137, 144].

I.3 High-throughput screening in plants

Increasing costs, research times and a low success rate during the development of new biopharmaceuticals (I.1.2.1) emphasize the need for efficient high-throughput screening tools to accelerate process development, especially in early stages [145, 146]. So far, high throughput screening tools have been mainly described for prokaryotic expression platforms [147, 148], which cannot carry out complex PTMs, thus limiting the range of target proteins that can be expressed as discussed above (I.2.1). Mammalian cell cultures allow for complex PTMs, but high sterility requirements complicate high-throughput applications [149]. Similar to mammalian cell cultures, plant-based expression systems can carry out complex PTMs and moreover allow heterologous protein expression within days [150] and under non-sterile conditions [151]. However, compared to bacteria, yeast and mammalian cells [148, 152–157], few tools for high throughput expression screening are available in plants. High-throughput screening tools that are of particular interest to overcome the design-build-test bottleneck in plant-based expression systems span cloning, expression and quantification as well as combinations thereof [158].

I.3.1 Automated cloning of vector libraries

The first step in high-throughput screening, namely generation of expression vectors, represented a long-lasting bottleneck in molecular biology [159, 160], but fortunately several high-throughput compatible methods for DNA assembly have become available by now. These cloning methods can be classified into (i) restriction enzyme-based cloning, (ii) recombination-

based cloning or (iii) ligation-independent cloning [161]. Cloning based on restriction enzymes and DNA ligase has been used for more than four decades and is hence well established in many laboratories. The technique is simple, efficient, universal and cost efficient, and since the implementation of type IIS restriction enzymes a viable option for high-throughput applications [161]. Specifically, type IIS restriction enzymes cleave DNA 1 – 20 base pairs (bp) away from their recognition sequences [162], thus allowing to assemble DNA fragments without introducing unwanted sequences, as well as one-pot restriction and assembly [163]. A prominent example for restriction enzyme-based cloning with type IIS enzymes is Golden Gate assembly [163].

Recombination-based cloning relies on site-specific recombinases to exchange DNA fragments between vectors, without the need for restriction enzymes or ligase [161]. The implementation of Seamless Ligation Cloning Extract, which uses bacterial cell extract as an alternative to expensive commercial kits has facilitated the use of recombination-based cloning in high-throughput settings [164]. A prominent example for recombination-based cloning is Gateway cloning [161].

An alternative approach for cloning of expression vector libraries is ligation-independent cloning, which relies on regions of homology (10 – 30 bp [165]) to assemble DNA fragments that have been linearized by PCR or with restriction enzymes [166]. Complementary single-stranded overhangs (cohesive ends) are generated on these DNA fragments by treatment with an exonuclease. Annealing of DNA fragments is mediated by the cohesive ends and the resulting DNA complexes can be directly transformed into *E. coli* without the need for *in vitro* ligation [167], because nicks are repaired by host repair mechanisms [167]. Ligation-independent cloning is simple, efficient [166] and compatible with high-throughput settings [147, 165]. Examples for cloning methods that are based on ligation-independent cloning include Gibson assembly, overlap extension cloning and In-Fusion cloning [161].

Standardization of workflows has led to increasing automation of the DNA assembly methods discussed above, thereby improving their reliability and accuracy, and ultimately allowing more complex projects [168, 169]. Cloning benchmarks that have been achieved by automating DNA assembly with the help of liquid handling stations reach 500 – 1000 assembly reactions per day at costs of < \$3 [170]. However, cloning throughput has previously far exceeded expression throughput in major plant-based expression platforms including *Nicotiana* spp., because of a low transformation efficiency and large footprint [158]. Only now have technologies become available in these platforms that allow expression of several hundred constructs per day [151, 171].

I.3.2 High-throughput expression in plant cell packs

One example for a high-throughput expression tool in plants (*N. tabacum*) is a leaf disc-based screening assay, which allows to conduct 14 *Agrobacterium*-mediated infiltration events in parallel [137]. A screening throughput of ~500 (manual) – 2,500 samples (automated) per day at costs of < \$0.5 per sample is possible with so called plant cell packs, hereafter referred to as PCPs [171]. PCPs are cast into 96-well plates by depriving plant cells from a suspension culture of liquid medium, using filters with a cut-off size $\leq 40 \mu\text{m}$ in combination with vacuum (50 kPa, 1 minute [171]) or centrifugation ($1800 \times g$, 1 minute [151]). The resulting cell pellet is infiltrated with recombinant *A. tumefaciens* containing vectors for transient protein expression. After incubation for 30 minutes to several hours, surplus *A. tumefaciens* cell suspension is removed by vacuum or centrifugation and PCPs are incubated at 90 – 95% relative humidity for 3 – 5 days before protein extraction [171]. The PCP technology is scalable between ~60 mg and at least ~100 g and compatible with different plant cell suspension cultures, for example *N. tabacum* Bright Yellow 2 (BY-2). In approximately 3 years after the technology has been introduced, PCPs have been successfully used to assess the accumulation of various target protein classes in plants, including but not limited to antibodies, biofilm degrading enzymes, immunotoxins, lectins as well as model proteins such as DsRed, GB1 and SpA [81, 143, 172–174]. Analysis often remains a bottleneck during high-throughput screening [175]. Therefore, to make full use of PCPs as a screening tool, an analysis method is required that is selective, sensitive and can keep up with a throughput of ~500 samples per day. Assays based on surface plasmon resonance (SPR) spectroscopy fulfil these requirements and can be automated and multiplexed to facilitate high-throughput assays [176–178].

I.3.3 Quantification with surface plasmon resonance spectroscopy

SPR is an optical effect that occurs when exciting a thin metal film (typically gold or silver) with monochromatic polarized light and some of the incident light interacts with delocalized electrons (plasmons) of the metal film, thus reducing the intensity of the reflected light [179]. The angle of incident light at which minimal light reflectance is observed (resonance angle or SPR angle [179, 180]) depends on the refractive index of the medium in close proximity (~300 nm [177]) of the metal film. The refractive index changes proportionally to mass of e.g. analyte molecules binding to the surface of the metal film, which can be measured (in real time) by the change in the resonance angle [176], typically expressed in resonance or response units (RU). A resonance angle shift of 0.0001° is defined as 1 RU, corresponding to the binding of 1 pg mm^{-2} protein [179, 181].

Analyte concentrations can be determined based on calibration curves or with calibration free concentration analysis (CFCA), depending on the availability of standards [180]. Direct or indirect assay formats are available for analyte quantification in the former application.

In a direct SPR assay, an analyte in solution binds to an immobilized ligand without additional sample preparation. A calibration curve is constructed from the change of the RU over time (i.e. the slope) and the concentration of the standards [179]. Instead of the slope, the response signal obtained at the end of an analyte injection can be used for quantification as well [180]. Because the resonance signal is proportional to the molecular mass of the analyte, small target proteins (< 10 kDa [182]) are difficult to quantify in direct assays.

In contrast to direct SPR assays, indirect assays (based on competition or binding inhibition) are independent of the target proteins size and are therefore preferable for small target proteins [182, 183]. In an indirect assay, the analyte (or a conjugate thereof) is immobilized on the sensor surface and the sample is mixed with a defined amount of ligand (typically larger than the analyte) before injection [184]. Only ligand molecules that retain free binding valencies after incubation can bind to the sensor surface [184]. Consequently, the resonance signal in indirect assays is inversely proportional to the amount of analyte in the sample [182].

Calibration-free concentration analysis (CFCA) does not require standards, but knowledge about the molar mass and diffusion coefficient of the analyte [180]. The analyte concentration in a sample is calculated from the change of the initial binding rates measured at different flow rates (e.g. the lower and upper limit of the device) and the diffusion coefficient of the analyte [185]. In CFCA, measurements are conducted under diffusion limited conditions, indicated by a linear RU slope during injection.

Because ligands cannot be easily coupled to an inert gold surface, commercial sensor chips are often covered with a self-assembled monolayer of lipids or dextran, which typically extends ~ 100 nm from the gold surface and provides functional groups for bioconjugation chemistry techniques [186]. A frequently used example is amine coupling, which relies on primary amino groups for covalent binding [187].

If the surface of the sensor chip is functionalized with a ligand that specifically binds the target protein, target detection and quantification is possible even in crude mixtures of proteins [179, 180], thus omitting the need for purification and facilitating the evaluation of expression studies. When combined with a high-throughput expression platform such as PCPs (I.3.2), target protein detection with SPR assays can facilitate screening and process development.

I.4 Aim of the thesis and workflow

This thesis aims to advance the low success rate during the development of new biopharmaceuticals by increasing the screening throughput across the entire development process (Figure 1A – D), and by identifying parameters that can guide selection of candidate proteins and expression vectors (Figure 1E). This concept was applied to transient expression in *Nicotiana* spp., which can rapidly supply recombinant proteins, for example in response to emerging pandemics [110]. Model proteins required to set up and refine high-throughput tools for biopharmaceutical protein production in plants were specifically selected to suit a global objective, namely treatment of infections with MRSA (I.1.1). An overarching objective was to investigate the physiological mechanisms that govern (i) recombinant protein accumulation, (ii) variation and (iii) correlation factors in plant-based expression systems, using data generated with these model proteins (Figure 1E).

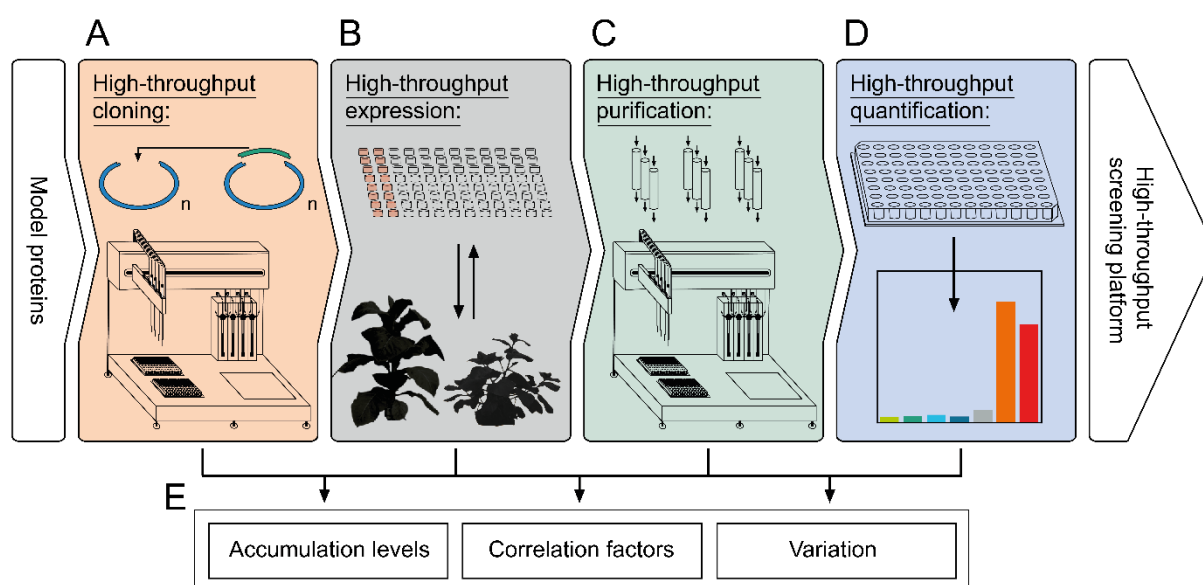


Figure 1: Workflow and work packages for establishing a plant-based high-throughput screening platform. A. Modular vectors and automation on a liquid handling station were combined for high-throughput cloning of vector libraries for *Agrobacterium*-mediated transient expression. B. Expression vectors cloned in (A) were used to establish correlation factors between BY-2 PCPs and differentiated plants. C. Miniaturized chromatography columns and automation on a liquid handling station were combined for high-throughput screening of chromatography conditions. D. Surface plasmon resonance (SPR) spectroscopy assays were developed to facilitate high-throughput quantification. E. Data from multiple work packages were combined to investigate physiological mechanisms that govern recombinant protein accumulation, correlation factors and variation in plant-based expression systems.

I.4.1 Model protein classes and molecular targets

Model protein classes selected to establish and refine high-throughput screening tools were chosen to suit a multi-layered strategy for the treatment of infections with MRSA (Figure 2). Specifically, interleukins were selected as model protein class, because they can be used to

modulate an immune response and thus potentially counter *S. aureus* immune evasion strategies such as interference with chemokine signaling [188]. The biological activity of plant-made inflammatory and anti-inflammatory cytokines has already been demonstrated [189, 190], which is a prerequisite for this strategy. Beyond modulating an immune response, cytokines are receiving increasing attention as defined medium additives for human and animal cell culture, currently often supplied in the form of crude mixtures [191–193].

S. aureus-specific antibodies were selected as model protein class, because no effective vaccine that protects against *S. aureus* infections is currently available [45, 194], and because antibiotics have become less and less effective against *S. aureus* [195]. Because *S. aureus* can bind and neutralize commonly used IgG1 antibodies through SpA [36, 37], anti-*S. aureus* antibodies were designed based on an IgG3 scaffold, which cannot be neutralized by SpA. However, IgG3 antibodies have so far been difficult to produce in established expression systems, including CHO cells and plants [196–198].

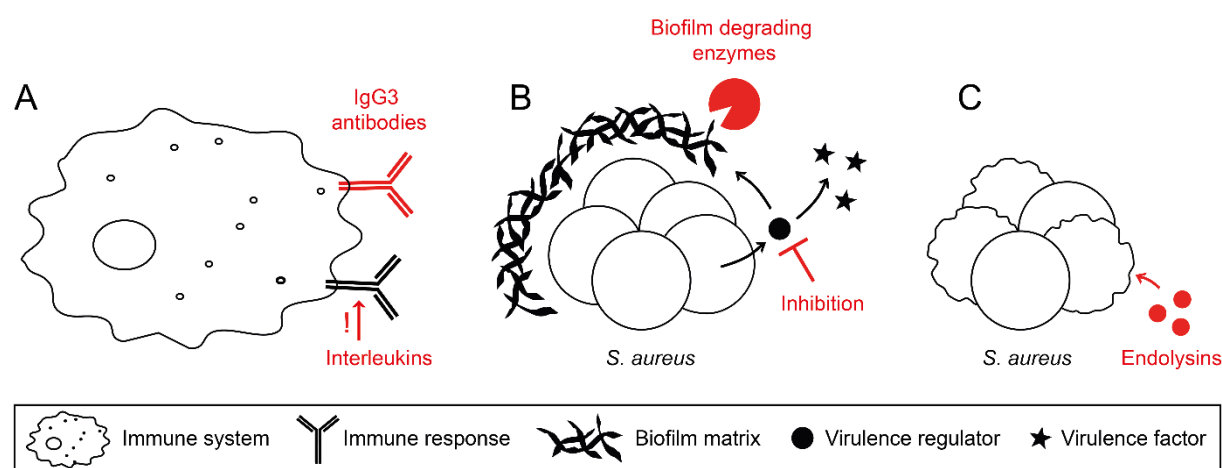


Figure 2: Schematic representation of molecular targets for treatment of infections with MRSA. A. Stimulation of an immune response with recombinant cytokines and antibodies that cannot be neutralized by *S. aureus*. B. Targeting of the biofilm matrix as well as virulence regulating proteins in *S. aureus* (co-) infections. C. Lysis of *S. aureus* cells with endolysins that are specific for the pathogen. Targets that were addressed in this project are displayed in red.

Treatment of infections with MRSA is complicated by the pathogen's ability to form biofilms, which protect the bacterium against environmental threats such as disinfectants, antibiotics or host immune effector mechanisms [27]. Because harsh methods for biofilm removal are unsuitable for the removal of *S. aureus* biofilms in the human body, biofilm degrading enzymes were investigated as a third model protein class to allow removal of biofilms under mild conditions. Beyond the medical sector, biofilm degrading enzymes have a wide range of potential applications in different branches of industry, for example in the food processing industry [199].

The fourth model protein class, namely polyphosphate kinases (PPKs), was selected as potential drug target [200]. PPKs are involved in virulence, biofilm formation and quorum sensing [201] and are widely conserved in bacteria including major pathogens such as *Pseudomonas aeruginosa*, *Helicobacter pylori* or *Mycobacterium tuberculosis* [202, 203]. *S. aureus* does not possess PPK homologs, but PPKs still represent an interesting drug target in the context of co-infections of *S. aureus* and other pathogens such as *P. aeruginosa* [203]. Seemingly contrasting their name, the kinetics of PPKs from the PPK2 family favor the polyphosphate-driven synthesis of nucleoside diphosphates and nucleoside triphosphates rather than their degradation [203, 204], which is desirable for cofactor regeneration [204, 205]. Consequently, PPKs are receiving increasing attention for ATP regeneration in enzymatic reactions, allowing to harness ATP-dependent enzymes for industrial applications without the need to add stoichiometric quantities of cofactor [204].

An additional model protein class chosen for further investigation were phage-derived endolysins, which represent a possible alternative for antibiotics [195, 206]. Endolysins are utilized by phages during the lytic cycle to digest the host cells peptidoglycan layer and release virions from the cytosol. Topical application of endolysins is especially effective against gram-positive bacteria such as *S. aureus* due to the freely accessible outer peptidoglycan layer [207].

I.4.2 State of completion

To assess whether plant-based expression systems can support a multi-layered strategy against *S. aureus*, the individual model proteins (I.4.1) had to be produced, purified and tested for activity. The state of completing for each model protein class is displayed hereafter (Table 2).

Table 2: State of completion during assessment of *Nicotiana* spp. for the production of different model protein classes directed against emerging MRSA.

Model protein class	Expression screening in PCPs	Transfer to differentiated plants	Scalable purification strategy	Characterization
Cytokines (IL6, IL8)	Completed	Completed	Completed	n.a. ^a
PPKs (PPK-RO/TA)	Completed	Completed	Completed	Completed
Antibodies (IgG1/3)	Completed	Completed	Completed	Completed
Biofilm degrading enzymes (DspB)	Completed for one UTR	Completed for <i>N. tabacum</i>	Completed	Completed
Endolysins (LyK-L)	Completed	Pending	Pending	Pending

^a The biological activity of plant-made cytokines has already been demonstrated in the literature [189].

II. Materials and Methods

II.1 Equipment and chemicals

All equipment used in this study is listed together with the manufacturers' information in the appendix, section VII.4. All chemicals and buffers are listed in the appendix, sections VII.5 and VII.6, respectively.

II.2 Expression vectors and cloning

All vectors for *Agrobacterium*-mediated transient expression were based on pTRA, a derivative of pPAM (GenBank AY027531), kindly provided by Dr. Thomas Rademacher (Fraunhofer IME, Aachen, Germany). Vectors included a β -lactamase gene for selection in *A. tumefaciens* and *E. coli*. The expression cassette was flanked by RB7 matrix attachment regions (GenBank U67919) to facilitate a potential comparison with stable transgenic plants by using identical construct designs [144].

II.2.1 Gene synthesis and codon optimization

The coding sequences for all model proteins produced in this study were codon optimized for *N. benthamiana* using the GeneOptimizer tool [208] and synthesized by GeneArt (Thermo Fisher Scientific, Darmstadt, Germany) with flanking 5' NcoI/BspHI/PciI and 3' NotI sites for subcloning. Constructs encoding the native heavy chain of human IgG3 (Uniprot ID P01860) or the IgG1 antibody M12 [209] combined with a human lambda light chain were synthesized with flanking 5' NcoI and 3' XhoI sites for subcloning. Sequences encoding polyphosphate kinases were kindly provided by Dr. Dirk Tischler (Ruhr University, Bochum, Germany).

II.2.2 PCR amplification

Q5 High-Fidelity DNA polymerase was used for cloning, whereas OneTaq DNA polymerase (both from New England Biolabs, Ipswich, USA) was used for analytical PCRs. The polymerases were used according to the manufacturer's recommendations using a total reaction volume of 10 μ L and a Biometra Trio thermal cycler (Analytik Jena, Jena, Germany). All PCR primers (Supporting Table 1) were synthesized by Eurofins (Eurofins Genomics, Ebersberg, Germany). PCR products intended for cloning were purified with a NucleoSpin Gel and PCR Clean-up kit (Macherey-Nagel, Düren, Germany) or with ultrafiltration plates (II.2.9.1). DNA concentrations after purification were quantified with a NanoDrop 2000 spectral photometer (Thermo Fisher Scientific).

II.2.3 Restriction digest

Restriction reactions were performed with 1 unit enzyme (New England Biolabs) per μg DNA in a total volume of 10 μL using ~ 300 ng template DNA (analytical) or in a total volume of 50 μL using ~ 5 μg template DNA (preparative) according to the manufacturer's recommendations. DNA fragments from preparative restriction reactions were purified by agarose gel electrophoresis (II.2.4) or with ultrafiltration plates (II.2.9.1).

II.2.4 Agarose gel electrophoresis

DNA fragments from restriction (II.2.3) were mixed with Gel Loading Dye (New England Biolabs) and separated on 1.2% (m v⁻¹) agarose gels containing 0.25 mg L⁻¹ ethidium bromide at 120 V in TAE buffer (VII.6) for 40 minutes. Analytical gels were analyzed in a Gel Doc (Bio-Rad, Hercules, USA) using an excitation wavelength of 365 nm and emission wavelength of 580 nm. Preparative gels were analyzed on a Dual UV transilluminator (VWR, Langenfeld, Germany), using an excitation wavelength of 365 nm. DNA fragments were cut from gels with a scalpel and isolated from the gel fragments with a NucleoSpin Gel and PCR Clean-up kit (Macherey-Nagel). DNA concentrations were quantified as described for PCR (II.2.2).

II.2.5 Ligation

Ligation reactions were performed with T4 DNA ligase (New England Biolabs) using ~ 30 ng vector backbone and a threefold molar excess of the insert in a total volume of 10 μL at 16°C overnight (16 hours). Ligation reactions were heat inactivated by incubation at 65°C for 10 minutes in a Biometra Trio thermal cycler (Analytik Jena) before transformation into *E. coli* (II.3.1.2) or *A. tumefaciens* (II.3.2.2).

II.2.6 Gibson assembly

Gibson assembly [210] was performed with commercial Gibson Assembly Mastermix (New England Biolabs) using ~ 100 ng vector backbone and a threefold molar excess of insert in a total volume of 5 μL at 50°C for 1 hour. Completed assembly reactions were stored at -20°C until transformation into *E. coli* (II.3.1.2) or *A. tumefaciens* (II.3.2.2).

II.2.7 Assembly of modular expression vectors

Vectors with modular expression cassettes composed of a promotor, 5' and 3' UTRs, 5' and 3' signal sequences, a purification tag and a terminator were created with Gibson assembly (II.2.6) and restriction cloning (II.2.3). Homologous regions for Gibson assembly were introduced into

DNA fragments through primer overhangs using PCR (II.2.2). Restriction sites between expression cassette elements were introduced similarly.

DNA fragments spanning the pTRA backbone upstream of the gene of interest, containing either a CHS [211], omega [212] or TL [213] 5' UTR, were amplified from the vectors pTRAc_CHS_PHACTR1, pTRAc_omega_PHACTR1 and pTARc_TL_PHACTR1 [214] by PCR (Supporting Table 1). DNA fragments spanning the pTRA backbone downstream of the gene of interest, containing either a His₆-tag or a His₆-tag in combination with an ER retention signal were amplified from pTRAc_000101 and pTRAc_000104 (Supporting Table 2) by PCR (Supporting Table 1). Upstream and downstream DNA fragments and a DNA fragment encoding the model protein IL6 (Supporting Table 1) were assembled into vectors for cytosolic expression (no signal sequence) and intermediate constructs with an ER retention signal. Next, the mAb24 leader peptide (LPH) for targeting the secretory pathway [215] was fused N-terminally to the DNA sequence encoding IL6 by PCR (Supporting Table 1) and the PCR product was introduced into the intermediate constructs by restriction cloning with NcoI and NotI, thus completing the vectors for ER retention. The same PCR product was introduced into the constructs for cytosolic expression to generate vectors for target protein secretion to the apoplast. Vectors for plastid-targeting were generated by introducing the RuBisCO transit peptide from *Solanum tuberosum* (rbcS [216]) into the constructs for cytosolic expression. The rbcS signal sequence was amplified from the vector pTRAc_TP_CHS_PHACTR1 [214] by PCR (Supporting Table 1) and introduced at the NcoI site. The correct orientation was confirmed by sequencing (Fraunhofer IME sequencing service).

The 1008 bp Rb7 matrix attachment regions flanking the expression cassette appeared to interfere with Gibson assembly. Vector backbones without such homologous regions were hence used for Gibson assembly hereafter.

II.2.8 Cloning of multi-subunit constructs for antibody expression

To facilitate subcloning into modular expression vectors (II.2.7) sequences encoding antibody heavy and light chains were fused in frame with a self-excising linker peptide [217]. Initial constructs for expression of IgG3 and IgG1 antibodies were synthesized (II.2.1) with an N-terminal LPH signal sequence for targeting the secretory pathway [215] and a C-terminal SEKDEL sequence for retention in the ER [218]. Additional vectors for antibody expression in the apoplast, vacuole and plastids were generated from these vectors by deleting the SEKDEL sequence (targeting to the apoplast) and replacing the SEKDEL sequence with a KISIA signal sequence (targeting to the vacuole [219]) or replacing the LPH leader peptide with the rbcS signal sequence (plastid-targeting) using PCR primers with overhangs (Supporting Table 1) in

combination with restriction enzymes (II.2.3) and Gibson assembly (II.2.6). Domain exchange variants were generated by amplifying IgG1 domains from the initial construct for IgG1 expression by PCR (Supporting Table 1) and introducing the PCR products into the constructs for IgG3 expression in different compartments by Gibson assembly (II.2.6). The identity of the resulting constructs was confirmed by sequencing (Fraunhofer IME sequencing service) using the primers 35SS_FI and 35SS_PARI (Supporting Table 1). Gibson assembly reactions were conducted in pMA/K vectors to avoid interference of the matrix attachment regions flanking the expression cassette in pTRAc vectors (II.2.7).

II.2.9 Cloning automation

II.2.9.1 PCR cleanup with ultrafiltration plates

II.2.9.1.1 Removal of DNA polymerase

Removal of DNA polymerase from PCR reactions was investigated with 100 kDa AcroPrep filter plates (Pall, Dreieich, Germany), using 5 units Q5 polymerase in 50 μ L Q5 reaction buffer (both from New England Biolabs) and a centrifugal force of $1000 \times g$ (Rotina 380R, Hettich, Kirchling, Germany) for 10 minutes at 22°C. Polymerase that was retained by the membrane was resuspended in 50 μ L Q5 reaction buffer.

Inactivation of Q5 polymerase was investigated by adding 0.001 – 1.000 mg L⁻¹ proteinase K to 5 units Q5 polymerase in 10 μ L polymerase buffer, followed by incubation at 50°C for 20 minutes. Residual polymerase activity was subsequently assessed in a PCR reaction using the template vector pTRAc_000006 (Supporting Table 2) and primers 35SS_FI and 35SS_PARI (Supporting Table 1).

Inactivation of proteinase K before restriction cloning was investigated by adding 0.2 mg L⁻¹ proteinase K to 10 μ L polymerase buffer containing 200 ng vector pTRAc_000006 (Supporting Table 2) followed by incubation at 90°C for 10 or 20 minutes. Residual proteinase activity was investigated by adding CutSmart buffer and the restriction enzymes (1 U μ g_{DNA}⁻¹) AscI, BlnI and NotI (all from New England Biolabs) to the reaction mix, followed by incubation for 1 hour at 37°C.

II.2.9.1.2 Removal of primers, dNTPs and salt

Removal of primers, dNTPs and salt from PCR reactions was investigated with 30 kDa AcroPrep filter plates (Pall), using 40 mM dNTPs, 20 mM magnesium chloride and 0.01 mM 35SS_PARI (Supporting Table 1) in a total volume of 50 μ L nuclease free water and a centrifugal force of $1000 \times g$ (Rotina 380R, Hettich) for 10 minutes at 22°C. Components

retained by the membrane were resuspended in 50 μL nuclease free water. The concentration of magnesium chloride in retentates and permeates was quantified by freezing point osmometry using an Osmomat 3000 (Gonotec, Berlin, Germany). Primer and dNTP concentrations were quantified with a NanoDrop 2000 spectral photometer (Thermo Fisher Scientific).

II.2.9.2 Separation of DNA fragments with ultrafiltration plates

For separation of different DNA fragments, size-dependent precipitation with PEG was combined with ultrafiltration membranes to split precipitated and soluble DNA.

First, Acropep 0.2 μm PTFE filter plates (Pall) were sanitized and pre-wet with 175 μL of 70% (v v^{-1}) ethanol followed by centrifugation at $2000 \times g$ (Rotina 380R, Hettich) for 2 minutes. After pre-wetting, membranes were washed with 100 μL nuclease free water and 100 μL of the respective buffer using the same settings.

For separation experiments 1.0 μg digested DNA was mixed with 20% PEG-6000 and 2.0 M sodium chloride to a final concentration of 6.3 % (m v^{-1}) PEG and 0.9 M sodium chloride [220] in a final volume of 50 μL (final DNA concentration of 20 mg L^{-1}). The PEG-DNA mixture was transferred into AcroPrep 0.2 μm filter plates and soluble and precipitated DNA were separated by centrifugation at $1000 \times g$ (Rotina 380R, Hettich) for 10 minutes. Precipitated DNA that was retained by the filter plates was re-solubilized in 50 μL TRIS buffer (VII.6). Remaining PEG was removed by filtration with 30 kDa membranes as described for the removal of primers, dNTPs and salt (II.2.9.1.2).

II.2.9.3 Optimization of size-dependent DNA precipitation

Optimization of size-dependent DNA precipitation with PEG was investigated by mixing 0.5 μg digested DNA with Sera-Mag Select reagent (Cytiva, Uppsala, Sweden) and nuclease free water to final concentration of 30 – 70% (v v^{-1}) in a total volume of 20 μL (final concentration of 25 mg L^{-1} DNA). Samples were incubated for 10 minutes at 22°C before precipitating the carboxylate-modified, magnetic beads in a magnetic rack, removal of the supernatant and washing with 70% (v v^{-1}) ethanol. Residual ethanol was removed by incubation at 40°C for 10 minutes. Precipitated DNA (bound to the beads) was resolubilized by incubation in 20 μL TRIS buffer (VII.6) for 15 minutes at 40°C. Sera-Mag Select reagent was brought to room temperature on a rotary shaker for 30 minutes before experiments.

II.2.9.4 Automation on a liquid handling station

Automated cloning protocols were carried out on a Vantage liquid handling station (Hamilton, Bonaduz, Swiss), using 4titude 96-well PCR plates (Brooks Life Sciences, Chelmsford, USA), 50 μL and 300 μL pipetting tips, and an on-deck thermal cycler (Hamilton). Enzymes and

template vectors for automated protocols were supplied in 96-well PCR plates (pre-dispensed and stored at -20°C until needed).

Restriction reactions (II.2.3) were prepared in a total volume of $50\text{ }\mu\text{L well}^{-1}$, by dispensing nuclease-free water, CutSmart buffer, restriction enzymes and template DNA into 96-well PCR plates, followed by incubation at 37°C for 1 hour. Reactions providing vector backbones were additionally supplemented with alkaline phosphatase to prevent re-ligation.

For separation of DNA fragments (II.2.9.2), sodium chloride, PEG and nuclease-free water were dispensed into $0.2\text{ }\mu\text{m}$ filter plates and mixed (3 pipetting cycles) with the restriction products to a total volume of $100\text{ }\mu\text{L well}^{-1}$ and subjected to centrifugation at $1000\times g$ in a HiG5000 centrifuge (GC biotech, Cambridge, UK) for 10 minutes. Because the labware gripper can only carry two plates simultaneously, filter plates and 96-well plates for separation of DNA fragments (II.2.9.2) were stacked sequentially into the HiG5000 centrifuge. After centrifugation, vector backbones were resuspended (in nuclease-free water) from the $0.2\text{ }\mu\text{m}$ filter plates, whereas inserts were resuspended from the 30 kDa membranes.

For ligation (II.2.5), vector backbones and inserts were re-combined in a new 96-well PCR plate, using the same workflow described for restriction.

II.3 Bacterial cultivation and recombinant expression

II.3.1 *Escherichia coli*

E. coli DH5 α (Thermo Fisher Scientific) was used for cloning and *E. coli* 10-beta (New England Biolabs) served as (non-T7 based) expression host for comparison of target proteins that were produced in *E. coli* and in plants.

II.3.1.1 Preparation of chemically competent *E. coli*

For preparation of chemically competent *E. coli*, 5.0 mL lysogeny broth (LB) pre-cultures were inoculated from *E. coli* glycerol stocks and incubated overnight (16 hours) at 37°C and 160 rpm. Main cultures (50 mL LB medium in 0.5 L baffled flasks) were inoculated with a 1:100 ratio (v v^{-1}) of the pre-cultures and incubated similarly until reaching an $\text{OD}_{600\text{nm}}$ of 0.4 – 0.6. Cells were harvested by centrifugation at $3220\times g$ (5810 R, Eppendorf, Hamburg, Germany) for 10 minutes at 4°C , resuspended in 10 mL cold (4°C) 100 mM magnesium chloride and incubated for 30 minutes on ice. After a second centrifugation cycle using the same conditions, cells were resuspended in 1.0 mL cold (4°C) 100 mM calcium chloride containing 15% (v v^{-1}) glycerol. Aliquots (50 μL) were prepared in pre-chilled (4°C) 1.5 mL reaction tubes and stored at -80°C until needed.

II.3.1.2 Transformation of *E. coli*

Chemically competent *E. coli* were transformed by mixing ~100 ng plasmid DNA, 10.0 μL ligation mix (II.2.5) or 5.0 μL Gibson assembly mix (II.2.6) with 50 μL competent cells (II.3.1.1). The cell suspension was incubated on ice for 30 minutes, subjected to a 30 second heat shock at 42°C and immediately transferred onto ice again. Cells were regenerated by adding 1.0 mL LB medium (VII.7) followed by incubation at 37°C and 160 rpm for 1 hour. After regeneration, the cell suspension (50 μL plate⁻¹) was plated onto LB agar plates (VII.7) supplemented with 100 mg L⁻¹ ampicillin or 50 mg L⁻¹ kanamycin. Plates were incubated at 37°C overnight (16 hours) before picking single clones for preparation of LB master plates supplemented with the same antibiotics.

II.3.1.3 Preparation of *E. coli* glycerol stocks

For preparation of glycerol stocks, 5.0 mL LB cultures containing 100 mg L⁻¹ ampicillin were inoculated from master plates (II.3.1.2) and incubated overnight (16 hours) at 37°C and 160 rpm. Cultures were adjusted to an OD_{600nm} of 2.0 using the same medium and mixed with 50% (v v⁻¹) sterile glycerol in a 1:1 ratio (final OD_{600nm} of 1.0). Aliquots (1.0 mL) were prepared in Nalgene cryogenic vials (Merck, Darmstadt, Germany) and stored at -80°C.

II.3.1.4 *SacB* negative selection with *E. coli*

For *SacB* negative selection, 50 μL chemically competent *E. coli* DH5 α (II.3.1.1) were transformed with ~100 ng pTRAc_000431 (Supporting Table 2) as described above (II.3.1.2) and regenerated for 1.5 hours at 37°C and 160 rpm in 1.0 mL LB medium (VII.7), which was optionally supplemented with 100 g L⁻¹ sucrose. The cell suspension (50 μL plate⁻¹) was then plated on LB agar plates containing 50 g L⁻¹ sucrose or used to inoculate 5.0 mL LB liquid cultures containing 100 g L⁻¹ sucrose. Plates were incubated at 37°C for 16 hours in the dark. Liquid cultures were incubated at the same conditions at 160 rpm. Sodium chloride was omitted from LB medium for negative selection with *SacB* (VII.7). Ampicillin was added during all steps except regeneration at a concentration of 50 mg L⁻¹.

II.3.1.5 Recombinant protein expression in *E. coli*

Model proteins were produced in *E. coli* as controls for their plant-made counterparts, using a pASK-IBA33plus expression vector. Pre-cultures and main cultures were prepared as described for the preparation of competent cells (II.3.1.1), using 50 mg L⁻¹ ampicillin to maintain selective pressure. After reaching an OD_{600nm} of 0.2 – 0.4, expression was induced by adding

anhydrotetracycline hydrochloride (Merck) to a final concentration of 200 $\mu\text{g L}^{-1}$, followed by incubation overnight (16 hours) at 28°C (temperature during expression) and 160 rpm.

II.3.2 *Agrobacterium tumefaciens* (*Rhizobium radiobacter*)

A. tumefaciens GV3101:pMP90RK was used for transient expression and cultivation studies.

II.3.2.1 Preparation of competent *A. tumefaciens*

II.3.2.1.1 Electrocompetent *A. tumefaciens*

For preparation of electrocompetent *A. tumefaciens*, 5.0 mL YEB (VII.7) pre-cultures (supplemented with 25 mg L^{-1} kanamycin and rifampicin) were inoculated from *A. tumefaciens* glycerol stocks and incubated overnight (16 hours) at 28°C and 160 rpm. Main cultures (50 mL YEB medium in 500 mL baffled flasks) supplemented with the same antibiotics and concentrations were inoculated with 50 μL of the pre-cultures and incubated similarly for 24 hours until reaching an $\text{OD}_{600\text{nm}}$ of ~ 5.0 . Cells were harvested by centrifugation at $3220 \times g$ (5810 R, Eppendorf) for 10 minutes at 4°C, washed twice with cold (4°C) deionized water and once with cold (4°C) 10% (v v⁻¹) glycerol before resuspension in 3 mL 10% (v v⁻¹) glycerol. Aliquots (50 μL) were prepared in chilled (4°C) 1.5 mL reaction tubes and stored at -80°C.

II.3.2.1.2 Chemically competent *A. tumefaciens*

For preparation of chemically competent cells, *A. tumefaciens* main cultures were inoculated as described for electrocompetent cells and harvested after reaching an $\text{OD}_{600\text{nm}}$ of 0.5 – 0.8 by centrifugation at $3220 \times g$ (5810 R, Eppendorf) for 10 minutes at 4°C. Cells were washed with 5.0 mL cold (4°C) 20 mM calcium chloride and resuspended in 1.0 mL cold (4°C) 20 mM calcium chloride [221]. Aliquots were prepared as described for electrocompetent cells and stored at -80°C until needed.

II.3.2.2 Transformation of *A. tumefaciens*

II.3.2.2.1 Transformation of electrocompetent *A. tumefaciens*

Electrocompetent *A. tumefaciens* were transformed by mixing ~ 500 ng plasmid DNA or 10.0 μL ligation mix (II.2.5) with 50 μL competent cells (II.3.2.1). The cell suspension was transferred into chilled (4°C) 0.2 cm electroporation cuvettes (Bio-Rad) and subjected to electroporation at 2400 V, 25 μF and 200 Ω [221]. Cells were regenerated by adding 0.5 mL YEB medium (VII.7) followed by incubation at 28°C and 160 rpm for 2.5 hours. After regeneration, the cell suspension (10 $\mu\text{L plate}^{-1}$) was plated onto PAM4 agar plates (VII.7) supplemented with 25 mg L^{-1} rifampicin, 25 mg L^{-1} kanamycin and 50 mg L^{-1} carbenicillin.

Plates were incubated at 28°C for 72 hours before picking single clones for preparation of PAM4 master plates supplemented with the same antibiotics.

II.3.2.2.2 Transformation of chemically competent *A. tumefaciens*

Chemically competent *A. tumefaciens* were transformed by mixing ~500 ng plasmid DNA or 10.0 µL ligation mix (II.2.5) with 50 µL competent cells (II.3.2.1) followed by freezing in dry ice and ethanol for 5 minutes [221]. Cells were thawed by incubation at 37°C for 5 minutes and regenerated and plated as described for electrocompetent cells.

II.3.2.3 Preparation of *A. tumefaciens* glycerol stocks

For preparation of glycerol stocks, 5.0 mL PAM4 cultures containing 25 µg mL⁻¹ rifampicin, 25 µg mL⁻¹ kanamycin and 50 µg mL⁻¹ carbenicillin were inoculated from master plates (II.3.2.2) and incubated for 24 hours at 28°C and 160 rpm. Cultures were adjusted to an OD_{600nm} of 2.0 using the same medium and mixed with 50% (v v⁻¹) sterile glycerol in a 1:1 ratio (final OD_{600nm} of 1.0). Aliquots were prepared as described for *E. coli* (II.3.1.3).

II.3.2.4 SacB negative selection with *A. tumefaciens*

For SacB negative selection 50 µL aliquots of competent *A. tumefaciens* (II.3.2.1) were transformed with ~100 ng pTRAc_000431 (Supporting Table 2) as described above (II.3.2.2) and regenerated for 4.5 hours at 28°C and 160 rpm in 1.0 mL PAM4 medium (VII.7), which was optionally supplemented with 100 g L⁻¹ sucrose. The cell suspension (25 µL plate⁻¹) was then plated on PAM4 plates or used to inoculate 5.0 mL PAM4 liquid cultures, both containing 100 g L⁻¹ sucrose. Plates were incubated at 28°C for 80 hours in the dark. Liquid cultures were incubated for 100 h at the same conditions at 160 rpm. During all steps except regeneration kanamycin and rifampicin were added at a concentration of 25 mg L⁻¹ and carbenicillin was added at a concentration of 100 mg L⁻¹. Antibiotics were re-added in liquid cultures to 25 mg L⁻¹ (kanamycin, rifampicin) and 50 mg L⁻¹ (carbenicillin) after 48 hours.

II.3.2.5 Limiting dilution cloning with *A. tumefaciens*

For limiting dilution cloning 10 µL ligation mix containing ~500 ng backbone DNA and a threefold molar excess of insert DNA were mixed with 50 µL chemically competent *A. tumefaciens* (II.3.2.1) and subjected to a single round of freeze-thaw cycling (II.3.2.2.2). Cells were regenerated by adding 0.5 mL PAM4 medium (VII.7) followed by incubation at 28°C and 160 rpm for 3 hours (in 2 mL 96-well plates) before harvesting cells by centrifugation at 3220 × g (5810 R, Eppendorf) for 5 minutes. After removing the supernatant cells were resuspended in PAM4 medium supplemented with 25 mg L⁻¹ rifampicin, 25 mg L⁻¹ kanamycin

and 100 mg L⁻¹ carbenicillin. The cell suspension was then subjected to a two-fold serial dilution in 96-well plates using the same medium (final cultivation volume of 100 µL) and incubated at 28°C and 160 rpm for 96 hours in the dark. Antibiotics were re-added to 25 mg L⁻¹ (kanamycin, rifampicin) and 50 mg L⁻¹ (carbenicillin) after 48 hours of incubation.

II.3.2.6 Small scale *A. tumefaciens* cultures for infiltration of PCPs

For infiltration of PCPs, 0.5 mL well⁻¹ PAM4 cultures in 2.0 mL deep well plates (Ritter, Schwabmünchen, Germany) were inoculated with 20 µL well⁻¹ *A. tumefaciens* glycerol stock (II.3.2.3) and incubated on a rotary shaker at 30°C and 1000 rpm for 24 hours, using an automated protocol for cultivation and sub-cultivation [151]. Cultures were subjected to a single round of sub-cultivation, using an inoculation OD_{600nm} of 0.1 and the same cultivation conditions as above. Plates were sealed with gas permeable membranes with a vapor transmission rate of 4200 g m² d⁻¹ (Macherey-Nagel), mounted on a custom sealing lid [151]. Rifampicin, kanamycin (25 mg L⁻¹) and carbenicillin (50 mg L⁻¹) were added during all cultivation steps.

II.3.2.7 Large scale *A. tumefaciens* cultures for infiltration of whole plants

For infiltration of whole plants, 15 mL PAM4 (VII.7) pre-cultures in 50 mL shake flasks (Schott, Mainz, Germany) were inoculated with 0.6 mL *A. tumefaciens* glycerol stock (II.3.2.3) and incubated on a rotary shaker at 28°C and 160 rpm for 24 hours. Next, 0.5 L PAM4 main cultures in 2.5 L Thomson Ultra Yield flasks (VWR) were inoculated from the pre-cultures to an OD_{600nm} of 0.1, using the same cultivation conditions. Rifampicin, kanamycin (25 mg L⁻¹) and carbenicillin (50 mg L⁻¹) were added during all cultivation steps. The typical harvest OD_{600nm} of *A. tumefaciens* cultures for infiltration of plants was between 6.0 and 9.0.

II.3.3 *Staphylococcus aureus*

S. aureus Rosenbach 1884 was used for all biofilm degradation assays. First, a 5 mL terrific broth (TB, VII.7) pre-culture was inoculated with 50 µL *S. aureus* glycerol stock and incubated at 160 rpm at 37°C for 16 hours. Cells were harvested by centrifugation in an aerosol-tight rotor at 4000 × g for 5 minutes at 22°C, resuspended in MSgg medium (VII.7) and adjusted to an OD_{600nm} of 0.1 using the same medium. For formation of static biofilms, 200 µL well⁻¹ of the cell suspension was pipetted into sterile Cellstar 96-well plates (Greiner BioOne, Kremsmünster, Austria). Plates were sealed with gas-permeable membranes with a vapor transmission rate of 700 g m⁻² d⁻¹ (Merck) and incubated for 24 hours at 37°C without agitation.

Blanks (200 μL well⁻¹ MSgg) were incubated similarly. Supernatants were removed from biofilms and blanks before enzymatic treatment.

II.4 Plant cultivation and recombinant expression

II.4.1 BY-2 cells

N. tabacum cv. Bright Yellow 2 (BY-2) cells were used for all expression studies in PCPs and cultivated either in shake flasks (II.4.1.1) or stirred tank bioreactors (II.4.1.2).

II.4.1.1 Cultivation of BY-2 cells in shake flasks

Shake flask BY-2 cultivations were conducted in 0.25 L glass flasks (Schott, Mainz, Germany) containing 0.05 L medium for routine cultivations or in 0.10 L glass flasks containing 0.02 L medium for cultivation in a LEDitSHAKE device [222]. Routine cultivations were conducted under artificial white light (Osram Lumilux Cool White, HO 49W/840), whereas the LEDitShake device was used to test exposure to defined light wavelengths. MS medium (VII.7) containing 30 g L⁻¹ sucrose or 30 g L⁻¹ glucose as carbon source was used for all shake flask cultures. Shake flasks were inoculated with a seeding cell density of 2×10^8 cells L⁻¹ and cultivated at 160 rpm (50 mm eccentricity) and 26°C for 5 – 8 days in a Climo-Shaker ISF1-X (Kuhner, Birsfelden, Germany). The relative humidity was ~50%. BY-2 cultures were passaged after 7 days using the same seeding cell density.

II.4.1.2 Cultivation of BY-2 cells in stirred tank bioreactors

Stirred tank BY-2 cultivations were conducted in fed-batch mode [223], using a 5.0 L double-walled glass bioreactors (Applikon, Schiedam, Netherlands) for 20 – 60 days. MS medium (VII.7) containing 30 g L⁻¹ sucrose was used for the batch phase. The carbon source was replaced with 20 g L⁻¹ sucrose or 20 g L⁻¹ glucose in the feed for the fed-batch phase. Optionally, a modified feed composed of twofold concentrated MS medium (VII.7) supplemented with 40 g L⁻¹ sucrose was used for the fed-batch phase. For all stirred tank cultivations, the medium was supplemented with 0.01% (v v⁻¹) Pluronic L61 (BASF, Burgbernheim, Germany) to reduce foaming and wall growth [224]. Stirred tanks were inoculated with 20 g L⁻¹ BY-2 cells from 7 days old shake flask cultures (II.4.1) and incubated at 26°C (P = 10, I = 2,700, D = 0), using a dissolved oxygen tension (DOT) set point of 20%, which was maintained through a 100 – 160 rpm stirrer cascade (P = 20, I = 150, D = 6); the DOT is equivalent to the oxygen partial pressure. The temperature and DOT were maintained through a Proportional-Integral-Derivative (PID) controller. The effects of the individual constants on the controller output are described through Equation 3.

The fed-batch phase was started after reaching a BY-2 wet cell mass of 100 g L⁻¹, corresponding to a packed cell volume of 30 – 40% (v v⁻¹). The feed (VII.7) was controlled through a 12 × 320 mm capacity sensor (Aber instruments, Aberystwyth, UK) coupled to a Futura head amplifier and transmitter (Aber instruments, Aberystwyth, UK) to maintain a BY-2 wet cell mass of 95 – 105 g L⁻¹ (P = 5, I = 0, D = 0). The aeration rate was 1.0 L min⁻¹ (air) corresponding to 0.25 vvm in a filled tank (4.0 L) and 0.4 vvm after harvesting (2.5 L). The DOT was measured with a 12 × 235 mm Z010023525 dissolved oxygen sensor and the pH (not controlled) was measured with a 12 × 235 mm Z001023551 pH sensor (both from Applikon). All stirred tanks were controlled with an EZ-Control Unit (Applikon).

$$C_{out} = K_P e(t) + K_I \int_0^t e(\tau) d\tau + K_D \frac{d}{dt} e(t) \quad \text{Equation 3}$$

Where C_{out} represents the control signal, e represents the difference between the measured process variable and the desired setpoint (the control error), K_P is the proportional gain, K_I is the integral gain and K_D is the derivative gain.

II.4.1.3 Characterization of BY-2 cell cultures

The BY-2 wet cell mass was measured by removing the cultivation medium from 10 mL cell suspension with a PC600 suction pump, using 11.0 µm Whatman filter papers (Cytiva, Uppsala, Sweden) and applying an 80 kPa vacuum for 15 seconds. Cultures were agitated before measurements to prevent sedimentation. The BY-2 dry cell was measured by drying the wet cell mass obtained as described above at 65°C for 5 days.

The fraction of dead BY-2 cells was determined by mixing 1.0 mL cell suspension with 50.0 µL tryptophan blue (VII.5) before adding the cell suspension into a Fuchs-Rosenthal chamber. For cell counting 5 large squares (each corresponding to 4 × 4 small squares) were counted diagonally through the chamber (4 squares on the diagonal, 1 square next to the diagonal) using a trinocular microscope (BMS, Breukhoven, Netherlands) equipped with a 40 × objective and a 10 × eye piece. Cells with a damaged cell wall appeared blue after addition of tryptophan blue, whereas cells with an intact membrane excluded the dye.

For osmolality measurements, the cultivation medium was removed from 10 mL BY-2 cell suspension as described for the wet cell mass. The osmolality of the cell-free supernatant was then measured by freezing point osmometry using an Osmomat 3000 (Gonotec) and 0.0 mM and 500.0 mM glucose standards for calibration.

II.4.1.4 Transient expression in BY-2 PCPs

II.4.1.4.1 PCP casting

PCPs were cast manually from BY-2 cells, because a previously established automated protocol for PCP casting [151] was not compatible with multiple different BY-2 cultures. For generation of PCPs, BY-2 suspension cultures were concentrated to a wet cell mass of 200 g L⁻¹ by sedimentation (1 × g, 30 minutes), followed by decanting the supernatant. To obtain PCPs with a wet cell mass of 60 mg, 300 µL well⁻¹ of the BY-2 cell suspension was pipetted into 96-well AcroPrep Advance filter plates with a pore size of 30 – 40 µm (Pall) using wide bore tips (Ratiolab, Dreieich, Germany), followed by centrifugation at 1800 × g (Rotina 380R, Hettich) for 1 minute to remove the cultivation medium. If the wet cell mass was > 200 g L⁻¹, the volume of BY-2 suspension for PCP casting was reduced instead of diluting the cell suspension with fresh MS medium, which would compromise harvest time point experiments.

II.4.1.4.2 Infiltration

Infiltration of BY-2 PCPs with *A. tumefaciens* was conducted with an automated protocol [151]. Briefly, *A. tumefaciens* cultures from 96-well plates (II.3.2.6) were harvested by centrifugation at 3800 × g (Rotina 380R, Hettich) for 5 minutes, followed by removal of the cultivation supernatant and re-suspension in infiltration buffer (VII.6). For PCP infiltration, the *Agrobacterium* cell suspension was adjusted to an OD_{600nm} of 0.4 with the same infiltration buffer and induced for 1 hour at 28°C and 160 rpm. PCPs were infiltrated by adding 100 µL PCP⁻¹ of the *Agrobacterium* cell suspension, followed by incubation for 1 hour at 22°C. The infiltration solution was removed by centrifugation at 1800 × g (Rotina 380R, Hettich) for 1 minute. Infiltrated PCPs were incubated at 26°C and 80% relative humidity for 48 – 96 hours over a water reservoir [151].

II.4.2 Differentiated plants

N. benthamiana and *N. tabacum* cv. K326 plants were used for all expression studies in differentiated plants. Both species were cultivated in a phytotron for 7 weeks (II.4.2.1).

II.4.2.1 Cultivation of differentiated plants in a phytotron

N. benthamiana and *N. tabacum* seeds were germinated on stone-wool blocks (Cultilene, Tilburg, Netherlands) for 7 days and then transferred to a phytotron for cultivation at 25/22°C (day/night), 70% relative humidity and a 16-hour photo period. Plants were illuminated with red (285 µmol m⁻² s⁻¹, 660 nm peak) and blue (39 µmol m⁻² s⁻¹, 450 nm peak) light wavelengths using 120 cm GreenPower LED modules (Philips, Amsterdam, Netherlands). Plants were irrigated for 15 minutes per hour with the nutrient film technique [100], using 0.12 m wide

polypropylene gullies and a $\sim 0.8 \text{ g L}^{-1}$ Ferty 2 Mega solution (Planta Düngemittel, Regenstauf, Germany) corresponding to a conductivity of 1.2 mS cm^{-1} . The concentration of Ferty 2 Mega was increased to 1.4 mS cm^{-1} after 2 weeks of cultivation and to 1.6 mS cm^{-1} after 4 weeks of cultivation.

II.4.2.2 Transient expression in differentiated plants

II.4.2.2.1 Infiltration

For infiltration of differentiated plants, 5.0 L infiltration solution with an $\text{OD}_{600\text{nm}}$ of 0.5 were prepared from *A. tumefaciens* cultures (II.3.2.7) by dilution with twofold concentrated plant infiltration buffer (VII.6) and deionized water. The cell suspension was induced for 1 hour at room temperature and 100 rpm. The stem and leaves of *N. benthamiana* or *N. tabacum* plants were carefully submerged in the cell suspension using a 5.0 L bucket placed in a desiccator before applying a $\sim 10 \text{ kPa}$ vacuum for 2 minutes, which was released instantaneously. Before infiltration, all plants were thoroughly watered for 1 hour.

II.4.2.2.2 Incubation after infiltration

After infiltration with *A. tumefaciens* (II.4.2.2.1), *N. benthamiana* and *N. tabacum* plants were incubated in foil-covered incubation racks in an inverted position for 5 days at $22.2 \pm 1.5^\circ\text{C}$ and constant illumination (24 hours day^{-1}). Plants were illuminated with a total light intensity of $\sim 50 \mu\text{mol s}^{-1} \text{ m}^{-2}$ using 8 Lumilux 58W/830 warm white and 8 Lumilux 58W/840 cool white fluorescent tubes (Osram, Munich, Germany). Plants were irrigated every 1.5 hours for 7.7 seconds using MRS-10122 nozzles (Micro Rain Systems, Altenburg, Germany) with a water flow rate of $149 \pm 5 \text{ mL min}^{-1}$ (30% relative humidity before irrigation and 80% relative humidity after each irrigation cycle).

II.5 Downstream processing

II.5.1 Extraction of *E. coli*

E. coli cultures (II.3.1.5) were harvested by centrifugation at $5000 \times g$ for 15 minutes at 4°C and resuspended in 10 mL cold (4°C) extraction buffer (VII.6) supplemented with 1.0 g L^{-1} lysozyme, 1.0 g L^{-1} DNase I, $1.0 \mu\text{M}$ PMSF and 100 mM magnesium chloride. After incubation for 15 minutes on ice, cells were extracted with a SonoPuls MS73 ultrasonic homogenizer (Bandelin, Berlin, Germany) for 3×90 seconds on ice, using 10 second pulses and an amplitude of 50%. Cell debris was removed by centrifugation at $13,000 \times g$ for 5 minutes at 4°C , followed by sterile filtration with a Sartopore Capsule with a retention rating of $0.2 \mu\text{m}$ (Sartorius-Stedim, Göttingen, Germany).

II.5.2 Extraction of BY-2 PCPs

II.5.2.1 Bead mill

PCPs were extracted with a 3 v m⁻¹ ratio of extraction buffer, which was optionally supplemented with detergents (VII.6), in a MM 300 bead mill (Retsch, Han, Germany). Briefly, PCPs and a single 3 mm chrome steal bead per PCP (Spherotech, Fulda, Germany) were transferred into Chromabond collection tubes (Macherey-Nagel), sealed with PTFE coated silicone mats and extracted for 2 × 3 minutes at 28 Hz. Plates were inverted after the first extraction cycle. Extracts were clarified by centrifugation at 5100 × g (Rotina 380R, Hettich) for 8 minutes at 4°C. Supernatants were stored at -20°C.

II.5.2.2 Infiltration-centrifugation

PCPs were cast as described above (II.4.1.4.1) using glucose as carbon source for BY-2 cultivation (II.4.1.1). PCPs were infiltrated with *A. tumefaciens* containing the vectors pTRAc_0000101 or pTRAc_000102 (Supporting Table 2) using an infiltration OD_{600nm} of 0.4. After 96 hours of incubation (II.4.1.4), PCPs were subjected to infiltration-centrifugation by adding 100 µL of the respective buffer (VII.6) per PCP, followed by application of a 10 kPa vacuum for 1 minute and incubation for 30 minutes at 22°C. Apoplastic fluid was subsequently collected by centrifugation at 1500 × g (Rotina 380R, Hettich) for 1 minute.

II.5.3 Extraction of differentiated plants

Differentiated plants were harvested by cutting shoots 3 – 4 cm above the stone-wool blocks. Whole plants including the stem were extracted with a 3 v m⁻¹ ratio of extraction buffer (VII.6) in a ProBlend 6 (Philips, Amsterdam, Netherlands) for 3 × 30 seconds with 30-second breaks between mixing cycles [128]. Extracts intended only for analysis were clarified by centrifugation (twice at 16,000 × g for 20 minutes at 4°C). Extracts intended for process development were clarified using a BP-410 bag filter (Fuhr, Klein-Winterheim, Germany) with a nominal retention rating of 1.0 µm and a 22 cm² PDH4 depth filter composed of K700 and KS50 filter layers (Pall) with ~10.0 and ~0.6 µm nominal retention ratings, respectively, using a flow rate of 12 mL minute⁻¹ [225]. As an alternative for PDH4, 17.3 cm² Sartopure GF Plus glass fiber filters (Sartorius-Stedim) with a nominal retention rating of 1.2 µm were tested for clarification, using a flow rate of 10 mL minute⁻¹. Before chromatography (II.5.5), clarified extracts were additionally passed through Sartopore Capsules with a retention rating of 0.2 µm (Sartorius-Stedim).

II.5.4 Ultrafiltration/diafiltration

All ultrafiltration/diafiltration (UF/DF) experiments were conducted with a Sartocoon Slice 200 bench-top system (Sartorius-Stedim). Regenerated cellulose membranes with a filter area of 200 cm² were used for all experiments (Sartorius-Stedim). The UF/DF purification process consisted of a 100 kDa ultrafiltration step for removal of host cell proteins and a 10 kDa (IL8) or 30 kDa (DspB) diafiltration step for removal of bulk water (Table 3). By default, 3 cycles of fourfold feed (II.5.3) concentration were conducted during the ultrafiltration step, using extraction buffer (VII.6) to restore the feed starting volume after each concentration cycle. All retentate and permeate fractions were kept on ice during the UF/DF process.

Table 3: UF/DF settings for purification of different target proteins.

Target protein	Ultrafiltration step				Diafiltration step	
	Initial volume [L]	Final volume [L]	TMP [kPa]	TFF [mL min ⁻¹]	TMP [kPa]	TFF [mL min ⁻¹]
IL6/8	0.20	0.05	200 (2.0 bar)	550	50 (0.5 bar)	550
DspB	0.50	0.50	50 (0.5 bar)	550	50 (0.5 bar)	550

TMP – transmembrane pressure, TFF – tangential flow rate.

Ultrafiltration membranes were regenerated by washing with extraction buffer (VII.6), 1.0 M sodium hydroxide and ultra-pure water, using a wash volume of 10 L m² (extraction buffer, sodium hydroxide) or 20 L m² (ultra-pure water) per membrane area. Membranes were stored in 20% (v v⁻¹) ethanol at 4°C.

II.5.5 Chromatography

High-throughput chromatography screening was carried out with a Janus G3 liquid handling station (PerkinElmer, Waltham, USA). Laboratory scale chromatography was carried out with an Äkta Pure FPLC system (Cytiva, Uppsala, Sweden). The Unicorn v6.4 software (Cytiva) was used to automate chromatography methods.

II.5.5.1 Immobilized metal affinity chromatography

High-throughput screening of IMAC conditions was conducted with 0.2 mL RoboColumns (Supporting Table 18) packed with Chelating Sepharose FF resin (Repligen, Weingarten, Germany). Resins were charged with nickel ions (VII.6) and equilibrated with 5 column volumes IMAC equilibration buffer (VII.6) before loading 10 column volumes 0.2 µm filtered extract (II.5.3). Columns were washed with 5 column volumes IMAC equilibration buffer

(VII.6) and 5 column volumes IMAC washing buffer containing 10 – 60 mM imidazole (VII.6) before eluting the target protein with 5 column volumes IMAC elution buffer (VII.6). The contact time was 2.0 minutes during all steps.

Laboratory scale experiments were conducted with prepacked 1.0 mL Chelating Sepharose FF columns (Cytiva) or an XK26/20 column (Kronlab, Dinslaken, Germany) packed with the same resin (Supporting Table 18). Resins were charged and equilibrated as described for RoboColumns before loading 10 or 50 column volumes 0.2 μm filtered (II.5.3) or UF/DF-purified extract (II.5.3). Washing and elution were conducted as described for RoboColumns, using 30 mM imidazole for the washing buffer (VII.6). A volumetric flow rate of 0.5 mL minute^{-1} (linear flow rate of 0.8 m hour^{-1}) was used during all steps when working with prepacked 1.0 mL columns, corresponding to a contact time of 2.0 minutes. For the 50 mL column a flow rate of 15 mL minute^{-1} (linear flow rate of 1.7 m hour^{-1}) was used, corresponding to a contact time of 3.3 minutes.

II.5.5.2 Protein G chromatography

Prepacked 1.0 mL HiTrap Protein G HP columns (Cytiva) were used for protein G chromatography (Supporting Table 18). Columns were equilibrated with 5 column volumes equilibration buffer (VII.6) before loading 100 column volumes 0.2 μm filtered extract (II.5.3). Columns were then washed with 5 column volumes equilibration buffer (VII.6) and 5 column volumes washing buffer (VII.6) before eluting the target protein with 5 column volumes elution buffer (VII.6). Elution fractions were immediately neutralized with 15% (v v⁻¹) neutralization buffer (VII.6). A volumetric flow rate of 0.5 mL minute^{-1} (linear flow rate of 0.8 m hour^{-1}) was used during all steps, corresponding to a contact time of 2.0 minutes.

II.6 Protein quantification and characterization

II.6.1 Bradford assay

The quantity of total soluble protein (TSP) in supernatants (II.5) was determined using the Bradford method [226]. Briefly, 5.0 μL sample or bovine serum albumin standards with concentrations of 0, 125, 250, 500, 750, 1000, 1500 and 2000 mg L^{-1} [227] were pipetted into flat-bottom 96-well plates (Sarstedt, Nümbrecht, Germany) and mixed with 195 μL Bradford reagent (Thermo Fisher Scientific). After incubation for 10 minutes at 22°C, the absorbance at 595 nm was measured using a Synergy H1 plate reader (Agilent, Frankfurt, Germany). The TSP concentration in samples was calculated based on a standard curve build from the serum albumin standards. Samples and standards were analyzed in triplicates.

II.6.2 Fluorescence spectroscopy

II.6.2.1 DsRed extract concentration

The quantity of DsRed in supernatants (II.5) was determined by fluorescence spectroscopy. Briefly, 50 μL sample or DsRed standards with concentrations of 0, 5, 15, 25, 75, 125, 175 and 225 mg L^{-1} [144] were pipetted into black half-area 96-well plates (Greiner BioOne) and fluorescence was measured at an emission wavelength of 586 nm (excitation at 556 nm, automated read height and gain), using a Synergy H1 plate reader (Agilent). The DsRed concentration in samples was calculated based on a standard curve build from the DsRed standards. Samples and standards were analyzed in triplicates.

II.6.2.2 DsRed surface fluorescence

The surface fluorescence of BY-2 PCPs expressing DsRed was used as surrogate for the DsRed concentration in PCP extracts. The DsRed surface fluorescence was measured with the same device and settings used for quantification of DsRed in extracts (II.6.2.1), using a consistent read height (8.9 mm) and a constant gain value (52).

II.6.3 Surface plasmon resonance spectroscopy

A Sierra SPR2/4 (Bruker Daltonics SPR, Hamburg, Germany) and a Biacore T200 (Cytiva) were used for SPR experiments. High Capacity Amine sensors (Bruker) were used with the Sierra SPR 2/4, whereas CM5 sensors were used with the Biacore T200 (Cytiva). Assays were conducted at 25°C. All peptides used for SPR assays were synthesized by Thermo Fisher Scientific.

II.6.3.1 Quantification of His-tagged proteins

An indirect SPR assay format based on binding inhibition was used to quantify model proteins through their His₆-tag, using monoclonal anti-His antibody as ligand. Different peptide designs were tested to functionalize sensors with His₆ epitopes (Supporting Table 20), using ethyl-3-diaminopropyl-carbodiimide/N-hydroxysuccinimide (EDC/NHS) chemistry [228] for peptide coupling. Briefly, sensor surfaces were conditioned by alternating exposure to 30 mM hydrochloric acid and 25 mM sodium hydroxide, followed by activation with a mixture of 0.48 M EDC and 0.10 M NHS for 10 minutes and coupling with 500 μM peptide in coating buffer (VII.6) for 15 minutes. Excess reactive groups were deactivated by injection of 1.0 M ethanolamine for 10 minutes, followed by conditioning with 5 injections of regeneration buffer (VII.6). Reference surfaces were functionalized similarly, omitting the coupling of peptides. Functionalized sensors were stored in sterile PBS at 4°C.

Binding inhibition assays were conducted by diluting supernatants (II.5) in PBS-T running buffer (VII.6) until they were in the range of the calibration curve (0.4 – 100.0 nM His-tagged peptide in PBS-T), typically 1:40 or 1:80, before mixing 50 μL sample or standard with 50 μL of 20 nM MonoRab anti-His antibody (GenScript, Piscataway, USA), prepared in the same buffer. After incubation for 1 hour on a rotary shaker at 22°C, samples were injected over peptide-coated sensors for 3 minutes at a flow rate of 10 $\mu\text{L minute}^{-1}$ to capture antibody molecules with unoccupied binding sites. The quantity of His-tagged protein in a sample was calculated based on the relative binding inhibition measured with His-tagged standards using a Boltzmann function (Equation 4). Sensors were regenerated with a 30 second injection of regeneration buffer (VII.6), using a flow rate of 30 $\mu\text{L minute}^{-1}$.

$$y = \frac{A_1 - A_2}{1 + e^{-\frac{x - x_0}{dx}}} + A_2 \quad \text{Equation 4}$$

Where y (in %) is the inhibition (dependent variable), x (in nM) is the analyte concentration (independent variable), A_1 is the initial value (minimal inhibition in %), A_2 is the final value (maximal inhibition in %), x_0 is the center (in nM) and dx is the slope.

II.6.3.2 Quantification of IgG1 and IgG3 antibodies

A direct SPR assay format was used to quantify IgG1 or IgG3 antibodies with immobilized protein A/G. Sensors were functionalized as described for the coating of peptides (II.6.3.1), using 100 mg L^{-1} recombinant protein A (quantification of IgG1) or protein G (quantification of IgG3) produced in *E. coli* (Thermo Fisher Scientific). Typical protein A/G immobilization levels were ~ 5000 resonance units (RU).

Direct SPR assays were conducted by diluting supernatants (II.5) in HBS-EP running buffer (VII.6) until the signal was in the linear range of the calibration curve (0.0 – 2.0 mg L^{-1} 2G12 in HBS-EP), typically 1:40 or 1:80, before injection over protein A/G coated sensors for 3 minutes at a flow rate of 30 $\mu\text{L minute}^{-1}$. The quantity of IgG1 or IgG3 in a sample was calculated based on the resonance signal measured with 2G12 standards [229], using Equation 5. Measurements were corrected with the RU recorded with extracts from wildtype plants. Sensors were regenerated with a 30 second injection of 30 mM hydrochloric acid [230].

$$c_{\text{sample}} = \frac{RU_{\text{sample}} \times M_{\text{m, std}} \times \text{oligo}_{\text{std}}}{M_{\text{m, sample}} \times \text{oligo}_{\text{sample}}} \times \frac{c_{\text{std}}}{RU_{\text{std}}} \times \text{dil}_{\text{sample}} \xrightarrow{\text{monomer authentic std}} c_{\text{sample}} = RU_{\text{sample}} \times \frac{c_{\text{std}}}{RU_{\text{std}}} \quad \text{Equation 5}$$

Where RU_{sample} is the reference-corrected resonance signal of the sample, RU_{std} is the reference-corrected resonance signal of the 2G12 standard, $M_{\text{m, std}}$ and $M_{\text{m, sample}}$ are the molar masses of

the standard and sample, and $oligo_{std}$ and $oligo_{sample}$ describe the oligomerization state of standard and sample. The term $c_{std} RU_{std}^{-1}$ describes the slope that is obtained from a dilution series of standards with a known concentration (c_{std}), and dil_{sample} is the sample dilution factor.

II.6.3.3 Binding kinetics of IgG3 antibodies

Binding kinetics were measured with protein G-purified IgG3 (II.5.5.2) derived from the ER or apoplast and recombinant alpha toxin (antigen) produced in *E. coli* (Abcam, Cambridge, United Kingdom), using a Biacore T200 (Cytiva) and HBS-EP running buffer (VII.6). Briefly, IgG3 antibodies were captured on protein G-coated sensors (II.6.3.2) at a concentration of 7.35 mM (ER derived IgG3) or 10.62 mM (apoplast derived IgG3), followed by injection of 24 – 400,000 pM alpha toxin in HBS-EP. Alpha toxin was dialyzed against HBS-EP for 16 hours at 4°C to remove glycerol (20% v v⁻¹) from the formulation. After every antigen injection the sensor surface was regenerated as described for IgG3 quantification (II.6.3.2), followed by the next cycle of IgG3 capture and antigen injection. The association rate constant k_a and the dissociation rate constant k_d of the antibody-antigen complex were derived from the signal measured with different alpha toxin concentrations, using the Biacore T200 evaluation software. The equilibrium dissociation constant K_D was calculated from k_d and k_a using Equation 6.

$$K_D = \frac{k_d}{k_a} \quad \text{Equation 6}$$

II.6.4 Polyacrylamide gel electrophoresis

Precast 4 – 12 % (m v⁻¹) BIS-TRIS polyacrylamide gels (Thermo Fisher Scientific) were used for gel electrophoresis with MES running buffer (Thermo Fisher Scientific). Samples were prepared by mixing 26 µL supernatant (II.5) with 10 µL lithium dodecyl sulfate (LDS) Loading Buffer and 4 µL Reducing Agent (both from Thermo Fisher Scientific) followed by denaturation at 80°C for 10 minutes. Gels were loaded with 15 µL sample per lane and 5 µL PageRuler pre-stained protein standard (Thermo Fisher Scientific). Electrophoresis was performed in an X-Cell SureLock Mini-Cell (Thermo Fisher Scientific) at 200 V for 40 minutes.

II.6.4.1 Coomassie staining

Coomassie staining was performed at room temperature (22°C) subsequently to gel electrophoresis (II.6.4). Gels were washed twice in ultra-pure water for 5 minutes, stained with Simply Blue Safe Stain (Thermo Fisher Scientific) for 4 hours and de-stained in ultra-pure water overnight. All washing and incubation steps were conducted at 16 rpm using a rotary shaker. Gels were scanned at 600 dpi using a Canon 5600 scanner (Canon, Krefeld, Germany).

II.6.4.2 Silver staining

Silver staining was performed at room temperature (22°C) subsequently to gel electrophoresis (II.6.4), using a custom protocol. Gels were fixated in solution I (VII.6) for 1 hour, washed twice with solution II for 20 minutes (VII.6) and incubated in solution III (VII.6) for 1 minute. After washing (twice) in ultra-pure water for 1 minute, gels were incubated in solution IV (VII.6) for 20 minutes and developed in solution V (VII.6). The reaction was stopped by addition of solution VI (VII.6). All washing and incubation steps were conducted at 16 rpm using a rotary shaker. Gels were scanned as described for Coomassie gels (II.6.4.1).

II.6.4.3 Western blotting

After separation by gel electrophoresis (II.6.4) samples were transferred onto nitrocellulose membranes (Merck) in an X-Cell II Blot Module (Thermo Fisher Scientific) or a Trans-Blot Cell (Bio-Rad) at 30 V for 1 hour in blotting buffer (VII.6). After blocking with 5% (w v⁻¹) milk powder in PBS-T (VII.6), proteins were specifically detected with primary and (optionally) secondary antibodies (Table 4), using an incubation time of 1 hour for each antibody. Membranes were washed 3 times for 5 minutes in PBS-T after each incubation step. Secondary antibodies were conjugated with alkaline phosphatase (AP), which was used for colorimetric protein detection with a mixture of 0.30 g L⁻¹ nitroblue tetrazolium (NBT) and 0.15 g L⁻¹ 5-bromo-4-chloro-3-indolyl phosphate (BCIP) as substrate. All washing and incubation steps were conducted at 16 rpm. Blots were dried and scanned as described for Coomassie gels (II.6.4.1).

Table 4: Overview of antibody combinations used for target protein detection on western blots.

Target protein or domain	Primary antibody	Concentration [mg L ⁻¹]	Secondary antibody	Concentration [mg L ⁻¹]
His ₆	Rabbit anti-His ₆ (GenScript A00174)	0.10	Goat anti-rabbit IgG AP (Jackson 111-045-045)	0.06
DsRed	Goat anti-mCherry (Thermo Fisher TA150126)	0.20	Rabbit anti-goat IgG AP (Jackson 305-055-046)	0.06
Human IgG (quantification)	Goat anti-human IgG (H+L) AP (Jackson 109-055-003)	0.12	n.a.	n.a.
IgG (detection)	Goat anti-human IgG (H+L) AP (Jackson 109-055-003)	0.12	n.a.	n.a.
	Goat anti-human Ig λ AP (Merck AP506A)	0.15		

Antibody solutions were prepared in 5% (w v⁻¹) milk powder in PBS-T (VII.6). AP – alkaline phosphatase, H – antibody heavy chain, L – antibody light chain, n.a. – not applicable.

II.6.5 Dot blot analysis

His₆-tagged model proteins were optionally quantified by dot blot analysis, using the same antibody pair used for detection of His₆-tagged proteins on western blots (II.6.4.3) and authentic purified model proteins as standards (II.5.5.1). Briefly, 5 µL supernatant (II.5) or authentic standards with concentrations of 0.5, 2.0, 4.0, 6.0, 8.0, 10.0, 12.5 and 15.0 mg L⁻¹ [174] in PBS (VII.6) were pipetted on nitrocellulose membranes (Merck). Membranes were air-dried for 5 minutes, blocked with 5% (w v⁻¹) milk powder in PBS-T (VII.6) and His₆-tagged proteins were specifically detected as described for western blots. The signal from the alkaline phosphatase color reaction was quantified by densitometric analysis.

II.6.6 PPK activity assay

The activity of recombinant PPKs produced in plants or *E. coli* was assessed in an enzymatic assay [231], using adenosine diphosphate (ADP) as substrate and hexametaphosphate (both from Merck) as phosphate donor. Briefly, 100 µL assay solution I (VII.6) and 700 µL assay solution II (VII.6) were heated to 37°C in a thermo shaker, omitting the addition of PPK in solution I and the addition of NAD⁺ in solution II. After equilibration for 2 minutes, assay solution I and assay solution II were mixed and the reaction was started by addition of purified PPK (II.5.5.1) and NAD⁺. The ADP consumption rate was measured indirectly through the phosphorylation of glucose to glucose-6-phosphate, catalyzed by hexokinase, and the oxidation of glucose-6-phosphate to 6-phosphogluconolactone, catalyzed by glucose-6-phosphate dehydrogenase [231]. The reduction of NAD⁺ to NADH in the latter reaction was monitored by measuring the absorbance at 340 nm for 1 hour in a spectrometer, using a quartz glass cuvette. The PPK activity was calculated from the change in absorbance over time using the Lambert-Beer law (Equation 7).

$$\Delta A = \varepsilon \cdot d \cdot \Delta c \quad \text{Equation 7}$$

Where ΔA is the change in absorbance, ε is the molar extinction coefficient ($\varepsilon_{\text{NADH } 340\text{nm}} = 6220 \text{ M}^{-1} \text{ cm}^{-1}$), d is the path length of the cuvette (in cm) and Δc is the change in concentration.

II.6.7 Biofilm degradation assay

The activity of recombinant DspB produced in plants or *E. coli* was assessed against authentic MRSA biofilms in an experimental biofilm assay [174]. Briefly, tenfold serial dilutions of 0.04 – 400.00 mg L⁻¹ purified DspB (II.5.5.1) were prepared in biofilm assay buffer (VII.6) and 200 µL well⁻¹ were added to preformed *S. aureus* biofilms in 96-well plates (II.3.3). After enzymatic treatment for 2 or 6 hours at 37°C without agitation, supernatants were discarded and plates

were washed twice with ultrapure water. Remaining biofilm was stained with 200 $\mu\text{L well}^{-1}$ 0.1% (m v^{-1}) crystal violet (Carl Roth, Karlsruhe, Germany) for 5 minutes at 22°C. After washing (twice) with ultrapure water and air drying for 10 minutes at 22°C, crystal violet was resolubilized by addition of 200 $\mu\text{L well}^{-1}$ acetic acid and incubation on a rotary shaker at 300 rpm for 10 minutes. Signals were readout at 595 nm using a Synergy H1 plate reader (Agilent). The activity of DspB was calculated by fitting the enzyme concentration and remaining biofilm (compared to untreated controls) with a dose response function (Equation 8).

$$y = A_1 + \frac{A_2 - A_1}{1 + 10^{(\log x_0 - x)p}} \quad \text{Equation 8}$$

Where A_1 is the minimum biofilm signal (in % of the untreated control), A_2 is the maximum biofilm signal (in % of the untreated control), $\log x_0$ is the enzyme concentration at half-maximal response (IC_{50} in g L^{-1}) and p is the Hill slope (the slope of a tangent to the curve at half-maximal response).

II.7 Data evaluation and visualization

Advanced image data analyzer (AIDA) v5.1 (Raytest, Straubenhardt, Germany) and ImageJ v1.51j8 [232] were used for densitometric evaluation of LDS gels (II.6.4) and dot blots (II.6.5). Design Expert v13 (Stat-Ease, Minneapolis, USA) was used to set up and analyze statistical designs (II.7.1). OriginPro 2015 SR2 vb9.2.272 (OriginLab, Northampton, USA) was used to plot data and for statistical analysis (II.7.2).

II.7.1 Design of experiments

A statistical design of experiments (DoE) approach was used to establish predictive models that characterize the impact of the expression cassette design (II.7.1.1), BY-2 cultivation conditions (II.7.1.2) or exposure to light (II.7.1.3) on model protein accumulation or integrity (II.7.1.4). Significant model factors were preselected by automatic backwards selection from a quadratic base model, using a p-value threshold of 0.10. Factors with a p-value > 0.05 were manually removed. Exceptions were made to maintain model hierarchy if needed [90].

II.7.1.1 Expression models

The effect of the 5' UTR, target compartment and antibody scaffold on the accumulation of IgG3 in *N. benthamiana* and *N. tabacum* was investigated using historical response surface models with 122 runs (Table 5).

Table 5: Factors and factor ranges investigated for building an IgG3 expression model.

Factor	Level				
	1	2	3	4	5
5' UTR [-]	CHS	omega	TL	n.a.	n.a.
Target compartment [-]	Apoplast	ER (1 × LPH)	ER (2 × LPH)	Vacuole	Chloroplast
Antibody scaffold [-]	IgG3	IgG3 (IgG1 CH3)	IgG3 (IgG1 CH3/2)	n.a.	n.a.

n.a. – not applicable.

II.7.1.2 Harvest time model

The effect of the BY-2 cultivation time and PCP incubation time on the accumulation of DsRed in different cell compartments was investigated using a D-optimal response surface design with 92 runs, conducted in two blocks (Table 6).

Table 6: Factors and factor ranges investigated for building a BY-2/PCP harvest time model.

Factor	Level			
	1	2	3	4
BY-2 cultivation time [h]	120	144	168	192
PCP incubation time [h]	48	72	96	n.a.
Target compartment [-]	Apoplast	ER	Chloroplast	Cytosol

n.a. – not applicable.

II.7.1.3 Light exposure model

The effect of different light wavelengths, intensities and the duration of BY-2 light exposure on the accumulation of DsRed in different cell compartments was investigated using a D-optimal response surface-mixture design with 144 runs (Table 7).

Table 7: Factors and factor ranges investigated for building a BY-2 light exposure model.

Factor	Level			
	1	2	3	4
Light wavelength [-]	Far red	red	Green	Blue
Light intensity [$\mu\text{mol s}^{-1} \text{m}^{-2}$]	20	30	40	n.a.
Exposure time [weeks]	1	2	3	n.a.
Compartment [-]	Apoplast	ER	Chloroplast	Cytosol

n.a. – not applicable.

II.7.1.4 IgG integrity model

The effect of the 5' UTR, target compartment, IgG scaffold, BY-2 cultivation time and PCP incubation time on IgG integrity was investigated using an I-optimal split-plot response surface design with 216 runs (Table 8).

Table 8: Factors and factor ranges investigated for building an IgG integrity model.

Factor	Level			
	1	2	3	4
BY-2 cultivation time [h]	120	144	168	192
PCP incubation time [h]	48	72	96	n.a.
Compartment [-]	Apoplast	ER	Chloroplast	Cytosol
Antibody scaffold [-]	IgG3	IgG3 (IgG1 CH3)	IgG3 (IgG1 CH3/2)	IgG1

The PCP harvest time point was treated as hard-to-change factor. n.a. – not applicable.

II.7.2 Statistical methods

A Shapiro-Wilk test was used to test for normality and an F -test was used to confirm equal variance of data sets [233]. Unpaired two-sample, two-sided t -tests were used to compare normally distributed data from negative selection, plant (cell) cultivation and activity tests, using a significance level of $\alpha = 0.05$. Welch's t -test was used if variances differed significantly and a Mann-Whitney U -test (Wilcoxon test) was used to compare non-normally distributed data [234]. Screening studies in PCPs or differentiated plants were evaluated by analysis of variance (ANOVA) using Design Expert (Stat-Ease) or OriginPro (OriginLab) with a *post hoc* Bonferroni test [235] and a significance level of $\alpha = 0.05$.

In statistical tests comparing two groups, N refers to the total number of samples from both groups, whereas n refers to the number of samples from a single group.

III. Results and discussion

Results presented in the following sections have been published as denoted hereafter:

- III.2.3.3.1 Opdensteinen, P., Buyel, J.F., Reducing water uptake into BY-2 cells by
- III.2.3.3.2 systematically optimizing the cultivation parameters increases product yields
- III.2.3.3.4 achieved by transient expression in plant cell packs. *Biotechnology Journal* 2022, 17(10), 2200134, DOI: 10.1002/biot.202200134.
- III.2.4.1 Opdensteinen, P., Sperl, L.E., Mohamadi, M., Kündgen-Redding, N., Hagn, F. and Buyel, J.F., The transient expression of recombinant proteins in plant cell packs facilitates stable isotope labeling for NMR spectroscopy. *Plant Biotechnology Journal* 2022, 20(10), 1928-1939, DOI: 10.1111/pbi.13873.
- III.4.2.2 Opdensteinen, P., Meyer, S., Buyel, J.F., *Nicotiana* spp. for the expression and purification of functional IgG3 antibodies directed against the *Staphylococcus aureus* alpha toxin. *Frontiers in Chemical Engineering* 2021, 3, 737010, DOI: 10.3389/fceng.2021.737010.

III.1 High-throughput cloning

The standardization of workflows and synthetic biology tools has facilitated the automation of DNA assembly [236–238], which is the starting point for many projects in molecular biology, thus allowing to generate and explore increasingly complex construct libraries [168]. By applying the same concept to plant biotechnology, a high-throughput platform for cloning of transient expression vectors was established that facilitates a systematic investigation of current limitations of plant-based expression systems, e.g. low yields, and batch to batch variation [78, 90]. Establishing a high-throughput cloning platform comprised generation of modular vectors (III.1.1), implementation of negative selection to maximize the cloning success rate (III.1.2) and automation to increase the cloning throughput (III.1.3).

III.1.1 Modular expression vectors

The first step towards high-throughput cloning was to set up modular vectors based on pTRA, a derivative of pPAM (GenBank AY027531), to facilitate the rapid exchange of vector elements. An approach based on restriction enzymes was chosen, because after more than 50 years of application [239] this technique is established in many laboratories, compatible with PCR amplification [240] and parallelization, especially when combined with type IIS restriction enzymes, which allow one-pot assembly reactions [241].

III.1.1.1 Selection of target proteins

The model proteins (Table 9) used to establish a high-throughput screening platform for recombinant protein production in plants were chosen to suit a multi-layered strategy for treatment of infections with MRSA (I.4.1).

Specifically, the proinflammatory cytokine IL6 (Uniprot ID P05231) was chosen as a model protein because of its ability to promote bacterial killing by neutrophils [242], aiming to support the treatment of *S. aureus* infections by stimulating the immune response [243]. So far recombinant IL6 production has proven to be challenging with established expression platforms including plants and bacteria due to aggregation and susceptibility to degradation [189, 244]. In the same context IL8 (Uniprot ID P10145) was chosen as model protein, because *S. aureus* evasion protein SSL5 interferes with normal neutrophil activation and migration through IL8 [188]. Additionally, IL8 has a longer half-life time than IL6 [245], thus allowing to compare the effect of intrinsic protein stability on recombinant accumulation levels in plants.

Polyphosphate kinases from *Thermococcus agreste* and *Rhodococcus opacus* (PPK-RO) were selected not only as conserved anti-bacterial drug targets, but also because they can be used for co-factor regeneration in industrial application. Specifically, the PPK from *T. agreste* (PPK-TA) was chosen as model, because of its origin from a thermostable organism [246], thus facilitating a potential purification from plants by heat treatment of leaf tissue or plant extracts in the future [247]. For example, a thermal stability of $\geq 60^{\circ}\text{C}$ enables blanching of leaf tissue, which has been shown to simplify purification of (heat-stable) recombinant from plants tremendously by precipitating ~80% of plant HCPs before chromatography [247]. The PPK from *R. opacus* (PPK-RO) was selected as a counterpart from a mesophilic organism.

Antibodies directed against *S. aureus* toxins have been successfully used to treat infections with MRSA [195]. This concept was developed further by using an IgG3 antibody scaffold (Uniprot ID P01860), which unlike the commonly used IgG1 cannot be bound and neutralized by *S. aureus* SpA. Compared to IgG1, IgG3 offers additional advantages like a more potent complement activation [248] and a more flexible hinge region, but has so far been difficult to produce recombinantly due to aggregation and degradation [249]. IgG1 antibodies directed against the same target (*S. aureus* alpha toxin) were selected as a control for IgG3.

DspB (Uniprot ID Q840G9) was chosen as a model for biofilm degrading enzymes, because it is one of only two reported enzymes capable of hydrolyzing poly- β -1,6-*N*-acetyl-d-glucosamine (PNAG), which is a key element in bacterial biofilms [250] and highly conserved among diverse bacteria including *S. aureus* [251, 252]. DspB has so far been produced in stable

transgenic plants to protect them from pathogens [253], but the transgenic production of DspB has not been investigated in detail in plants.

The chimeric enzyme LysK-L (Uniprot IDs Q6Y7T6 and P10547) was selected as a model for endolysins, because it combines amidase, alanyl-glycyl endopeptidase and glycyl-glycyl endopeptidase activities, thus achieving efficient lysis of antibiotic-resistant *S. aureus* [254]. The plant-based production of LysK-L has been difficult with viral vectors, likely due to their size limitation [116, 255], thus representing an interesting target for the *Agrobacterium* system used herein, which is compatible with genes > 2.0 kb [114].

Table 9: Overview of model proteins used to set up and test modular expression vectors.

Protein [-]	Organism of origin [-]	Molecular mass [kDa]	Isoelectric point [-]	Instability index [-]	Aliphatic index [-]
PPK-RO	<i>Rhodococcus opacus</i>	81.50	5.48	37.01	96.73
PPK-TA	<i>Thermocrisum agreste</i>	80.10	5.51	43.03	96.71
IL6	<i>Homo sapiens</i>	20.80	6.21	57.89	84.81
IL8	<i>Homo sapiens</i>	11.10	9.10	24.95	101.52
IgG3 ^a	<i>Homo sapiens</i>	54.58	8.16	49.37	61.24
IgG3 (IgG1 CH3 domain) ^a	<i>Homo sapiens</i>	54.58	8.16	49.63	62.40
IgG3 (IgG1 CH3/2 domain) ^a	<i>Homo sapiens</i>	54.58	8.16	49.23	61.82
IgG1 (M12) ^a	<i>Homo sapiens</i>	49.40	8.36	45.56	67.39
DspB	<i>Actinobacillus actinomycetemcomitans</i>	41.00	5.70	30.83	81.36
LysK-L ^b	Staphylococcal phage K, <i>Staphylococcus simulans</i>	71.30	9.48	31.32	60.68

^a protein properties correspond to the antibody heavy chain. All mAbs contained the variable domain of the M12 antibody (Figure S1). ^b LysK-L is a fusion protein of LysK and lysostaphin [254]. All protein properties were calculated with ExPASy ProtParam [256].

A C-terminal hexa histidine-tag (His₆-tag) was fused in frame with the respective target protein coding sequences to facilitate purification and quantification (Figure 3). The His₆-tag was chosen, because it is one of the smallest affinity tags available (0.84 kDa [257]), thus likely minimizing the impact on target protein properties such as solubility or function [258, 259]. The purification tag was omitted for target proteins of the IgG class, because these can be

readily detected with group specific antibodies and can be quantified and purified with protein A, G or L.

III.1.1.2 Selection of vector elements for screening studies

The expression cassette elements selected for an initial set of modular vectors constitute promoters, UTRs and signal sequences, because they have been shown to strongly affect recombinant expression in plants [144]. Systematically screening libraries of these elements facilitates the identification of combinations that achieve high product accumulation. The double-enhanced *Cauliflower mosaic virus* 35S promoter was selected as an example for a strong constitutive promoter, conferring high transgene transcription in plants [260]. Three different 5' UTRs, namely the *Petroselinum hortense* chalcone synthase 5' UTR (CHS [211]), the *Tobacco mosaic virus* omega prime sequence (omega [212]) and the *Tobacco etch virus* leader sequence (TL [213]) were selected for screening of promoter and UTR combinations that confer high transgene expression [144]. Because of compartment-specific differences in protein modification and degradation [85], the LPH, rbcS [216] and KISIA signal sequences [219] as well as the SEKDEL retention signal [218] were included in the modular vector system to investigate the effect of sub-cellular targeting on recombinant protein accumulation and activity (Table 10, Figure 3).

Table 10: Overview of signal sequence combinations used in the modular vectors system and the resulting targeted sub-cellular compartment.

5' signal sequence	3' signal sequence	Targeted compartment
None	None	Cytosol
rbcS	None	Plastid (BY-2), chloroplast (differentiated plants)
LPH	None	Apoplast
LPH	SEKDEL	Endoplasmic reticulum
LPH	KISIA	Central vacuole

KDEL – ER retention signal from the chaperone protein grp78. KISIA – vacuolar targeting signal from the *Amaranthus hypochondriacus* 11S globulin. LPH – leader peptide of the antibody mAb24 heavy chain. rbcS – transit peptide from the ribulose-1,5-bisphosphate carboxylase/oxygenase small subunit of *Solanum tuberosum*. Amino acid sequences are provided in the appendix (Supporting Table 3).

III.1.1.3 Assembly of modular vectors

To assemble modular expression vectors, DNA fragments containing the expression cassette elements chosen for initial screening studies (III.1.1.2) were amplified by PCR (Figure 3A), thereby introducing restriction enzyme recognition sequences and complementary sites for homologous recombination via primer overhangs (II.2.2). Gibson assembly (II.2.6) was then

used to join the amplified DNA fragments resulting in expression vectors with restriction enzyme recognition sites flanking the sequence coding for the protein of interest as well as expression cassette elements with a strong influence on recombinant protein expression in plants (Figure 3A).

Whereas additional or modified nucleotides in untranscribed regions resulting from restriction cloning did not affect the coding sequence of the target protein, the restriction sites directly flanking the latter had to be selected carefully to maintain the target protein's native amino acid sequence. NcoI was chosen for the 5' end of the target protein, because the enzyme recognition site encompasses the translation start codon (ATG) and overhangs generated by NcoI are compatible with overhangs from multiple other restriction enzymes (Supporting Table 4). These enzymes can be used instead of NcoI depending on the nucleotide sequence of the target protein and omit the need to alter the target protein sequence for restriction cloning. However, such "NcoI-ReX" cloning events caused the original restriction sites to disappear, effectively trapping the target protein coding sequence in the vector. NotI was chosen for the target protein's 3' end (Figure 3A), because the enzyme recognition site encompasses three alanine, a small and neutral amino acid that can simultaneously act as a spacer to ensure tag accessibility without being susceptible to degradation [261].

To simplify cloning of antibodies which are composed of two polypeptides, the sequences coding for the heavy and light chain were fused in frame with a self-excising linker peptide consisting of an intein and F2A peptide [217], thus generating a single open reading frame, which can be readily introduced into the modular vectors (Figure 3A). Using the same strategy, the modular vectors can be used to express other multi-chain proteins or for protein co-expression. Up to 3 proteins have been simultaneously expressed with a self-excising linker in the literature without compromising expression levels compared to single-protein vectors [217]. Moreover, T-DNAs of at least 150 kb have been transformed into *N. tabacum* plants [119], hence not posing an issue to further expanding the expression cassette in a transient expression setting. Because antibodies did not require a tag, they were cloned into the modular vectors through NcoI and XhoI, thereby removing the C-terminal His₆-tag and the SEKDEL or KISIA signal sequences present in the modular vectors (Figure 3A). If retention in the ER or trafficking to the vacuole was desired, the respective signal sequences were fused in frame to the 5' end of the leading peptide chain, i.e. the heavy chain by PCR (Figure S1). Equipping one of the two fused peptide chains with a signal sequence has shown to be sufficient for correct trafficking before [262]. After assembling modular vectors (Supporting Table 2), restriction cloning with type II enzymes was used to exchange target proteins (III.1.1.1) and expression cassette

elements (III.1.1.2), in order to investigate their interplay while maintaining sub-cloning capability (Figure 3B).

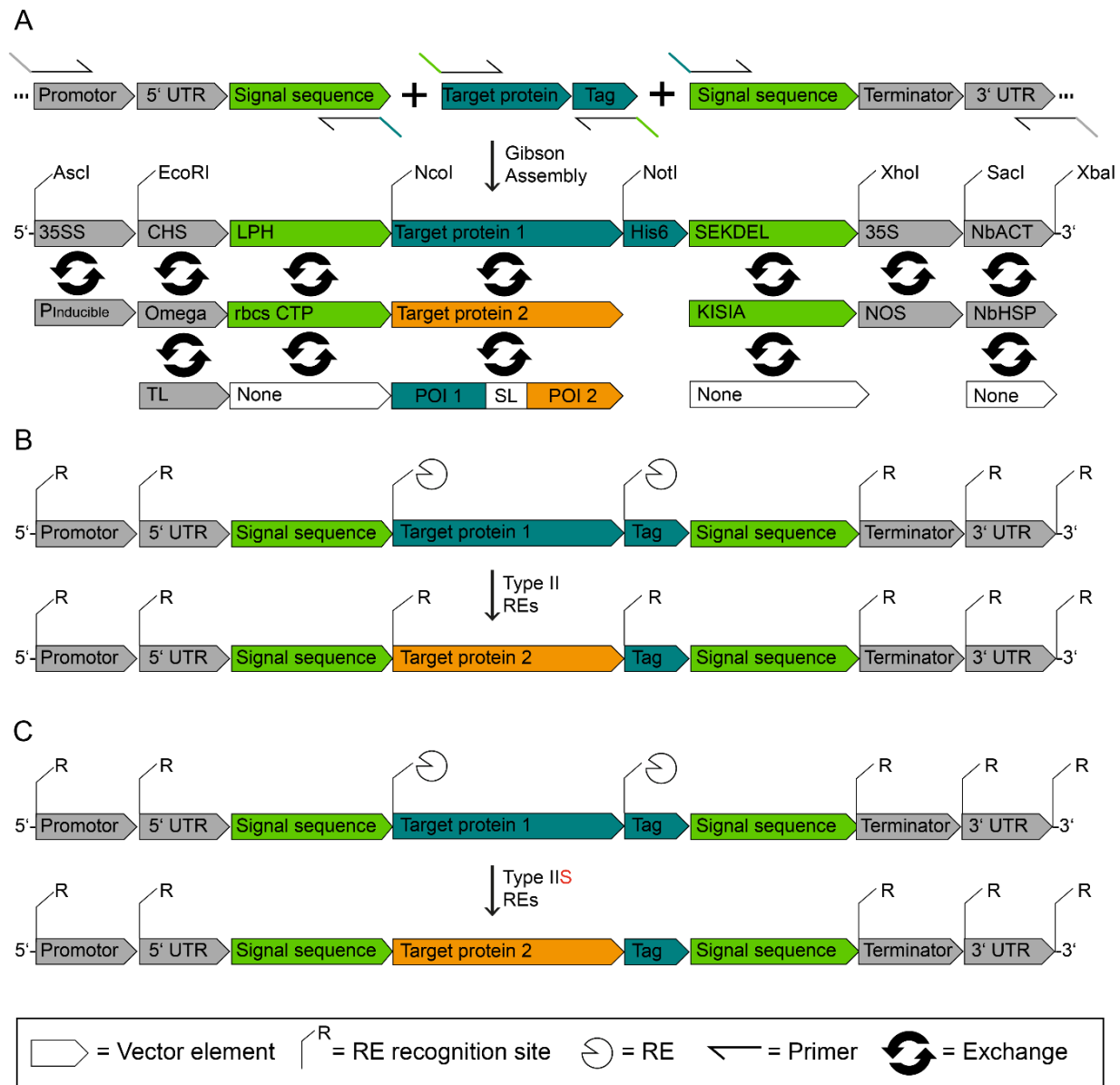


Figure 3: Schematic representation of a modular vector design for *Agrobacterium*-mediated transient protein expression in plants and exchange of vector elements with endonucleases. A. Assembly of modular expression vectors using Gibson assembly [210]. Homologous regions for the assembly of modular expression vectors were introduced into PCR products with primer overhangs, simultaneously adding restriction enzyme recognition sites (II.2.7). B. Exchange of vector elements with type II restriction enzymes. When using type II enzymes for restriction cloning, enzyme recognition sites and sub-cloning capability are preserved. C. Exchange of vector elements with type IIS restriction enzymes. When using type IIS enzymes for restriction cloning, enzyme recognition sites disappear in the final DNA sequence. Depending on the combinations of signal sequences used, recombinant proteins can be targeted to the cytosol, apoplast, plastid, ER or vacuole (Table 10). RE – restriction enzyme, SL – self-excising linker.

In the future, aiming for a commercial application, type II restriction enzymes will be replaced by type IIS enzymes to increase the throughput when exchanging genetic elements (Figure 3C). Because type IIS restriction enzyme recognition sites can be designed so they do not appear in

the final DNA sequence, these enzymes are most suitable for applications where sub-cloning capability is not required anymore (Figure 3C).

In total, 430 constructs were cloned with the modular vector system, out of which 206 were used in this thesis (Supporting Table 2). The cloning efficiency (i.e. the number of correct clones obtained from the cloning reaction) with type II enzymes was $83.5 \pm 19.3\%$ ($n = 692$), which was, as expected, lower than the efficiency ($> 97\%$) reported for type IIS enzymes [263]. Clones that were negative during colony PCR typically contained the original template vector instead of the intended cloning product. To remove such false-positive clones and increase the reliability of DNA assembly, a negative selection strategy was next implemented into the modular vector system.

III.1.2 Negative selection with SacB

Levan sucrase from *Bacillus subtilis* hydrolyses sucrose to form levan, which is toxic to gram-negative bacteria like *A. tumefaciens* and *E. coli* [263], even though its specific mode of action is still under investigation. Including the SacB cassette (native SacB promoter, SacR control region and SacB encoding gene sequence (Figure S2) as a default insert in the modular vector system (III.1.1.3) can therefore be used as a negative selection strategy in the presence of sucrose [264]. Specifically, in the cloning process, the SacB cassette is replaced by a new DNA sequence to be tested and only cells containing vectors where the SacB cassette was successfully replaced can grow on sucrose selective media. Sodium chloride was omitted from SacB selection media (VII.7), because SacB sensitivity has been reported to decrease in the presence of $\geq 5 \text{ g L}^{-1}$ sodium chloride [265]. For example, lysogeny broth (LB) medium used for routine cultivation of *E. coli* contained 10 g L^{-1} sodium chloride (VII.7) and can thus be expected to impair SacB selection.

The SacB gene cassette was functional in *E. coli* as well as *A. tumefaciens* (the two species relevant for the cloning strategy) as indicated by the absence of colonies when plating SacB^+ cells from both species, on solid media containing 50 g L^{-1} (*E. coli*) or 100 g L^{-1} (*A. tumefaciens*) sucrose (Figure 4). The same cells survived when omitting sucrose (Figure 4C, F), but growth was impaired compared to control constructs, as indicated by a $\sim 50\%$ smaller colony size after 16 hours (*E. coli*) and 80 hours (*A. tumefaciens*) of incubation (Figure 4C, F). However, because the replacement of the SacB cassette with a gene of interest was the desired cloning outcome, the impaired growth did not pose a problem and even acted in favor of negative selection against SacB. The cloning efficiency increased from $83.5 \pm 19.3\%$ ($n = 692$) to $95.8 \pm 7.2\%$ ($n = 20$) after implementing SacB negative selection into the modular expression vectors.

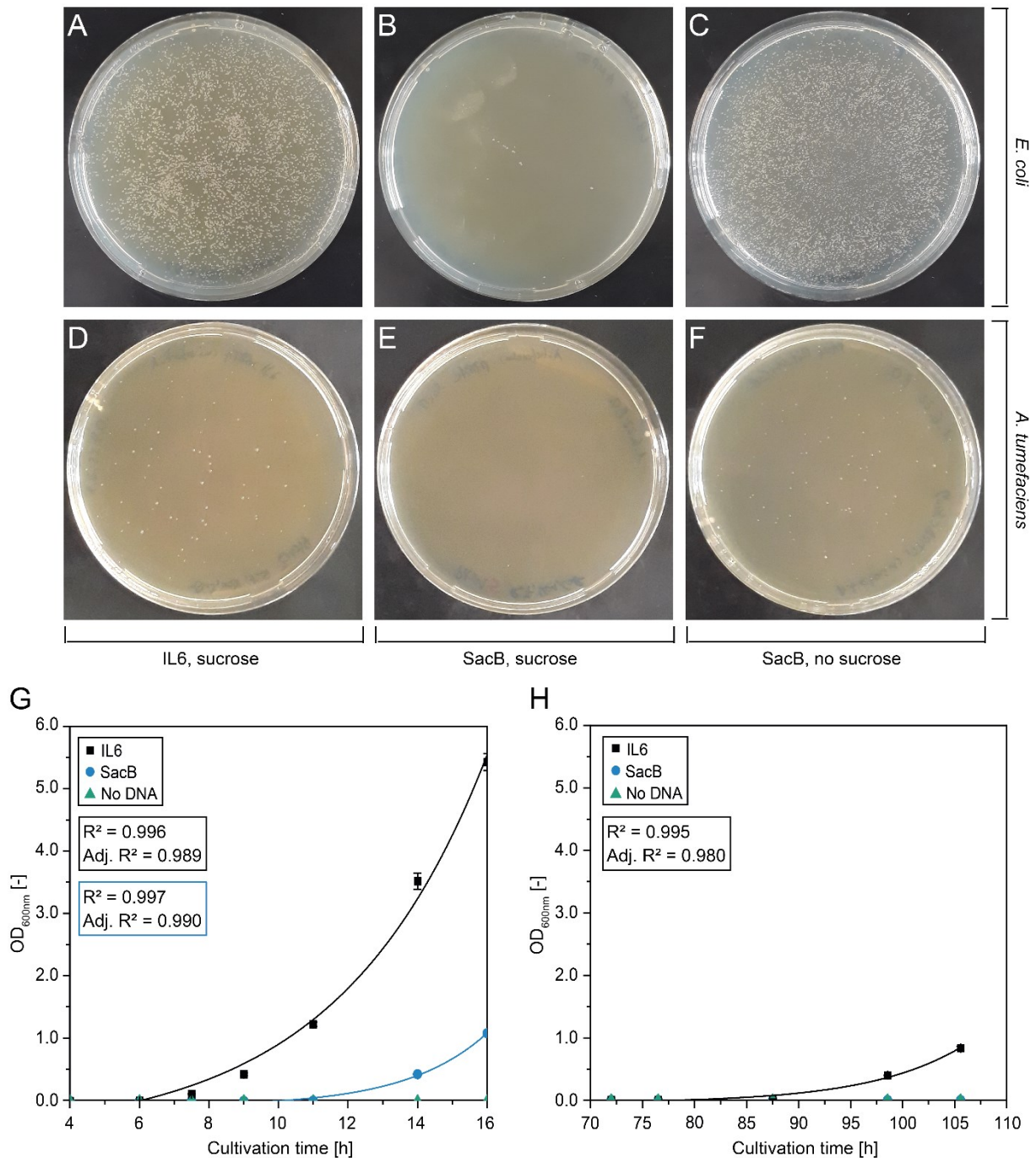


Figure 4: Evaluation of SacB functionality in *E. coli* and *A. tumefaciens*. A – C. Negative selection with *E. coli* SacB⁺ and SacB⁻ on agar plates. Chemically competent *E. coli* dh5 α (II.3.1.1) were transformed with pTRAc_000431 or pTRAc_000001 (Supporting Table 2) and regenerated in the presence of sucrose (II.3.1.4). Plates were incubated for 16 hours at 37°C. D – F. Negative selection with *A. tumefaciens* SacB⁺ and SacB⁻ on agar plates. Electrocompetent *A. tumefaciens* cells (II.3.2.1) were transformed with the same constructs used for *E. coli* and regenerated in the presence of sucrose (II.3.2.4). Plates were incubated for 80 hours at 28°C. G. Growth of with *E. coli* SacB⁺ and SacB⁻ in liquid cultures. Liquid cultures were inoculated with the same *E. coli* cell suspensions used for plates and incubated at 37°C for 16 hours (II.3.1.4). H. Negative selection with *A. tumefaciens* SacB⁺ and SacB⁻ in liquid cultures. Liquid cultures were inoculated with the same *A. tumefaciens* cell suspensions used for plates and incubated at 28°C and 160 rpm for 106 hours (II.3.2.4). Negative controls were treated similarly, omitting the addition of DNA. Antibiotics were re-added in *A. tumefaciens* liquid cultures to 25 $\mu\text{g mL}^{-1}$ (kanamycin, rifampicin) and 50 $\mu\text{g mL}^{-1}$ (carbenicillin) every 48 hours. Growth curves were fitted to an exponential growth function (Equation 9, Supporting Table 5) using the software OriginPro. Error bars represent the standard deviation from $n = 3$ cultures.

In liquid cultures containing 100 g L⁻¹ sucrose, SacB⁺ but sucrose-resistant *E. coli* became detectable through an increasing OD_{600nm} after ~11 hours of incubation (Figure 4G). The appearance of sucrose-resistant mutants after > 10 hours of incubation was in agreement with the literature [265] and has previously been attributed to mutations in the SacB cassette [266]. The time until the emerging of sucrose-resistant mutants in liquid cultures was estimated by recording growth curves of SacB⁺ *E. coli* and *A. tumefaciens* in the presence of sucrose and converting the OD_{600nm} to colony forming units (CFU) using a conversion factor of $7.94 (\pm 2.00) \times 10^8$ CFU OD_{600nm}⁻¹ for *E. coli* and a conversion factor of $13.66 (\pm 7.06) \times 10^8$ CFU OD_{600nm}⁻¹ for *A. tumefaciens* [267]. The growth curves recorded for both organisms were then fitted to an exponential growth function (Equation 9) and the time where the number of CFU first exceeded zero (CFU > 0) was derived by rearranging the exponential growth function for the cultivation time (Equation 10).

$$y = y_0 + A_1 e^{\frac{x}{t_1}} \quad \text{Equation 9}$$

$$x = \ln\left(\frac{y-y_0}{A_1}\right) t_1 \quad \text{Equation 10}$$

Where x is the incubation time (the independent variable), y is the number of CFU (the dependent variable), y_0 is the y-offset (number of CFU at $t = 0$), A_1 is the amplitude (pre-exponential scaling factor) and t_1 is the growth constant. Uncertainties on the incubation time x were calculated by error propagation (Equation 22).

Adding 50 g L⁻¹ sucrose already during regeneration increased the negative selection efficiency by delaying the emergence of sucrose-resistance clones by ~2 hours, i.e. from 7.5 ± 4.8 hours to 9.1 ± 3.1 hours in *E. coli* (Figure S3, Supporting Table 6). The mean time until the emergence of sucrose-resistant clones (y_0) was significantly different in both settings when comparing the fitting parameters (Supporting Table 6) using an F -test and OriginPro ($p < 0.001$, $\alpha = 0.05$). When testing a similar setting with *A. tumefaciens*, no sucrose-resistant clones emerged (Figure 4H), probably reflecting the concurrence of the *A. tumefaciens* cultivation temperature (28°C) and the optimum of SacB expression (30°C [268]). SacB⁺ but sucrose-resistant clones did thus not pose an issue in *A. tumefaciens* liquid cultures. In *E. coli* liquid cultures sucrose-resistant clones only emerged after 9.1 ± 3.1 hours, when SacB⁻ clones had already reached the exponential growth phase [269]. This data indicated that SacB negative selection can be used in *E. coli* liquid cultures, given that cells are harvested before resistant clones emerge. The

possibility to use liquid cultures during cloning simplifies automation by omitting the need for plating and picking of individual colonies.

III.1.3 Automated cloning of expression vectors

Automation in the context of DNA assembly is desirable, because it increases the throughput, reliability and accuracy of cloning, thus facilitating the generation and testing of extensive construct libraries [168]. Multi-well plates featuring (ultra-) filtration membranes were especially interesting for this application, because they are compatible with automated liquid handling stations, can be operated with centrifugal force or vacuum [270] and do not compromise DNA integrity and transformational ability [271]. Additionally, using filter membranes for purification of DNA prevents the risk to damage DNA by exposure to ethidium bromide and UV light [272], which is still widely used in the context of DNA purification [273].

III.1.3.1 High-throughput DNA purification of cloning intermediates

Universal buffers are available for restriction and ligation [163], but they are often incompatible with high fidelity polymerases such as Q5 [274]. Therefore, rapid DNA purification from PCR, restriction or ligation preparations is necessary to ensure maximum flexibility in enzyme selection.

To establish a rapid PCR cleanup method, 96-well plates featuring ultrafiltration membranes with molecular weight cut offs (MWCOs) of 100 kDa and 30 kDa were challenged with PCR reaction mix containing DNA fragment sizes typically cloned with the modular vector system. DNA fragments in the range of 0.5 – 6.0 kbp readily passed a 100 kDa membrane (Figure 5A), but interestingly also the ~105 kDa DNA polymerase was detected in the permeate instead of the retentate (Figure S4). Because residual DNA polymerase might interfere with subsequent cloning steps, for example due to exonuclease activity, addition of a proteinase directly to the completed PCR reaction was tested as a measure to inactivate the polymerase. As anticipated, incubation with 0.01 mg L⁻¹ proteinase K completely inactivate the polymerase within 20 min (Figure S4B). Vice versa, proteinase K was readily inactivated by a 90°C heat treatment within 10 min and did thus not interfere with subsequent restriction (Figure S4C).

Filtration with a 30 kDa membrane retained both 0.5 kbp and 6.0 kbp DNA fragments (Figure 5A), while deoxyribonucleotide triphosphates (dNTPs) and primers that might interfere with subsequent applications passed the 30 kDa membrane (Figure 5B). The recovery of DNA re-suspended from the 30 kDa membrane was ~70%, which matched the literature [275], but indicated that a fraction of the DNA remained on the membrane. However, protocols for removal of residual DNA have already been proposed in the literature, for example based on

phosphoric acid for degradation of DNA [276], thus allowing to re-use the filter plates. The removal efficiency of primers and dNTPs with 30 kDa membranes was ~78% and ~98% (Table 11) respectively, which was several times more efficient than the 10 – 30% removal reported in the literature for a comparable setup using 13 kDa membranes [277]. The higher efficiency during the removal of primers and dNTPs can be attributed to the larger membrane pore size compared to the literature.

To achieve a rapid concentration of DNA fragments, the same setup can be used by reducing the buffer volume for re-suspension of DNA fragments from the 30 kDa membrane (Figure 5A). Similarly, a buffer exchange or desalting can be conducted with 96-well plates featuring 30 kDa membranes, as indicated by the efficient removal of salt ions with 30 kDa membranes (Table 11).

Table 11: PCR cleanup using 96-well filter plates with a retention rating of 30 kDa.

Component [-]	Concentration [mM]	Removal [% initial]
Deoxyribonucleotide triphosphate mix	40 (200-fold PCR)	98.0% \pm 0.1
Magnesium chloride (polymerase buffer)	20 (10-fold PCR)	100.0 \pm 0.0%
Primer 35SPARI (20 nt)	0.01 (100-fold PCR)	78.0% \pm 2.1

For all experiments a single centrifugation cycle ($1000 \times g$ for 10 min) was used with a sample volume of 50 μ L (II.2.9.1.2). Data are means \pm standard deviations from $n = 3$ purifications. The concentration of magnesium chloride was derived from the osmolality measured with a Gonotec Osmomat (II.2.9.1.2).

III.1.3.2 Automated separation of DNA fragments

Automating the separation of DNA fragments of different length on a liquid handling station is desirable because it allows to automate permutation of genetic elements between expression vectors generated with the modular vectors system (III.1.1.3). Exchanging genetic elements in the modular vectors always results in a large DNA fragment, i.e. the vector backbone (~6.0 kbp), and a much smaller DNA fragment, i.e. the element that is exchanged (~0.5 – 2.5 kbp), for example a promotor, signal sequence, UTR or the sequence coding for the protein of interest. However, despite the size difference it was not possible to separate these DNA fragments on a liquid handling station using miniaturized (600 μ L) size exclusion chromatography (data not shown). As an alternative to SEC, membranes were hence tested for a size separation of DNA fragments. Membrane-based separation processes have been successfully used to separate open, circular and supercoiled vector isoforms [278] and the selectivity of such separation processes has been further improved by optimizing the ionic strength and pH of the buffers used [271]. However, the underlying mechanism, i.e. a change in the vector size and conformation [278],

cannot be utilized to separate linear DNA fragments of different length. In order to induce conformational changes in linear DNA fragments comparable to vector isoforms and thus facilitate separation by filtration, PEG was tested as an additive.

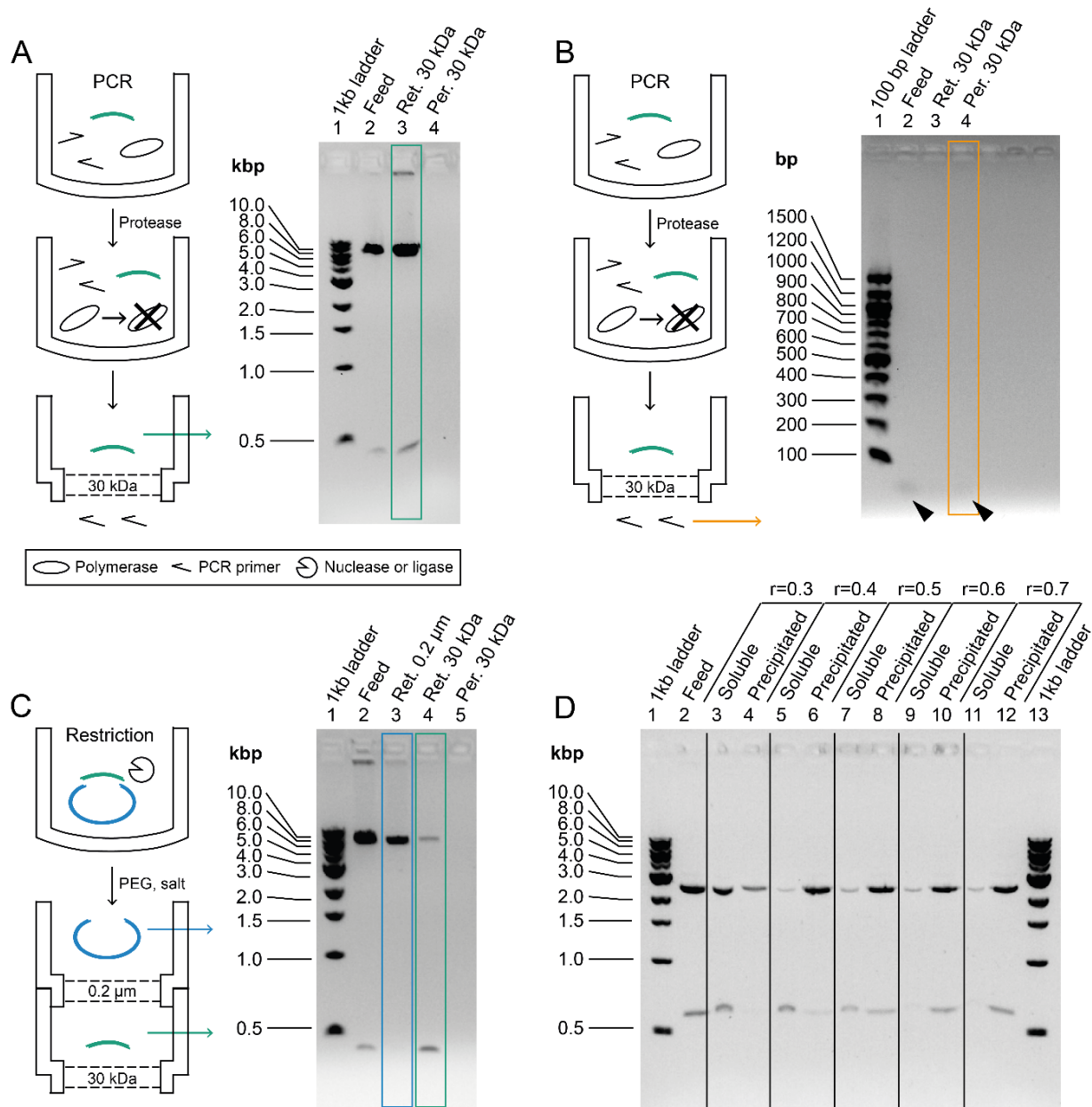


Figure 5: PCR cleanup and separation of DNA fragments with combinations of 96-well filter plates as well as optimization of the separation selectivity. A. DNA fragments in the range of 0.45 – 5.85 kbp were generated by cutting the vector pTRAc_000001 (Supporting Table 2) with BstXI, FseI and EcoRI and concentrated with a 30 kDa filter plate. DNA fragments were applied in 50 μL TRIS buffer at a concentration of 20 mg L⁻¹ (II.2.9.1) and re-suspended from the 30 kDa membrane in 25 μL of the same buffer. B. Removal of PCR primers with 30 kDa filter plates. The 20 nt primer 35SPARI (Supporting Table 1) was removed by ultrafiltration with a 30 kDa membrane. The primer concentration used for ultrafiltration was 0.01 mM. C. Separation of DNA fragments in the range of 0.45 – 5.85 kbp by PEG precipitation and filtration with 0.2 μm and 30 kDa filter plates (II.2.9.2). DNA fragments and concentrations were similar to (A). D. Optimization of separation selectivity by modifying the binding buffer volume fraction. DNA fragments for separation were generated by cutting the vector pMA_IRES (Supporting Table 2) with EcoRI and NcoI, yielding 0.60 kbp and 2.40 kbp DNA fragments. A DNA concentration of 25 mg L⁻¹ was used. Carboxyl-coated magnetic beads were used to capture precipitated DNA. Numbers denote the volume fraction of the binding buffer (II.2.9.3).

The addition of neutral polymers such as PEG allows to convert DNA from an extended configuration to a condensed, globular conformation [279]. DNA molecules with higher molecular mass precipitate at lower PEG concentrations than DNA molecules with lower molecular mass [280] and the concentration required to achieve this conformation change can be predicted [281], which simplifies the implementation of PEG precipitation in automated protocols.

By combining PEG precipitation of DNA fragments with multi-well filter plates featuring retention ratings of 0.2 μm and 30 kDa it was possible to separate a 6.0 kbp vector backbone and a 0.5 kbp DNA fragment excised from the same vector (Figure 5C). After a single purification cycle the retained backbone was $\sim 99\%$ pure (recovery of $\sim 33\%$), whereas the insert was $\sim 68\%$ pure (89% recovery). The selectivity during separation of small and large DNA fragments can be further fine-tuned by optimizing the concentration of PEG and salt used for precipitation as demonstrated with a 2.4 and 0.6 kbp DNA fragment and carboxyl-coated beads (Figure 5D). Additionally, multiple rounds of purification are possible to increase the purity. However, a complete separation was not necessary, because dephosphorylation of vector backbones with an alkaline phosphatase prevented re-ligation. As described for the PCR cleanup (III.1.3.1), membranes can be regenerated by removing DNA contaminations with phosphoric acid [276], thus allowing to re-use membranes. Membrane fouling was not observed in the literature when using DNA concentrations of $250 \text{ ng } \mu\text{L}^{-1}$, which is more than tenfold the concentration used here [282].

III.1.3.3 Automation workflow

Two different workflows were used for automated cloning, depending on whether template vectors (Figure 6A) had restriction sites compatible with the modular expression vectors (Figure 6, grey background) or whether compatible restriction sites had to be introduced by PCR (Figure 6, orange background). When backbone and insert originated from vectors with compatible restriction sites, both vectors were directly cut with type II restriction enzymes (Figure 6B). Following heat-inactivation of the restriction enzymes, the resulting DNA fragments were separated with 96-well filter plates (Figure 6C) as described above (III.1.3.2). Vector backbones and inserts from different reactions were combined and ligated into new expression vectors (Figure 6D) and transformed into *E. coli* or *A. tumefaciens* (Figure 6E).

When restriction sites were not compatible between template vectors, DNA sequences of interest were amplified from template vectors by PCR (Figure 6F), introducing compatible restriction sites via primer overhangs. After inactivation of the DNA polymerase potentially interfering with subsequent cloning steps (Figure 6G), PCR products were purified with 96-

well filter plates (III.1.3.1) and cut with type II or type IIS restriction enzymes (Figure 6H). When restriction sites for regular type II enzymes had been introduced by PCR (Figure 6, solid lines), the workflow proceeded as described above for vectors with compatible restriction sites. Introducing restriction sites for type IIS enzymes allowed one-pot restriction and ligation, because restriction sites were removed upon ligation into the desired product, thus increasing the cloning throughput at the expense of the sub-cloning capability.

All above workflows required at least one reaction providing a backbone and one reaction providing an insert with an upper limit of 96 reactions per plate. To maximize the cloning efficiency, alkaline phosphatase (AP) was added to all reactions providing vector backbones to dephosphorylate DNA fragments and prevent re-ligation. Similarly, DpnI was added after PCR reactions to degrade template vectors.

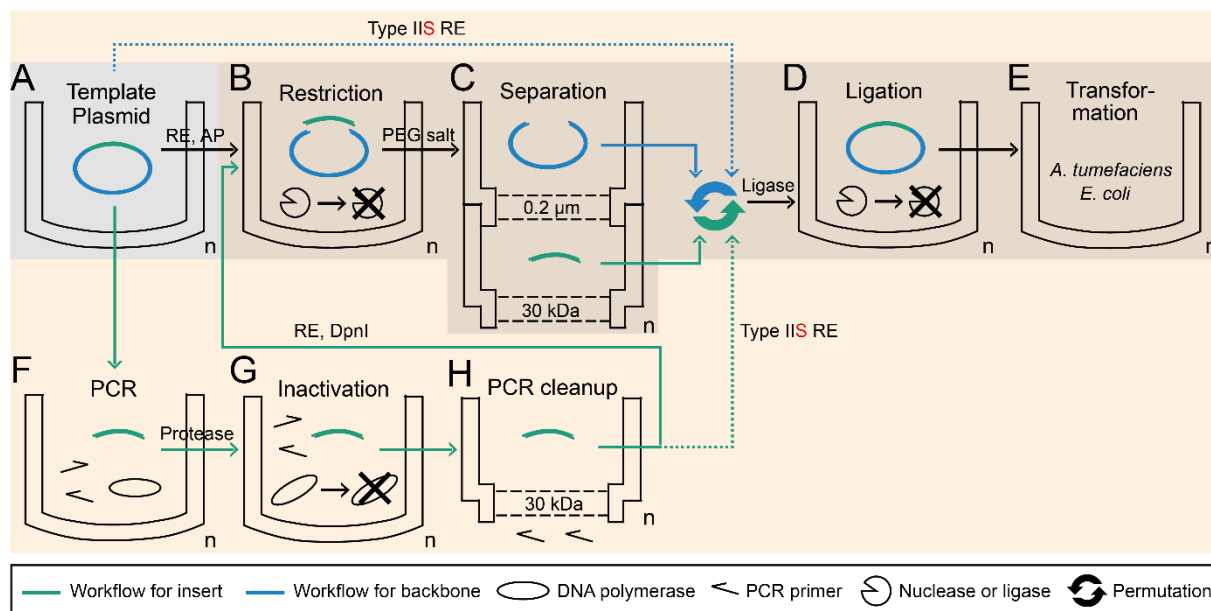


Figure 6: Schematic representation of the automated cloning workflow. Two different workflows were used for automated cloning, depending on whether template vectors had compatible restriction sites (grey background) or whether compatible restriction sites had to be introduced by PCR (orange background). Template vectors (A) with compatible restriction sites were directly cut with type II restriction enzymes (B), DNA fragments were purified with filter membranes (C) and re-combined for ligation (D) and transformation (E). If template vectors did not have compatible restriction sites, PCR was used to introduce compatible restriction sites via primer overhangs (F), followed by inactivation of the polymerase (G) and PCR cleanup with filter plates (H). Depending on the type of restriction site introduced, DNA fragments were either cut and purified as described above (type II restriction enzymes, solid lines) or were directly combined with vector backbones, restriction enzymes and ligase, thus omitting the need for purification (type IIS restriction enzymes, dashed lines). A Vantage liquid handling station was used for protocol automation (II.2.9.4). AP – alkaline phosphatase, RE – restriction enzyme.

Automation of DNA assembly using the above workflow with a Vantage liquid handling station (II.2.9.4) increased the throughput from ~100 manual assembly reactions per week, to 288 assembly reactions per day without relying on plate stack carriers. Multiplexing up to 10 96-

well plates per day was possible when utilizing plate stack carriers for the cloning protocol, thus reaching the range of commercial applications [170].

III.1.3.4 High-throughput transformation of *A. tumefaciens*

Vectors for transient expression in plants are typically assembled in *E. coli* before mobilization into *A. tumefaciens* [283–286]. Omitting the transformation into *E. coli* [264] can therefore simplify and accelerate the workflow. Whereas *E. coli* is transformed by a simple heat shock, *A. tumefaciens* requires electroporation, which increases consumable costs especially in a high-throughput context. For example, multi-well electroporation plates cost > \$300 per item. Transformation by conjugation is a potential alternative, but the requirement for virulent donor strains might raise safety concerns [287].

To overcome above limitations, direct transformation of *A. tumefaciens* with ligation mix was investigated, using freeze-thaw cycling as transformation method. Freeze-thaw cycling relies on rapid freezing and thawing of cells to create temporary lesions in the cell wall and membrane, allowing DNA to diffuse into the cells [288]. Freezing can be achieved using dry ice or liquid nitrogen [288]. Because the latter is difficult to handle on automated platforms and requires additional safety measures for the operator, a bath of dry ice and ethanol was used here. However, the transformation efficiency in this setting was on average ~22% of the efficiency observed with liquid nitrogen (Table 12), which was in agreement with the literature [289]. The transformation efficiency decreased to 8%, when using ligation mix instead of purified vector for transformation (Table 5), which reflected the lower concentration of assembled vector [290]. However, a single freeze-thaw cycle with ligation mix containing 500 ng vector backbones and different inserts (three-fold molar excess) was still sufficient to obtain *A. tumefaciens* clones (4 ± 1 CFU $\mu\text{g}_{\text{DNA}}^{-1}$) that contained the desired genetic constructs (Table 12).

Table 12: Freeze-thaw cycling transformation efficiency depending on the template DNA and freezing agent. A single freeze-thaw cycle was used for every combination (II.3.2.2.2).

Freezing agent [-]	Template DNA [-]	Colony forming units [CFU $\mu\text{g}_{\text{DNA}}^{-1}$]
Liquid nitrogen	Purified vector	50 ± 3
Dry ice in pure ethanol	Purified vector	11 ± 3
Dry ice in pure ethanol	Ligation mix	4 ± 1^a

For generation of ligation mix, the 5' UTR, signal sequence and target protein in the vectors pTRAc_000009 and pTRAc_000037 (Supporting Table 2) were exchanged using the restriction enzymes EcoRI and XbaI. Ligation was conducted with a threefold molar excess of the insert (II.2.5). Data are means with standard deviations from $n = 3 - 4$ transformations. ^a The DNA concentration in ligation mix refers to the vector backbone. A threefold molar excess was used for the insert.

All six clones investigated by colony PCR were positive (Figure 7A), which was in agreement with the success rate of 73 – 97% reported for transformation of *A. tumefaciens* with ligation mix by electroporation [291]. Increasing the number of freeze-thaw cycles offers the potential to further improve the currently low transformation efficiency, however, a low transformation efficiency was desired to facilitate separation of *A. tumefaciens* clones subsequently to transformation to achieve monoclonality. The effect of SacB selection on this process has not yet been tested, but will be investigated in the future.

A well-established approach for single clone isolation is limited dilution cloning, which refers to serial dilution of cells in multi-well plates until a theoretical concentration of < 1 cell well⁻¹ is reached [292]. After an incubation period, wells from the most thorough dilution that still show growth are expanded and screened for expression [292]. Disadvantages of the method are the time-consuming dilution and the requirement for often more than one round of dilution to ensure monoclonality [292]. However, the time required to prepare dilutions can be greatly reduced by using pipetting robots, whereas computing confidence intervals on the probability of monoclonality can simplify the selection of dilution steps [293]. The probability of monoclonality can be assessed through different approaches, for example based on the number of wells without cells (i.e. wells without growth), which can be reliably assessed [293], assuming a Poisson distribution for limiting dilution (Equation 11).

$$P(k) = \frac{\mu^k}{k!} e^{-\mu} \quad \text{Equation 11 [294]}$$

Where $P(k)$ is the probability that a well contains k cells, k is zero or a positive integer and μ is the mean number of cells per well [294].

The probability that a cell line is monoclonal after one round of limiting dilution can be derived by counting the wells without growth and the total number of surveyed wells (Equation 12):

$$PM_1 = \frac{P_\mu(1)}{1 - P_\mu(0)} = \frac{-\ln(s)}{1-s} \quad \text{Equation 12 [293]}$$

Where PM_1 is the probability of monoclonality after one round of limiting dilution cloning and s is the proportion of empty wells, $s = P(0) = e^{-\mu}$ [294].

For calculating confidence intervals on the probability of monoclonality (Equation 12), the proportion of empty wells, s , is replaced with the lower or higher bond of the confidence interval calculated for s (Equation 13).

$$CI_{s_L} = \hat{s} - \kappa \sqrt{\frac{\hat{s}(1-\hat{s})}{T^*}} \quad \text{Equation 13 [293]}$$

$$T^* = T + \kappa^2 \quad \text{Equation 14 [293]}$$

$$\hat{s} = \frac{X + 0.5\kappa^2}{T^*} \quad \text{Equation 15 [293]}$$

Where CI_{s_L} is the lower bond of the confidence interval of the proportion of empty wells, \hat{s} is an estimate for s , X is the number of wells without growth, T is the total number of surveyed wells and κ is the $1-\alpha$ quantile of the normal distribution, $\kappa = z_{1-\alpha}$ [294].

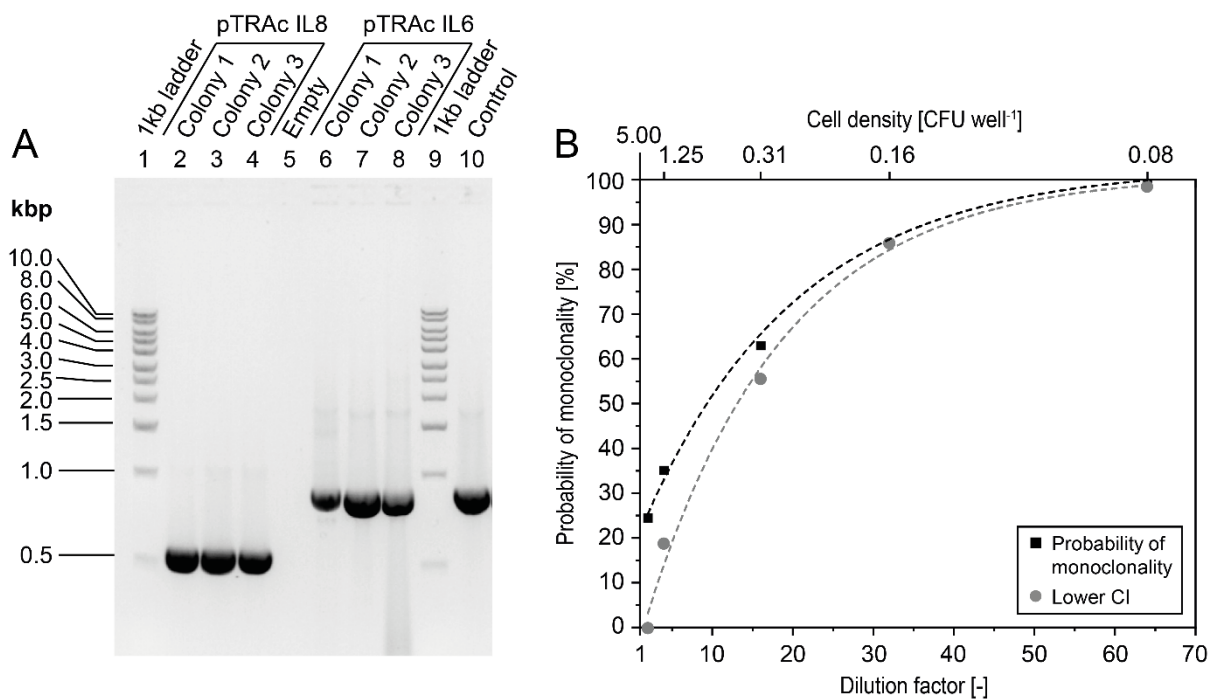


Figure 7: Transformation of *A. tumefaciens* with ligation mix by freeze-thaw cycling and clone isolation by limiting dilution cloning. A. Colony PCR of *A. tumefaciens* after transformation with ligation mix by freeze-thaw cycling. For generation of ligation mix, a DNA fragment spanning the 5' UTR, signal sequence and target protein was exchanged in the vectors pTRAc_000009 and pTRAc_000037 (Supporting Table 2), using the restriction enzymes EcoRI and XbaI. Ligation was conducted with a threefold molar excess of the insert (II.2.5). B. Assessment of monoclonality after limiting dilution cloning. Chemically competent *A. tumefaciens* cells were transformed with the same ligation mix as in (A), using a single cycle of freeze-thaw cycling with dry ice (II.3.2.2.2). After regeneration, the cell suspension (input cell density of 5.0 CFU well⁻¹) was subjected to twofold serial dilution in PAM4 medium supplemented with 25 mg L⁻¹ rifampicin, 25 mg L⁻¹ kanamycin and 100 mg L⁻¹ carbenicillin and incubated at 28°C and 160 rpm for 96 hours (II.3.2.5). Antibiotics were re-added to 25 µg mL⁻¹ (kanamycin, rifampicin) and 50 µg mL⁻¹ (carbenicillin) after 48 hours of incubation. The probability of monoclonal was calculated from the number of wells without growth (Equation 12). A significance level of $\alpha = 0.05$ ($\kappa = 1.645$) was used to calculate confidence intervals (Equation 13).

The probability of monoclonality calculated after 1 round of limiting dilution cloning with *A. tumefaciens* directly transformed with ligation mix was 99% (using a significance level of

$\alpha = 0.05$) after six steps of two-fold serial dilution (Figure 7B) and thus exceeded the 95% probability typically accepted in the literature [295].

These data indicated that a probability of monoclonality $> 95\%$ can be achieved in a single round of limiting dilution with the proposed setting. Specifically, the synergy of limiting dilution cloning with the low transformation efficiency of the freeze-thaw cycling method simplified clone isolation. Template DNA impurities that could compromise the clones obtained, can be minimized through the addition of sucrose to the cultivation medium, to trigger the growth-inhibiting effect of SacB present in the template vectors (III.1.2). Because the SacB cassette is active in *A. tumefaciens* and *E. coli*, the limiting dilution approach can be used for the isolation of single colonies from both bacteria.

Following limiting dilution, the presence of the target vector was confirmed by colony PCR, using universal primers that are compatible with all vectors generated with the modular vector system (Supporting Table 1). After ensuring monoclonality, *A. tumefaciens* cultures were either expanded to a 500 μL scale for infiltration of PCPs, or were used to prepare glycerol stocks for long-term storage.

III.2 High-throughput expression in BY-2 PCPs

Combining high-throughput cloning and high-throughput expression offers the potential to rapidly generate and screen expression vector libraries. However, an expression platform is required that can keep up with an automated cloning throughput of at least 100 assembly reactions per day (III.1.3.3). Plant cell packs (PCPs), which refer to plant cells from a suspension culture that are deprived of medium and infiltrated with *A. tumefaciens* [171], are ideal for this application, because they can be adapted to different plant species and casting and infiltration can be automated, which allows for > 1000 samples to be tested per day at costs less than \$0.5 per sample [151]. Here, screening in PCPs was combined with a design of experiments (DoE) approach to establish descriptive models and predict ideal expression cassettes (III.2.1). The transferability of results obtained in PCPs to differentiated plants was then investigated by establishing correlation factors between both systems (III.2.3). This comprised investigation of the origin of variability in both systems to improve prediction accuracy. Lastly, novel applications of the PCP technology were explored by using BY-2 PCPs for labeling recombinant proteins with isotopes (III.2.4) and by using infiltration centrifugation for high-throughput extraction of recombinant proteins from PCPs.

III.2.1 Prediction of ideal expression cassettes

Previous research has been limited to a single target protein (DsRed) and only a limited number of combinations of expression cassette elements have been tested. Here all possible permutations of the CHS, omega and TL 5' UTRs with signal sequences directing target proteins to the apoplast, ER, plastids, cytosol or vacuole were cloned using the modular vector system discussed above (III.1.1.3). The resulting expression vectors (Supporting Table 2) were tested by transient expression in BY-2 PCPs, *N. benthamiana* and *N. tabacum* plants, using IgG3 antibodies, interleukins (ILs), polyphosphate kinases (PPKs), biofilm degrading enzymes and endolysins as model proteins. Expression data were used to establish descriptive models that can accurately predict target protein accumulation levels depending on the expression cassette elements used.

Models established from accumulation levels of IgG3 antibodies in *N. benthamiana* indicated that the 5' UTR did not have a substantial effect on IgG3 accumulation (Figure 8, Figure S5, Supporting Table 7), which was in agreement with previous experiments [143]. In contrast, the CHS and omega 5' UTRs typically outperformed the TL 5' UTR when using DsRed [144], IL8, PPKRO (Figure 8E – H), DspB or endolysins (Figure S6) as model proteins. The lower target protein accumulation levels observed with the TL 5' UTR were in agreement with the literature and have previously been linked to lower (~50%) mRNA levels, which was attributed to a reduced mRNA half-life time [296]. The subcellular localization had a substantial influence on the accumulation levels of all target proteins tested, but the ideal compartment differed for each target protein class (Figure 8). For example, accumulation levels of native IgG3 antibodies were highest in the ER ($31.8 \pm 14.5 \text{ mg kg}^{-1}$), followed by the apoplast ($12.2 \pm 5.2 \text{ mg kg}^{-1}$), vacuole ($9.5 \pm 3.6 \text{ mg kg}^{-1}$) and plastids ($2.5 \pm 1.7 \text{ mg kg}^{-1}$, Figure 8A, B). In contrast, the highest accumulation of IL8 was observed in plastids ($8.5 \pm 2.6 \text{ mg kg}^{-1}$), followed by the cytosol ($3.5 \pm 2.6 \text{ mg kg}^{-1}$), apoplast ($3.2 \pm 3.0 \text{ mg kg}^{-1}$) and ER ($1.9 \pm 1.7 \text{ mg kg}^{-1}$, Figure 8E, F), whereas PPK accumulation was more than fivefold higher in the cytosol ($7.9 \pm 2.4 \text{ mg kg}^{-1}$) and plastids ($5.4 \pm 4.2 \text{ mg kg}^{-1}$) compared to the apoplast ($0.7 \pm 0.8 \text{ mg kg}^{-1}$) and ER ($0.6 \pm 0.7 \text{ mg kg}^{-1}$, Figure 8G, H).

The ideal compartment for target protein expression appeared to reflect the target protein origin. For example, PPKs and DspB, which are derived from bacteria and do not contain complex post translational modifications based on an analysis with ModPred [297], accumulated well in plastids, which are thought to have a bacterial origin [298] and do not possess the machinery for complex PTMs such as glycosylation [86, 299].

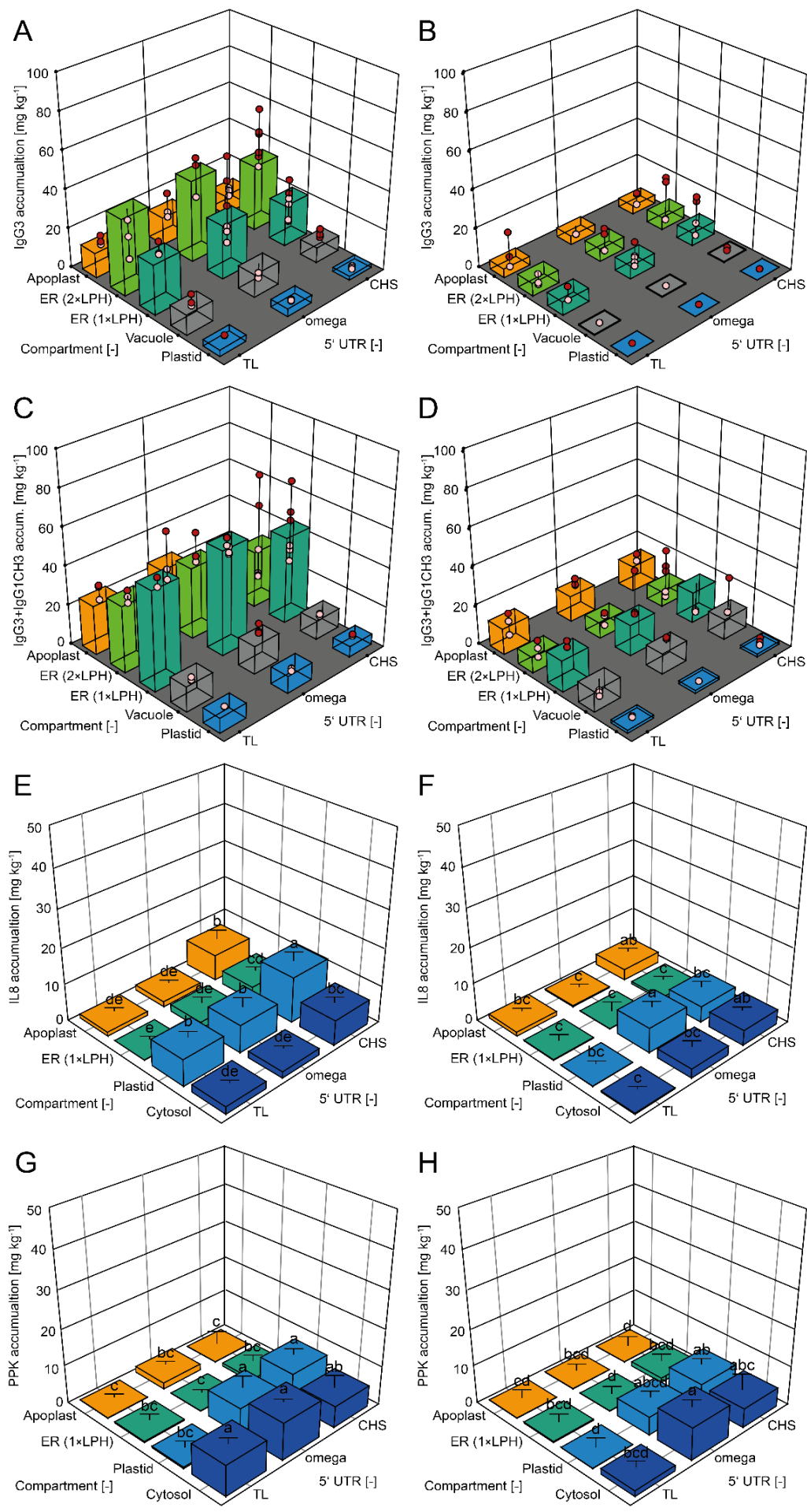


Figure 8: Comparison of IgG3, IL8 and PPK accumulation in *N. benthamiana* and *N. tabacum* plants depending on the expression cassette design. A, B. Models predicting the accumulation of native IgG3 antibodies in *N. benthamiana* (A) and *N. tabacum* (B) when using a CHS, omega or TL 5' UTR and targeting IgG3 to the apoplast, ER, vacuole or plastids (Supporting Table 7). Seven weeks old plants were infiltrated and harvested after 5 dpi. C, D. Models predicting the accumulation of IgG3 domain exchange variants (Figure S1) in *N. benthamiana* (C) and *N. tabacum* (D) testing the same UTRs and compartments as for native IgG3 (Supporting Table 7). Results from additional domain exchange variants are displayed in the appendix section (Figure S5). E, F. Accumulation of human IL8 in *N. benthamiana* (E) and *N. tabacum* (F) when using the same UTRs as above and directing IL8 to the apoplast, ER, plastid or cytosol. G, H. Accumulation of PPK-RO in *N. benthamiana* (G) and *N. tabacum* (H) testing the same UTRs and cell compartments as for IL8. Error bars represent the standard deviation from $n = 3 - 6$ plants. Lowercase letters indicate significance groups. Conditions that share the same letter were not significantly different ($p > 0.05$).

Antibodies originating from eukaryotes are typically glycosylated and showed the highest accumulation levels in the compartments that enable glycosylation, namely the ER and apoplast [300]. Based on these findings the selection of a suitable compartment for expression of a target protein of interest can be guided by the protein origin, thus reducing the number of constructs during screening. Considering that PTM sites can be predicted with *in silico* tools [301], an *a priori* analysis of PTM sites can further support the selection of a suitable compartment for expression of a target protein.

Even though the number of potential combinations of expression cassette elements can be narrowed down as described above, the ideal combination of expression cassette elements that maximized target protein accumulation was protein specific. For example, even within the same protein class, the ideal compartment differed between target protein sub-classes (Figure 8A – D, Figure S5) as indicated by a significant interaction of the antibody heavy chain scaffold and the subcellular localization (Supporting Table 7). Multiple expression cassette designs must therefore be screened in order to maximize target protein accumulation levels. However, the screening effort can be reduced tremendously by using modular expression vectors in combination with high-throughput expression in PCPs as proposed here.

III.2.2 Effect of intrinsic protein properties on accumulation levels

The different target proteins expressed in this work were next used to investigate the impact of intrinsic protein properties such as overall stability on recombinant accumulation levels in *Nicotiana* spp., aiming to determine the feasibility of a plant-based production *a priori*. Stability is a fundamental protein property and can be assessed based on different principles, for example the amino acid sequence, flexibility or hydropathy [302]. Here, the aliphatic index was used as a measure for (thermal) protein stability and flexibility (thermostability and flexibility are inversely related [303]), whereas the dipeptide composition-based instability index was used as a measure for susceptibility to *in vivo* degradation [304]. The aliphatic index is defined as the

relative volume occupied by aliphatic amino acid side chains and higher values indicate a higher (thermal) stability [305]. The instability index provides an estimate for the stability of a protein or peptide based on the presence of certain dipeptides in the primary amino acid sequence. Instability indices < 40 indicate that a protein is likely stable in a test tube, whereas instability indices > 40 indicate that the protein might be unstable [304].

The relationship of the instability index and recombinant accumulation levels within the same protein class was investigated with IgG antibodies as model proteins (Figure S7A). Within this protein class the instability index correlated well with recombinant IgG accumulation levels when targeted to different cell compartments in BY-2 PCPs (Pearson's $r = -0.61 - -0.99$, Supporting Table 9). The same trends were observed when comparing IL6 and IL8 or PPK-RO and PPK-TA produced in different cell compartments (Supporting Table 9). Because the instability index does not account for any stability gained from folding, antibodies reached high accumulation levels ($\sim 50 - 100 \text{ mg kg}^{-1}$) despite unfavorable instability indices (> 40 , Figure S7A) due to the presence of stabilizing disulfide bonds [304]. This observation emphasizes that several mechanisms have to be considered for accurate stability predictions [304].

Within the IgG class the aliphatic index correlated positively (Pearson's $r = 0.81 - 0.98$, Supporting Table 10) with recombinant accumulation levels in different cell compartments (Figure S7B). Again, the same trends were observed when comparing IL6 and IL8 or PPK-RO and PPK-TA produced in different cell compartments (Supporting Table 10). These data indicated that a higher (thermal) stability might contribute to increased target protein accumulation levels in plants.

When comparing different target protein classes, the situation was more complex: Even though recombinant protein accumulation levels were still negatively correlated with the instability index, there appeared to be different clusters, corresponding to high and low base accumulation levels (Figure S7C). Proteins from the cluster showing high base accumulation levels shared a near neutral isoelectric point (pI), whereas more extreme pI values were common in the protein cluster showing low base accumulation levels (Figure S7). These findings indicated that multiple protein properties have to be considered when attempting *a priori* predictions that involve different protein classes. When comparing the aliphatic index and recombinant accumulation levels of different target protein classes, the highest accumulation levels were observed with an aliphatic index between 75 – 80, whereas recombinant accumulation levels declined at higher or lower aliphatic indices. This finding might indicate that a balance between stability and flexibility contributed to high recombinant accumulation levels in plants.

However, due to the limited data available additional investigations are required to confirm or refine these observations.

Overall, these data indicate that an *in silico* stability assessment, for example based on the instability index, can differentiate between promising and unsuitable product candidates within the same target protein class. However, when comparing different target protein classes, additional parameters have to be considered to allow reliable predictions [306]. Machine learning approaches that combine different parameters can hence be expected to advance *a priori* stability investigations in the future [302, 307]. The high-throughput tools implemented here facilitate the generation of bigger datasets, thus allowing to address the limited availability of experimental data, which is a major drawback of protein stability prediction methods [302].

III.2.3 Transferability between PCPs and differentiated plants

Even though BY-2 cells used to cast PCPs originate from *N. tabacum*, expression levels measured in BY-2 PCPs cannot directly be transferred to differentiated *N. tabacum* plants and its wild relative *N. benthamiana* due to tissue specific differences. For example, BY-2 cells lack veins, which are present in differentiated plants, but do not contribute to expression of recombinant proteins [90]. Hence, individual correlation factors between these systems have to be derived to allow predictions based on screening results in PCPs [151].

III.2.3.1 Correlation factors

To establish correlation factors between BY-2 PCPs and differentiated *Nicotiana* plants, interleukins, polyphosphate kinases and antibodies were expressed in both systems. Differentiated plants were infiltrated by vacuum infiltration, while a previously established, automated protocol was used to infiltrate PCPs [151]. PCPs were incubated for 72 hours after infiltration, because this incubation time has previously achieved higher levels of correlation between PCPs and differentiated plants (Pearson's $r = 0.98$; 3 dpi) compared to longer PCP incubation times (Pearson's $r = 0.66$; 4 dpi [308]) when using DsRed as a model protein. The harvest time of differentiated plants was 5 dpi, which was reported to maximize transient accumulation of various target proteins including antibodies or DsRed [296, 309, 310]. *N. benthamiana* and *N. tabacum* plants were extracted as a whole to mimic the situation in a vertical farming unit, where whole plants are inverted and harvested by cutting the plant stem with blades [100].

Correlation factors were derived by linear correlation analysis based on target protein accumulation levels in BY-2 PCPs and in differentiated plants (Figure 9). A strong positive

correlation (Pearson's $r = 0.88$), was found when comparing accumulation levels in PCPs and *N. benthamiana* plants (Figure 9A), which was in agreement with previous literature [171].

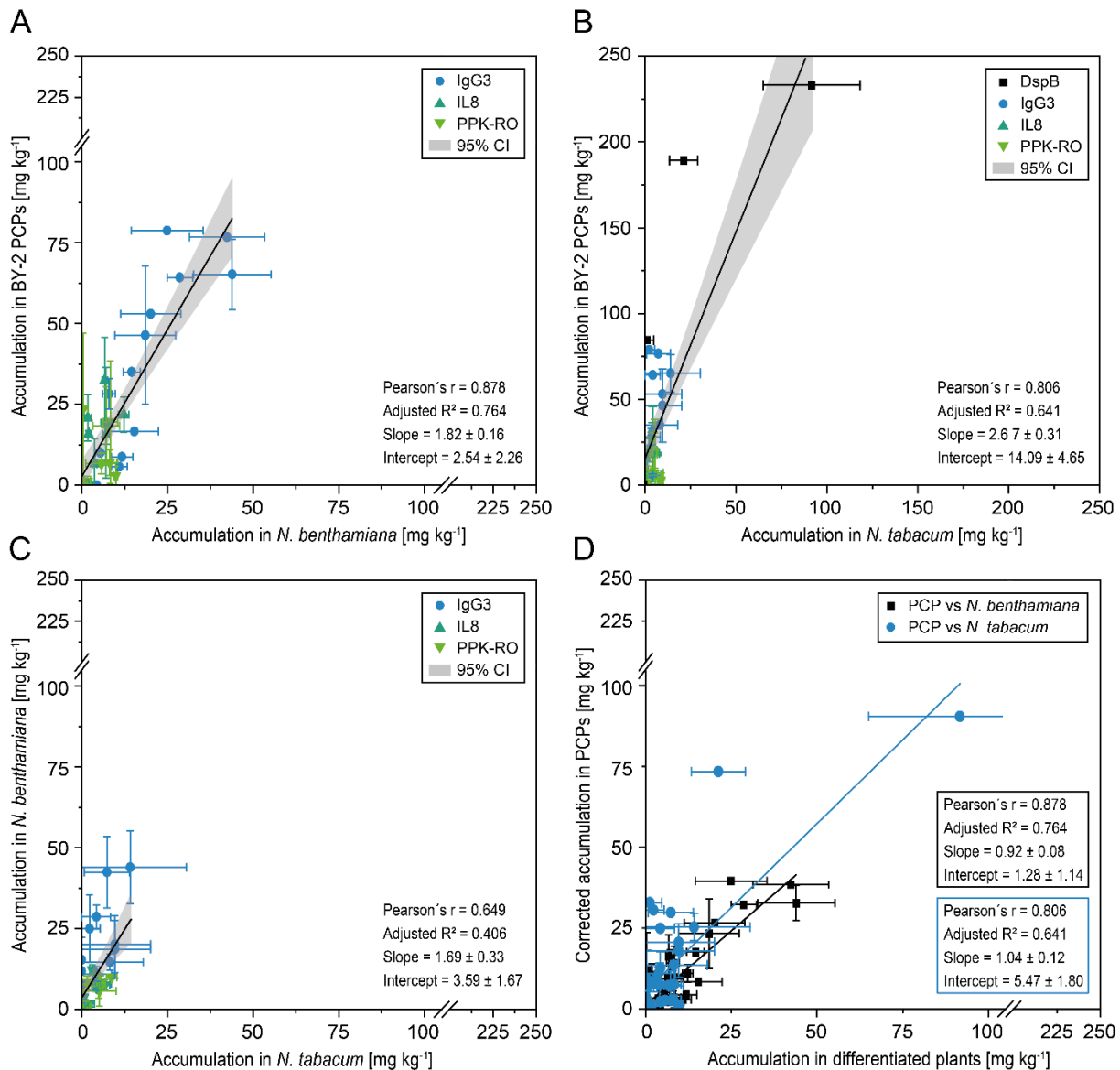


Figure 9: Correlation between transient protein accumulation levels in PCPs and differentiated plants. A – D. The transferability of results between BY-2 PCPs and differentiated plants (A, B) or between different plant species (C) was investigated by expressing IL8, PPK-RO, IgG3 and DspB in the respective system and assessing the correlation of target protein accumulation levels by linear regression. D. Target protein accumulation levels in PCPs were optionally corrected for biosynthetically active biomass (III.2.3.2) before assessing correlation. Both PCPs and differentiated plants were extracted with a 3 v m⁻¹ ratio of extraction buffer (VII.6). BY-2 cells used to cast PCPs were harvested after 168 hours of cultivation in shake flasks with sucrose as carbon source (II.4.1.1). PCPs were incubated for 72 hours after infiltration. Whole plants were extracted after 5 dpi. Accumulation levels of IL8, PPK-RO and DspB were quantified by dot blot (II.6.5) and accumulation levels of IgG3 were quantified by SPR (II.6.3.2). Slopes and confidence intervals of linear regression functions were calculated with OriginPro. Regression functions were not error weighted, because direct and instrumental weighting were not compatible with missing error values. If available, error bars represent the standard deviation from $n = 3 - 6$ PCPs or plants.

The actual correlation factors, i.e. the slope of the respective regression lines, were 1.82 ± 0.16 when comparing PCPs and *N. benthamiana* plants (Figure 9A) and 2.67 ± 0.31 when comparing BY-2 PCPs and *N. tabacum* plants (Figure 9B). Thus, target protein accumulation in BY-2 PCPs was about twofold higher compared to *N. benthamiana* and about threefold higher when compared to *N. tabacum*.

When comparing target protein accumulation levels in *N. benthamiana* and *N. tabacum* (Figure 9C), again a positive correlation was found (Pearson's $r = 0.65$). Overall, these data indicated that expression in PCPs and plants correlated well across different types of protein products, which is a prerequisite when using BY-2 PCPs as a surrogate for screening in differentiated plants.

III.2.3.2 Physiological origin of correlation factors

To investigate the mechanistic origin of these correlation factors, the fraction of biosynthetically active biomass was estimated for *N. benthamiana* and *N. tabacum* plants. Herein active biomass was defined as biomass that contributes to target protein production. For example, the plant stem [100], leaf veins [90] and leaf areas that were not successfully infiltrated with *A. tumefaciens* cell suspension produce little or no target protein. The active biomass was derived from the total biomass by correcting for (i) the mass fraction of the plant stem, (ii) the mass fraction of veins and (iii) non-infiltrated leaf areas using Equation 16.

$$m_a = m_t \cdot m_l \cdot \eta_v \cdot a_e \quad \text{Equation 16}$$

Where m_a is the active biomass (i.e. biomass contributing to target protein expression), m_t is the total biomass, m_l is the ratio of leaf biomass and total biomass, η_v is the ratio of leaf tissue other than veins and total leaf tissue and a_e is the ratio of the infiltrated leaf area and total leaf area.

Correction factors were derived from the fraction of active biomass in PCPs and the fraction of active biomass in differentiated plants using Equation 17.

$$CF_{plant} = \frac{m_{aPCP}}{m_{aplant}} \quad \text{Equation 17}$$

Where m_{aPCP} is the ratio of active biomass in BY-2 PCPs and m_{aplant} is the active biomass ratio in differentiated plants.

In *N. benthamiana* plants the stem accounted for $27 \pm 4\%$ of the total biomass (SD, $n = 106$), whereas it was only $18 \pm 7\%$ in *N. tabacum* (SD, $n = 81$). Veins accounted for approximately 35% of the leaf tissue (*N. tabacum* [90]) and infiltration efficiencies of approximately 95%

were observed for BY-2 PCPs and *N. benthamiana* plants. The infiltration efficiency measured for *N. tabacum* was $70 \pm 28\%$ (SD, $n = 26$). Based on these data the active biomass ratio was 0.48 ± 0.06 for *N. benthamiana* and 0.37 ± 0.20 for *N. tabacum* (Equation 16). The corresponding correction factors were 1.99 ± 0.24 for *N. benthamiana* and 2.58 ± 1.41 for *N. tabacum*, which was in the range of the experimentally derived correlation factors (Figure 9A, B). Similarly, the correlation factor between *N. benthamiana* and *N. tabacum* plants (1.69 ± 0.33) was in agreement with the experimentally derived correction factor of 1.44 ± 0.57 .

When assessing the correlation between expression levels in BY-2 PCPs and corrected expression levels in *N. benthamiana* and *N. tabacum*, the slopes of the regression curves were 0.92 ± 0.08 and 1.04 ± 0.12 , respectively, and thus close to a perfect correlation (Figure 9D).

These findings indicated that an estimate for correlation factors can be made, based on the fraction of biosynthetically active biomass in differentiated plants, assuming that plant cells of the same or a closely related species are used for screening in PCPs.

A remaining drawback that impaired the investigation of correlation factors between BY-2 PCPs and differentiated plants was the high variation of target protein accumulation levels of 19% observed in BY-2 PCPs, 25% in *N. benthamiana* and 62% in *N. tabacum* (Figure 9). The physiological origin of varying (transient) target protein accumulation levels in BY-2 PCPs and differentiated plants was investigated next.

III.2.3.3 Origin of variation in BY-2 PCPs

III.2.3.3.1 Effect of the carbon source and cultivation setting on BY-2 productivity

Interestingly, the variability in BY-2 PCPs was affected by the BY-2 cultivation setting and carbon source (Figure 10A). Specifically, a higher intra and inter batch variability, represented by the coefficient of variation (CV) of DsRed accumulation, was observed when cultivating BY-2 cells in stirred tanks instead of shake flasks before casting PCPs (Supporting Table 11). When replacing the default carbon source sucrose with glucose, the mean intra-batch variability (CV of DsRed accumulation within the same BY-2 batch) fell significantly from $\sim 15\%$ to $\sim 10\%$ (Mann-Whitney *U*-test, $\alpha = 0.05$, $p < 0.01$, $n = 44$), and the mean inter-batch variability (CV of DsRed accumulation across different BY-2 batches) fell significantly from $\sim 55\%$ to $\sim 30\%$ (Kruskal-Wallis ANOVA, $\alpha = 0.05$, $p < 0.01$, $n = 44$). The observed variabilities were in agreement with the literature [151].

The compartment-specific accumulation of DsRed in PCPs increased when glucose instead of sucrose was used as carbon source during BY-2 cultivation (Figure 10B). The effect was reproducible with additional target proteins and was strongest for target proteins that

accumulate at levels $> 50 \text{ mg kg}^{-1}$ such as DsRed or the SPA Z-domain, whereas the accumulation of IgG1, IgG3 and human ferritin only doubled (Figure S8).

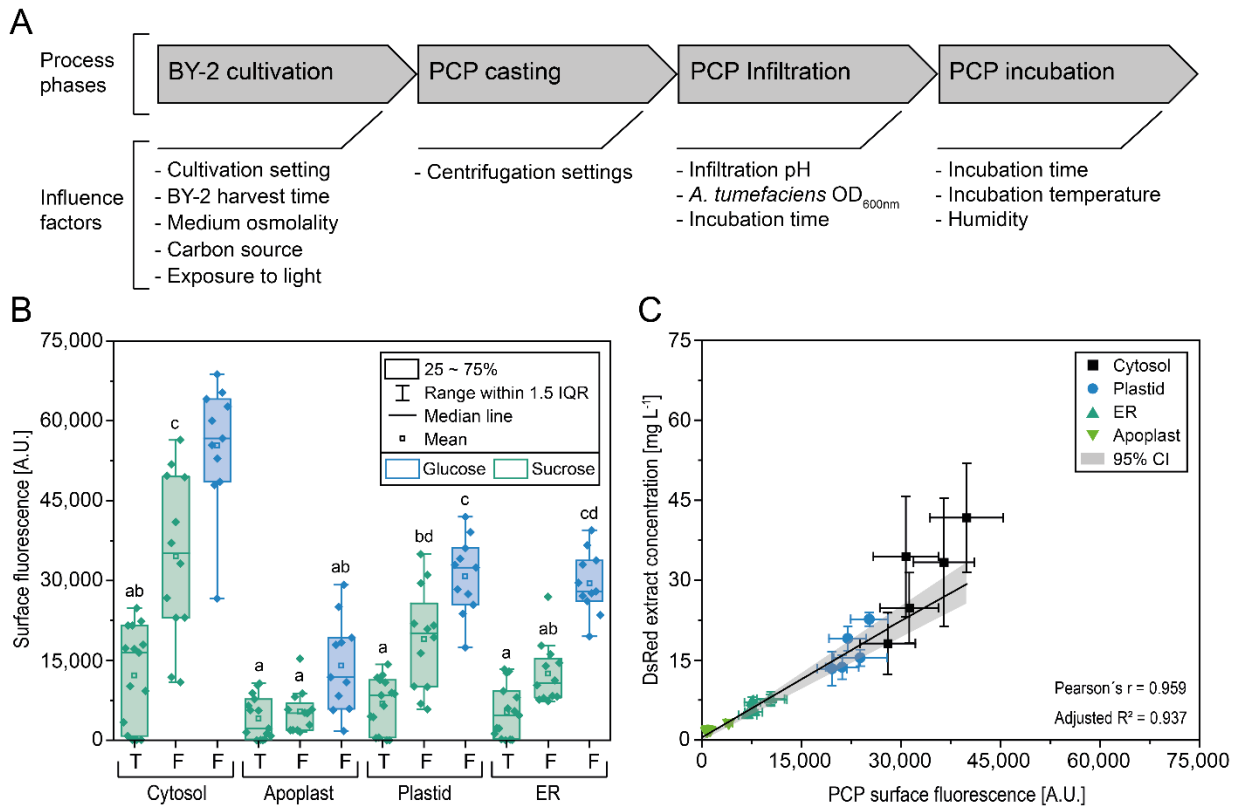


Figure 10: Phases during transient protein expression in PCPs and comparison of different BY-2 cultivation settings using DsRed as a model protein. A. Schematic representation of high-throughput screening in PCPs and influence factors investigated. B. Productivity of BY-2 PCPs depending on the targeted cell compartment, BY-2 cultivation setting and carbon source using the surface fluorescence as surrogate for DsRed accumulation (Supporting Table 11). C. Correlation between surface fluorescence and extract concentration of DsRed targeted to different cellular compartments. The slope and confidence interval of the error weighted (Equation 18) linear regression function was calculated with OriginPro. Error bars in (C) represent the standard deviation from $n = 3 - 7$ BY-2 PCPs. Lowercase letters indicate significance groups. Conditions that share the same letter were not significant different ($p > 0.05$). T – stirred tank, F – shake flask.

$$w_i = \frac{1}{\sigma_i^2} \quad \text{Equation 18}$$

Where w_i is the weighting factor and σ_i^2 is the variance of the data point.

The effect of the carbon source on BY-2 productivity was next investigated in detail by cultivating BY-2 cells in parallel with similar mass concentrations of sucrose and glucose and investigating macroscopic (wet cell mass and dry cell mass) and microscopic (cell number) properties of BY-2 cells under both conditions. DsRed was again used as a model to facilitate the evaluation of productivities under both conditions by measuring the PCP surface fluorescence. The latter correlated well (Pearson's $r = 0.96$) with the concentration of DsRed in PCP extracts (Figure 10C), which was in agreement with previous literature [151]. To avoid

artifacts from repeated sampling, multiple flasks were cultivated in parallel and only sampled a single time.

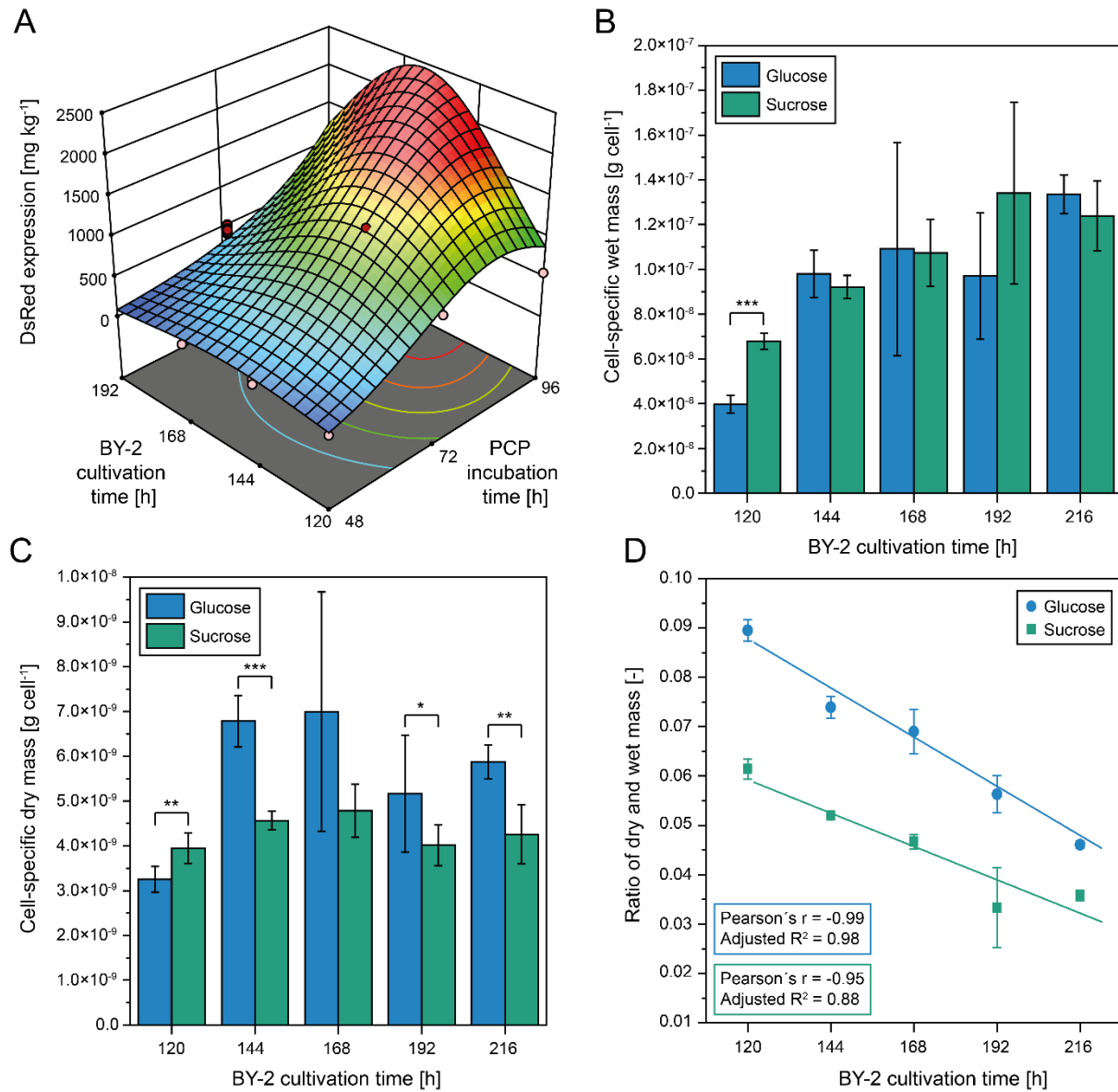


Figure 11: Analysis of different BY-2 cell harvest time points in shake flasks in terms of PCP productivity, cell growth and the cell-specific wet and dry mass. A. Model predicting the accumulation of DsRed in PCPs after infiltration with *A. tumefaciens* depending on the BY-2 and PCP harvest time point (Supporting Table 12). Data correspond to the expression of DsRed in BY-2 cells cultivated on glucose as carbon source. B. Cell-specific wet mass of BY-2 cells depending on the harvest time point in shake flasks. C. Cell-specific dry mass of the same samples as in (B). D. Ratio of the cell dry and wet mass during cultivation of BY-2 cells using sucrose or glucose as carbon source. The concentration of the carbon source was 30 g L⁻¹ in all settings. Error bars represent the standard deviation from n = 2 – 4 individual flasks with three technical replicates per measurement (*p < 0.05, **p < 0.01, ***p < 0.001).

The accumulation of DsRed in BY-2 PCPs correlated positively with the PCP incubation time after infiltration (Figure 11A), which was in agreement with the literature [151]. The highest DsRed accumulation (~2.0 g kg⁻¹) was observed when harvesting BY-2 cells after 144 – 168

hours to cast PCPs (Figure 11A). The cell-specific BY-2 wet mass continuously increased during BY-2 cultivation regardless of the carbon source used, reaching a plateau after ~216 hours. While the cell-specific BY-2 wet mass was comparable for both carbon sources (Figure 11B), the cell-specific dry mass was higher when using glucose instead of sucrose as carbon source (Figure 11C). The difference was significant ($p < 0.05$) for all but a single harvest time point, which exhibited a high variation of the cell number. The cell-specific dry mass reached a maximum after 144 – 168 hours of cultivation, which coincided with the maximum of DsRed accumulation (Figure 11A). The cell specific dry mass thus appeared to reflect the biosynthetic capacity per cell and can hence be used to estimate suitable BY-2 harvest time points.

The continuous increase of the BY-2 cell wet mass during cultivation can be attributed to a growth mode that is unique to plant cells, namely cell growth by elongation, i.e. the uptake of water into the central vacuole [311]. This hypothesis was supported by the decreasing ratio of cell-specific dry and wet mass during BY-2 cultivation (Figure 11D). Similarly, the increased productivity of BY-2 cells cultivated on glucose instead of sucrose was accompanied by a lower relative water content as indicated by the higher ratio of cell-specific dry mass and cell-specific wet mass (Figure 11D). Comparable observations have been reported in the literature, where a twofold reduction in the packed cell volume, a surrogate for the water content, resulted in 20-fold higher yields [139]. Likewise, the high yields achieved with BY-2 lysates (3.0 g L⁻¹ lysate [140]) can be partially attributed to the removal of water from BY-2 cells, i.e. a ~50% reduction of the cell volume by removing the vacuole [141].

III.2.3.3.2 Effect of the medium osmolality on BY-2 productivity

A major driver of water uptake into BY-2 cells is the osmolality of the cultivation medium [312], which is directly affected by the type and concentration of carbon source (i.e. a monosaccharide exhibits twice the osmolality than a disaccharide at similar mass concentrations). The effect of the medium osmolality on the productivity of BY-2 cells (in a PCP setting) was thus investigated next.

The productivity of BY-2 cells sampled through stirred tank cultivations varied severalfold in a PCP setting (Figure 12A). The productivity correlated with the medium osmolality measured at the respective cultivation time (Figure 12B) and was well described by a lognormal function (Equation 19). The BY-2 productivity reached a maximum at a medium osmolality of ~140 mOsmol kg⁻¹, while productivities declined at osmolality values < 100 and > 150 mOsmol kg⁻¹. A similar course was observed when changing the default infiltration pH from 5.6 to 7.5 (Figure 12B), which reduced the infiltration efficiency [313], indicating that the effect of the medium

osmolality had a generic effect on transient expression and was not limited to narrow experimental conditions.

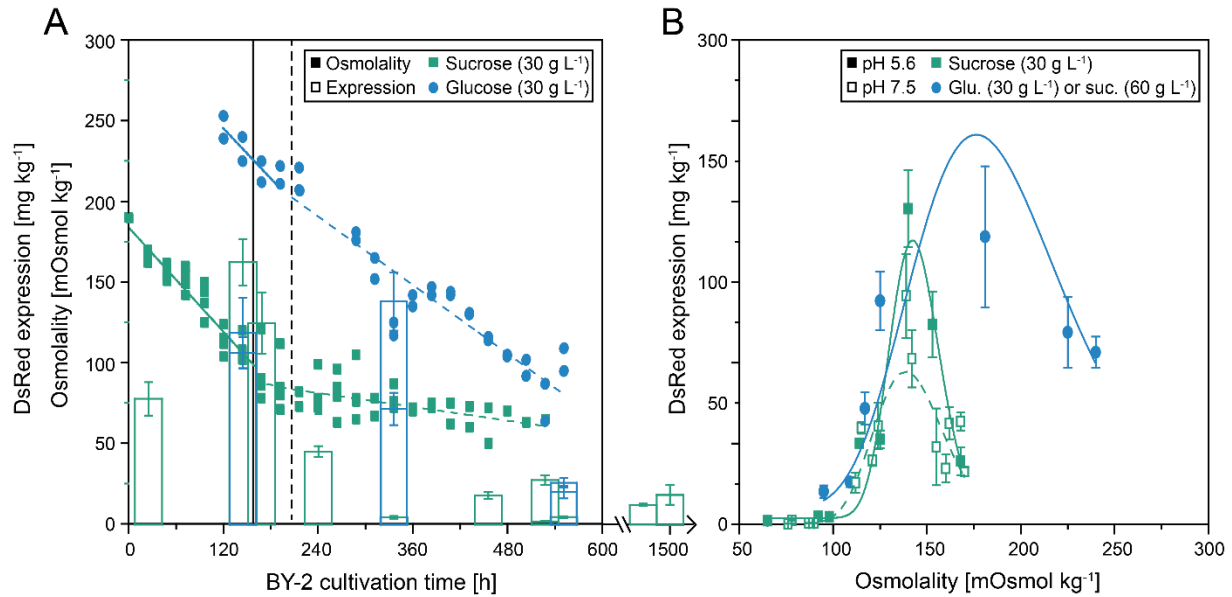


Figure 12: Effect of the carbon source on the medium osmolality and BY-2 productivity in stirred tank BY-2 cultures. A. Time course of the osmolality and BY-2 PCP productivity in stirred tank cultures depending on the carbon source. Sucrose (green) or glucose (blue) was used as the carbon source (30 g L⁻¹ in the batch phase, 20 g L⁻¹ in the fed-batch phase). Osmolality data were combined from four cultivations with sucrose and two cultivations with glucose as carbon source. The correlation between the medium osmolality and cultivation time was assessed by linear regression (batch phase sucrose, $r = -0.94$, adj. $R^2 = 0.88$; batch phase glucose, $r = -0.85$, adj. $R^2 = 0.65$; fed-batch phase sucrose, $r = -0.55$, adj. $R^2 = 0.28$; fed-batch phase glucose, $r = -0.93$, adj. $R^2 = 0.87$). B. Effect of the medium osmolality during BY-2 cultivation in stirred tanks with 30 or 60 g L⁻¹ sucrose or 30 g L⁻¹ glucose as carbon source on the productivity of BY-2 PCPs. The pH values refer to the conditions during infiltration with *A. tumefaciens*, which is most efficient under acidic conditions. Data were fitted to a lognormal model (Equation 19) using OriginPro (sucrose pH 5.6, adj. $R^2 = 0.85$; sucrose pH 7.5, adj. $R^2 = 0.86$; glucose pH 5.6, adj. $R^2 = 0.68$, Supporting Table 13). In all experiments PCPs were incubated for 72 hours after infiltration (II.4.1.4.2). Vertical lines in (A) denote the end of the batch phase for sucrose (solid line) and glucose dashed line). Error bars represent the standard deviation from $n = 4 - 7$ PCPs.

$$y = y_0 + \frac{A}{\sqrt{2\pi \cdot w \cdot x}} e^{-\frac{\left[\ln \frac{x}{x_c}\right]^2}{2w^2}} \quad \text{Equation 19}$$

Where y is the DsRed expression (the dependent variable), y_0 is the minimal DsRed expression (the minimal value (y -offset) of the distribution), x is the osmolality (the independent variable), x_c is the center of the distribution, w is the standard deviation (width) of the distribution, and A is the area under the curve.

Interestingly, the productivity decline at medium osmolalities > 140 mOsmol kg⁻¹ was less severe when using glucose instead of sucrose as carbon source or when doubling the sucrose concentration (Figure 12B). While the reduced BY-2 productivity at osmolalities < 100 mOsmol kg⁻¹ was linked to an increased water uptake as discussed above, the cause for the

effect of the high osmolality is not yet clear. One potential explanation is osmotic stress, leading to metabolic changes that limit protein biosynthesis as reported for the production of phenolic compounds [314].

The physiological origin of the productivity maximum observed when cultivating BY-2 cells at a medium osmolality of $\sim 145 \text{ mOsmol kg}^{-1}$ was investigated next, by converting the medium osmolality to osmotic pressure, followed by comparison with the osmotic potential reported for *N. tabacum* tissues in the literature. *N. tabacum* was chosen for comparison, because BY-2 cells originate from *N. tabacum* (root cells). Osmolality was converted to osmotic pressure π using Van't Hoff's law (Equation 20).

$$\pi = R * T * \frac{n}{V} \quad \text{Equation 20 [315]}$$

Where R is the gas constant, T is the absolute temperature in Kelvin (299°K at 26°C), n is the number of moles of a solute in solution, V is the mass of water in the solution and π is the osmotic pressure. The solute potential Ψ_s is related to the osmotic pressure as $\Psi_s = -\pi$ [316].

The medium osmolality that resulted in the highest productivities in BY-2 PCPs ($\sim 145 \text{ mOsmol kg}^{-1}$) corresponded to an osmotic potential of -0.36 MPa , which was close to the osmotic potential of $-0.42 \pm 0.07 \text{ MPa}$ reported for extracts of *N. tabacum* roots [317]. In contrast, a twofold higher osmolality ($\sim 288 \text{ mOsmol kg}^{-1}$) and consequently higher osmotic potential ($-0.65 \pm 0.04 \text{ MPa}$) was reported for extracts from *N. tabacum* leaves [317]. These data indicated that isotonic medium conditions might allow to boost the productivity of BY-2 cells, possibly because the cells have to spend less energy to maintain their turgor. The transferability to other plant cell lines has yet to be explored. In any case, the medium osmolality likely has to be optimized individually for different cell lines, given the differences in osmotic potential between plant species or different tissues of the same plant species [317].

III.2.3.3.3 Optimization of fed-batch cultivation conditions to improve BY-2 productivity

During stirred tank BY-2 cultivation with sucrose as carbon source, the medium osmolality fell below the critical threshold of $\sim 100 \text{ mOsmol kg}^{-1}$ within 7 days of cultivation, after which it stabilized at $\sim 75 \text{ mOsmol kg}^{-1}$ due to the constant feed that contained 20 g L^{-1} sucrose (Figure 12A). This agreed well with the low and varying DsRed expression over an extended duration (Figure 12A, Supporting Table 11), because BY-2 cells for casting PCPs were typically harvested after 14 – 60 days of stirred tank cultivation when the osmolality was already $< 100 \text{ mOsmol kg}^{-1}$. Consequently, there was only a narrow window where the medium osmolality was suitable for expression studies (Figure 12A).

When replacing sucrose with a similar mass concentration of glucose, it was possible to maintain medium osmolalities $> 100 \text{ mOsmol kg}^{-1}$ for approximately two weeks, thus stabilizing BY-2 productivities in the same timeframe (Figure 12A). This effect was transferred to routine BY-2 stirred tank cultivations next, by increasing the medium osmolality during the fed-batch phase with a twofold concentrated feed. As anticipated, BY-2 productivities stabilized during the fed-batch phase with DsRed accumulation levels of $\sim 250 \text{ mg kg}^{-1}$ (Figure S9A), which was more than fivefold of the accumulation observed with regular feed medium (Figure S9B). The vitality of BY-2 cells was not impaired by the increased medium osmolality as indicated by Evans blue staining [318]. However, the central vacuole in BY-2 cells appeared smaller compared to default cultivation conditions (Figure S10), thus indicating a reduced BY-2 water content. Because the medium osmolality resulting from the two-fold concentrated feed ($\sim 200 \text{ mOsmol kg}^{-1}$) exceeded the observed productivity optimum (Figure 12B), even higher BY-2 productivities might be possible by maintaining the medium osmolality in the range of the productivity optimum of $\sim 145 \text{ mOsmol kg}^{-1}$.

III.2.3.3.4 Effect of exposure to different light wavelengths on BY-2 productivity

An additional influence factor that might contribute to varying PCP productivities was the exposure of BY-2 cells to different light conditions during cultivation. Specifically, the mean productivity of PCPs cast from BY-2 cells cultivated in a stirred tank close to a window was higher ($26,985 \pm 13,015 \text{ AU}$, $154 \pm 74 \text{ mg kg}^{-1}$ DsRed, $n = 16$, data not shown) than the mean productivity of BY-2 cells cultivated in a stirred tank under artificial light ($12,186 \pm 9,265 \text{ AU}$, $69 \pm 53 \text{ mg kg}^{-1}$ DsRed, $n = 15$, Figure 10B). This observation was surprising at first, because the BY-2 cell line is derived from tobacco root cells and does not perform photosynthesis [319]. However, exposure to light has previously been shown to influence the ability of *A. tumefaciens* to transform plant cells, including those that are not photosynthetically active [320]. Because the spectra of artificial and natural light differed, i.e. artificial light featured narrow wavelengths while natural light was more homogenous (Figure S11), the effect of different light wavelengths on BY-2 cells was investigated systematically, using a DoE approach. UV light (350 – 380 nm) was excluded from the investigation, because this is known to induce programmed cell death in BY-2 cells [321]. BY-2 cells were continuously exposed to light (24 h d^{-1}) to accelerate the onset of light effects [320].

DsRed accumulation in PCPs increased with the proportion and intensity of blue light during BY-2 cultivation, whereas the productivity declined following exposure to far-red and red light compared to “white light”, which was simulated by exposure to equal intensities of blue, green, red and far-red light (Figure 13A).

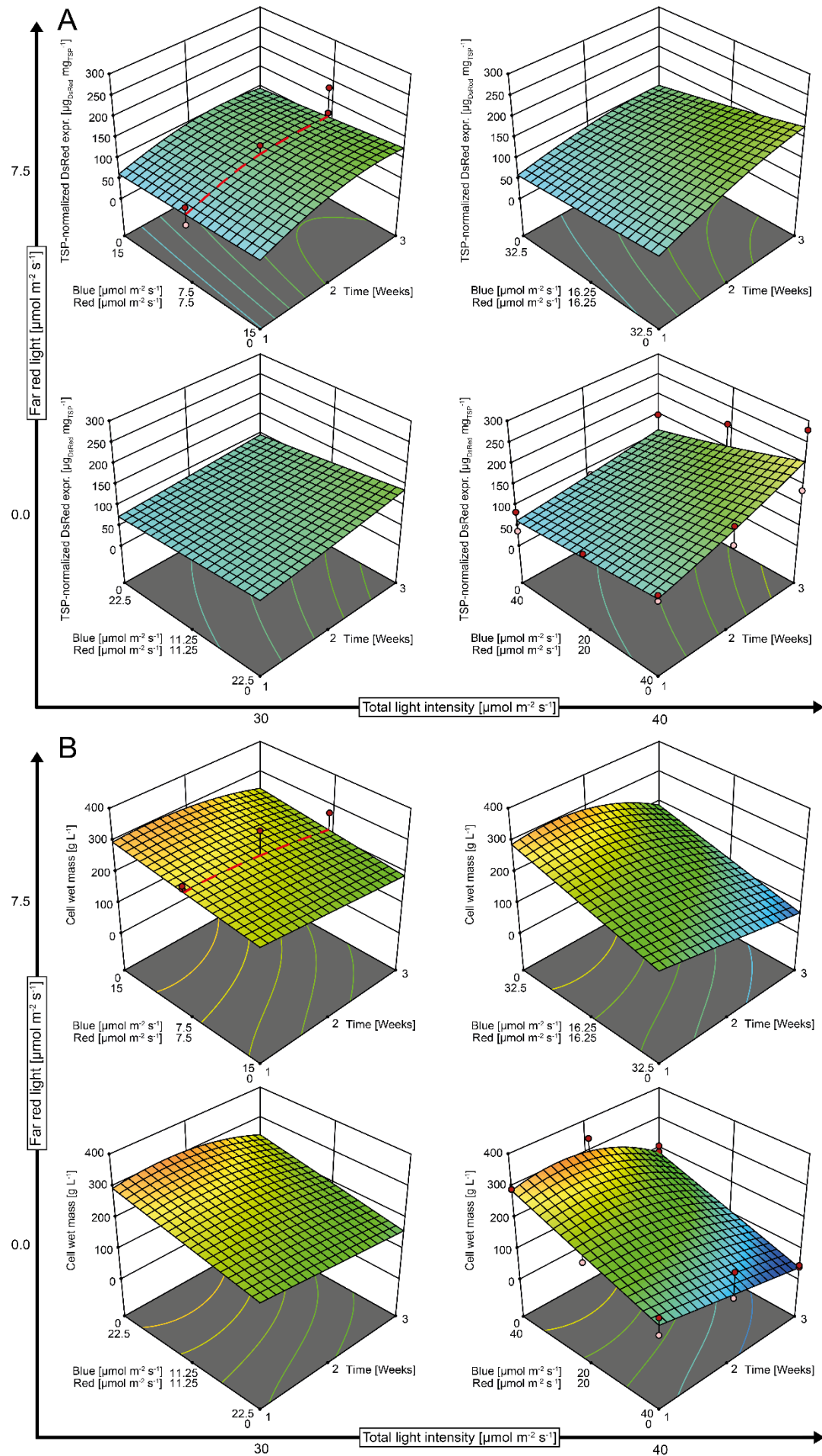


Figure 13: Models describing the effect of light on BY-2 cells and PCP productivity. A. Model for the concentration of DsRed in PCP extracts as quantified by fluorescence spectroscopy (Supporting Table 14). The DsRed concentration in PCP extracts was normalized to the TSP concentration in the same sample to compensate for differences during extraction. B. Model for the BY-2 cell mass following exposure to light as measured before casting PCPs for expression studies (Supporting Table 14). BY-2 cells were cultivated at 26°C, 160 rpm (II.4.1.1) and continuously (24 h d⁻¹) exposed to light in a LEDitSHAKE device [222]. BY-2 cells were harvested after 168 hours and PCPs were incubated for 72 hours post-infiltration with *A. tumefaciens*. Conditions representing “white light” (dashed red line) were simulated as mixtures of blue, green, red and far-red light (equal intensity).

The effect was independent of the targeted cell compartment and consistent with IgG1 as a second model protein [173]. An inverse effect was observed on the wet cell mass, i.e. the wet cell mass decreased when BY-2 cells were exposed to blue light and increased upon exposure to red or green light (Figure 13B). The effects on both DsRed accumulation and wet mass increased with longer exposure times.

Similar to the experiments discussed in the context of medium osmolality (III.2.3.3.2), light conditions resulting in the lowest wet cell mass coincided with the highest BY-2 productivity. These findings linked to the observations on osmolality and water uptake, because UV-B photoreceptors, which are typically upregulated in strongly illuminated environments with a large fraction of blue light, were also upregulated under osmotic stress conditions that limited cell expansion by preventing water uptake [322, 323]. It is currently unclear whether the effect of blue light is specific to root-derived cells, for which light stimuli have been reported [324], or whether it is a more widespread mechanism. However, exposure to different light conditions appeared to induce undesired variation in BY-2 productivity, even though BY-2 cells do not require light as an energy source, and should therefore be eliminated or controlled.

III.2.3.4 Origin of variation in differentiated plants

Even more than in BY-2 PCPs, screening in differentiated plants was complicated by a high inter and intra batch variation (15 – 50% [90]). An approach that has been proposed to overcome this issue is increasing the number of infiltrated plants [325]. However, this approach is not always feasible considering the additional foot print required for plant cultivation and incubation after infiltration. The focus here was hence to identify the major influence factors that affect transient protein accumulation, thus allowing to eliminate or control the origin of undesired variation (Figure 14A).

First, variation in the infiltrated leaf area was investigated in a vacuum infiltration setting, assuming that only leaf tissue that has been infiltrated with *A. tumefaciens* cell suspension can contribute to recombinant protein expression. Seasonal variation, which is known to influence recombinant protein expression [326, 327], was controlled by cultivating plants in a phytotron setting. Because the position of sampling spots and the age of plant leaves have been shown to

contribute to varying productivities [90], whole plants were infiltrated and extracted instead of sampling individual leaves.

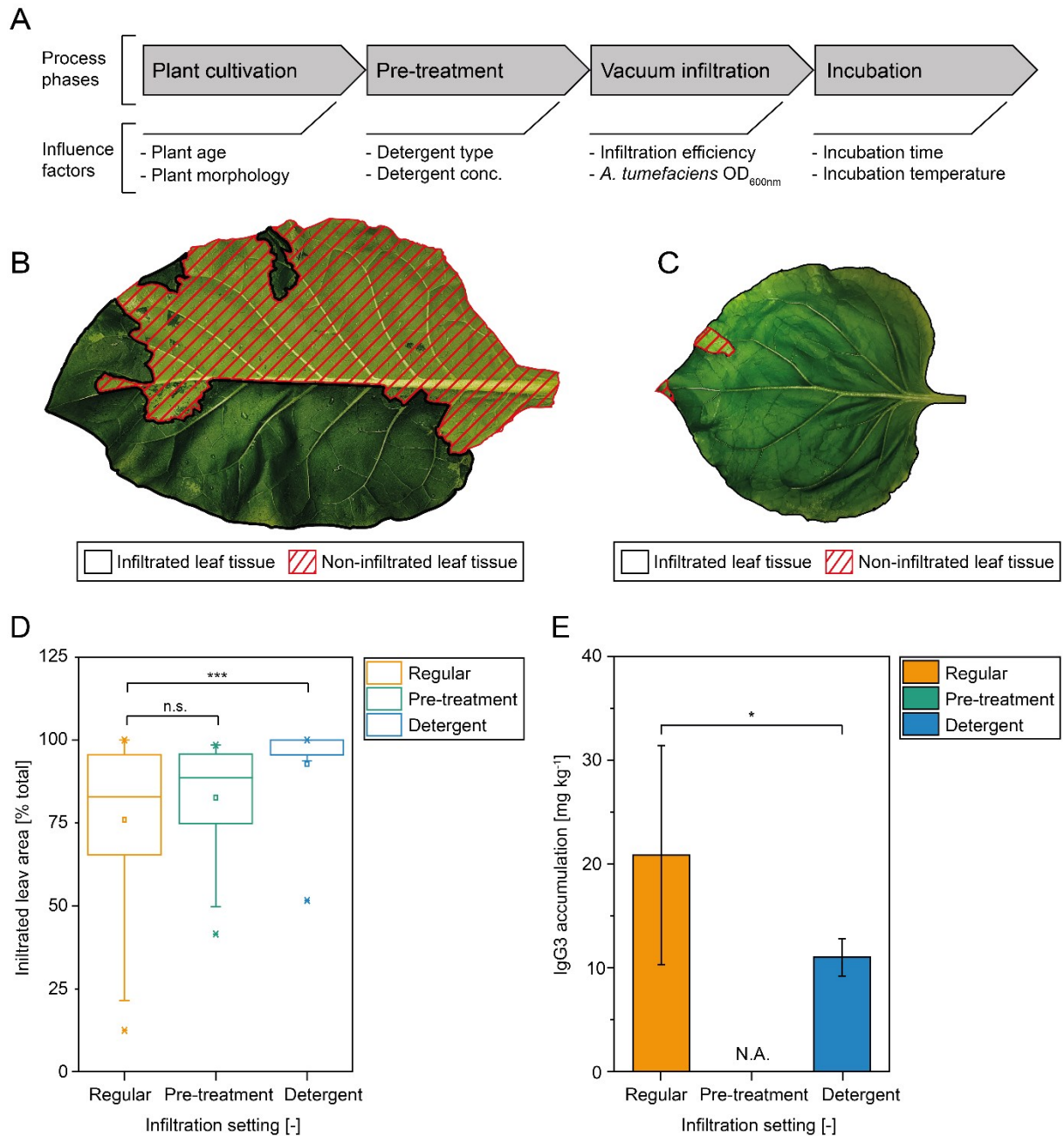


Figure 14: Phases during transient protein expression in whole plants and variation of the infiltrated leaf area in *Nicotiana* spp. A. Schematic representation of screening in whole plants and factors influencing productivity. B, C. Representative pictures of *N. tabacum* (A) and *N. benthamiana* (B) leaves after vacuum infiltration. Variation of the infiltrated leaf area was investigated by infiltrating 7 weeks old plants (II.4.2.2.1) and quantifying the total and infiltrated leaf area of each leaf using the software ImageJ. D, E. Infiltration efficiency and variation of target protein accumulation levels in different settings. Pre-treatment refers to the incubation of plants for 24 hours in plastic bags before infiltration. The detergent Silwet Gold was added to the infiltration solution at a concentration of 0.04% (v v⁻¹). IgG3 accumulation levels in plant extracts were quantified by SPR (II.6.3). Expression levels in (D) refer to total biomass. Error bars represent the standard deviation from n = 22 – 48 leaves (*p < 0.05, **p < 0.01, ***p < 0.001).

A monoclonal antibody (IgG3) was used as model protein, because antibodies can be accurately quantified in crude plant extracts using surface plasmon resonance spectroscopy [328], thus improving the signal to noise ratio and facilitating the identification of effects [329].

Whereas the infiltrated area of *N. benthamiana* leaves was ~95% after vacuum infiltration the infiltrated area of *N. tabacum* leaves was only $70 \pm 28\%$ after vacuum infiltration and varied considerably (Figure 14B, C). To improve the infiltration efficiency and reproducibly, an approach reported for *Arabidopsis thaliana* was tested, namely pre-incubation of plants in a plastic bag for 24 hours before infiltration to induce stomata opening [330]. The average infiltration efficiency increased from $70 \pm 28\%$ to $83 \pm 17\%$ after pre-incubation (Figure 14D), but the variation was not significantly different in both settings (Kruskal-Wallis ANOVA, $p = 0.411$, $N = 70$, $\alpha = 0.05$). Because the pre-incubation of plants in plastic bags doubled the hands-on time for vacuum infiltration from 10 minutes to 20 minutes per plant, the addition of a surface active agent to the infiltration solution was investigated as an alternative next. Surface active agents have again been successfully used to improve the infiltration efficiency in the context of *A. thaliana* plants [331]. The addition of 0.04% ($v v^{-1}$) Silwet Gold significantly (Kruskal-Wallis ANOVA, $p < 0.001$, $N = 74$, $\alpha = 0.05$) reduced the variation of the infiltrated leaf area of *N. tabacum* plants (Figure 14D). The average infiltrated leaf area increased to $93 \pm 13\%$, which was close to the efficiency observed with *N. benthamiana*. As anticipated, the significantly reduced variation of the infiltrated leaf area translated to a significantly reduced (two-sided, two-sample *F*-test, $p = 0.028$, $N = 6$, $\alpha = 0.05$) variation during recombinant protein expression (Figure 14E). However, the overall expression decreased by about half, indicating that the surface active agent negatively affected either *A. tumefaciens* or plants or potentially impaired DNA transfer between both. Consequently, future research should focus on identifying a suitable detergents and concentration ranges to benefit from the reduced variation of the infiltrated leaf area.

The plant age is known to influence transient protein expression in *N. benthamiana*, with a proposed optimal infiltration age of 8 – 10 weeks [332]. To investigate whether a defined harvest time point is sufficient to control variation in productivity resulting from differences in plant morphology, whole *N. benthamiana* and *N. tabacum* plants were infiltrated with constructs for expression of IgG3 as described above. Plants were infiltrated after 7 weeks of cultivation to simplify submerging of entire plants in *Agrobacterium* cell suspension for vacuum infiltration. Despite cultivating plants in a phytotron (to control seasonal variation) and harvesting after a defined time, i.e. 7 weeks of cultivation, the fresh biomass varied considerably between individual plants (Figure 15A, B).

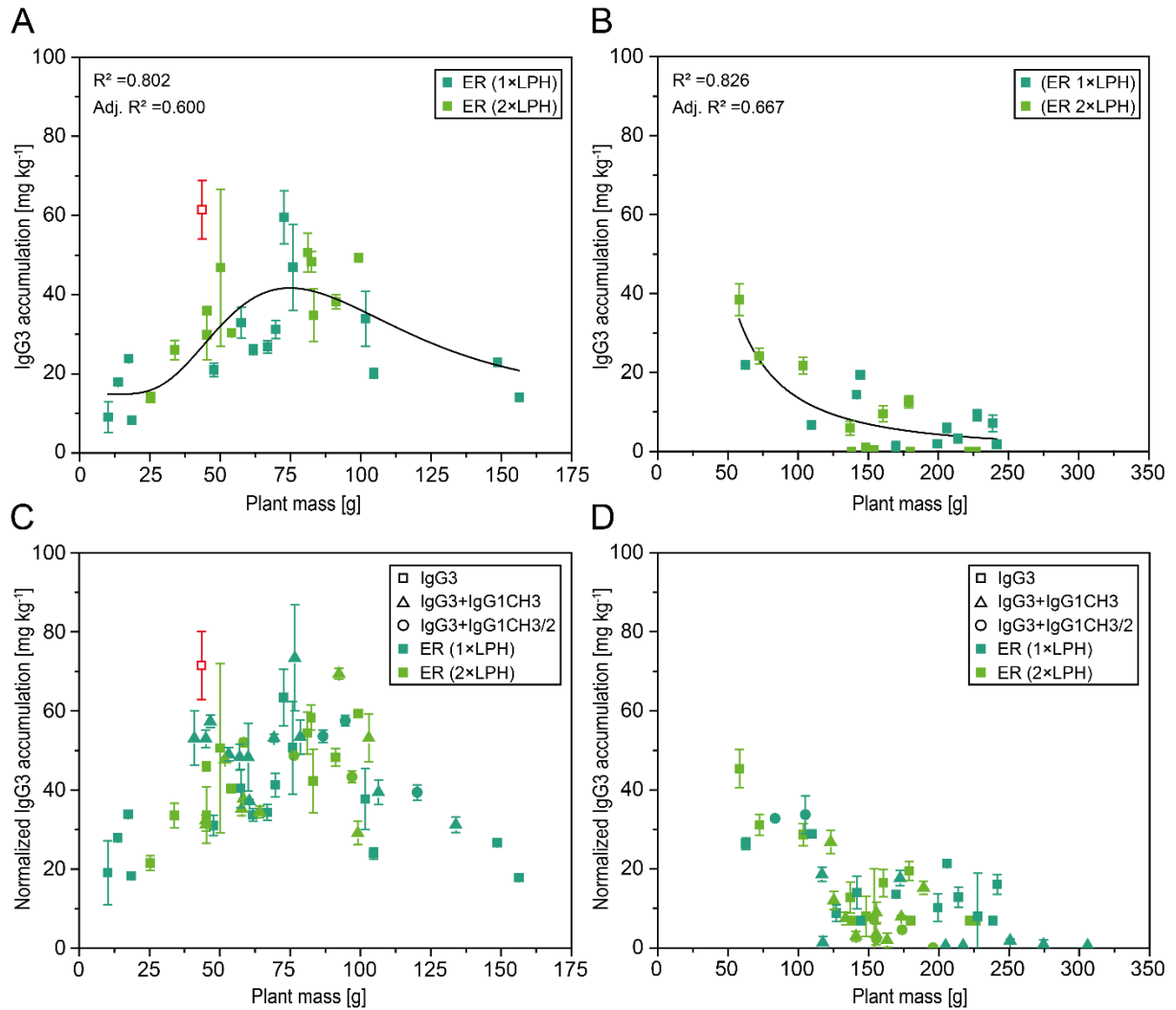


Figure 15: Effect of the plant morphology on the productivity during transient protein expression in *N. benthamiana* and *N. tabacum*. A, B. Expression of native IgG3 antibodies (single and duplicate leader peptide) in the ER in *N. benthamiana* (A) and *N. tabacum* plants (B). IgG3 accumulation levels with a single and duplicate leader peptide were combined for curve fitting because both can be regarded as derived from the same population (i.e. both data sets were normally distributed and the variance and mean did not differ significantly). Data from *N. benthamiana* were fitted to a lognormal model (Equation 19) and data from *N. tabacum* were fitted to an allometric model (Equation 21). Statistical analysis and fitting (Supporting Tables 15, 16) were conducted with OriginPro. C, D. Expression of native IgG3 and IgG1 domain exchange variants in the ER in *N. benthamiana* plants (C) and in *N. tabacum* plants (D). DoE model coefficients (Supporting Table 8) were used to normalize for the effects of different antibody scaffolds, allowing to compare the accumulation levels of native IgG3 and IgG1 domain exchange variants. Data points marked in red correspond to partially withered plants, which artificially reduced the water content. Error bars represent the standard deviation from $n = 3 - 6$ plants. ER – endoplasmic reticulum, LPH – leader peptide of the antibody mAb24 heavy chain, IgG3+IgG1CH3 – IgG3 domain exchange variant containing an IgG1 CH3 domain, IgG3+IgG1CH3-2 – IgG3 domain exchange variant containing IgG1 CH2 and CH3 domains.

$$y = a x^b$$

Equation 21

Where y is the IgG3 accumulation (dependent variable), x is the plant mass (independent variable), a is the coefficient and b the power.

The productivity, as assessed by the accumulation of IgG3 antibodies, correlated with the biomass and was well described by a lognormal function (Equation 19) in *N. benthamiana* plants (Figure 15A) and an allometric function (Equation 21) in *N. tabacum* plants (Figure 15B). The highest IgG3 accumulation in both *N. benthamiana* and *N. tabacum* was observed for plants with a biomass of ~80 g, whereas IgG3 accumulation decreased in plants with a biomass > 80 g. Interestingly, IgG3 accumulation also decreased in *N. benthamiana* plants with a biomass < 80 g (Figure 15A, C). Similar trends were observed, when including the accumulation levels of additional IgG variants (Figure 15C, D).

A comparable relationship of fresh biomass and productivity has been reported for *N. benthamiana* plants that were harvested and infiltrated after 4 – 12 weeks of cultivation, with the highest recombinant protein accumulation observed in plants that were cultivated for 8 – 10 weeks before infiltration [332]. The observation has previously been attributed to sequential senescence, i.e. the programmed decrease of soluble protein in aging leaves [333]. In agreement with this hypothesis, a reduced productivity has been observed in old plant leaves compared to young leaves in multiple studies [332–334]. The hypothesis was also consistent with a positive correlation of TSP and IgG3 accumulation observed here (Figure S12).

These data indicated that harvesting plants based on a defined physiology rather than based on a defined time point can help to reduce inter and intra batch variation during recombinant protein production. In the context of automated cultivation in a vertical farm setting, 2D or 3D imaging can be used to monitor the plant physiology during cultivation and sort out plants that don't match predefined criteria, as recently proposed [100]. However, whether plants with a sub-optimal morphology have to be discarded or can still be used at a different harvest time point has to be investigated in the future.

III.2.4 Novel applications for PCPs

Section III.2.4.1 is a shortened version of the following manuscript: Opdensteinen, P., Sperl, L.E., Mohamadi, M., Kündgen-Redding, N., Hagn, F. and Buyel, J.F. (2022), The transient expression of recombinant proteins in plant cell packs facilitates stable isotope labeling for NMR spectroscopy. *Plant Biotechnology Journal*, 20(10), 1928-1939. The Co-authors have contributed to the manuscript as follows: Laura Sperl und Mariam Mohamadi cloned control constructs for GB1 expression in *E. coli*, expressed GB1 in *E. coli* and conducted NMR measurements. Nicole Kündgen-Redding cultivated BY-2 cells. Johannes Felix Buyel und Franz Hagn secured funding, supported data analysis and revised the manuscript.

III.2.4.1 Isotope labeling in PCPs

Labeling recombinant proteins with stable isotopes allows to investigate protein structures and dynamics in solution [335], which can help to understand disease mechanisms and facilitate the development of therapeutics [336, 337], as recently demonstrated for the SARS-CoV-2 spike protein [338]. To facilitate the characterization of proteins that are difficult to produce in established bacterial systems, for example due to the need for post translational modifications (PTMs), the suitability of BY-2 PCPs for labeling of transiently expressed proteins with isotopes was investigated. Because previous research in BY-2 cells has focused on a single isotope (^{15}N [339]), labeling experiments were carried out with deuterium oxide (^2H), ^{15}N , and combinations of both isotopes (Supporting Table 17). GB1 was used as a model for expression studies, because it has been well characterized by NMR [340, 341], allowing to compare plant-made GB1 with the bacterial counterpart. The protein was cloned with a C-terminal His₆ tag to facilitate purification by IMAC.

GB1 expression in PCPs was successful with BY-2 cells cultivated in media containing deuterium oxide (50% v v⁻¹), ^{15}N or both isotopes (Figure S13A, B). The highest GB1 accumulation was ~55 mg kg⁻¹ (Figure S13B), which matched accumulation levels of labeled GB1 in *E. coli* [342]. Interestingly, GB1 accumulation levels in media containing isotopes were significantly higher compared to a control without isotopes (Figure S13B), despite a reduced cell vitality (Supporting Table 17). While the increased productivity of BY-2 cells cultivated in the presence of labeled nitrogen might reflect altered protein expression levels (compared to ^{14}N [343]), the increased productivity of BY-2 cells cultivated in the presence of deuterium oxide appeared to result from a reduced water content as indicated by a reduced wet cell mass at the time of PCP preparation. Specifically, BY-2 cells cultivated in 50% v v⁻¹ deuterium oxide only reached a wet cell mass of 90.5 g L⁻¹ compared to 280.0 ± 14.7 g L⁻¹ in the other media (Supporting Table 17). A potential explanation for the reduced water content is the inhibition of cell elongation (i.e. the uptake of water), which has been reported for root cells of other plant species in the presence of deuterium oxide [344]. The effect of the water uptake on the productivity of BY-2 cells was consistent with the systematical investigations of water uptake and BY-2 productivity discussed above (III.2.3.3.2).

For analysis by ESI-MS and NMR spectroscopy GB1 was purified from extracts of BY-2 PCPs cultivated on all isotope containing media as well as a control without isotopes by immobilized metal affinity chromatography (IMAC, Figure 16A, B). The IMAC protocol was designed to facilitate rapid purification of target proteins from PCP extracts, using a 30 mM imidazole

washing step to remove non-specifically bound HCPs, before eluting GB1 with 300 mM imidazole.

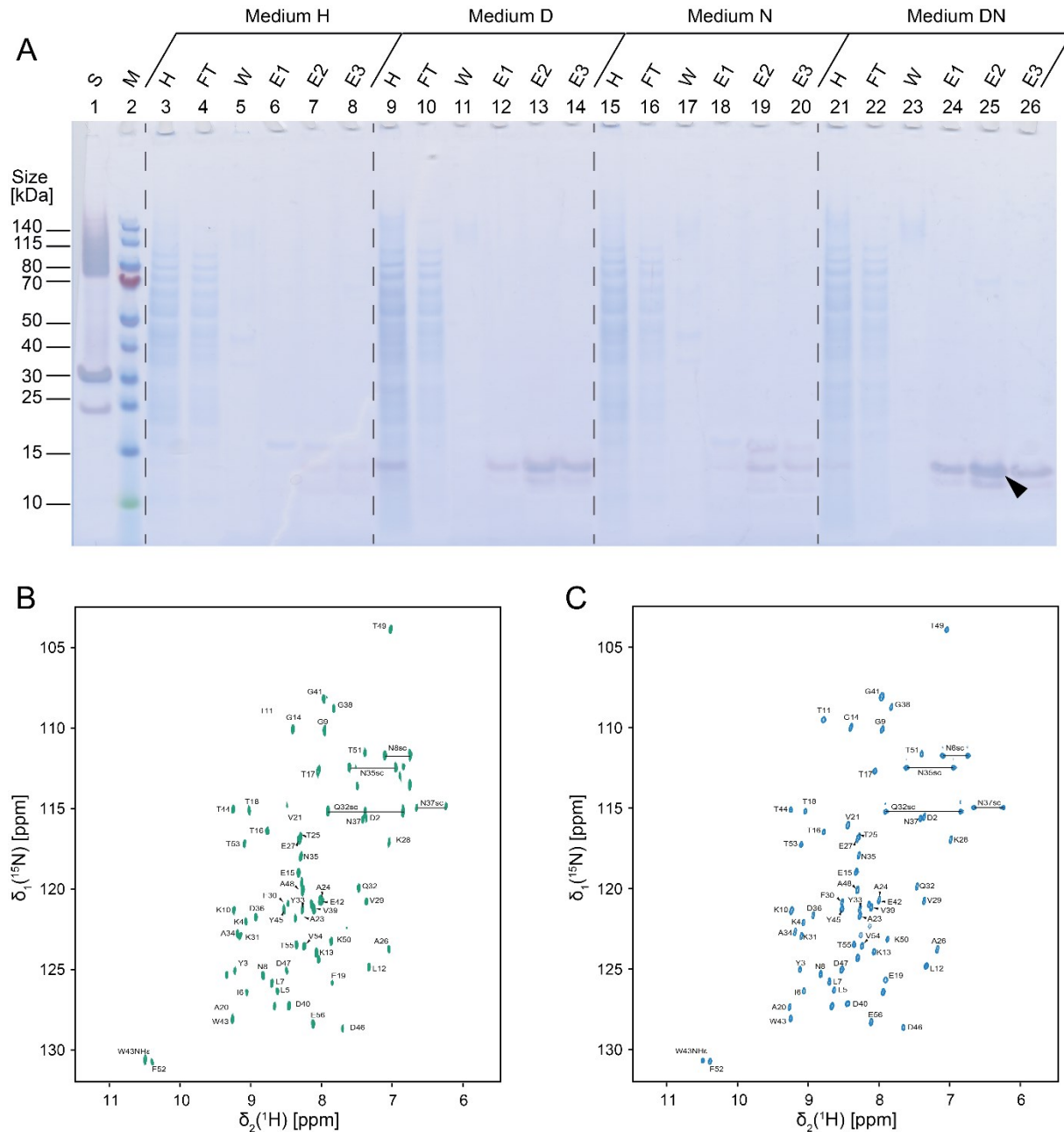


Figure 16: Production of isotope-labeled GB1 in BY-2 PCs and characterization by 2D-NMR spectroscopy. A. Overlay of a Coomassie-stained LDS gel and western blot with samples from purification of plastid-targeted GB1 from BY-2 PCs by IMAC. BY-2 cells were cultivated in MS medium containing 30 g L⁻¹ glucose and optionally 50% (v v⁻¹) deuterium oxide (medium D, VII.7), ¹⁵N-labelled ammonium nitrate (medium N, VII.7) or both isotopes (medium DN, VII.7). MS medium without isotopes was used as control (medium H, VII.7). BY-2 cells were cultivated for 7 days and incubated for 96 hours after infiltration with *A. tumefaciens* (II.4.1.1). A rabbit anti-His₆ primary antibody and an alkaline phosphatase-labeled goat anti-rabbit secondary antibody were used for GB1 detection on the western blot. C, D. Comparison of 2D-[¹⁵N,¹H]-HSQC spectra of plant-made GB1 (C) and GB1 produced in *E. coli* (D). Identical construct designs (C-terminal His₆-tag) and isotopes (¹⁵N and ²H) were used for GB1 production in *E. coli* and BY-2 PCs. D – medium prepared with 50% (v v⁻¹) deuterium oxide, N – medium prepared with labeled ammonium nitrate, DN – medium prepared with 50% (v v⁻¹) deuterium oxide and labeled ammonium nitrate, S – DsRed standard (10 µg mL⁻¹), M – marker, H – homogenate, FT – flowthrough, W – imidazole buffer wash, E – eluate.

Using this strategy, GB1 was obtained with a high purity ($> 95\%$) and recovery ($80 \pm 28\%$), despite using low extract volumes (≤ 15 mL) for chromatography.

NMR spectra of plant-made GB1 and GB1 produced in *E. coli* were almost identical (Figure 16C, D), indicating that the plant-made GB1 was folded correctly. The labeling efficiency was close to 100% for labeled nitrogen, which matched labeling efficiencies in *E. coli* [345]. Resulting from the relatively low deuterium oxide volume fraction of $50\% \text{ v v}^{-1}$, the labeling efficiency of deuterium oxide was only 16%. To allow the analysis of proteins > 30 kDa [346] the efficiency of deuterium labeling needs to be improved to $> 70\%$ [347], which can be achieved e.g. by adapting BY-2 cells to deuterium oxide volume fractions $> 50\%$ over time (Supporting Table 17).

Overall, these data indicated that PCPs can complement existing systems for the production of isotopically labeled proteins, especially in the context of target proteins that are incompatible with mammalian cells or difficult to produce in bacteria due to the need for complex PTMs. However, to facilitate multi-dimensional NMR experiments, 1 – 10 mg of labeled target protein would be required depending on the target protein size. Such amounts of labeled target proteins can be produced for example by scaling up PCPs to 100 g [171] or improving the productivity of PCPs, as demonstrated above (III.2.3.3).

III.2.4.2 High throughput infiltration-centrifugation in BY-2 PCPs

Plant-based expression systems allow to direct target proteins to different cell compartments, thus offering a high degree of flexibility for recombinant protein expression. Targeting recombinant proteins to the apoplast is especially interesting, because this extracellular compartment is located outside of the plasma membrane and proteins can be extracted without disrupting the plant tissue by infiltration-centrifugation [348]. Infiltration-centrifugation refers to the replacement of the air space in the apoplast with an infiltration solution, which is then recovered by centrifugation [132]. The technique has been tested with plant tissues from various species [349] as well as non-differentiated BY-2 cells [171], but to date the method has not been adapted to a high-throughput format. To facilitate high-throughput screening of plant-made proteins, infiltration-centrifugation was therefore adapted to BY-2 PCPs cast in 96-well plates.

The efficacy of infiltration-centrifugation with BY-2 PCPs was tested by infiltrating PCPs cast in 96-well plates with constructs for targeting DsRed to the apoplast and cytosol, respectively. DsRed was used as a model protein to facilitate quantification by measuring the fluorescence in a plate reader. DsRed was additionally targeted to the cytosol to confirm that DsRed in elution fractions did not originate from rupture of the cell tissue during centrifugation. Three different

buffer formulations were tested for infiltration-centrifugation, namely tap water, regular extraction buffer (VII.6) and extraction buffer supplemented with detergent (VII.6) to investigate the potential for optimization of infiltration-centrifugation in the context of PCPs.

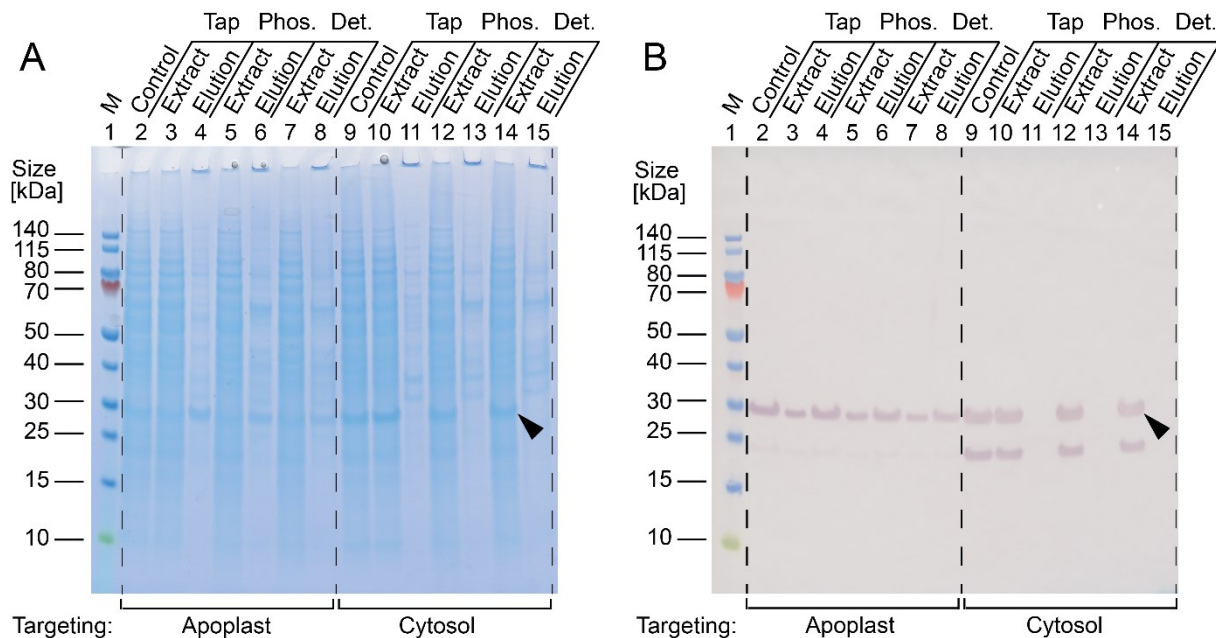


Figure 17: Extraction of recombinant proteins from BY-2 PCPs in 96-well plates by infiltration-centrifugation. A, B. Analysis of PCP extracts (II.5.2.1) and infiltration-centrifugation eluates (II.5.2.2) from PCPs expressing DsRed in the cytosol and apoplast by LDS gel electrophoresis and staining with Coomassie Brilliant Blue (A) or western blotting (B) using goat anti-mCherry (TA150126) and AP-labeled anti-goat antibodies. PCPs were cast from BY-2 cells cultivated in shake flasks using 30 g L⁻¹ glucose as carbon source. PCPs were incubated for 96 hours after infiltration with *A. tumefaciens*. Tap – tap water, Phos. – regular extraction buffer (VII.6), Det. – detergent extraction buffer (VII.6).

As anticipated, the model protein DsRed was only detectable in infiltration-centrifugation elution fractions when DsRed had been targeted to the apoplast (Figure 17). No DsRed was present in elution fractions when targeting DsRed to the cytosol despite extract accumulation levels of 620 mg kg⁻¹ in this compartment, indicating that the centrifugal force used (1500 × g) did not damage the cell tissue. These results were in agreement with literature recommending centrifugal forces of ~1000 × g for infiltration-centrifugation [349]. Maintaining the cell integrity is a prerequisite of multiple infiltration-centrifugation rounds, which allows for continuous harvest of protein directed to the apoplast as previously suggested for leaves of differentiated plants [350].

The highest DsRed purity (57.8 ± 12.0% TSP) was observed when using tap water for infiltration-centrifugation (Table 13), whereas the DsRed purity decreased when using phosphate extraction buffer (39.2 ± 7.7% TSP) or extraction buffer supplemented with detergent (24.4 ± 3.6% TSP) for infiltration-centrifugation (Table 13). The decreasing DsRed purity appeared to reflect the ability of the respective buffers to solubilize host cell proteins

(HCPs), as indicated by LDS gel electrophoresis, i.e. more HCPs were eluted when using complex buffer formulations compared to tap water, thus decreasing the DsRed purity (Figure 17A). In agreement with this hypothesis, the zwitterionic detergent CHAPS, which was used for the buffer with the lowest DsRed purity, has been reported to improve protein solubilization [351].

When compared to extraction in a bead mill, the DsRed recovery after a single cycle of infiltration-centrifugation was $49.8 \pm 10.6\%$, resulting in a DsRed yield of $210.8 \pm 23.5 \text{ mg kg}^{-1}$ (Table 13). The recovery was in agreement with literature reporting a DsRed recovery of 40% [171], while the DsRed yield was threefold higher, which can be attributed to optimized BY-2 cultivation conditions (III.2.3.3.1). The reduced recovery compared to bead mill extraction was expected, considering that some DsRed molecules are still being trafficked through the secretory pathway. However, unlike PCP extraction with a bead mill, infiltration-centrifugation offers the possibility for repeated target protein harvest by applying multiple rounds of infiltration-centrifugation to the same PCPs, thus allowing to increase the product recovery or recover labile target proteins [171].

Table 13: Comparison of different infiltration-centrifugation buffers for elution of DsRed from the apoplast of BY-2 PCPs cast in 96-well plates. BY-2 PCPs were infiltrated by applying a vacuum of 10 kPa for 1 minute (II.5.2.2). A single centrifugation cycle was used to harvest apoplastic fluid.

Buffer [-]	Purity bead mill extraction [% TSP]	Purity infiltr. centrifugation [% TSP]	Recovery infiltr. centrifugation [% bead mill]	Yield infiltr. centrifugation [mg kg ⁻¹]
Tap water	8.5 ± 0.5	57.8 ± 12.0	49.8 ± 10.6	210.8 ± 23.5
Phosphate buffer	7.5 ± 1.1	39.2 ± 7.7	45.8 ± 8.9	193.8 ± 18.3
Detergent buffer	7.3 ± 1.5	24.4 ± 3.6	33.6 ± 5.7	142.0 ± 9.7

BY-2 cells used to cast PCPs were cultivated on glucose, harvested after 7 days of cultivation and were incubated for 72 hours post infiltration with *A. tumefaciens*. An incubation time of 30 minutes and $1500 \times g$ was used for infiltration centrifugation (II.5.2.2). Data values with variance indicate the standard deviation from $n = 4$ PCPs. Buffer formulations are provided in the appendix section (VII.6).

Overall, these data indicated that infiltration-centrifugation can simplify the extraction of target proteins from PCPs cast in 96-well plates, thus omitting the need for tissue disruption and chromatography before the functionality of a target protein can be assessed.

III.3 Purification of target proteins from plant extracts

To facilitate a potential application of the plant-made target proteins expressed in this work in the context of infections with MRSA (III.1.1.1), purification processes were established for all target protein classes. Similar to cloning (III.1) and expression (III.2), automation with a liquid

handling station was used to increase the throughput during screening for ideal chromatography conditions (III.3.1). Based on the screening results in miniaturized chromatography columns, which are compatible with automation on a liquid handling station, scalable purification processes were established in the laboratory scale (III.3.2).

III.3.1 High-throughput screening of chromatography conditions

To be able to keep up with the increased throughput resulting from automation of cloning and expression, target proteins cloned with the modular vector system featured a His₆-tag to facilitate rapid purification by IMAC (III.1.1.1). IMAC was chosen for target protein purification, because this method is cost efficient and compatible with mild elution conditions such as physiological pH [352], thus simplifying the retrieval of active target proteins [353]. Compared to other affinity separation technologies IMAC is considered less specific [352], but target protein purities up to 95% can still be achieved by carefully optimizing the chromatography conditions [354]. To increase the purity of His-tagged proteins purified from plant extracts, the removal of plant HCPs that persist after IMAC was investigated by washing with low concentrations of imidazole (10 – 60 mM). Imidazole acts as a competitor to histidine during IMAC, thus releasing bound protein [355]. PPKs were used as model proteins with moderate accumulation levels, because high concentrations of specifically binding target proteins can displace non-specifically binding HCPs, thus increasing the purity of elution fractions disproportionately. Miniaturized chromatography columns (0.2 mL, Supporting Table 18) were used in combination with a liquid handling station to parallelize and speed-up screening of imidazole concentrations for washing.

Imidazole concentrations ≥ 10 mM eluted a distinct group of HCPs that co-purified with His-tagged PPK-RO and PPK-TA expressed in *N. benthamiana* (Figure 18A, B). These HCPs were enriched about fourfold compared to the feed (based on densitometric evaluation), indicating that certain *N. benthamiana* HCPs preferentially interacted with the nickel-charged chromatography resin. This observation can be attributed to the presence of consecutive histidine residues in HCPs, which is more prominent in eukaryotic expression systems such as mammals compared to bacterial expression systems [354]. The HCPs persisting after IMAC (Figure 18A, red arrows) were analyzed by mass spectrometry and corresponded to serine hydroxymethyltransferase, glutamine synthetase, xyloglucan hydrolase and a major latex protein (Supporting Table 19). Serine hydroxymethyltransferase and glutamine synthetase form large oligomers of ~475 kDa and ~200 kDa, whereas xyloglucan hydrolase and the major latex protein are small (17 and 34 kDa), thus facilitating size-based separation methods for removal of these HCPs. This was investigated below by implementing ultrafiltration/diafiltration

(UF/DF) before IMAC (III.3.2.3). The concentration of TSP in IMAC wash fractions, i.e. the amount of HCPs eluted, increased with the concentration of imidazole in the wash buffer (Figure S14).

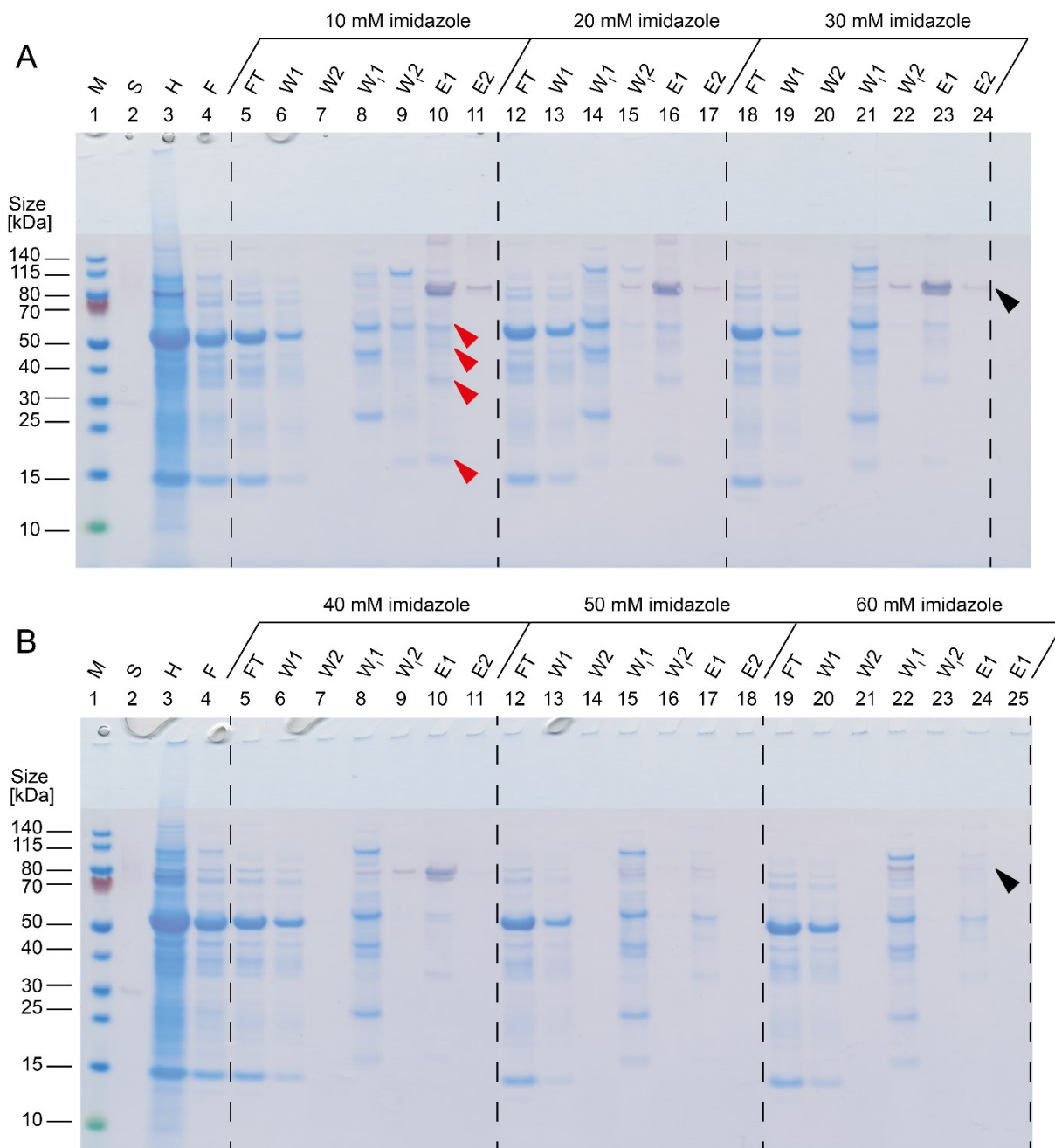


Figure 18: High-throughput screening of IMAC wash buffers on a liquid handling station. A, B. Overlay of Coomassie-stained LDS gels and western blots with samples from purification of His-tagged PPK-RO from *N. benthamiana*. Chromatography was performed with pre-packed Chelating Sepharose FF columns (0.2 mL column volume) on a Janus G3 liquid handling station, using 2 mL clarified *N. benthamiana* extract as feed (II.5.3) and 500 μ L buffer for washing (no imidazole, VII.6), removal of HCPs (10 – 60 mM imidazole, VII.6) and elution (300 mM imidazole, VII.6). The contact time was 2 min during all steps. Black arrows indicate the expected molecular mass of PPK-RO, red arrows indicate HCPs. His-tagged PPK-RO was detected on western blots using rabbit anti-His₆ and AP-labelled goat anti-rabbit antibodies. M – marker, S – DsRed standard (10 μ g mL⁻¹), H – homogenate, F – IMAC feed, FT – IMAC flow-through, W – equilibration buffer wash, W₁ – imidazole buffer wash, E – IMAC elution fractions.

A maximum PPK-RO purity of ~20% (assessed by densitometric evaluation of LDS gels) was achieved in IMAC elution fractions when washing with 30 mM imidazole (Figure S14), corresponding to a threefold increased purity compared to washing with 10 mM imidazole and an approximately fortyfold increased purity compared to the feed. When exceeding an imidazole concentration of 30 mM in the wash buffer, the PPK-RO purity in IMAC elution fractions dropped to < 5% (Figure 18B). This observation can be attributed to the elution of the target protein as indicated by analysis of IMAC fractions by LDS gel electrophoresis and western blotting (Figure 18, black arrows). To allow an effective separation of His-tagged target proteins from HCPs that co-purified during IMAC, the target protein affinity to the resin should be equivalent to approximately 70 mM imidazole (Figure S14C, D). Because the binding affinity of the His-tag correlates with the tag lengths [356], such an increase in affinity can be achieved by extend the His₆-tag, for example to 7 or 8 histidine residues. However, the effect of additional histidine residues on the tagged protein should be carefully investigated. A major drawback that was observed during screening of chromatography conditions with miniaturized columns (200 µL) was drop carry-over during elution, which essentially mixed different IMAC fractions. This problem was overcome by inverting the flow direction for 20 µL after every elution fraction, using the lowest possible flowrate of the device (~50 µL min⁻¹) to avoid disturbing the resin.

Overall, these results indicated that liquid handling stations in combination with miniaturized chromatography columns can facilitate the screening of chromatography conditions in the context of plant extracts. The transferability of the screening results from miniaturized chromatography columns to the laboratory scale was investigated next (III.3.2).

III.3.2 Laboratory scale target protein purification

III.3.2.1 Clarification of plant extracts in the laboratory scale

A major bottleneck that limited target protein yields when establishing scalable purification processes in the laboratory scale was clarification, which is typically conducted by filtration and/or centrifugation [357]. When using diatomite filters [358] to clarify plant extracts containing target proteins other than IgG, low recoveries ≤ 20% were common (Table 14), which have previously been attributed to binding of proteins to diatomaceous earth [358]. However, when directly mixing plant extracts containing IL8 with 5 g L⁻¹ (0.5% m v⁻¹ [359]) diatomaceous earth, IL8 recoveries were 99.3 ± 3.8% (n = 3), thus indicating that diatomaceous earth was not the cause for low target protein recoveries. It appears hence likely that the low target protein recoveries originated from adsorption to the positively-charged resin binder rather than diatomaceous earth, as previously reported [360]. Clarification by ultra-centrifugation

restored target protein recoveries to $> 90\%$ (Table 14), but the scalability of ultra-centrifugation can be difficult due to changes in the apparatus geometry [357]. To overcome these limitations glass fiber (GF) filters, which are scalable but do not contain diatomaceous earth nor a positively charged resin, were tested for clarification of plant extracts next. GF filters with a nominal retention rating of $1.2\ \mu\text{m}$ restored the recovery of IL8 and DspB during clarification to $> 60\%$ (Table 14), albeit at the cost of a \sim twentyfold increased turbidity ($97.8 \pm 9.1\ \text{NTU}$) compared to filtration with a diatomite filter ($5.4 \pm 2.3\ \text{NTU}$). However, the increased turbidity did not seem to impair the purification of these target proteins by UF/DF as discussed below (Figure 19C, D, Figure 20A, B). Further improvements of target protein recovery as well as filtrate turbidity can be expected by systematically testing combinations of GF filters with different retention ratings, which will be investigated in the future.

III.3.2.2 Transferability between liquid handling station and laboratory scale

Next, the transferability of screening results from miniaturized chromatography columns (III.3.1) to the laboratory scale was investigated, again using PPKs as model proteins. The purity of PPK-RO (assessed by densitometric evaluation) in IMAC elution fractions from 1.0 mL and 50.0 mL columns ($18.8 \pm 6.9\%$, $n = 4$) matched the purity observed with the miniaturized 0.2 mL columns (18.3%), using a 30 mM imidazole washing step in all settings. HCPs persisting after IMAC in the laboratory scale matched the HCPs observed in the miniaturized format (Figure 19A, E_{step}), indicating that screening results from miniaturized chromatography columns were transferable to the laboratory scale.

A limitation of the liquid handling station was the difficulty to realize gradients for target protein elution, as each chromatography column was connected to a single pump [361]. Gradient elution experiments (Figure 19A, Table 14) can be used to refine the conditions for a step elution and are hence a powerful tool for chromatography optimization [362]. An approach that has been proposed to implement gradients on liquid handling stations is to mimic gradients with a series of step elutions, using multiple different buffers [363]. However, additional time is required to prepare the respective buffers, thus depreciating the reduced hands-on time during chromatography screening with a liquid handling station.

III.3.2.3 Combined UF/DF and IMAC purification process

Because the purity of recombinant proteins required for pharmaceutical applications typically exceeds 95% [364] and thus far exceeded the $\sim 20\%$ purity obtained after a single IMAC purification step (III.3.1), IMAC was next combined with size-based separation using UF/DF. A size-based purification method was chosen, because major HCPs persisting after IMAC

formed large multimers of ~ 475 kDa and ~ 200 kDa (III.3.1), thus facilitating their separation from smaller recombinant proteins based on size. [130]. Similarly, RuBisCO, which alone accounts for up to $\sim 30\%$ of TSP in *N. tabacum* [130], forms a ~ 560 kDa hetero-hexadecamer and can thus be removed with the same approach. UF/DF was chosen for size-based purification, because the method is gentle, scalable [365] and can be used to remove bulk water before chromatography, thus reducing processing times [130].

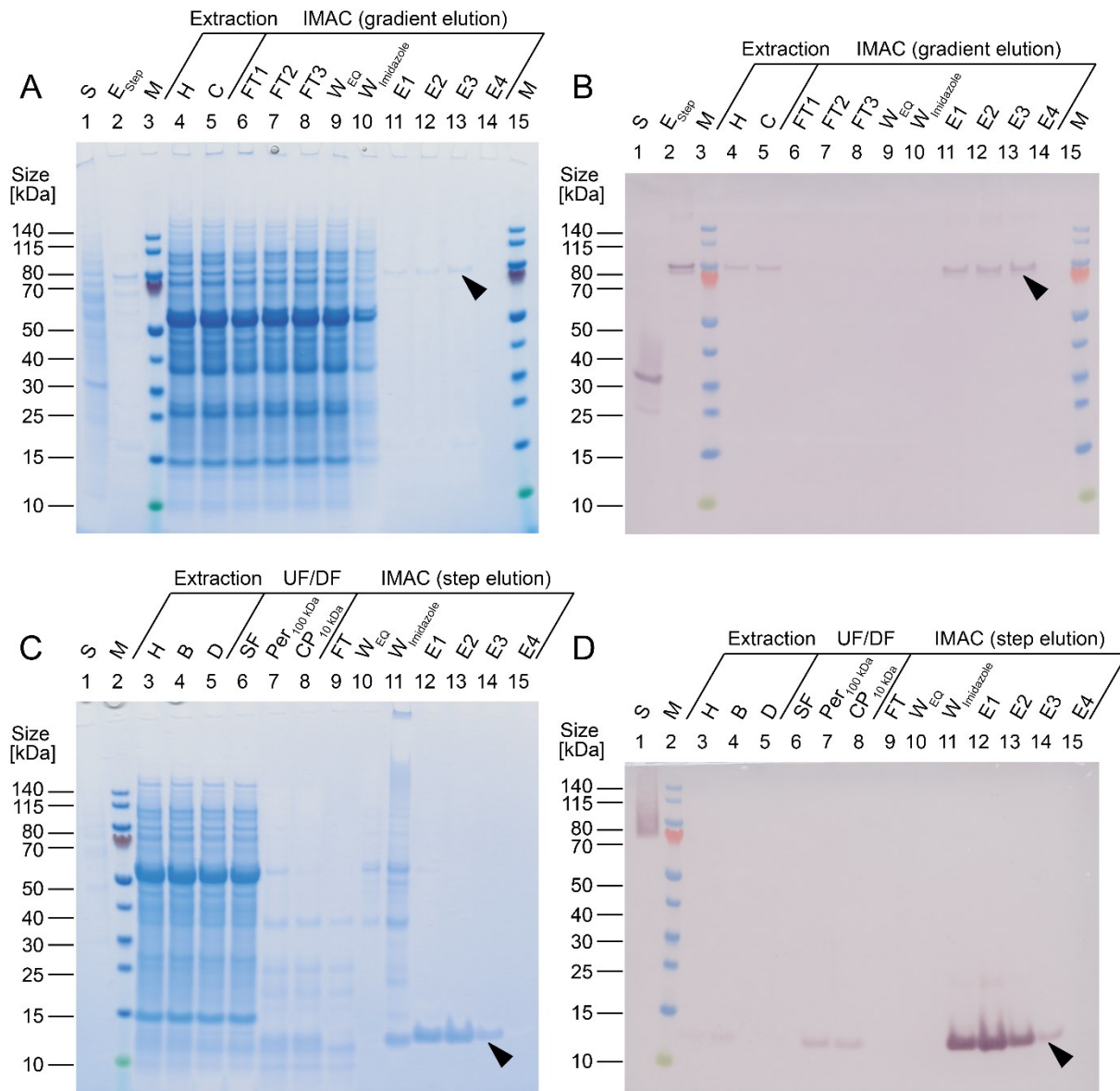


Figure 19: Laboratory scale purification of PPK-RO and IL8 from *N. benthamiana*. A, B. Samples from PPK-RO purification were analyzed on a Coomassie-stained LDS gel (A) and by western blot (B) using rabbit anti-His and AP-labeled goat anti-rabbit antibodies. Gradient elution was performed with 100 mM imidazole over 10 column volumes. C, D. Samples from IL8 purification were analyzed similarly. S – DsRed standard ($10 \mu\text{g mL}^{-1}$), H – homogenate, B – bag filtrate, C – centrifugation supernatant, D – depth filtrate (glass fiber filter), SF – sterile ($0.2 \mu\text{m}$) filtrate, FT – flow-through, W_{Eq} – equilibration buffer wash, W_{imidazole} – imidazole buffer wash, E – IMAC eluate.

Hydrophilic regenerated cellulose (RC) membranes were chosen over commonly used hydrophobic polyether sulfone or polypropylene membranes to minimize membrane fouling [366], i.e. the loss of membrane performance through deposition of dissolved substances on the membrane surface or pores. Limited by the current lack of RC membranes with cut-off sizes between 100 and 300 kDa [130], a 100 kDa membrane was initially tested for pre-purification of plant extracts before IMAC. To facilitate testing, the small (< 50 kDa) target proteins IL6, IL8 and DspB were used as models, because they should readily permeate a 100 kDa membrane.

As anticipated, oligomeric HCPs persisting after IMAC (III.3.1) were retained by a 100 kDa membrane, whereas recombinant IL6 (20.9 kDa) and IL8 (8.4 kDa) accumulated in the permeate (Figure 19C, D, Table 14). The permeate from the 100 kDa membrane was re-concentrated with a 10 kDa membrane to remove bulk water and thus accelerate subsequent chromatographic purification by IMAC [130]. The combination of UF/DF and IMAC achieved an IL8 purity > 95%, thus meeting the anticipated purity threshold. The same purification strategy was successfully applied for the purification recombinant DspB (42.0 kDa) from plant extracts (Figure 20A, B), again achieving a purity > 95% (Figure 20A, B, Table 14). These data indicated that UF/DF can simplify the purification of target proteins of at least ~40 kDa from plant extracts, while maintaining scalability of the process. For larger or multimeric target proteins an inverse strategy can be utilized, for example by using a 300 kDa membrane to retain the target protein and wash out smaller HCPs [130]. Further improvements of the selectivity during UF/DF can be expected by optimizing the UF/DF pH, which had a major impact on protein retention [130]. Specifically, a pH close to the isoelectric point of major *Nicotiana* HCPs favored HCP permeation, whereas a higher pH favored HCP retention [130].

Implementing UF/DF before chromatography allowed to remove bulk water from the purification process, which reduced the overall processing time and process footprint [130].

Additionally, pre-concentrating the target protein before IMAC was desirable, because the target protein purity in IMAC elution fractions has been shown to correlate with the amount of His-tagged protein in the sample. The effect has previously been attributed to displacement of HCPs by the His-tagged target protein, given the higher affinity of the latter to the ion-charged resin due to the dedicated tag [354]. For purification of antibodies protein A chromatography is the industry standard [367]. However, IgG3 antibodies produced herein are not bound by protein A, thus facilitating a potential application in the context of MRSA, but complicating IgG3 purification. As an alternative to protein A, protein G chromatography was thus investigated for IgG3 purification. As anticipated, protein G chromatography achieved high

IgG3 purities of ~95% (Figure 20C, D, Table 14) in a single step, thus matching the literature [368]. However, the recovery during protein G chromatography was < 20% (Table 14), whereas the recovery after IMAC was typically > 70%, which was in agreement with the literature [369]. Because the low recovery limited the overall process yields during IgG3 purification, future research should focus on optimizing protein G chromatography, for example by replacing the acidic elution currently used, with gentler elution compared to the currently used acidic (pH 2.0 – 3.0) elution to prevent IgG3 denaturation [370].

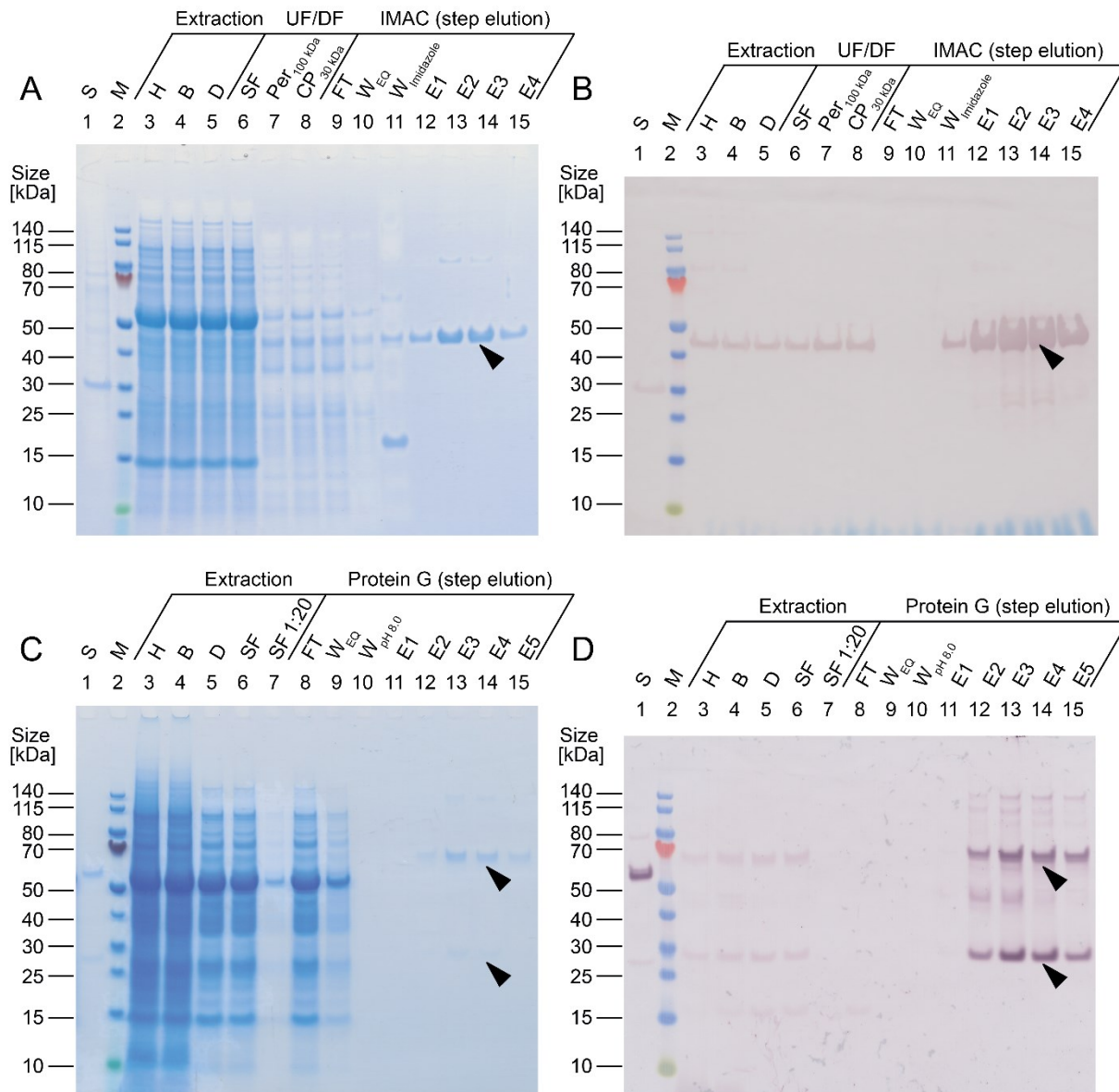


Figure 20: Laboratory scale purification of DspB and IgG3 from *N. benthamiana*. A, B. Samples from DspB purification were analyzed on a Coomassie stained LDS gel (A) and by western blot (B) using rabbit anti-His and AP-labeled goat anti-rabbit antibodies. C, D. Samples from IgG3 purification were analyzed similarly using AP-labeled goat anti-human IgG and goat anti-human Ig λ antibodies for the western blot. S – Standard (10 $\mu\text{g mL}^{-1}$ DsRed (A, B) or 7.5 $\mu\text{g mL}^{-1}$ IgG1 (C, D)), H – homogenate, B – bag filtrate, D – depth filtrate (glass fiber filter (A, B) or PDH4 (C, D)), SF – sterile (0.2 μm) filtrate, FT – flow-through, W_{EQ} – equilibration buffer wash, W_{imidazole} – imidazole buffer wash, W_{pH 8.0} – alkaline buffer wash, E – IMAC (A, B) or protein G (C, D) eluate.

Table 14: Purification of polyphosphate kinases, interleukins, dispersin B and IgG3 antibodies from *N. benthamiana*. Data correspond to 7 week old plants infiltrated without any silencing suppressor. Entire plants (including the stem) were extracted after 5 dpi.

	PPK-RO		PPK-TA		IL6		IL8		DspB		IgG3	
Process step [-]	Step purity [%]	Step recovery [%]	Step purity [%]	Step recovery [%]	Step purity [%]	Step recovery [%]	Step purity [%]	Step recovery [%]	Step purity [%]	Step recovery [%]	Step purity [%]	Step recovery [%]
Extraction^a	Regular: < 0.5 Detergent: (< 1.0)	100	Regular: < 0.1 Detergent: (< 0.5)	100	Regular: < 0.5	100	Regular: < 0.5	100	Regular: < 0.5	100	Regular: < 0.5	100
Bag filtration	< 0.5	98.7	n.a.	n.a.	< 0.5	84.3	< 0.5	99.4 ± 0.8	< 0.5	89.3 ± 2.6	< 0.5	72.2 ± 3.1
Clarification^b	Diatomite: (< 1.0) Centrifuge: < 0.5	Diatomite: (10.8 ± 5.1) Centrifuge: 96.7	Diatomite: (< 0.5) Centrifuge: n.a.	Diatomite: (16.5 ± 5.1) Centrifuge: n.a.	Diatomite: < 0.5	Diatomite: 48.2 ± 10.2	Diatomite: (< 0.5) GF: < 0.5	Diatomite: (20.8 ± 2.1) GF: 66.6 ± 5.2	Diatomite: (< 0.5) GF: < 0.5	Diatomite: (13.4) GF: 93.3 ± 6.2	Diatomite: < 0.5	Diatomite: 72.2 ± 3.5
UF/DF^c	Not used		Not used		(3.1 ± 0.3)	(84.2 ± 6.4)	8.3 ± 3.9	89.5 ± 5.7	4.4 ± 3.8	79.2 ± 11.8	Not used	
Affinity chromatography^d	Step elution: 18.8 ± 6.9 Gradient: 94.6	Step elution: 79.1 ± 3.9 Gradient: 70.5	Step elution: 21.6	Step elution: 79.6	Step elution: 4.6 ± 1.0	Step elution: 78.8 ± 28.3	Step elution: 97.8	Step elution: 64.5	Step elution: 96.1 ± 1.6	Step elution: 74.7 ± 5.4	Step elution: 94.9 ± 3.2	Step elution: 16.7 ± 3.2
Yield [mg kg⁻¹]	7.76 ± 0.83		8.13		0.16		8.86		5.99 ± 1.05 164.0 ^e		1.51 ± 0.24 9.5 ^e	

^a plants were extracted with 3 v m⁻¹ of regular or modified extraction buffer (VII.6). ^b extracts were clarified (II.5.3) with a diatomite filter, by centrifugation or with a 1.2 µm glass fiber (GF) filter. ^c UF/DF was conducted with a 100 kDa membrane (II.5.4), followed by re-concentration of the permeate with a 10 kDa (IL) or 30 kDa membrane (DspB). ^d PPKs, ILs and DspB were purified by IMAC using a 30 mM imidazole washing step (II.5.5.1), whereas IgG3 was purified by protein G chromatography (II.5.5.2). ^e Process yields when suppressing gene silencing in *N. benthamiana* with the tombusvirus p19 protein (non-optimized setting). If available, standard deviations were calculated from n = 3 – 4 processes. Values in brackets correspond to exploratory experiments that were not used for the subsequent process steps.

III.4 High-throughput target protein quantification and characterization

After combining high-throughput cloning using modular vectors (III.1) with high-throughput expression in PCPs (III.2), quantification and characterization of target proteins became a bottleneck that limited the screening throughput, thus emphasizing the need for high-throughput compatible assays. Surface plasmon resonance (SPR) spectroscopy assays allow real time monitoring of binding interactions without the need for labeling [371] and state of the art instruments offer a throughput of ~100 – 400 assays per day [371], thus matching the throughput during screening in PCPs. Compared to widely used methods such as enzyme-linked immunosorbent assay (ELISA), SPR assays are less dependent on the operator experience, reducing the variability from > 10% observed in ELISA assays [372] to ~2% (CV, n = 14) in SPR assays. Thus, to facilitate target protein quantification, a high-throughput compatible SPR assay was established that is independent of the target protein class and size (III.4.1). To simplify the characterization of biofilm degrading enzymes, the DoE approach was combined with a multi-well based biofilm degradation assay (III.4.2).

III.4.1 High-throughput quantification of His-tagged proteins by SPR

III.4.1.1 Sensor functionalization

Small target proteins (< 10 kDa [182]) are difficult to quantify in direct SPR assays (Figure 21A), because the resonance signal is directly proportional to the molecular mass of the analyte. To facilitate the rapid quantification of target proteins regardless of their size, an indirect SPR assay based on binding inhibition was thus chosen for high-throughput quantification. The assay was based on the His₆-tag to facilitate detection of target proteins from different classes. The tag-based detection has a high synergy with the indirect assay format (Figure 21A), because simple peptides rather than complex molecules can be used for immobilization. Peptides are typically more stable than proteins [373], thus increasing the sensor lifetime, which is desirable because of high costs of SPR sensor chips [374].

First, different peptide designs were compared, aiming to improve accessibility of the His₆-tag after immobilization (Supporting Table 20). Peptides were immobilized by amine coupling through primary amine groups present at the N-terminus of peptide chains as well as in the amino acid lysine [187]. Because the peptides used did not contain lysine, immobilization was expected to occur at the N-terminus. To mimic the anticipated application, i.e. quantification of target proteins in crude samples, extracts of wildtype *N. benthamiana* plants were diluted in different assay buffers and spiked with anti-His antibody as ligand to assess the assay specificity

under different conditions (Supporting Table 20). The highest ratio of specific to non-specific binding was observed with peptide P1, when using PBS-T assay buffer in combination with a flow rate of $10 \mu\text{L min}^{-1}$ (Supporting Table 20). The peptide design that performed best (P1) featured 3 alanine acting as spacer and was thus identical to the tag design used for recombinant proteins expressed in *Nicotiana* spp. (III.1.1.1). The lower ratio of specific and unspecific binding with HBS-EP assay buffer compared to PBS-T was surprising, because binding of anti-His antibodies to His-tagged proteins was not affected by EDTA or high sodium chloride concentrations (up to 1.0 M) in the literature [375], which constitute the main differences between both buffers (VII.6). In agreement with these data, the signal from specific binding of the anti-His antibody was only $\sim 19\%$ lower in HBS-EP compared to PBS-T, whereas the signal from unspecific binding increased twofold, indicating that the assay buffer primarily affected the binding of HCPs rather than binding of the anti-His antibody (Supporting Table 20).

Peptide-coated sensors were stable for at least 6 months when stored in sterile PBS at 4°C . A capacity loss of $\sim 6\%$ was observed after 40 injections (Figure S15A, B), allowing to use functionalized sensors for extended periods of time, which is desirable given the high costs of SPR sensor chips [374]. In contrast, direct SPR assays based on an immobilized antibodies often fail after only 10 regeneration cycles [376, 377]. The increased stability of the peptide sensor compared to an antibody-based sensor can be attributed to the higher stability of small peptides compared to complex proteins as discussed above. Nevertheless, to compensate for a changing sensor capacity and to increase the assay accuracy, injections with a defined standards should be included in routine assays, for example after 5 – 10 cycles of sample injection and regeneration.

III.4.1.2 Sensor characterization

Because a stable interaction between analyte and ligand is required for a reliable assay, the dissociation rates (k_d) of several commercial anti-his antibodies were assessed next, by injecting different antibody concentrations on a sensor functionalized with peptide P1. The dissociation rate was independent of the antibody concentration in these experiments (Figure 21B), but the signal to noise ratio improved, when increasing the antibody concentration (Figure S15C). The dissociation rates derived for MonoRab and THE-His anti-His antibodies were in the range of $9.0 \times 10^{-5} - 1.0 \times 10^{-4} \text{ s}^{-1}$ (Supporting Table 21), indicating a stable interaction between antibody and immobilized peptide. The dissociation rate measured with a control antibody (Dianova anti-His₆) was in the range of dissociation rates reported in the literature (Supporting Table 21).

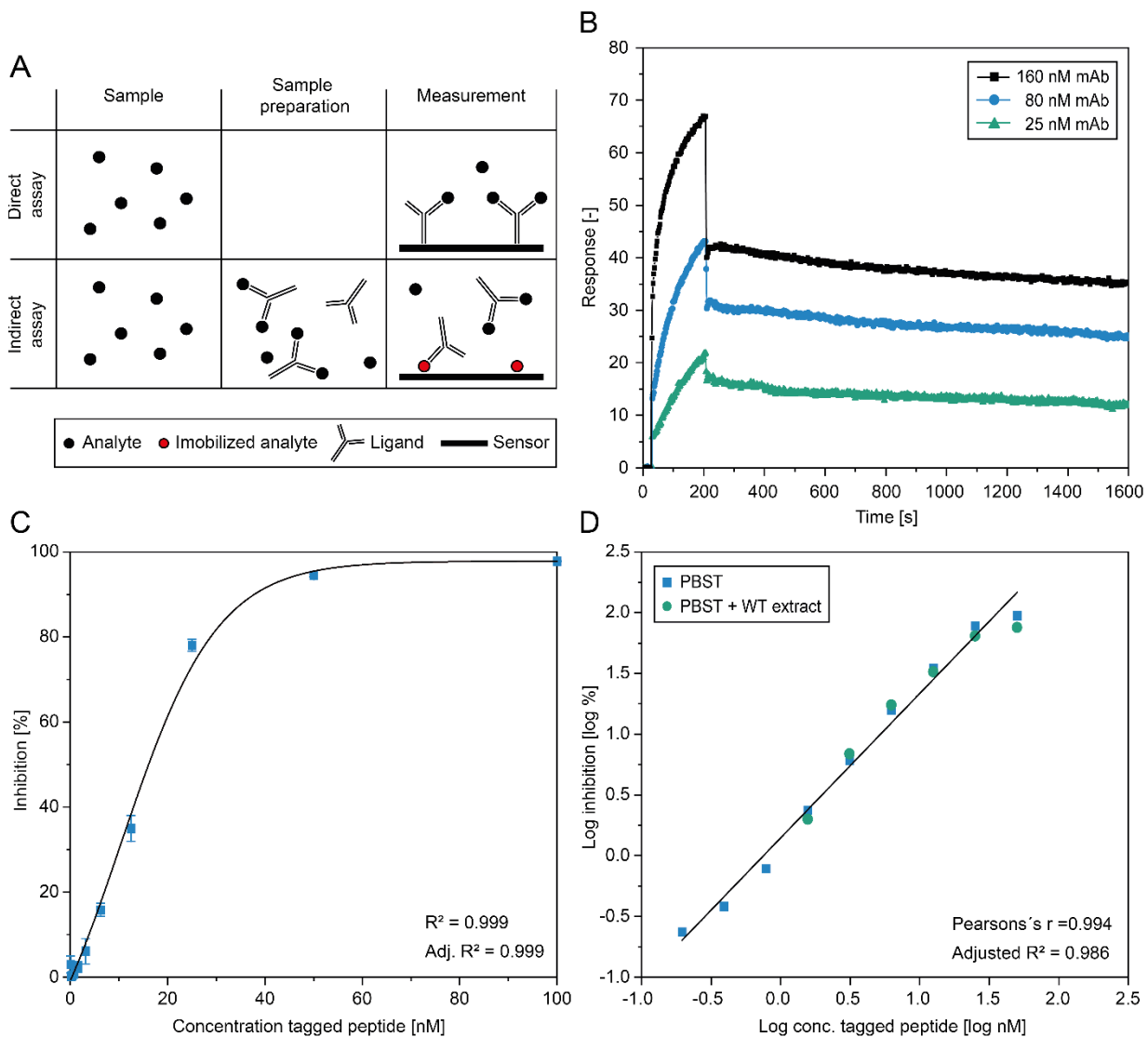


Figure 21: Development of an indirect SPR assay based on binding inhibition for quantification of His-tagged target proteins. A. Schematic representation of direct and indirect SPR assay formats for analyte quantification. B. Stability of the antibody-antigen interaction. MonoRab anti-His antibody was captured on sensors coated with peptide P1 (Supporting Table 20) followed by a 30 min dissociation phase. Low P1 immobilization levels (~ 20 RU) were used to prevent rebinding or steric hindrance. The flow rate was $30 \mu\text{L min}^{-1}$ during dissociation. C. Effect of the analyte concentration on binding inhibition. A constant concentration of 20 nM MonoRab anti-His antibody was mixed with 11 concentrations of peptide P1 in the range of 0.4 – 100.0 nM before injection on a sensor coated with P1 (II.6.3.1). High P1 immobilization levels (~ 180 RU) were used to ensure binding of all free antibody molecules remaining in the sample. Error bars represent the standard deviation from $n = 3$ measurements. Prior injection, mixtures of samples and antibody were incubated for 1 hour at 22°C on a rotary shaker. Inhibition curves were fitted to a Boltzmann function (Equation 4). D. Transformation of analyte concentration and binding inhibition to establish a linear relationship between both. A log transformation was applied to data from binding inhibition assays in PBS-T or clarified *N. benthamiana* extract diluted (1:40) in PBS-T. Assays were conducted similar to (C). A Sierra SPR 2/4 device was used for all experiments. OriginPro was used to plot and fit data.

Next, the assay stoichiometry was investigated by fitting experimental binding inhibition curves obtained with MonoRab anti-His antibody and peptide P1 (Figure 21C) to a 1:1 and 1:2 binding stoichiometry (Figure S16). Interestingly, even when using a small (~ 1.0 kDa) His-tagged peptide as analyte, the experimental inhibition curve was closer to a 1:1 stoichiometry than a

2:1 stoichiometry as indicated by an adjusted R^2 value of 0.99 compared to 0.88 (Figure S16, Supporting Table 22). These data indicate that binding of one molecule of tagged peptide restricted the accessibility of the second binding site of the antibody as previously reported for a comparable setting [378]. Considering that the molecular mass of even small (10 kDa) proteins is tenfold larger than the molecular mass of His-tagged peptides used as analyte in the inhibition experiment, the assay can be expected to follow a 1:1 rather than a 2:1 stoichiometry under experimental conditions.

It is further noteworthy that the proposed assay can be used to assess the dissociation rate constant, K_D , between a His-tagged molecule and an anti-His antibody by recording binding inhibition curves and fitting the experimental data to different stoichiometries as demonstrated here for MonoRab anti-His antibody and peptide P1 (Figure S16, Supporting Table 22). This provides flexibility in the assay design for measuring K_D , because binding of small (≤ 10 kDa) molecules to immobilized antibody is often difficult to detect due to the low molecular mass as discussed above.

The relationship between the concentration of analyte and the measured binding inhibition was well described by a Boltzmann function (Figure 21C, Supporting Table 22), which can be used to calculate the analyte concentration from the measured binding inhibition (Equation 4). To simplify the evaluation of binding inhibition assays, a log transformation was applied to the analyte concentration and the measured inhibition, thus establishing a linear correlation between both (Figure 21D). This held true in the presence of *N. benthamiana* HCPs when using an incubation time of 1 hour (Figure 21D). The target protein concentrations derived from the binding inhibition assay were in good agreement (Pearson's $r = 0.99$) with data from a dot blot assay using authentic standard and DspB as a model protein (Figure S15D). However, the SPR assay was overall more precise than the dot blot assay as indicated by a fourfold lower standard deviation when using the same anti-His antibody (Figure S15D). Even better results can be expected when using more sensitive devices for the SPR assay such as a Biacore S200.

A remaining drawback of the proposed SPR assay are the consumable costs resulting from the commercial anti-His antibody, which accounted for \$1.30 per reaction when using commercial anti-His antibody for the assay. An alternative to using commercial antibody is the production in-house. For example, the cloning of monoclonal anti-His antibodies has already been described more than 20 years ago [379] and structures and sequences of anti-His antibodies are available in the literature [380]. Even when assuming a low antibody yield and production costs of \$20,000 g^{-1} in a plant-based expression system [357, 372], the in-house production would reduce the consumable costs resulting from the anti-His antibody to ~\$0.01 cent per reaction.

III.4.2 Assessment of target protein functionality

After establishing high-throughput cloning (III.1), expression (III.2) and purification (III.3.1) in *Nicotiana*-based expression systems, the functionality of plant-made target proteins was assessed. Exceptions were made for IL6 and IL8, because the integrity and biological activity of plant-made cytokines including IL6 has already been demonstrated [189, 190].

III.4.2.1 Functionality of plant-made polyphosphate kinases

The activity of purified (III.3.2) plant-made PPKs and their counterparts produced in *E. coli* was assessed in an enzymatic assay using hexametaphosphate and ADP as substrates (Figure 22A). The enzymatic assay indicated that plant-made PPKs were active, but the activity was < 10% of the same PPKs produced in *E. coli* (Figure 22B). The activity was not significantly different when expressing PPKs in the cytosol, which resembled bacterial hosts closest in terms of PTMs, compared to expression in the apoplast (Figure 22B), which enabled complex PTMs such as *N*-glycosylation. Complex PTMs are common in eukaryotes but restricted to a limited range of bacteria [381].

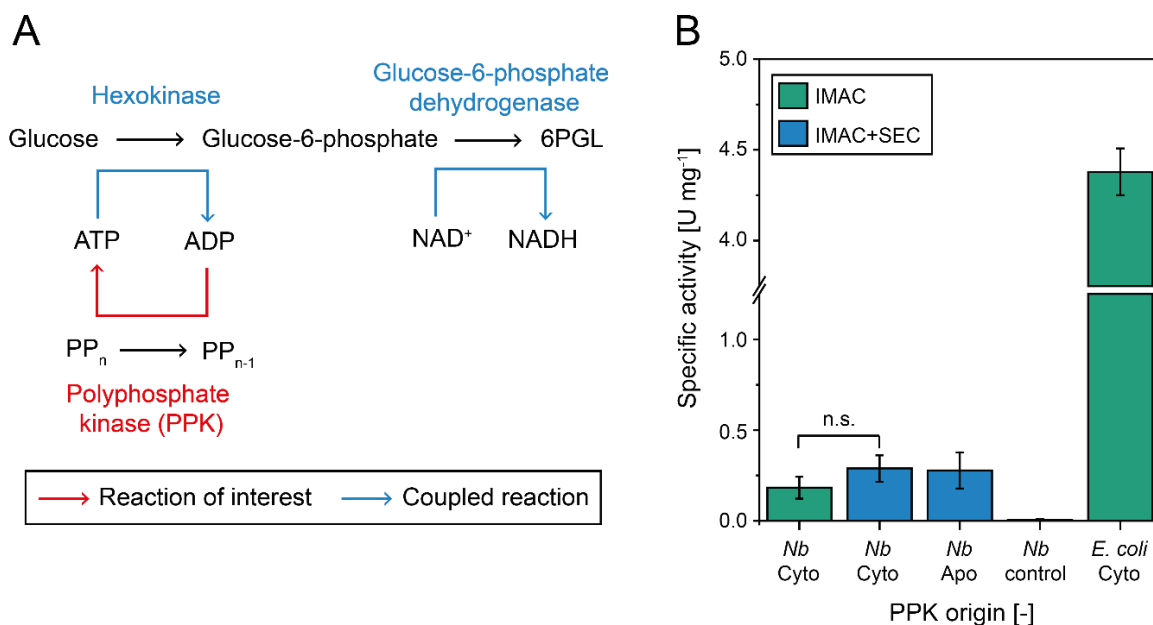


Figure 22: Functionality assessment of PPKs transiently expressed in *N. benthamiana*. A. Schematic representation of the enzymatic assay used to measure PPK activity (II.6.6). B. Activity of PPK-RO derived from the cytosol or apoplast after purification by IMAC and optionally SEC. A preliminary control for the enzymatic assay was generated by subjecting wildtype *N. benthamiana* extract to the same purification procedure as PPK-RO. Plant-made PPK-RO purified by IMAC was 48% pure, whereas plant-made PPK-RO purified by IMAC and SEC was 72% pure, based on densitometric evaluation of LDS gels (II.6.4). Error bars represent the standard deviation from $n = 3 - 6$ reactions. Nb – *Nicotiana benthamiana*, PP_n – polyphosphate, 6PGL – 6-phosphogluconolactone.

These findings indicated that PTMs were not the origin of the reduced activity of plant-made PPKs compared to PPKs produced in *E. coli*. In contrast, the PPK purity potentially affected

the activity measured in the enzymatic assay, as indicated by a lower PPK activity after purification by IMAC, compared to purification by IMAC and size exclusion chromatography (SEC, Figure 22B), although the difference was not significant (two-sided, two-sample *t*-test, $p = 0.070$, $n = 6$, $\alpha = 0.05$). Further supporting this hypothesis, the ATP-dependent HCP glutamine synthetase co-purified with PPKs during IMAC (III.3.1), thus potentially interfering with the assay. The effect of plant HCPs on the PPK activity assay was further investigated with extracts from wildtype *N. benthamiana* plants. A net activity of $\sim 0.025 \text{ U mg}_{\text{TSP}}^{-1}$ was measured in clarified *N. benthamiana* extract (Figure S17A), which increased from ~ 0.025 to $\sim 0.035 \text{ U mg}_{\text{TSP}}^{-1}$ after incubation at 45°C , corresponding to a 10% reduction of TSP (Figure S17B). The difference in activity before and after heat treatment was significant (two-sided, two-sample *t*-test, $p = 0.044$, $n = 3$, $\alpha = 0.05$). However, because the net activity of plant extract was only $\sim 10\%$ of the activity of PPKs produced in *E. coli*, it appeared unlikely that HCPs were the cause for the lower activity of plant-made PPKs compared to PPKs derived from *E. coli*. Incubation at 65°C , which corresponds to a $\sim 85\%$ TSP reduction (Figure S17A), completely suppressed the activity of *N. benthamiana* HCPs in the enzymatic assay. This observation can be useful for the purification and characterization of PPKs from thermophilic organisms such as *T. agreste* [246, 382], which will be investigated in the future.

Because neither PTMs, nor HCPs were the apparent cause of the reduced activity of plant-made PPKs compared to their bacterial counterparts, the effect of the tag location on the PPK activity should be investigated next. For instance, the bacterial PPKs contained an N-terminal His₆-tag, whereas the plant-derived PPKs contained a C-terminal His₆-tag. It is therefore possible that the C-terminal his-tag interfered with the enzymatic activity of PPKs, as observed for other enzymes in the literature [383]. Routinely testing different tag positions with the modular vector system can facilitate the production of functional target proteins in plants in the future.

III.4.2.2 Functionality of plant-made IgG3 antibodies

IgG3 antibodies were transiently expressed in *N. benthamiana* in the two compartments with the highest accumulation levels, namely the ER and apoplast (III.2.1), and purified by protein G chromatography (III.3.2). The activity of the plant-made IgG3 antibodies, i.e. their ability to bind the antigen alpha toxin (AT), was assessed by capturing IgG3 antibodies on a protein G-coated SPR sensor and injecting recombinant AT (produced in *E. coli*) in the range of 0.024 to 400 nM (Figure 23A).

As anticipated, IgG3 antibodies derived from the ER or apoplast were able to bind their antigen (Figure 23A). ER-targeted IgG3 had a higher association rate and lower dissociation rate compared to apoplast-targeted IgG3, resulting in overall stronger AT binding (Supporting Table

24). The lower affinity of IgG3 antibodies derived from the apoplast compared to the ER coincided with a ~15% lower integrity of both IgG1 and IgG3 antibodies in the apoplast compared to the ER (Figure 23B).

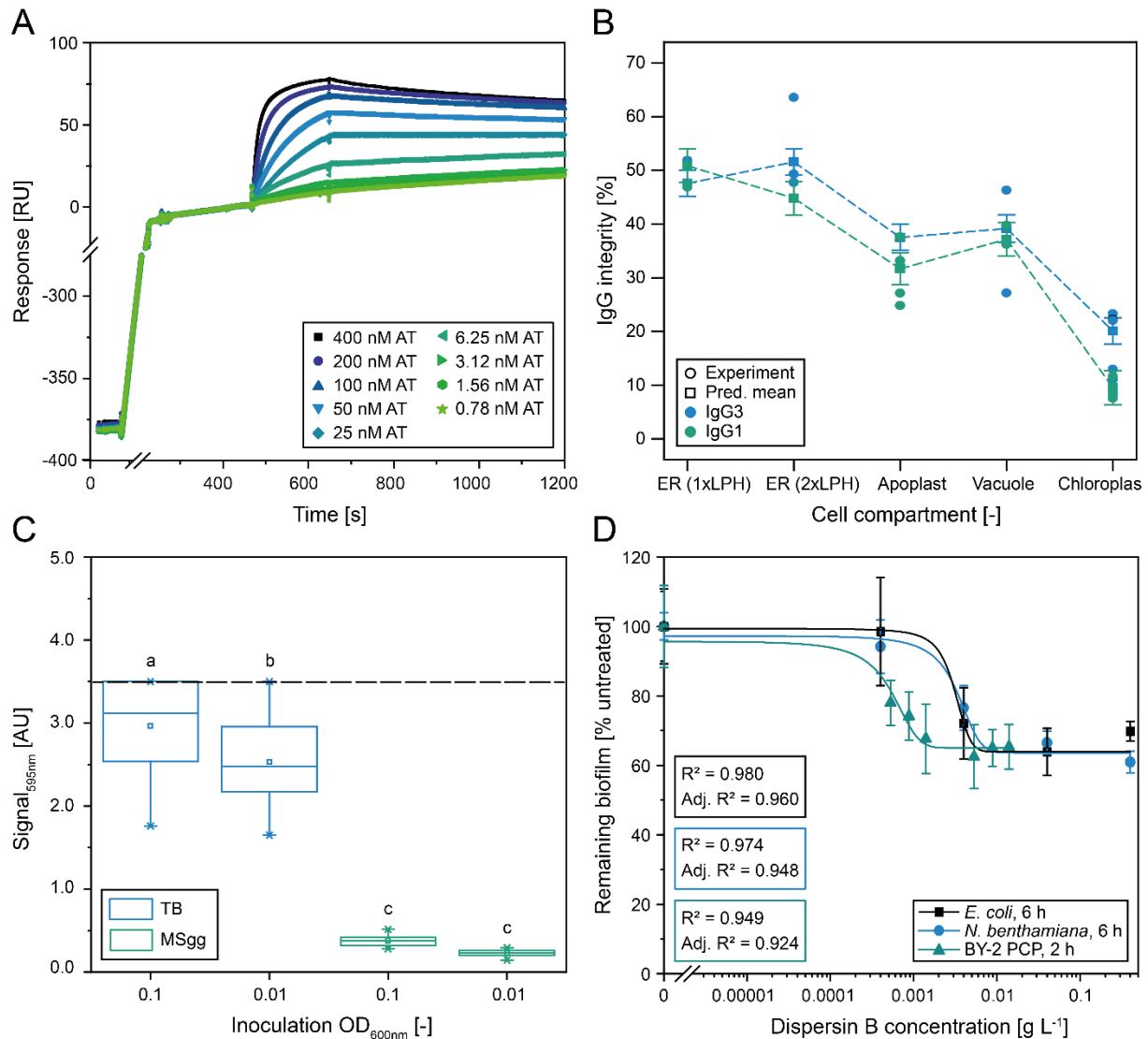


Figure 23: Activity tests with plant-made IgG3 and DspB. A. Functionality test of plant-derived IgG3 antibodies with the antigen alpha toxin (AT). In the first protocol phase (50 – 230 seconds) IgG3 antibodies were captured on a protein G coated SPR sensor (II.6.3.3). In the second protocol phase (500 – 680 seconds) 0.024 – 400 nM recombinant AT were injected (II.6.3.3). AT concentrations < 0.780 nM were not displayed for clarity. Data are raw resonance units without correction for a baseline drift, recorded on a Biacore T200. B. Model predicating the integrity of IgG1 and IgG3 antibodies in different plant cell compartments (Supporting Table 25). The antibody integrity was assessed by densitometric analysis of silver-stained LDS gels and western blotting (II.6.4). Data correspond to a BY-2 cultivation time of 168 hours and a PCP incubation time of 72 hours. Error bars represent least significant difference (LSD) bars around the model predicted means (95% confidence interval), calculated with Design-Expert. C. Cultivation of MRSA biofilms in complex and defined media. Glycerol, the main carbon source in MSgg medium (VII.7), is reportedly taken up by *S. aureus* [384]. The dashed line denotes the upper detection limit of the device. D. Enzymatic treatment of mature MRSA biofilms with DspB. Biofilms were quantified by staining with crystal violet and read out at 595 nm after solubilization with acetic acid (II.6.7). Data were fitted with a dose response function (Equation 8) using OriginPro. Error bars denote the standard deviation from $n \geq 3$ biological replicates.

This observation indicated that the lower activity of apoplast-derived IgG3 resulted from degradation in the apoplast, which has previously been attributed to proteolytic activity of e.g. serine proteases in this compartment [85, 385]. The differences in IgG integrity between different cell compartments were significant as indicated by non-overlapping least significant difference (LSD) bars around the model predictions (Figure 23B). In contrast to secreting mAbs to the apoplast, retention in the ER has been reported to promote the folding and stability of antibody-derived proteins [386], thus matching the results observed here.

Plant-made IgG3 antibodies showed an approximately fivefold lower affinity (K_D) compared to the affinity reported for IgG1 mAbs with the same CDRs produced in murine B-cell hybridomas [387]. However, only the association rate (k_a) was lower compared to the literature, whereas the dissociation rate (k_d) of the plant-made IgG3 antibodies was similar to the murine IgG1 counterparts (Supporting Table 24). This observation indicated that the lower affinity might be related to the antigen batch used, possibly originating from differences in the AT amino acid sequence observed when comparing multiple suppliers, or from a loss of activity during dialysis used to remove glycerol (20% v v⁻¹) from the supplied AT before SPR measurements. Additionally, many literature reports suggest that plant-made mAbs perform similar to their counterparts produced in mammalian cells [388, 389]. A fair comparison of antibodies produced in plants and mammalian cells would therefore require parallel measurements, using identical antigens and reagent batches as suggested for SPR assays before [390, 391]. Potential differences resulting from the IgG scaffold will be investigated in the future by comparing IgG3 antibodies directed against *S. aureus* AT with IgG1 antibodies directed against the same antigen that have been expressed as a control for IgG3 (Figure 23B).

III.4.2.3 Functionality of plant-made biofilm degrading enzymes

To investigate the functionality of plant-made biofilm degrading enzymes, DspB was transiently expressed in *N. benthamiana* plants in the compartment with the highest accumulation, namely the chloroplast (III.2.1), and purified by IMAC using a C-terminal His₆-tag (III.3.2). DspB with an identical amino acid sequence and tag was produced in *E. coli* and purified similarly to be able to compare the activity of plant-derived DspB with its bacterial counterpart. The activity of purified DspB was tested against experimental MRSA biofilms in a static biofilm reduction assay, which has been successfully used to detect biofilm degrading activity in the context of *S. aureus* in the literature [392]. A clinically relevant MRSA strain (Rosenbach 1884) was used for the production of experimental biofilms to simulate a clinical application, considering that the biofilm composition differs between *S. aureus* strains [9]. A physiological temperature of 37°C was used for biofilm cultivation and degradation, because

sensitive equipment or even human patients, both representing potential applications for the recombinant DspB, cannot be exposed to harsh conditions such as high temperatures [393]. Chemically defined medium was used for biofilm cultivation, because biofilms cultivated on complex terrific broth (TB) exceeded the detection limit (Figure 23C). Moreover, the variation during biofilm formation could be significantly reduced with defined compared to complex medium, when using experimental *Bacillus subtilis* biofilms as surrogate for *S. aureus* biofilms [174].

As anticipated, plant-made DspB was active and reduced mature MRSA biofilms even at low concentrations $< 0.004 \text{ g L}^{-1}$ (Figure 23D), which was in agreement with the disruption of mature *S. epidermidis* biofilms with $\sim 0.002 \text{ g L}^{-1}$ DspB in the literature [394]. The relative IC_{50} was $0.0032 \pm 0.0006 \text{ g L}^{-1}$ ($0.0800 \pm 0.0150 \text{ mM}$) for DspB derived from *N. benthamiana* and $0.0031 \pm 0.0001 \text{ g L}^{-1}$ ($0.0775 \pm 0.0025 \text{ mM}$) for DspB derived from *E. coli* (Supporting Table 26) and thus not significantly different (*F*-test, $p = 0.598$, $\alpha = 0.05$). Biofilm removal in the static assay stagnated at $\sim 40\%$ (compared to untreated controls), even when increasing the DspB concentration to 0.4 g L^{-1} (Figure 23D). The incomplete biofilm removal was expected, because biofilms are not only composed of EPS like poly- β -1,6-*N*-acetyl-d-glucosamine (PNAG), but also contain extracellular DNA and proteins [395], which are not targeted by DspB. A similar stagnation in biofilm removal was observed with DspB produced in *E. coli*, further supporting the assumption that the incomplete biofilm removal originated from properties of the MRSA biofilm rather than a lack of DspB activity. The extend of biofilm persistence can be attributed to the strain used, because several clinically relevant MRSA strains are known to produce biofilms with little EPS, thus making them less susceptible to DspB compared to other strains [9]. It is noteworthy that PCP extracts containing DspB achieved a similar biofilm removal as purified DspB from *N. benthamiana* and *E. coli* at tenfold lower concentrations, albeit at a shorter incubation time of 2 hours (Figure 23D, Supporting Table 26). This observation indicated that extracts of BY-2 cells containing DspB could be directly used against MRSA biofilms and that other anti-microbial components may be found in plant extracts, which will be investigated in the future along with short (2 hours) incubation times for purified DspB. The proposed biofilm assay facilitates testing of multi-enzyme mixtures for removal of biofilms, which should be the focus of future research. Enzyme combinations that have been suggested to completely eradicate *S. aureus* biofilms include combinations of DspB with DNase or protease [9, 396, 397]. However, enzyme mixtures containing proteases with a broad substrate spectrum should be carefully tested to rule out any autolysis or unintended proteolysis of other biofilm-degrading enzymes [174].

IV. Conclusion and outlook

IV.1 High-throughput screening in plants

High-throughput screening tools facilitate the development of biopharmaceuticals, but few high-throughput tools have been available for plant-based expression platforms compared to dominant production hosts like *E. coli* or CHO cells. To advance biopharmaceutical development in plants, high-throughput techniques were therefore implemented during (i) cloning, (ii) expression, (iii) purification and (iv) quantification in *Nicotiana* species.

Combining modular vectors with automation on a liquid handling station allowed a cloning throughput comparable to established platforms, i.e. ~1000 DNA assembly reactions per day [170]. To achieve a matching throughput during construct evaluation, high-throughput expression in PCPs was complemented with automated quantification by SPR, thus omitting the need to purify PCP extracts before product quantification.

Combining high-throughput cloning, expression, and quantification with a DoE approach allowed to rapidly generate and screen libraries of expression cassette elements and identify combinations that maximize product accumulation. This strategy achieved IgG3 accumulation levels that were threefold higher than in the literature (~50 mg kg⁻¹ compared to 16 mg kg⁻¹ [196]), thus emphasizing the potential that high-throughput screening tools offer for optimization of expression cassettes. Using the same strategy, DspB accumulation levels of ~300 mg kg⁻¹ (~75 mg L⁻¹ extract) were achieved, thus matching yields reported in *E. coli* (~60 mg L⁻¹ culture, after purification [398]). Even higher accumulation levels can be expected in the future by expanding the set of expression cassette elements used for screening, particularly with synthetic promoters, 3' UTRs or terminators. For instance, optimization of terminator-UTR combinations improved recombinant protein accumulation levels ~25-fold in *Nicotiana* spp. [399]. Additional improvements can be expected from silencing suppression. For example, co-infiltration with a silencing suppressor more than doubled IgG3 accumulation levels from ~50 mg kg⁻¹ to ~130 mg kg⁻¹ in a non-optimized setting [143].

Beyond expression cassette optimization, productivities can also be increased (at least fourfold) by optimizing cultivation conditions as demonstrated for the medium osmolality, harvest time or light exposure. This approach provides an additional handle to address low target protein accumulation in plants, which currently limits their broader application.

The PCP technology would greatly benefit from an overall increase in productivity, so that a typical PCP of ~60 mg (or triplicates thereof) can provide sufficient protein quantities for initial analysis and functional testing, e.g. 1 mg for NMR analysis [172]. Sufficient productivities

provided, PCPs can be used for high-throughput protein characterization, because recombinant proteins can be rapidly extracted from the apoplast by infiltration-centrifugation, as demonstrated in 96-well plates.

Establishing correlation factors between PCPs and differentiated plants allowed to estimate accumulation levels in differentiated plants (the anticipated production platform) from screening results in PCPs, thus reducing the screening footprint. Because mayor sources of variation were identified in both systems, even more accurate predictions can be derived in the future by controlling the respective influence factors. Understanding the physiological origin of correlation factors (i.e. the fraction of active biomass), will further facilitate the investigation of correlation factors in the future.

Future research should investigate the use of PCPs in commercial screening kits. This approach requires conservation of PCPs, which could be achieved for example by lyophilization, considering that lyophilized plant cells can be used as bioreactors [400, 401].

As an alternative to screening in PCPs, the proposed high-throughput screening platform can be adapted to cell-free expression systems, e.g. based on BY-2 lysates, which allow high productivities ($\sim 3 \text{ g L}^{-1}$ cell lysate [140]). This approach would facilitate rapid characterization of plant-made proteins through high yields and allow to express recombinant proteins that are difficult to produce in living plant cells due to toxicity [68].

IV.2 Smart candidate and strategy selection

A recent concept during development of biopharmaceuticals is the transition from a pure numbers game to a smart candidate selection [54, 56]. Aiming to incorporate this concept into plant-based expression platforms, model proteins expressed in this work were used to identify parameters that can guide the selection of e.g. expression vectors or model proteins.

A parameter that can guide the selection of a suitable expression compartment was the target protein origin. This means that target proteins derived from prokaryotes such as PPKs or DspB accumulated well in chloroplasts, which have a bacterial origin, whereas target proteins derived from eukaryotes accumulated best in compartments that enabled common eukaryotic post translational modifications such as glycosylation. [300]. Narrowing down the number of suitable expression compartments can speed up screening.

Assessing intrinsic protein stabilities based on the instability index or the aliphatic index can help to sort out product candidates that cannot be produced and hence save time and resources during screening. This approach was successful when comparing proteins within the same class (e.g. antibodies), whereas predictions involving multiple target protein classes have to consider

additional parameters such as the pI. Additional parameters for *a priori* stability predictions can be identified in the future by expanding the set of target proteins investigated. Further progress regarding *a priori* stability predictions involving multiple protein classes can be expected when employing machine learning approaches that combine multiple stability parameters [302, 307]. A potential limitation of machine learning approaches is that they are not deterministic.

A fundamental parameter that affected the productivity of plant cells from suspension cultures was the uptake of water, which was mainly driven by the medium osmolality. Productivities of plant cell cultures (or PCPs derived thereof) can be further increase in the future by adjusting cultivation conditions based on the critical osmolality thresholds identified herein ($\sim 100 - 150$ mOsmol kg⁻¹), as demonstrated in stirred tanks.

High-throughput screening of chromatography conditions with miniaturized columns and a liquid handling station allowed to identify HCPs that persist after IMAC. Identification and characterization of such HCPs can guide the selection of a purification strategy. For example, HCPs persisting after IMAC formed large (~ 475 kDa and ~ 200 kDa) oligomers and implementing size-based purification by UF/DF before IMAC allowed to remove these HCPs.

IV.3 Plant-made proteins for controlling MRSA

Plant-made proteins directed against MRSA were functional (except for low PPK activities), indicating that *Nicotiana* spp. can supply recombinant proteins for a multi-layered strategy to treat MRSA infections. Using the screening strategy established herein, additional plant-made proteins can be rapidly assessed for their usefulness against MRSA in the future. Of particular interest are antibodies directed against additional virulence factors or biofilm degrading enzymes that target biofilm building blocks other than PNAG. Because biofilm dispersion alone might cause an anaphylactic shock in human patients, combinations of biofilm degrading enzymes such as DspB and endolysins such as LysK-L should be investigated in the future, allowing to disperse biofilms and simultaneously inactivate the pathogen. Considering that biofilms are often exposed to shear forces in the human body, the activity of plant-made biofilm degrading enzymes should also be investigated in dynamic models [396].

A potential drawback of the proposed screening strategy is the requirement for an affinity tag. This limitation can be addressed by incorporating a protease-recognition site (e.g. for caspase-2) into the affinity tag [402]. When this approach is combined with chromatography, native protein can be eluted by injection a protease that specifically cleaves the affinity tag, thereby simultaneously removing HCPs that would otherwise co-elute with the target protein during chromatography [354].

V. Summary

Plants can complement dominant expression systems such as *Escherichia coli* and Chinese hamster ovary cells with additional production capacity in response to emerging infectious diseases, but compared to these hosts few high-throughput screening tools that facilitate biopharmaceutical development have been available in plants. To advance this situation, high-throughput techniques were implemented during cloning, expression, purification and quantification, thus increasing the screening throughput across the entire development process. This concept was applied to a transient expression in *Nicotiana* spp., which allows to establish production processes in as little as 3 weeks and thus quickly react to changing demands.

In combination with statistical design of experiments, the established high-throughput screening tools allowed to rapidly clone and test libraries of expression cassette elements such as promoters, 5' UTRs and signal sequences and identify combinations thereof that maximize target protein accumulation. This strategy was successfully employed to produce interleukins, polyphosphate kinases, IgG3 antibodies, biofilm degrading enzymes and endolysins selected for a multilayered strategy directed against methicillin-resistant *Staphylococcus aureus* (MRSA). Notably, IgG3 accumulation levels achieved by systematically screening expression cassette elements were threefold higher than the literature. Using the same strategy, dispersin B accumulation levels equivalent to *E. coli* were reached. Further improvement can be expected by expanding the set of expression cassette elements used for screening, particularly with synthetic promoters, 3' UTRs and terminators. Plant-derived target proteins were functional, except for a reduced enzymatic activity of polyphosphate kinases, indicating that *Nicotiana* spp. can supply recombinant proteins to counter emerging MRSA. Using the high-throughput screening tools established herein, additional plant-made proteins can be rapidly assessed for their usefulness against MRSA in the future.

In accordance with a recent approach in biopharmaceutical development, data generated with the different target proteins were used to identify parameters that can guide the selection of candidate proteins and even optimization strategies. For instance, the target protein origin had a major impact on the ideal expression compartment, thus allowing to pre-select suitable expression compartments and reduce the screening workload. Assessing intrinsic protein stability parameters allowed to sort out unsuitable candidate proteins, albeit currently limited to comparisons within the same protein class. A parameter that can guide the optimization of plant cell cultivation media is the medium osmolality, essentially controlling the uptake of water into plant cells. Characterization of host cell proteins that persist after chromatography allowed to derive purification strategies that facilitate their removal.

Zusammenfassung

Pflanzen können etablierte Expressionssysteme wie *Escherichia coli* und „Chinese hamster ovary“ Zellen im Kontext von Infektionskrankheiten durch zusätzliche Produktionskapazitäten ergänzen. Im Vergleich zu diesen Systemen sind jedoch nur wenige Hochdurchsatz-Screening-Tools verfügbar, die die Entwicklung von Biopharmazeutika in Pflanzen erleichtern. Um diesen Zustand zu verbessern, wurden Hochdurchsatztechniken während der Klonierung, Expression, Reinigung und Quantifizierung implementiert, um den Durchsatz während des gesamten Entwicklungsprozesses zu erhöhen. Dieses Konzept wurde auf eine transiente Expression in *Nicotiana* spp. angewandt, da transiente Produktionsprozesse in rund 3 Wochen etabliert werden können und damit schnell auf neue Anforderungen reagieren können.

Kombiniert mit statistischer Versuchsplanung ermöglichten es die etablierten Hochdurchsatz-Screening-Tools Kombinationen von Promotoren, 5' UTRs und Signalsequenzen zu identifizieren, die die Akkumulation von Zielproteinen maximieren. Diese Strategie wurde eingesetzt, um Interleukine, Polyphosphatkinasen, IgG3-Antikörper, Biofilm-abbauende Enzyme und Endolysine für eine holistische Strategie gegen Methicillin-resistenten *Staphylococcus aureus* (MRSA) herzustellen. Durch das systematische Screening von Vektorelementen wurde in Pflanzen eine dreifach höhere IgG3-Akkumulation erreicht als in der Literatur beschrieben. Dispersin B erreichte Akkumulationslevel äquivalent zu *E. coli*.

Weitere Verbesserungen können durch die Erweiterung der untersuchten Vektorelemente, insbesondere mit synthetischen Promotoren, 3' UTRs und Terminatoren erreicht werden.

Die aus Pflanzen gewonnenen Zielproteine waren funktionsfähig, mit Ausnahme einer verminderten Aktivität von Polyphosphatkinasen, was dafürspricht, dass *Nicotiana* spp. rekombinante Proteine zur Bekämpfung von MRSA produzieren kann. Mit Hilfe der etablierten Screening-Tools können in Zukunft weitere Proteine in Pflanzen produziert und auf ihre Aktivität gegen MRSA untersucht werden.

Basierend auf einem aktuellen Ansatz in der Entwicklung von Biopharmazeutika wurden Parametern identifiziert, die die Auswahl von Proteinkandidaten und Optimierungsstrategien leiten können. So erlaubte beispielsweise der Ursprung eines Zielproteins eine Vorauswahl geeigneter Expressionskompartimente und eine Verringerung des Screening Aufwandes. Die Bewertung der intrinsischen Proteinstabilität ermöglichte es, ungeeignete Proteinkandidaten innerhalb einer Proteinklasse auszusortieren. Die Medium Osmolalität (Wasser Aufnahme) kann für die Optimierung von Medien für die Pflanzenzellkultur herangezogen werden. Die Charakterisierung von Wirtszellproteinen, die nach der Chromatographie bestehen blieben, ermöglichte die Entwicklung von Reinigungsstrategien, die ihre Entfernung erleichtern.

VI. References

- [1] Baker, R. E., Mahmud, A. S., Miller, I. F., Rajeev, M. et al., Infectious diseases in an era of global change. *Nature Reviews Microbiology* 2022, 20, 193–205, DOI: 10.1038/s41579-021-00639-z.
- [2] Shanmugaraj, B., Phoolcharoen, W., Addressing demand for recombinant biopharmaceuticals in the COVID-19 era. *Asian Pacific Journal of Tropical Medicine* 2021, 14, 49–51, DOI: 10.4103/1995-7645.306736.
- [3] Simonsen, L., Viboud, C., Mortality: A comprehensive look at the COVID-19 pandemic death toll. *eLife Journal* 2021, 10, e71974, DOI: 10.7554/eLife.71974.
- [4] Wang, H., Paulson, K. R., Pease, S. A., Watson, S. et al., Estimating excess mortality due to the COVID-19 pandemic: A systematic analysis of COVID-19-related mortality, 2020–21. *The Lancet* 2022, 399, 1513–1536, DOI: 10.1016/S0140-6736(21)02796-3.
- [5] Guo, Y., Song, G., Sun, M., Wang, J. et al., Prevalence and therapies of antibiotic-resistance in *Staphylococcus aureus*. *Frontiers in Cellular and Infection Microbiology* 2020, 10, 107, DOI: 10.3389/fcimb.2020.00107.
- [6] Schuhmacher, A., Hinder, M., Gassmann, O., Value creation in the pharmaceutical industry: The critical path to innovation, *John Wiley & Sons*, 2016.
- [7] O'Neill, J., Review on antimicrobial resistance - Tackling drug-resistant infections globally: Final report and recommendations. *Antimicrobial Resistance Review* 2016.
- [8] Nieuwlaat, R., Mbuagbaw, L., Mertz, D., Burrows, L. L. et al., Coronavirus disease 2019 and antimicrobial resistance: Parallel and interacting health emergencies. *Clinical Infectious Disease* 2021, 72, 1657–1659, DOI: 10.1093/cid/ciaa773.
- [9] Craft, K. M., Nguyen, J. M., Berg, L. J., Townsend, S. D., Methicillin-resistant *Staphylococcus aureus* (MRSA): Antibiotic-resistance and the biofilm phenotype. *Medicinal Chemistry* 2019, 10, 1231–1241, DOI: 10.1039/C9MD00044E.
- [10] González-García, S., Hamdan-Partida, A., Bustos-Hamdan, A., Bustos-Martínez, J., Factors of nasopharynx that favor the colonization and persistence of *Staphylococcus aureus*. *IntechOpen* 2021, DOI: 10.5772/intechopen.95843.
- [11] Hammer, N. D., Skaar, E. P., Molecular mechanisms of *Staphylococcus aureus* iron acquisition. *Annual Review of Microbiology* 2011, 65, 129–147, DOI: 10.1146/annurev-micro-090110-102851.
- [12] Lowy, F. D., *Staphylococcus aureus* Infections. *New England Journal of Medicine* 1998, 339, 520–532, DOI: 10.1056/NEJM199808203390806.
- [13] Chambers, H. F., DeLeo, F. R., Waves of resistance: *Staphylococcus aureus* in the antibiotic era. *Nature Reviews Microbiology* 2009, 7, 629–641, DOI: 10.1038/nrmicro2200.
- [14] Stryjewski, M. E., Corey, G. R., Methicillin-resistant *Staphylococcus aureus*: An evolving pathogen. *Clinical Infectious Disease* 2014, 58, S10-S19, DOI: 10.1093/cid/cit613.
- [15] Jevons, M. P., Celbenin-resistant staphylococci. *British Medical Journal* 1961, 1, 124, DOI: 10.1136/bmj.1.5219.124-a.
- [16] Hiramatsu, K., Cui, L., Kuroda, M., Ito, T., The emergence and evolution of methicillin-resistant *Staphylococcus aureus*. *Trends in Microbiology* 2001, 9, 486–493, DOI: 10.1016/S0966-842X(01)02175-8.

- [17] Arêde, P., Ministro, J., Oliveira, D. C., Redefining the role of the β -lactamase locus in methicillin-resistant *Staphylococcus aureus*: β -lactamase regulators disrupt the MecI-mediated strong repression on *mecA* and optimize the phenotypic expression of resistance in strains with constitutive *mecA* expression. *Antimicrobial Agents and Chemotherapy* 2013, 57, 3037–3045, DOI: 10.1128/AAC.02621-12.
- [18] Bagcigil, A. F., Taponen, S., Koort, J., Bengtsson, B. et al., Genetic basis of penicillin resistance of *S. aureus* isolated in bovine mastitis. *Acta Veterinaria Scandinavica* 2012, 54, 69, DOI: 10.1186/1751-0147-54-69.
- [19] Ito, T., Classification of Staphylococcal cassette chromosome *mec* (SCC*mec*): Guidelines for reporting novel SCC*mec* elements. *Antimicrobial Agents and Chemotherapy* 2009, 53, 4961–4967, DOI: 10.1128/AAC.00579-09.
- [20] Ito, T., Kuwahara-Arai, K., Katayama, Y., Uehara, Y. et al., Staphylococcal cassette chromosome *mec* (SCC*mec*) analysis of MRSA, in: Ji, Y. (Ed.). *Methicillin-resistant Staphylococcus aureus (MRSA) protocols*, Humana Press 2014, pp. 131–148, DOI: 10.1007/978-1-62703-664-1_8.
- [21] Deurenberg, R. H., Vink, C., Kalenic, S., Friedrich, A. W. et al., The molecular evolution of methicillin-resistant *Staphylococcus aureus*. *Clinical Microbiology and Infection* 2007, 13, 222–235, DOI: 10.1111/j.1469-0691.2006.01573.x.
- [22] Hiramatsu, K., Cui, L., Kuroda, M., Ito, T., The emergence and evolution of methicillin-resistant *Staphylococcus aureus*. *Trends in Microbiology* 2001, 9, 486–493, DOI: 10.1016/S0966-842X(01)02175-8.
- [23] Otto, M., Staphylococcal biofilms. *Microbiology Spectrum* 2018, 6, 6.4.27, DOI: 10.1128/microbiolspec.GPP3-0023-2018.
- [24] Flemming, H.-C., Wingender, J., The biofilm matrix. *Nature Reviews Microbiology* 2010, 8, 623–633, DOI: 10.1038/nrmicro2415.
- [25] Mah, T.-F. C., O'Toole, G. A., Mechanisms of biofilm resistance to antimicrobial agents. *Trends in Microbiology* 2001, 9, 34–39, DOI: 10.1016/S0966-842X(00)01913-2.
- [26] Cheung, G. Y. C., Bae, J. S., Otto, M., Pathogenicity and virulence of *Staphylococcus aureus*. *Virulence* 2021, 12, 547–569, DOI: 10.1080/21505594.2021.1878688.
- [27] Del Pozo, J. L., Biofilm-related disease. *Expert Review of Anti-Infective Therapy* 2018, 16, 51–65, DOI: 10.1080/14787210.2018.1417036.
- [28] Schwartz, K., Ganesan, M., Payne, D. E., Solomon, M. J. et al., Extracellular DNA facilitates the formation of functional amyloids in *Staphylococcus aureus* biofilms. *Molecular Microbiology* 2016, 99, 123–134, DOI: 10.1111/mmi.13219.
- [29] Payne, D. E., Boles, B. R., Emerging interactions between matrix components during biofilm development. *Current Genetics* 2016, 62, 137–141, DOI: 10.1007/s00294-015-0527-5.
- [30] Arciola, C. R., Campoccia, D., Ravaioli, S., Montanaro, L., Polysaccharide intercellular adhesin in biofilm: Structural and regulatory aspects. *Frontiers in Cellular and Infection Microbiology* 2015, 5, DOI: 10.3389/fcimb.2015.00007.
- [31] Skurnik, D., Merighi, M., Grout, M., Gadjeva, M. et al., Animal and human antibodies to distinct *Staphylococcus aureus* antigens mutually neutralize opsonic killing and protection in mice. *The Journal of Clinical Investigation* 2010, 120, 3220–3233, DOI: 10.1172/JCI42748.
- [32] Valle, J., Fang, X., Lasa, I., Revisiting *bap* multidomain protein: More than sticking bacteria together. *Frontiers in Microbiology* 2020, 11, DOI: 10.3389/fmicb.2020.613581.

- [33] Cucarella, C., Tormo, M. A., Ubeda, C., Trotonda, M. P. et al., Role of biofilm-associated protein bap in the pathogenesis of bovine *Staphylococcus aureus*. *Infection and Immunity* 2004, 72, 2177–2185, DOI: 10.1128/IAI.72.4.2177-2185.2004.
- [34] Molin, S., Tolker-Nielsen, T., Gene transfer occurs with enhanced efficiency in biofilms and induces enhanced stabilisation of the biofilm structure. *Current Opinion in Biotechnology* 2003, 14, 255–261, DOI: 10.1016/S0958-1669(03)00036-3.
- [35] Palmqvist, N., Foster, T., Tarkowski, A., Josefsson, E., Protein A is a virulence factor in *Staphylococcus aureus* arthritis and septic death. *Microbial Pathogenesis* 2002, 33, 239–249, DOI: 10.1006/mpat.2002.0533.
- [36] Atkins, K. L., Burman, J. D., Chamberlain, E. S., Cooper, J. E. et al., *S. aureus* IgG-binding proteins SpA and Sbi: Host specificity and mechanisms of immune complex formation. *Molecular Immunology* 2008, 45, 1600–1611, DOI: 10.1016/j.molimm.2007.10.021.
- [37] Falugi F., Keun H. K., Missiakas D. M., Schneewind O., Role of protein A in the evasion of host adaptive immune responses by *Staphylococcus aureus*. *American Society for Microbiology* 2013, 4, e00575-13, DOI: 10.1128/mBio.00575-13.
- [38] Hoven, G. von, Qin, Q., Neukirch, C., Husmann, M. et al., *Staphylococcus aureus* α -toxin: Small pore, large consequences. *Biological Chemistry* 2019, 400, 1261–1276, DOI: 10.1515/hsz-2018-0472.
- [39] Caiazza N. C., O'Toole G. A., Alpha-toxin is required for biofilm formation by *Staphylococcus aureus*. *Journal of Bacteriology* 2003, 185, 3214–3217, DOI: 10.1128/JB.185.10.3214-3217.2003.
- [40] Menzies, B. E., Kourteva, I., *Staphylococcus aureus* α -toxin induces apoptosis in endothelial cells. *FEMS Immunology and Medical Microbiology* 2000, 29, 39–45, DOI: 10.1111/j.1574-695X.2000.tb01503.x.
- [41] Bhakdi, S., Trantum-Jensen, J., Alpha-toxin of *Staphylococcus aureus*. *Microbiological Reviews* 1991, 55, 733–751, DOI: 10.1128/mr.55.4.733-751.1991
- [42] Hall A. E., Domanski P. J., Patel P. R., Vernachio John H. et al., Characterization of a protective monoclonal antibody recognizing *Staphylococcus aureus* protein clumping factor A. *Infection and Immunity* 2003, 71, 6864–6870, DOI: 10.1128/IAI.71.12.6864-6870.2003.
- [43] Walsh, E. J., Miajlovic, H., Gorkun, O. V., Foster, T. J., Identification of the *Staphylococcus aureus* clumping factor B (ClfB) binding site in the alpha C-domain of human fibrinogen. *Microbiology* 2008, 154, 550–558, DOI: 10.1099/mic.0.2007/010868-0.
- [44] Hua, L., Hilliard, J. J., Shi, Y., Tkaczyk, C. et al., Assessment of an anti-alpha-toxin monoclonal antibody for prevention and treatment of *Staphylococcus aureus*-induced pneumonia. *Antimicrobial Agents and Chemotherapy* 2014, 58, 1108–1117, DOI: 10.1128/AAC.02190-13.
- [45] Miller, L. S., Fowler, Vance G, Jr, Shukla, S. K., Rose, W. E. et al., Development of a vaccine against *Staphylococcus aureus* invasive infections: evidence based on human immunity, genetics and bacterial evasion mechanisms. *FEMS Microbiology Review* 2020, 44, 123–153, DOI: 10.1093/femsre/fuz030.
- [46] Gadakh, B., van Aerschot, A., Renaissance in antibiotic discovery: Some novel approaches for finding drugs to treat bad bugs. *Current Medicinal Chemistry* 2015, 22, 2140–2158.

- [47] DiMasi, J. A., Grabowski, H. G., Hansen, R. W., Innovation in the pharmaceutical industry: New estimates of R&D costs. *Journal of Health Economics* 2016, 47, 20–33, DOI: 10.1016/j.jhealeco.2016.01.012.
- [48] Pramod, K., Tahir, M. A., Charoo, N. A., Ansari, S. H. et al., Pharmaceutical product development: A quality by design approach. *International Journal of Pharmaceutical Investigation* 2016, 6, 129–138, DOI: 10.4103/2230-973X.187350.
- [49] Wong, C. H., Siah, K. W., Lo, A. W., Estimation of clinical trial success rates and related parameters. *Biostatistics* 2019, 20, 273–286, DOI: 10.1093/biostatistics/kxx069.
- [50] Woods, T., Live Longer with AI: How artificial intelligence is helping us extend our healthspan and live better too, *Packt Expert Insight*, 2020.
- [51] Schuhmacher, A., Gassmann, O., Hinder, M., New innovation models in pharmaceutical R&D. In: Value creation in the pharmaceutical industry - The critical path to innovation. *John Wiley & Sons* 2016, 1, 400–415. DOI:10.1002/9783527693405.ch18
- [52] Mayr, L. M., Fuerst, P., The Future of high-throughput screening. *SLAS Discovery* 2008, 13, 443–448, DOI: 10.1177/1087057108319644.
- [53] Taylor, D., The Pharmaceutical industry and the future of drug development, in: Pharmaceuticals in the environment, *The Royal Society of Chemistry*, 2016, pp. 1–33, DOI: 10.1039/9781782622345-00001.
- [54] Rees, S., Gribbon, P., Birmingham, K., Janzen, W. P. et al., Towards a hit for every target. *Nature Reviews Drug Discovery* 2016, 15, 1–2, DOI: 10.1038/nrd.2015.19.
- [55] Pritchard, J. F., Jurima-Romet, M., Reimer, M. L. J., Mortimer, E. et al., Making better drugs: Decision gates in non-clinical drug development. *Nature Reviews Drug Discovery* 2003, 2, 542–553, DOI: 10.1038/nrd1131.
- [56] Hughes, J. P., Rees, S., Kalindjian, S. B., Philpott, K. L., Principles of early drug discovery. *British Journal of Pharmacology* 2011, 162, 1239–1249, DOI: 10.1111/j.1476-5381.2010.01127.x.
- [57] Carnero, A., High throughput screening in drug discovery. *Clinical and Translational Oncology* 2006, 8, 482–490, DOI: 10.1007/s12094-006-0048-2.
- [58] Paul, S. M., Mytelka, D. S., Dunwiddie, C. T., Persinger, C. C. et al., How to improve R&D productivity: The pharmaceutical industry's grand challenge. *Nature Reviews Drug Discovery* 2010, 9, 203–214. DOI: 10.1038/nrd3078
- [59] Gabrielsson, J., Lindberg, N. O., Lundstedt, T., Multivariate methods in pharmaceutical applications. *Journal of the Chemometrics Society* 2002, 16, 141–160, DOI: 10.1002/cem.697.
- [60] Brühlmann, D., Sokolov, M., Butté, A., Sauer, M. et al., Parallel experimental design and multivariate analysis provides efficient screening of cell culture media supplements to improve biosimilar product quality. *Biotechnology and Bioengineering* 2017, 114, 1448–1458, DOI: 10.1002/bit.26269.
- [61] Esbensen, K. H., Guyot, D., Westad, F., Houmoller, L. P., Multivariate data analysis in practice: An introduction to multivariate data analysis and experimental design, *Camo Process*, 2002.
- [62] Kleppmann, W., Versuchsplanung: Produkte und Prozesse optimieren, *Carl Hanser Verlag*, 2020.
- [63] Guo, H., Design of experiments and data analysis, in: Mettas, A. (Ed.). *Annual Reliability and Maintainability Symposium*, 2012.

- [64] Krishnaiah, K., Shahabudeen, P., Applied design of experiments and Taguchi methods, *PHI Learning*, 2012.
- [65] Beg, S., Swain, S., Rahman, M., Hasnain, M. S. et al., Chapter 3: Application of design of experiments (DoE) in pharmaceutical product and process optimization, in: Beg, S., Hasnain, M. S. (Ed.). *Pharmaceutical quality by design*, *Academic Press*, 2019, pp. 43–64, DOI: 10.1016/B978-0-12-815799-2.00003-4.
- [66] Dhoot, A. S., Fernandes, G. J., Naha, A., Rathnanand, M. et al., Design of experiments in pharmaceutical development. *Pharmaceutical Chemistry Journal* 2019, 53, 730–735, DOI: 10.1007/s11094-019-02070-4.
- [67] Castillo, J. C., Ahuja, A., Athey, S., Baker, A. et al., Market design to accelerate COVID-19 vaccine supply. *Science* 2021, 371, 1107–1109. DOI: 10.1126/science.abg0889
- [68] Schillberg, S., Finnern, R., Plant molecular farming for the production of valuable proteins: Critical evaluation of achievements and future challenges. *Journal of Plant Physiology* 2021, 258–259, 153359, DOI: 10.1016/j.jplph.2020.153359.
- [69] He, W., Baysal, C., Lobato Gómez, M., Huang, X. et al., Contributions of the international plant science community to the fight against infectious diseases in humans: Affordable drugs in edible plants for endemic and re-emerging diseases. *Plant Biotechnology Journal* 2021, 19, 1921–1936, DOI: 10.1111/pbi.13658.
- [70] Rybicki, E., I Hitzeroth, I., Meyers, A., Jose Dus Santos, M. et al., Developing country applications of molecular farming: Case studies in South Africa and Argentina. *Current Pharmaceutical Design* 2013, 19, 5612–5621, DOI: 10.2174/1381612811319310015.
- [71] Barbier, A. J., Jiang, A. Y., Zhang, P., Wooster, R. et al., The clinical progress of mRNA vaccines and immunotherapies. *Nature Biotechnology* 2022, 40, 840–854, DOI: 10.1038/s41587-022-01294-2.
- [72] Margolin, E., Schäfer, G., Allen, J. D., Gers, S. et al., A plant-produced SARS-CoV-2 spike protein elicits heterologous immunity in hamsters. *Frontiers in Plant Science* 2023, 14. DOI: 10.3389/fpls.2023.1146234
- [73] Badr, S., Okamura, K., Takahashi, N., Ubbenjans, V. et al., Integrated design of biopharmaceutical manufacturing processes: Operation modes and process configurations for monoclonal antibody production. *Computers & Chemical Engineering* 2021, 153, 107422, DOI: 10.1016/j.compchemeng.2021.107422.
- [74] Tusé, D., Nandi, S., McDonald, K. A., Buyel, J. F., The emergency response capacity of plant-based biopharmaceutical manufacturing - What it is and what it could be. *Frontiers in Plant Science* 2020, 11. DOI: 10.3389/fpls.2020.594019
- [75] Rapp, E., Reichl, U., Advances in Glycobiotechnology, *Springer* 2021, DOI: 10.1007/978-3-030-69590-3.
- [76] Walsh, G., Biopharmaceutical benchmarks 2018. *Nature Biotechnology* 2018, 36, 1136–1145, DOI: 10.1038/nbt.4305.
- [77] Kesik-Brodacka, M., Progress in biopharmaceutical development. *Biotechnology and Applied Biochemistry* 2018, 65, 306–322, DOI: 10.1002/bab.1617.
- [78] Schillberg, S., Raven, N., Spiegel, H., Rasche, S. et al., Critical analysis of the commercial potential of plants for the production of recombinant proteins. *Frontiers in Plant Science* 2019, 10, DOI: 10.3389/fpls.2019.00720.
- [79] Santos, R. B., Abranches, R., Fischer, R., Sack, M. et al., Putting the spotlight back on plant suspension cultures. *Frontiers in Plant Science* 2016, 7, DOI: 10.3389/fpls.2016.00297.

- [80] Chung, Y. H., Church, D., Koellhoffer, E. C., Osota, E. et al., Integrating plant molecular farming and materials research for next-generation vaccines. *Nature Reviews Materials* 2022, 7, 372–388, DOI: 10.1038/s41578-021-00399-5.
- [81] Gengenbach, B. B., Keil, L. L., Opdensteinen, P., Müschen, C. R. et al., Comparison of microbial and transient expression (tobacco plants and plant-cell packs) for the production and purification of the anticancer mistletoe lectin viscumin. *Biotechnology and Bioengineering* 2019, 116, 2236–2249, DOI: 10.1002/bit.27076.
- [82] Schreiber, C., Müller, H., Birrenbach, O., Klein, M. et al., A high-throughput expression screening platform to optimize the production of antimicrobial peptides. *Microbial Cell Factories* 2017, 16, 1–13. DOI: 10.1186/s12934-017-0637-5
- [83] Walsh, G., Jefferis, R., Post-translational modifications in the context of therapeutic proteins. *Nature Biotechnology* 2006, 24, 1241–1252, DOI: 10.1038/nbt1252.
- [84] Faye, L., Boulaflous, A., Benchabane, M., Gomord, V. et al., Protein modifications in the plant secretory pathway: current status and practical implications in molecular pharming. *Vaccine* 2005, 23, 1770–1778, DOI: 10.1016/j.vaccine.2004.11.003.
- [85] Hehle, V. K., Paul, M. J., Drake, P. M., Ma, J. K. C. et al., Antibody degradation in tobacco plants: a predominantly apoplastic process. *BMC Biotechnology* 2011, 11, 1–12, DOI: 10.1186/1472-6750-11-128.
- [86] Burnett, M. J. B., Burnett, A. C., Therapeutic recombinant protein production in plants: Challenges and opportunities. *Plants, People, Planet* 2020, 2, 121–132, DOI: 10.1002/ppp3.10073.
- [87] Fischer, R., Buyel, J. F., Molecular farming - The slope of enlightenment. *Biotechnology Advances* 2020, 40, 107519. DOI: 10.1016/j.biotechadv.2020.107519
- [88] Twyman, R. M., Stoger, E., Schillberg, S., Christou, P. et al., Molecular farming in plants: host systems and expression technology. *Trends in Biotechnology* 2003, 21, 570–578, DOI: 10.1016/j.tibtech.2003.10.002.
- [89] Xu, S., Gavin, J., Jiang, R., Chen, H., Bioreactor productivity and media cost comparison for different intensified cell culture processes. *Biotechnology Progress* 2017, 33, 867–878, DOI: 10.1002/btpr.2415.
- [90] Buyel, J. F., Fischer, R., Predictive models for transient protein expression in tobacco (*Nicotiana tabacum* L.) can optimize process time, yield, and downstream costs. *Biotechnology and Bioengineering* 2012, 109, 2575–2588, DOI: 10.1002/bit.24523.
- [91] Twyman, R. M., Schillberg, S., Fischer, R., Transgenic plants in the biopharmaceutical market. *Expert Opinion on Emerging Drugs* 2005, 10, 185–218, DOI: 10.1517/14728214.10.1.185.
- [92] Knödler, M., Buyel, J. F., Plant-made immunotoxin building blocks: A roadmap for producing therapeutic antibody-toxin fusions. *Biotechnology Advances* 2021, 47, 107683, DOI: 10.1016/j.biotechadv.2020.107683.
- [93] Allahyari, H., Heidari, S., Ghamgosha, M., Saffarian, P. et al., Immunotoxins: A new tool for cancer therapy. *Journal of the International Society for Oncodevelopmental Biology and Medicine* 2017, 39, 1010428317692226, DOI: 10.1177/1010428317692226.
- [94] Polito, L., Bortolotti, M., Battelli, M. G., Calafato, G. et al., Ricin: An ancient story for a timeless plant toxin. *Toxins* 2019, 11, 324, DOI: 10.3390/toxins11060324.
- [95] van der Valk, J., Brunner, D., Smet, K. de, Svenningsen, Å. F. et al., Optimization of chemically defined cell culture media-replacing fetal bovine serum in mammalian in vitro methods. *Toxicology in vitro* 2010, 24, 1053–1063, DOI: 10.1016/j.tiv.2010.03.016.

- [96] van der Valk, J., Mellor, D., Brands, R., Fischer, R. et al., The humane collection of fetal bovine serum and possibilities for serum-free cell and tissue culture. *Toxicology in vitro* 2004, 18, 1–12, DOI: 10.1016/j.tiv.2003.08.009.
- [97] Grabowski, G. A., Golembo, M., Shaaltiel, Y., Taliglucerase alfa - An enzyme replacement therapy using plant cell expression technology. *Molecular Genetics and Metabolism* 2014, 112, 1–8, DOI: 10.1016/j.ymgme.2014.02.011.
- [98] Tekoah, Y., Shulman, A., Kizhner, T., Ruderfer, I. et al., Large-scale production of pharmaceutical proteins in plant cell culture: The protalix experience. *Plant Biotechnology Journal* 2015, 13, 1199–1208, DOI: 10.1111/pbi.12428.
- [99] Fischer, R., Schillberg, S., Molecular Farming, in: Thomas, B., Murray, B. G., Murphy, D. J. (Ed.). *Encyclopedia of Applied Plant Sciences (Second Edition)*, Academic Press 2017, pp. 77–82.
- [100] Huebbers, J. W., Buyel, J. F., On the verge of the market - Plant factories for the automated and standardized production of biopharmaceuticals. *Biotechnology Advances* 2021, 46, 107681. DOI: 10.1016/j.biotechadv.2020.107681
- [101] Castilho, A., Windwarder, M., Gattinger, P., Mach, L. et al., Proteolytic and N-glycan processing of human α 1-antitrypsin expressed in *Nicotiana benthamiana*. *Plant Physiology* 2014, 166, 1839–1851.
- [102] Hundleby, P. A. C., D'Aoust, M.-A., Finkle, C., Atkins, J. et al., Regulation of molecular farming products, in: Schillberg, S., Spiegel, H. (Ed.). *Recombinant proteins in plants: Methods and protocols*, Springer 2022, pp. 313–333.
- [103] Modarresi, M., Javaran, M. J., Shams-bakhsh, M., Zeinali, S. et al., Transient expression of anti-VEGFR2 nanobody in *Nicotiana tabacum* and *N. benthamiana*. *Three Biotech* 2018, 8, 484, DOI: 10.1007/s13205-018-1500-z.
- [104] Yang, S.-J., Carter, S. A., Cole, A. B., Cheng, N.-H. et al., A natural variant of a host RNA-dependent RNA polymerase is associated with increased susceptibility to viruses by *Nicotiana benthamiana*. *Proceedings of the National Academy of Sciences* 2004, 101, 6297–6302, DOI: 10.1073/pnas.0304346101.
- [105] Nosaki, S., Hoshikawa, K., Ezura, H., Miura, K., Transient protein expression systems in plants and their applications. *Plant Biotechnology* 2021, 38, 297–304, DOI: 10.5511/plantbiotechnology.21.0610a.
- [106] Fischer, R., Stoger, E., Schillberg, S., Christou, P. et al., Plant-based production of biopharmaceuticals. *Current Opinion in Plant Biology* 2004, 7, 152–158, DOI: 10.1016/j.pbi.2004.01.007.
- [107] Zvirin, T., Magrisso, L., Yaari, A., Shoseyov, O., Stable Expression of Adalimumab in *Nicotiana tabacum*. *Molecular Biotechnology* 2018, 60, 387–395, DOI: 10.1007/s12033-018-0075-6.
- [108] Fischer, R., Emans, N., Molecular farming of pharmaceutical proteins. *Transgenic Research* 2000, 9, 279–299, DOI: 10.1023/A:1008975123362.
- [109] Martine, G., Philippe, H., Myriam, S., Biosafety considerations associated with molecular farming in genetically modified plants. *Journal of Medicinal Plants Research* 2009, 3, 825–838.
- [110] D'Aoust, M.-A., Couture, M. M.-J., Charland, N., Trépanier, S. et al., The production of hemagglutinin-based virus-like particles in plants: A rapid, efficient and safe response to pandemic influenza. *Plant Biotechnology Journal* 2010, 8, 607–619, DOI: 10.1111/j.1467-7652.2009.00496.x.

- [111] Darbani, B., Eimanifar, A., Stewart Jr, C. N., Camargo, W. N., Methods to produce marker-free transgenic plants. *Biotechnology Journal* 2007, 2, 83–90, DOI: 10.1002/biot.200600182.
- [112] Giddings, G., Allison, G., Brooks, D., Carter, A., Transgenic plants as factories for biopharmaceuticals. *Nature Biotechnology* 2000, 18, 1151–1155, DOI: 10.1038/81132.
- [113] Andrews, L. B., Curtis, W. R., Comparison of transient protein expression in tobacco leaves and plant suspension culture. *Biotechnology Progress* 2005, 21, 946–952, DOI: 10.1021/bp049569k.
- [114] Voinnet, O., Rivas, S., Mestre, P., Baulcombe, D., An enhanced transient expression system in plants based on suppression of gene silencing by the p19 protein of tomato bushy stunt virus. *The Plant Journal* 2003, 33, 949–956, DOI: 10.1046/j.1365-313X.2003.01676.x.
- [115] Butaye, K. M.J., Goderis, I. J.W.M., Wouters, P. F.J., Poes, J. M.-T.G. et al., Stable high-level transgene expression in *Arabidopsis thaliana* using gene silencing mutants and matrix attachment regions. *The Plant Journal* 2004, 39, 440–449, DOI: 10.1111/j.1365-313X.2004.02144.x.
- [116] Peyret, H., Lomonossoff, G. P., When plant virology met *Agrobacterium*: The rise of the deconstructed clones. *Plant Biotechnology Journal* 2015, 13, 1121–1135.
- [117] Chilton, M.-D., Drummond, M. H., Merlo, D. J., Sciaky, D. et al., Stable incorporation of plasmid DNA into higher plant cells: The molecular basis of crown gall tumorigenesis. *Cell* 1977, 11, 263–271. DOI:10.1016/0092-8674(77)90043-5
- [118] Gordon, J. E., Christie, P. J., The *Agrobacterium* Ti plasmid. *Microbiology Spectrum* 2014, 2, DOI: 10.1128/9781555818982.ch17.
- [119] Shibata, D., Liu, Y. G., Technical focus-*Agrobacterium*-mediated plant transformation with large DNA fragments. *Trends in Plant Science* 2000, 5, 354–357, DOI: 10.1016/S1360-1385(00)01689-7.
- [120] Shah, K. H., Almaghrabi, B., Bohlmann, H., Comparison of expression vectors for transient expression of recombinant proteins in plants. *Plant Molecular Biology Reporter* 2013, 31, 1529–1538, DOI: 10.1007/s11105-013-0614-z.
- [121] Ibrahim, A., Odon, V., Kormelink, R., Plant viruses in plant molecular pharming: Toward the use of enveloped viruses. *Frontiers in Plant Science* 2019, 10, DOI: 10.3389/fpls.2019.00803.
- [122] Gleba, Y., Marillonnet, S., Klimyuk, V., Engineering viral expression vectors for plants: The full virus and the deconstructed virus strategies. *Current Opinion in Plant Biology* 2004, 7, 182–188, DOI: 10.1016/j.pbi.2004.01.003.
- [123] Avesani, L., Marconi, G., Morandini, F., Albertini, E. et al., Stability of potato virus X expression vectors is related to insert size: Implications for replication models and risk assessment. *Transgenic Research* 2007, 16, 587–597. DOI:10.1007/s11248-006-9051-1
- [124] Chen, Q., Lai, H., Hurtado, J., Stahnke, J. et al., Agroinfiltration as an effective and scalable strategy of gene delivery for production of pharmaceutical proteins. *Advanced Techniques in Biology & Medicine* 2013, 1, DOI: 10.4172/atbm.1000103.
- [125] Rybicki, E. P., Plant-made vaccines for humans and animals. *Plant Biotechnology Journal* 2010, 8, 620–637. DOI:10.1111/j.1467-7652.2010.00507.x
- [126] Buyel, J. F., Twyman, R. M., Fischer, R., Extraction and downstream processing of plant-derived recombinant proteins. *Biotechnology Advances* 2015, 33, 902–913, DOI: 10.1016/j.biotechadv.2015.04.010.

- [127] Buyel, J. F., Opdensteinen, P., Fischer, R., Cellulose-based filter aids increase the capacity of depth filters during the downstream processing of plant-derived biopharmaceutical proteins. *Biotechnology Journal* 2015, 10, 584–591, DOI: 10.1002/biot.201400611.
- [128] Buyel, J. F., Gruchow, H. M., Boes, A., Fischer, R., Rational design of a host cell protein heat precipitation step simplifies the subsequent purification of recombinant proteins from tobacco. *Biochemical Engineering Journal* 2014, 88, 162–170, DOI: 10.1016/j.bej.2014.04.015.
- [129] Opdensteinen, P., Lobanov, A., Buyel, J. F., A combined pH and temperature precipitation step facilitates the purification of tobacco-derived recombinant proteins that are sensitive to extremes of either parameter. *Biotechnology Journal* 2021, 16, 2000340, DOI: 10.1002/biot.202000340.
- [130] Opdensteinen, P., Clodt, J. I., Müschen, C. R., Filiz, V. et al., A Combined ultrafiltration/diafiltration step facilitates the purification of cyanovirin-N from transgenic tobacco extracts. *Frontiers in Bioengineering and Biotechnology* 2019, 6, DOI: 10.3389/fbioe.2018.00206.
- [131] Holland, T., Sack, M., Rademacher, T., Schmale, K. et al., Optimal nitrogen supply as a key to increased and sustained production of a monoclonal full-size antibody in BY-2 suspension culture. *Biotechnology and Bioengineering* 2010, 107, 278–289, DOI: 10.1002/bit.22800.
- [132] O'Leary, B. M., Rico, A., McCraw, S., Fones, H. N. et al., The infiltration-centrifugation technique for extraction of apoplastic fluid from plant leaves using *Phaseolus vulgaris* as an example. *Journal of Visualized Experiments* 2014, e52113, DOI: 10.3791/52113.
- [133] Jansing, J., Sack, M., Augustine, S. M., Fischer, R. et al., CRISPR/Cas9-mediated knockout of six glycosyltransferase genes in *Nicotiana benthamiana* for the production of recombinant proteins lacking β -1,2-xylose and core α -1,3-fucose. *Plant Biotechnology Journal* 2019, 17, 350–361, DOI: 10.1111/pbi.12981.
- [134] Strasser, R., Stadlmann, J., Schähs, M., Stiegler, G. et al., Generation of glyco-engineered *Nicotiana benthamiana* for the production of monoclonal antibodies with a homogeneous human-like N-glycan structure. *Plant Biotechnology Journal* 2008, 6, 392–402, DOI: 10.1111/j.1467-7652.2008.00330.x.
- [135] Smargiasso, N., Nader, J., Rioux, S., Mazzucchelli, G. et al., Exploring the N-glycosylation profile of glycoprotein B from human cytomegalovirus expressed in CHO and *Nicotiana tabacum* BY-2 cells. *International Journal of Molecular Sciences* 2019, 20, DOI: 10.3390/ijms20153741.
- [136] Rup, B., Alon, S., Amit-Cohen, B.-C., Brill Almon, E. et al., Immunogenicity of glycans on biotherapeutic drugs produced in plant expression systems: The taliglucerase alfa story. *Public Library of Science One* 2017, 12, e0186211, DOI: 10.1371/journal.pone.0186211.
- [137] Piotrkowski, N., Schillberg, S., Rasche, S., Tackling Heterogeneity: A leaf disc-based assay for the high-throughput screening of transient gene expression in Tobacco. *Public Library of Science One* 2012, 7, e45803, DOI: 10.1371/journal.pone.0045803.
- [138] Reuter, L. J., Bailey, M. J., Joensuu, J. J., Ritala, A., Scale-up of hydrophobin-assisted recombinant protein production in tobacco BY-2 suspension cells. *Plant Biotechnology Journal* 2014, 12, 402–410, DOI: 10.1111/pbi.12147.
- [139] Vasilev, N., Grömping, U., Lipperts, A., Raven, N. et al., Optimization of BY-2 cell suspension culture medium for the production of a human antibody using a combination

- of fractional factorial designs and the response surface method. *Plant Biotechnology Journal* 2013, 11, 867–874, DOI: 10.1111/pbi.12079.
- [140] Buntru, M., Vogel, S., Finnern, R., Schillberg, S., Plant-based cell-free transcription and translation of recombinant proteins, in: Schillberg, S., Spiegel, H. (Ed.). *Recombinant proteins in plants: Methods and protocols*, Springer, 2022, pp. 113–124, DOI: 10.1007/978-1-0716-2241-4_8.
- [141] Buntru, M., Vogel, S., Spiegel, H., Schillberg, S., Tobacco BY-2 cell-free lysate: An alternative and highly-productive plant-based in vitro translation system. *BMC Biotechnology* 2014, 14, 1–11. DOI: 10.1186/1472-6750-14-37
- [142] Pumplin, N., Voinnet, O., RNA silencing suppression by plant pathogens: Defence, counter-defence and counter-counter-defence. *Nature Reviews Microbiology* 2013, 11, 745–760, DOI: 10.1038/nrmicro3120.
- [143] Opdensteinen, P., Meyer, S., Buyel, J. F., Nicotiana spp. for expression and purification of functional IgG3 antibodies directed against the Staphylococcus aureus alpha toxin. *Frontiers in Chemical Engineering* 2021, 3. DOI: 10.3390/antibiotics9040202
- [144] Buyel, J. F., Kaever, T., Buyel, J. J., Fischer, R., Predictive models for the accumulation of a fluorescent marker protein in tobacco leaves according to the promoter/5'UTR combination. *Biotechnology and Bioengineering* 2013, 110, 471–482, DOI: 10.1002/bit.24715.
- [145] Bareither, R., Pollard, D., A review of advanced small-scale parallel bioreactor technology for accelerated process development: Current state and future need. *Biotechnology Progress* 2011, 27, 2–14, DOI: 10.1002/btpr.522.
- [146] Fink, M., Cserjan-Puschmann, M., Reinisch, D., Striedner, G., High-throughput microbioreactor provides a capable tool for early stage bioprocess development. *Scientific Reports* 2021, 11, 2056, DOI: 10.1038/s41598-021-81633-6.
- [147] Camilo, C. M., Polikarpov, I., High-throughput cloning, expression and purification of glycoside hydrolases using ligation-independent cloning (LIC). *Protein Expression and Purification* 2014, 99, 35–42. DOI: 10.1016/j.pep.2014.03.008
- [148] Kwon, K., Peterson, S. N., Expression and solubility testing in a high-throughput environment, in: Anderson, W. F. (Ed.). *Structural genomics and drug discovery: Methods and protocols*, Springer, 2014, pp. 75–88. DOI: 10.1007/978-1-4939-0354-2_6
- [149] Chen, A., Chitta, R., Chang, D., Amanullah, A., Twenty-four well plate miniature bioreactor system as a scale-down model for cell culture process development. *Biotechnology and Bioengineering* 2009, 102, 148–160. DOI: 10.1002/bit.22031
- [150] Tremblay, R., Feng, M., Menassa, R., Huner, N. et al., High-yield expression of recombinant soybean agglutinin in plants using transient and stable systems. *Transgenic Research* 2011, 20, 345–356. DOI: 10.1007/s11248-010-9419-0
- [151] Gengenbach, B. B., Opdensteinen, P., Buyel, J. F., Robot cookies - Plant cell packs as an automated high-throughput screening platform based on transient expression. *Frontiers in Bioengineering and Biotechnology* 2020, 8. DOI: 10.3389/fbioe.2020.00393
- [152] Shih, Y.-P., Kung, W.-M., Chen, J.-C., Yeh, C.-H. et al., High-throughput screening of soluble recombinant proteins. *Protein Science* 2002, 11, 1714–1719, DOI: 10.1110/ps.0205202.
- [153] Saez, N. J., Vincentelli, R., High-throughput expression screening and purification of recombinant proteins in E. coli, in: Chen, Y. W. (Ed.). *Structural genomics: General applications*, Humana Press, 2014, pp. 33–53. DOI: 10.1007/978-1-62703-691-7_3

- [154] Wang, H. M., Shih, Y. P., Hu, S. M., Lo, W. T. et al., Parallel gene cloning and protein production in multiple expression systems. *Biotechnology Progress* 2009, 25, 1582–1586, DOI: 10.1002/btpr.274.
- [155] Chapple, S. D. J., Crofts, A. M., Shadbolt, S. P., McCafferty, J. et al., Multiplexed expression and screening for recombinant protein production in mammalian cells. *BMC Biotechnology* 2006, 6, 49, DOI: 10.1186/1472-6750-6-49.
- [156] Wang, B., Albanetti, T., Miro-Quesada, G., Flack, L. et al., High-throughput screening of antibody-expressing CHO clones using an automated shaken deep-well system. *Biotechnology Progress* 2018, 34, 1460–1471, DOI: 10.1002/btpr.2721.
- [157] Bos, A. B., Luan, P., Duque, J. N., Reilly, D. Harms, P. D., Wong, A. W., Optimization and automation of an end-to-end high throughput microscale transient protein production process. *Biotechnology and Bioengineering* 2015, 112, 1832–1842, DOI: 10.1002/bit.25601.
- [158] Page, M. T., Parry, M. A., Carmo-Silva, E., A high-throughput transient expression system for rice. *Plant, Cell & Environment* 2019, 42, 2057–2064, DOI: 10.1111/pce.13542.
- [159] Esposito, D., Garvey, L. A., Chakiath, C. S., Gateway cloning for protein expression, in: Doyle, S. A. (Ed.). High throughput protein expression and purification: Methods and protocols, *Humana Press*, 2009, pp. 31–54, DOI: 10.1007/978-1-59745-196-3_3.
- [160] Dieckman, L., Gu, M., Stols, L., Donnelly, M. I. et al., High throughput methods for gene cloning and expression. *Protein Expression and Purification* 2002, 25, 1–7, DOI: 10.1006/prep.2001.1602.
- [161] Jia, B., Jeon, C. O., High-throughput recombinant protein expression in *Escherichia coli*: Current status and future perspectives. *Open Biology* 2016, 6, 160196, DOI: 10.1098/rsob.160196.
- [162] Szybalski, W., Kim, S. C., Hasan, N., Podhajska, A. J., Class-IIS restriction enzymes: A review. *Gene* 1991, 100, 13–26, DOI: 10.1016/0378-1119(91)90345-C.
- [163] Pryor, J. M., Potapov, V., Kucera, R. B., Bilotti, K. et al., Enabling one-pot Golden Gate assemblies of unprecedented complexity using data-optimized assembly design. *Public Library of Science One* 2020, 15, e0238592, DOI: 10.1371/journal.pone.0238592.
- [164] Zhang, Y., Werling, U., Edelmann, W., Seamless ligation cloning extract (SLiCE) cloning method. *Methods in Molecular Biology* 2014, 1116, 235–244, DOI: 10.1007/978-1-62703-764-8_16.
- [165] Schmid-Burgk, J. L., Schmidt, T., Kaiser, V., Höning, K. et al., A ligation-independent cloning technique for high-throughput assembly of transcription activator-like effector genes. *Nature Biotechnology* 2013, 31, 76–81, DOI: 10.1038/nbt.2460.
- [166] Thieme, F., Engler, C., Kandzia, R., Marillonnet, S., Quick and clean cloning: A ligation-independent cloning strategy for selective cloning of specific PCR products from non-specific mixes. *Public Library of Science One* 2011, 6, e20556, DOI: 10.1371/journal.pone.0020556.
- [167] Kinsland, C., Chapter 9.19: Bacterial protein overexpression systems and strategies, in: Liu, H.-W., Mander, L. (Ed.). Comprehensive natural products II, *Elsevier* 2010, pp. 695–721, DOI: 10.1016/B978-008045382-8.00199-4.
- [168] Storch, M., Haines, M. C., Baldwin, G. S., DNA-bot: A low-cost, automated DNA assembly platform for synthetic biology. *Synthetic Biology* 2020, 5, 010, DOI: 10.1093/synbio/ysaa010.

- [169] Walsh, D. I., Pavan, M., Ortiz, L., Wick, S. et al., Standardizing automated DNA assembly: Best practices, metrics, and protocols using robots. *Translating Life Sciences Innovation* 2019, 24, 282–290, DOI: 10.1177/2472630318825335.
- [170] Hillson, N., Caddick, M., Cai, Y., Carrasco, J. A. et al., Building a global alliance of biofoundries. *Nature Communications* 2019, 10, 2040, DOI: 10.1038/s41467-019-10079-2.
- [171] Rademacher, T., Sack, M., Blessing, D., Fischer, R. et al., Plant cell packs: A scalable platform for recombinant protein production and metabolic engineering. *Plant Biotechnology Journal* 2019, 17, 1560–1566, DOI: 10.1111/pbi.13081.
- [172] Opdensteinen, P., Sperl, L. E., Mohamadi, M., Kündgen-Redding, N. et al., The transient expression of recombinant proteins in plant cell packs facilitates stable isotope labelling for NMR spectroscopy. *Plant Biotechnology Journal* 2022, 20, 1928–1939, DOI: 10.1111/pbi.13873.
- [173] Opdensteinen, P., Buyel, J. F., Reducing water uptake into BY-2 cells by systematically optimizing the cultivation parameters increases product yields achieved by transient expression in plant cell packs. *Biotechnology Journal* 2022, 17, 2200134, DOI: 10.1002/biot.202200134.
- [174] Opdensteinen, P., Dietz, S. J., Gengenbach, B. B., Buyel, J. F., Expression of biofilm-degrading enzymes in plants and automated high-throughput activity screening using experimental *Bacillus subtilis* biofilms. *Frontiers in Bioengineering and Biotechnology* 2021, 714, DOI: 10.3389/fbioe.2021.708150.
- [175] Welch, C. J., High throughput analysis enables high throughput experimentation in pharmaceutical process research. *Reaction Chemistry & Engineering* 2019, 4, 1895–1911, DOI: 10.1039/C9RE00234K.
- [176] Ahmed, F. E., Wiley, J. E., Weidner, D. A., Bonnerup, C. et al., Surface plasmon resonance (SPR) spectrometry as a tool to analyze nucleic acid-protein interactions in crude cellular extracts. *Cancer Genomics & Proteomics* 2010, 7, 303–309.
- [177] Nguyen, H. H., Park, J., Kang, S., Kim, M., Surface plasmon resonance: A versatile technique for biosensor applications. *Sensors Journal* 2015, 15, 10481–10510, DOI: 10.3390/s150510481.
- [178] Tabasi, O., Falamaki, C., Recent advancements in the methodologies applied for the sensitivity enhancement of surface plasmon resonance sensors. *Analytical Methods* 2018, 10, 3906–3925, DOI: 10.1039/C8AY00948A.
- [179] Schasfoort, R. B. M., Chapter 1: Introduction to surface plasmon resonance, in: Handbook of surface plasmon resonance. *Royal Society of Chemistry* 2017. DOI: 10.1039/9781788010283.
- [180] Gaudreault, J., Forest-Nault, C., Crescenzo, G. de, Durocher, Y. et al., On the use of surface plasmon resonance-based biosensors for advanced bioprocess monitoring. *Processes* 2021, 9, DOI: 10.3390/pr9111996.
- [181] Yatabe, R., Onodera, T., Toko, K., Fabrication of surface plasmon resonance sensor surface with control of the non-specific adsorption and affinity for the detection of 2,4,6-trinitrotoluene using an antifouling copolymer. *Frontiers in Bioengineering and Biotechnology* 2014, 2. DOI: 10.3389/fbioe.2014.00010.
- [182] Shankaran, D. R., Gobi, K. V., Miura, N., Recent advancements in surface plasmon resonance immunosensors for detection of small molecules of biomedical, food and environmental interest. *Sensors and Actuators B: Chemical* 2007, 121, 158–177, DOI: 10.1016/j.snb.2006.09.014.

- [183] Cao, Y., McDermott, M. T., A surface plasmon resonance based inhibition immunoassay for measurement of steroid hormones. *Analytical Biochemistry* 2018, 557, 7–12, DOI: 10.1016/j.ab.2018.06.027.
- [184] Mariani, S., Minunni, M., Surface plasmon resonance applications in clinical analysis. *Analytical and Bioanalytical Chemistry* 2014, 406, 2303–2323, DOI: 10.1007/s00216-014-7647-5.
- [185] Grover Shah, V., Ray, S., Karlsson, R., Srivastava, S., Calibration-free concentration analysis of protein biomarkers in human serum using surface plasmon resonance. *Talanta* 2015, 144, 801–808, DOI: 10.1016/j.talanta.2015.06.074.
- [186] Wijaya, E., Lenaerts, C., Maricot, S., Hastanin, J. et al., Surface plasmon resonance-based biosensors: From the development of different SPR structures to novel surface functionalization strategies. *Current Opinion in Solid State and Materials Science* 2011, 15, 208–224, DOI: 10.1016/j.cossms.2011.05.001.
- [187] Fischer, M. J. E., Amine coupling through EDC/NHS: A practical approach, in: Mol, N. J., Fischer, M. J. E. (Ed.). Surface plasmon resonance: Methods and protocols, *Humana Press*, 2010, pp. 55–73, DOI: 10.1007/978-1-60761-670-2_3.
- [188] de Jong N. W., van Kessel K. P., van Strijp J. A. G., Immune evasion by *Staphylococcus aureus*. *Microbiology Spectrum* 2019, 7, 7.2.20, DOI: 10.1128/microbiolspec.GPP3-0061-2019.
- [189] Nausch, H., Mikschofsky, H., Koslowski, R., Meyer, U. et al., High-level transient expression of ER-targeted human interleukin 6 in *Nicotiana benthamiana*. *Public Library of Science One* 2012, 7, e48938, DOI: 10.1371/journal.pone.0048938.
- [190] Kolotilin, I., Plant-produced recombinant cytokines IL-37b and IL-38 modulate inflammatory response from stimulated human PBMCs. *Scientific Reports* 2022, 12, 19450, DOI: 10.1038/s41598-022-23828-z.
- [191] Bialek-Waldmann, J. K., Domning, S., Esser, R., Glienke, W. et al., Induced dendritic cells co-expressing GM-CSF/IFN- α /TWT1 priming T and B cells and automated manufacturing to boost GvL. *Molecular Therapy - Methods & Clinical Development* 2021, 21, 621–641, DOI: 10.1016/j.omtm.2021.04.004.
- [192] Elseberg, C. L., Salzig, D., Czermak, P., Bioreactor expansion of human mesenchymal stem cells according to GMP requirements, in: Turksen, K. (Ed.). Stem cells and good manufacturing practices: Methods, protocols, and regulations, *Springer* 2015, pp. 199–218, DOI: 10.1007/7651_2014_117.
- [193] Czapla, J., Matuszczak, S., Kulik, K., Wiśniewska, E. et al., The effect of culture media on large-scale expansion and characteristic of adipose tissue-derived mesenchymal stromal cells. *Stem Cell Research & Therapy* 2019, 10, 235, DOI: 10.1186/s13287-019-1331-9.
- [194] Redi, D., Raffaelli, C. S., Rossetti, B., Luca, A. de et al., *Staphylococcus aureus* vaccine preclinical and clinical development: Current state of the art. *The New Microbiologica* 2018, 41, 208–213.
- [195] Cheung, G. Y. C., Otto, M., The potential use of toxin antibodies as a strategy for controlling acute *Staphylococcus aureus* infections. *Expert Opinion on Therapeutic Targets* 2012, 16, 601–612, DOI: 10.1517/14728222.2012.682573.
- [196] Kallolimath, S., Hackl, T., Gahn, R., Grünwald-Gruber, C. et al., Expression profiling and glycan engineering of IgG subclass 1-4 in *Nicotiana benthamiana*. *Frontiers in Bioengineering and Biotechnology* 2020, 8, DOI: 10.3389/fbioe.2020.00825.

- [197] Kallolimath, S., Sun, L., Palt, R., Stiasny, K. et al., Highly active engineered IgG3 antibodies against SARS-CoV-2. *Proceedings of the National Academy of Sciences* 2021, 118, e2107249118, DOI: 10.1073/pnas.2107249118.
- [198] Senga, Y., Doi, M., Onitsuka, M., Honda, S., Live-cell imaging to analyze intracellular aggregation of recombinant IgG in CHO cells. *Cell Chemical Biology* 2022, 29, 120-132.e4, DOI: 10.1016/j.chembiol.2021.08.010.
- [199] Abdallah, M., Benoliel, C., Drider, D., Dhulster, P. et al., Biofilm formation and persistence on abiotic surfaces in the context of food and medical environments. *Archives of Microbiology* 2014, 196, 453–472, DOI: 10.1007/s00203-014-0983-1.
- [200] Neville, N., Roberge, N., Jia, Z., Polyphosphate kinase 2 (PPK2) enzymes: Structure, function, and roles in bacterial physiology and virulence. *International Journal of Molecular Sciences* 2022, 23, DOI: 10.3390/ijms23020670.
- [201] Batten, L. E., Bacterial kinases as potential targets for broad-spectrum antibiotics. Doctoral thesis, *University of Southampton* 2013.
- [202] Rao, N. N., Gómez-García, M. R., Kornberg, A., Inorganic polyphosphate: Essential for growth and survival. *Annual Review of Biochemistry* 2009, 78, 605–647, DOI: 10.1146/annurev.biochem.77.083007.093039.
- [203] Zhang, H., Ishige, K., Kornberg, A., A polyphosphate kinase (PPK2) widely conserved in bacteria. *Proceedings of the National Academy of Sciences* 2002, 99, 16678–16683, DOI: 10.1073/pnas.262655199.
- [204] Tavanti, M., Hosford, J., Lloyd, R. C., Brown, M. J. B., ATP regeneration by a single polyphosphate kinase powers multigram-scale aldehyde synthesis in vitro. *Green Chemistry* 2021, 23, 828–837, DOI: 10.1039/D0GC03830J.
- [205] Calhoun, K. A., Swartz, J. R., Energy systems for ATP regeneration in cell-free protein synthesis reactions. *Methods in Molecular Biology* 2007, 375, 3–17, DOI: 10.1007/978-1-59745-388-2_1.
- [206] Nakonieczna, A., Cooper, C. J., Gryko, R., Bacteriophages and bacteriophage-derived endolysins as potential therapeutics to combat Gram-positive spore forming bacteria. *Journal of Applied Microbiology* 2015, 119, 620–631, DOI: 10.1111/jam.12881.
- [207] Schmelcher, M., Donovan, D. M., Loessner, M. J., Bacteriophage endolysins as novel antimicrobials. *Future Microbiology* 2012, 7, 1147–1171, DOI: 10.2217/fmb.12.97.
- [208] Raab, D., Graf, M., Notka, F., Schödl, T. et al., The GeneOptimizer algorithm: Using a sliding window approach to cope with the vast sequence space in multiparameter DNA sequence optimization. *Systems and Synthetic Biology* 2010, 4, 215–225, DOI: 10.1007/s11693-010-9062-3.
- [209] Gaur, R. K., Structural study of human antibody fragments with specificity for Mucin-1 antigen. Doctoral thesis, *RWTH Aachen University* 2004.
- [210] Gibson, D. G., Young, L., Chuang, R.-Y., Venter, J. C. et al., Enzymatic assembly of DNA molecules up to several hundred kilobases. *Nature Methods* 2009, 6, 343–345, DOI: 10.1038/nmeth.1318.
- [211] Kreuzaler, F., Ragg, H., Fautz, E., Kuhn, D. N. et al., UV-induction of chalcone synthase mRNA in cell suspension cultures of *Petroselinum hortense*. *Proceedings of the National Academy of Sciences* 1983, 80, 2591–2593, DOI: 10.1073/pnas.80.9.2591.
- [212] Gallie, D. R., Sleat, D. E., Watts, J. W., Turner, P. C. et al., The 5'-leader sequence of tobacco mosaic virus RNA enhances the expression of foreign gene transcripts in vitro and in vivo. *Nucleic Acids Research* 1987, 15, 3257–3273, DOI: 10.1093/nar/15.8.3257.

- [213] Carrington, J. C., Freed, D. D., Cap-independent enhancement of translation by a plant potyvirus 5'nontranslated region. *Journal of Virology* 1990, 64, 1590–1597, DOI: 10.1128/jvi.64.4.1590-1597.1990.
- [214] Gengenbach, B. B., Müschen, C. R., Buyel, J. F., Expression and purification of human phosphatase and actin regulator 1 (PHACTR1) in plant-based systems. *Protein Expression and Purification* 2018, 151, 46–55, DOI: 10.1016/j.pep.2018.06.003.
- [215] Fischer, R., Schumann, D., Zimmermann, S., Drossard, J. et al., Expression and characterization of bispecific single-chain Fv fragments produced in transgenic plants. *European Journal of Biochemistry* 1999, 262, 810–816, DOI: 10.1046/j.1432-1327.1999.00435.x.
- [216] Wolter, F. P., Fritz, C. C., Willmitzer, L., Schell, J. et al., rbcS genes in *Solanum tuberosum*: Conservation of transit peptide and exon shuffling during evolution. *Proceedings of the National Academy of Sciences* 1988, 85, 846–850, DOI: 10.1073/pnas.85.3.846.
- [217] Zhang, B., Rapolu, M., Kumar, S., Gupta, M. et al., Coordinated protein co-expression in plants by harnessing the synergy between an intein and a viral 2A peptide. *Plant Biotechnology Journal* 2017, 15, 718–728, DOI: 10.1111/pbi.12670.
- [218] Munro, S., Pelham, H. R., A C-terminal signal prevents secretion of luminal ER proteins. *Cell* 1987, 48, 899–907, DOI: 10.1016/0092-8674(87)90086-9.
- [219] Petruccielli, S., Molina, M. I., Lareu, F. J., Circosta, A., Two short sequences from amaranth 11S globulin are sufficient to target green fluorescent protein and beta-glucuronidase to vacuoles in *Arabidopsis* cells. *Plant Physiology and Biochemistry* 2007, 45, 400–409, DOI: 10.1016/j.plaphy.2007.02.008.
- [220] Luechau, F., Ling, T. C., Lyddiatt, A., Selective partition of plasmid DNA and RNA in aqueous two-phase systems by the addition of neutral salt. *Separation and Purification Technology* 2009, 68, 114–118, DOI: 10.1016/j.seppur.2009.04.016.
- [221] Wise, A. A., Liu Z., Binns, N., Three methods for the introduction of foreign DNA into *Agrobacterium*, in: Wang, K. (Ed.), *Agrobacterium protocols*. *Humana Press*, 2006.
- [222] Beuel, A.-K., Jablonka, N., Heesel, J., Severin, K. et al., LEDitSHAKE: A lighting system to optimize the secondary metabolite content of plant cell suspension cultures. *Scientific Reports* 2021, 11, 1–15, DOI: 10.1038/s41598-021-02762-6.
- [223] Blessing, D., Holland, T., Sack, M., Buntru, M., Vogel, S., Fermentation systems (EP3136841B1), Fraunhofer-Gesellschaft eV, 2015.
- [224] Holland, T., Blessing, D., Hellwig, S., Sack, M., The in-line measurement of plant cell biomass using radio frequency impedance spectroscopy as a component of process analytical technology. *Biotechnology Journal* 2013, 8, 1231–1240, DOI: 10.1002/biot.201300125.
- [225] Buyel, J. F., Fischer, R., Scale-down models to optimize a filter train for the downstream purification of recombinant pharmaceutical proteins produced in tobacco leaves. *Biotechnology Journal* 2014, 9, 415–425, DOI: 10.1002/biot.201300369.
- [226] Bradford, M. M., A rapid and sensitive method for the quantitation of microgram quantities of protein utilizing the principle of protein-dye binding. *Analytical Biochemistry* 1976, 72, 248–254, DOI: 10.1016/0003-2697(76)90527-3.
- [227] Buyel, J. F., Fischer, R., Flocculation increases the efficacy of depth filtration during the downstream processing of recombinant pharmaceutical proteins produced in tobacco. *Plant Biotechnology Journal* 2014, 12, 240–252, DOI: 10.1111/pbi.12132.

- [228] Johnsson, B., Löfås, S., Lindquist, G., Immobilization of proteins to a carboxymethyl-dextran-modified gold surface for biospecific interaction analysis in surface plasmon resonance sensors. *Analytical Biochemistry* 1991, 198, 268–277, DOI: 10.1016/0003-2697(91)90424-R.
- [229] Ma, J. K.-C., Drossard, J., Lewis, D., Altmann, F. et al., Regulatory approval and a first-in-human phase I clinical trial of a monoclonal antibody produced in transgenic tobacco plants. *Plant Biotechnology Journal* 2015, 13, 1106–1120, DOI: 10.1111/pbi.12416.
- [230] Ramessar, K., Rademacher, T., Sack, M., Stadlmann, J. et al., Cost-effective production of a vaginal protein microbicide to prevent HIV transmission. *Proceedings of the National Academy of Sciences* 2008, 105, 3727–3732, DOI: 10.1073/pnas.0708841104.
- [231] Nocek, B., Kochinyan, S., Proudfoot, M., Brown, G. et al., Polyphosphate-dependent synthesis of ATP and ADP by the family-2 polyphosphate kinases in bacteria. *Proceedings of the National Academy of Sciences* 2008, 105, 17730–17735, DOI: 10.1073/pnas.0807563105.
- [232] Schneider, C. A., Rasband, W. S., Eliceiri, K. W., NIH Image to ImageJ: 25 years of image analysis. *Nature Methods* 2012, 9, 671–675, DOI: 10.1038/nmeth.2089.
- [233] Box, G. E. P., Non-normality and tests on variances. *Biometrika* 1953, 40, 318–335, DOI: 10.2307/2333350.
- [234] Ruxton, G. D., The unequal variance t-test is an underused alternative to Student's t-test and the Mann-Whitney U test. *Behavioral Ecology* 2006, 17, 688–690, DOI: 10.1093/beheco/ark016.
- [235] McHugh, M. L., Multiple comparison analysis testing in ANOVA. *Biochemia Medica* 2011, 21, 203–209, DOI: 10.11613/bm.2011.029.
- [236] Decoene, T., Paepe, B. de, Maertens, J., Coussement, P. et al., Standardization in synthetic biology: An engineering discipline coming of age. *Critical Reviews in Biotechnology* 2018, 38, 647–656, DOI: 10.1080/07388551.2017.1380600.
- [237] Malcı, K., Watts, E., Roberts, T. M., Auxillos, J. Y. et al., Standardization of synthetic biology tools and assembly methods for *Saccharomyces cerevisiae* and emerging yeast species. *ACS Synthetic Biology* 2022, 11, 2527–2547, DOI: 10.1021/acssynbio.1c00442.
- [238] Brasch, M. A., Hartley, J. L., Vidal, M., ORFeome cloning and systems biology: Standardized mass production of the parts from the parts-list. *Genome Research* 2004, 14, 2001–2009, DOI: 10.1101/gr.2769804.
- [239] Cohen, S. N., Chang, A. C. Y., Boyer, H. W., Helling, R. B., Construction of biologically functional bacterial plasmids in vitro. *Proceedings of the National Academy of Sciences* 1973, 70, 3240–3244, DOI: 10.1073/pnas.70.11.3240.
- [240] Sievert, V., Ergin, A., Büssow, K., High-throughput cloning with restriction enzymes, in: Kobe, B., Guss, M., Huber, T. (Ed.). *Structural proteomics - High-throughput methods*, Humana Press 2008, pp. 163–173. DOI: 10.1007/978-1-60327-058-8_9
- [241] Marillonnet, S., Grützner, R., Synthetic DNA assembly using Golden Gate cloning and the hierarchical modular cloning pipeline. *Current Protocols in Molecular Biology* 2020, 130, e115, DOI: 10.1002/cpmb.115.
- [242] Gierlikowska, B., Stachura, A., Gierlikowski, W., Demkow, U., The impact of cytokines on neutrophils' phagocytosis and NET formation during sepsis - A review. *International Journal of Molecular Sciences* 2022, 23, 5076, DOI: 10.3390/ijms23095076.
- [243] Rose-John, S., Winthrop, K., Calabrese, L., The role of IL6 in host defense against infections. *Nature Reviews* 2017, 13, 399–409, DOI: 10.1038/nrrheum.2017.83.

- [244] Nausch, H., Huckauf, J., Koslowski, R., Meyer, U. et al., Recombinant production of human interleukin 6 in *Escherichia coli*. *Public Library of Science One* 2013, 8, e54933, DOI: 10.1371/journal.pone.0054933.
- [245] Bishara, N., Chapter 18: The use of biomarkers for detection of early and late-onset neonatal sepsis, in: Ohls, R. K., Maheshwari, A. (Ed.). *Hematology, immunology and infectious disease: Neonatology questions and controversies*, Elsevier 2012, pp. 303–315, DOI: 10.1016/B978-1-4377-2662-6.00018-3
- [246] Kumpf, A., Kowalczykiewicz, D., Szymańska, K., Mehnert, M. et al., Immobilization of the highly active UDP-glucose pyrophosphorylase from *Thermocrisum agreste* provides a highly efficient biocatalyst for the production of UDP-glucose. *Frontiers in Bioengineering and Biotechnology* 2020, 8, 740, DOI: 10.3389/fbioe.2020.00740.
- [247] Buyel, J. F., Hubbuch, J., Fischer, R., Comparison of tobacco host cell protein removal methods by blanching intact plants or by heat treatment of extracts. *Journal of Visualized Experiments* 2016, e54343, DOI: 10.3791/54343.
- [248] Kurtovic, L., Beeson, J. G., Complement factors in COVID-19 therapeutics and vaccines. *Trends in Immunology* 2021, 42, 94–103, DOI: 10.1016/j.it.2020.12.002.
- [249] Saito, S., Namisaki, H., Hiraishi, K., Takahashi, N. et al., A stable engineered human IgG3 antibody with decreased aggregation during antibody expression and low pH stress. *Protein Science* 2019, 28, 900–909, DOI: 10.1002/pro.3598.
- [250] Di Martino, P., Extracellular polymeric substances, a key element in understanding biofilm phenotype. *AIMS Microbiology* 2018, 4, 274–288, DOI: 10.3934/microbiol.2018.2.274.
- [251] Kaplan, J. B., Therapeutic potential of biofilm-dispersing enzymes. *The International Journal of Artificial Organs* 2009, 32, 545–554, DOI: 10.1177/039139880903200903.
- [252] Cywes-Bentley, C., Skurnik, D., Zaidi, T., Roux, D. et al., Antibody to a conserved antigenic target is protective against diverse prokaryotic and eukaryotic pathogens. *Proceedings of the National Academy of Sciences* 2013, 110, E2209–E2218, DOI: 10.1073/pnas.1303573110.
- [253] Ragunath, C., Shanmugam, M., Bendaoud, M., Kaplan, J. B. et al., Effect of a biofilm-degrading enzyme from an oral pathogen in transgenic tobacco on the pathogenicity of *Pectobacterium carotovorum* subspecies *carotovorum*. *Plant Pathology* 2012, 61, 346–354, DOI: 10.1111/j.1365-3059.2011.02509.x.
- [254] Filatova, L. Y., Donovan, D. M., Ishnazarova, N. T., Foster-Frey, J. A. et al., A chimeric LysK-Lysostaphin fusion enzyme lysing *Staphylococcus aureus* cells: A study of both kinetics of inactivation and specifics of interaction with anionic polymers. *Applied Biochemistry and Biotechnology* 2016, 180, 544–557, DOI: 10.1007/s12010-016-2115-7.
- [255] Kovalskaya, N. Y., Herndon, E. E., Foster-Frey, J. A., Donovan, D. M. et al., Antimicrobial activity of bacteriophage derived triple fusion protein against *Staphylococcus aureus*. *AIMS Microbiology* 2019, 5, 158–175, DOI: 10.3934/microbiol.2019.2.158.
- [256] Gasteiger, E., Gattiker, A., Hoogland, C., Ivanyi, I. et al., ExPASy: The proteomics server for in-depth protein knowledge and analysis. *Nucleic Acids Research* 2003, 31, 3784–3788, DOI: 10.1093/nar/gkg563.
- [257] Young, C. L., Britton, Z. T., Robinson, A. S., Recombinant protein expression and purification: A comprehensive review of affinity tags and microbial applications. *Biotechnology Journal* 2012, 7, 620–634, DOI: 10.1002/biot.201100155.

- [258] Woestenenk, E. A., Hammarström, M., van den Berg, S., Härd, T. et al., His-tag effect on solubility of human proteins produced in *Escherichia coli*: A comparison between four expression vectors. *Journal of Structural and Functional Genomics* 2004, 5, 217–229, DOI: 10.1023/B:jsfg.0000031965.37625.0e.
- [259] Andersen, K. R., Leksa, N. C., Schwartz, T. U., Optimized *E. coli* expression strain LOBSTR eliminates common contaminants from His-tag purification. *Proteins* 2013, 81, 1857–1861, DOI: 10.1002/prot.24364.
- [260] Mitsuhashi, I., Ugaki, M., Hirochika, H., Ohshima, M. et al., Efficient promoter cassettes for enhanced expression of foreign genes in dicotyledonous and monocotyledonous plants. *Plant and Cell Physiology* 1996, 37, 49–59, DOI: 10.1093/oxfordjournals.pcp.a028913.
- [261] Tamada, Y., Swanson, B. A., Arabshahi, A., Frey, P. A., Preparation and characterization of a bifunctional fusion enzyme composed of UDP-galactose 4-epimerase and galactose-1-P uridylyltransferase. *Bioconjugate Chemistry* 1994, 5, 660–665, DOI: 10.1021/bc00030a023.
- [262] Felipe, P. de, Ryan, M. D., Targeting of proteins derived from self-processing polyproteins containing multiple signal sequences. *Traffic* 2004, 5, 616–626, DOI: 10.1111/j.1398-9219.2004.00205.x.
- [263] van Drisse, C. M., Escalante-Semerena, J. C., New high-cloning-efficiency vectors for complementation studies and recombinant protein overproduction in *Escherichia coli* and *Salmonella enterica*. *Plasmid* 2016, 86, 1–6, DOI: 10.1016/j.plasmid.2016.05.001.
- [264] Traore, S. M., Zhao, B., A novel Gateway-compatible binary vector allows direct selection of recombinant clones in *Agrobacterium tumefaciens*. *Plant Methods* 2011, 7, 1–8, DOI: 10.1186/1746-4811-7-42.
- [265] Blomfield, I. C., Vaughn, V., Rest, R. F., Eisenstein, B. I., Allelic exchange in *Escherichia coli* using the *Bacillus subtilis* *sacB* gene and a temperature-sensitive pSC101 replicon. *Molecular Microbiology* 1991, 5, 1447–1457, DOI: 10.1111/j.1365-2958.1991.tb00791.x.
- [266] Hashimoto, J. G., Stevenson, B. S., Schmidt, T. M., Rates and consequences of recombination between rRNA operons. *Journal of Bacteriology* 2003, 185, 966–972, DOI: 10.1128/JB.185.3.966-972.2003.
- [267] Myers, J. A., Curtis, B. S., Curtis, W. R., Improving accuracy of cell and chromophore concentration measurements using optical density. *BMC Biophysics* 2013, 6, 4, DOI: 10.1186/2046-1682-6-4.
- [268] Abdel-Fattah, A. F., Mahmoud, D. A. R., Esawy, M. A. T., Production of levansucrase from *Bacillus subtilis* NRC 33a and enzymic synthesis of levan and fructo-oligosaccharides. *Current Microbiology* 2005, 51, 402–407, DOI: 10.1007/s00284-005-0111-1.
- [269] Sezonov G., Joseleau-Petit D., D'Ari R., *Escherichia coli* physiology in Luria-Bertani broth. *Journal of Bacteriology* 2007, 189, 8746–8749, DOI: 10.1128/JB.01368-07.
- [270] Christensen, M., Yunker, L. P. E., Shiri, P., Zepel, T. Prieto, P., Grunert, S., et al., Automation isn't automatic. *Chemical Science* 2021, 12, 15473–15490, DOI: 10.1039/D1SC04588A.
- [271] Arkhangelsky, E., Steubing, B., Ben-Dov, E., Kushmaro, A. et al., Influence of pH and ionic strength on transmission of plasmid DNA through ultrafiltration membranes. *Desalination* 2008, 227, 111–119, DOI: 10.1016/j.desal.2007.07.017.

- [272] Gründemann, D., Schömig, E., Protection of DNA during preparative agarose gel electrophoresis against damage induced by ultraviolet light. *Biotechniques* 1996, 21, 898–903, DOI: 10.2144/96215rr02.
- [273] Hussein Ali, T., Mousa Mandal, A., Alhasan, A., Dehaen, W., Surface fabrication of magnetic core-shell silica nanoparticles with perylene diimide as a fluorescent dye for nucleic acid visualization. *Journal of Molecular Liquids* 2022, 359, 119345, DOI: 10.1016/j.molliq.2022.119345.
- [274] Sidore, A. M., Plesa, C., Samson, J. A., Lubock, N. B. et al., DropSynth 2.0: High-fidelity multiplexed gene synthesis in emulsions. *Nucleic Acids Research* 2020, 48, e95–e95, DOI: 10.1093/nar/gkaa600.
- [275] Manduzio, H., Martelet, A., Ezan, E., Fenaille, F., Comparison of approaches for purifying and desalting polymerase chain reaction products prior to electrospray ionization mass spectrometry. *Analytical Biochemistry* 2010, 398, 272–274, DOI: 10.1016/j.ab.2009.10.026.
- [276] Zhou, Y., Zhang, Y., He, W., Wang, J. et al., Rapid regeneration and reuse of silica columns from PCR purification and gel extraction kits. *Scientific Reports* 2018, 8, 1–11, DOI: 10.1038/s41598-018-30316-w.
- [277] Hannis, J. C., Muddiman, D. C., Characterization of a microdialysis approach to prepare polymerase chain reaction products for electrospray ionization mass spectrometry using on-line ultraviolet absorbance measurements and inductively coupled plasma-atomic emission spectroscopy. *Rapid Communications in Mass Spectrometry* 1999, 13, 323–330, DOI: 10.1002/(SICI)1097-0231(19990315)13:5<323::AID-RCM485>3.0.CO;2-B.
- [278] Li, Y., Currie, D., Zydney, A. L., Enhanced purification of plasmid DNA isoforms by exploiting ionic strength effects during ultrafiltration. *Biotechnology and Bioengineering* 2016, 113, 783–789, DOI: 10.1002/bit.25836.
- [279] Lerman, L. S., A transition to a compact form of DNA in polymer solutions. *Proceedings of the National Academy of Sciences* 1971, 68, 1886–1890, DOI: 10.1073/pnas.68.8.1886.
- [280] Lis, J. T., Schleif, R., Size fractionation of double-stranded DNA by precipitation with polyethylene glycol. *Nucleic Acids Research* 1975, 2, 383–390, DOI: 10.1093/nar/2.3.383.
- [281] Kleideiter, G., Nordmeier, E., Polyethylene glycol-induced DNA condensation in aqueous/methanol containing low-molecular-weight electrolyte solutions. Chapter I: Theoretical considerations. *Polymer* 1999, 40, 4013–4023, DOI: 10.1016/S0032-3861(98)00643-0.
- [282] Latulippe, D. R., Zydney, A. L., Salt-induced changes in plasmid DNA transmission through ultrafiltration membranes. *Biotechnology and Bioengineering* 2008, 99, 390–398, DOI: 10.1002/bit.21575.
- [283] Curtis, M. D., Grossniklaus, U., A gateway cloning vector set for high-throughput functional analysis of genes in planta. *Plant Physiology* 2003, 133, 462–469, DOI: 10.1104/pp.103.027979.
- [284] Karimi, M., Inzé, D., Depicker, A., Gateway vectors for *Agrobacterium*-mediated plant transformation. *Trends in Plant Science* 2002, 7, 193–195, DOI: 10.1016/s1360-1385(02)02251-3.
- [285] Earley, K. W., Haag, J. R., Pontes, O., Opper, K. et al., Gateway-compatible vectors for plant functional genomics and proteomics. *The Plant Journal* 2006, 45, 616–629, DOI: 10.1111/j.1365-3113X.2005.02617.x.

- [286] Chen, S., Songkumarn, P., Liu, J., Wang, G.-L., A versatile zero background T-vector system for gene cloning and functional genomics. *Plant Physiology* 2009, 150, 1111–1121, DOI: 10.1104/pp.109.137125.
- [287] Brigulla, M., Wackernagel, W., Molecular aspects of gene transfer and foreign DNA acquisition in prokaryotes with regard to safety issues. *Applied Microbiology and Biotechnology* 2010, 86, 1027–1041, DOI: 10.1007/s00253-010-2489-3.
- [288] Holsters, M., Waele, D. de, Depicker, A., Messens, E. et al., Transfection and transformation of *Agrobacterium tumefaciens*. *Molecular and General Genetics* 1978, 163, 181–187, DOI: 10.1007/BF00267408.
- [289] Chen, H., Nelson, R. S., Sherwood, J. L., Enhanced recovery of transformants of *Agrobacterium tumefaciens* after freeze-thaw transformation and drug selection. *Biotechniques* 1994, 16, 664–8, 670.
- [290] Horspool, D. R., Coope, R. J. N., Holt, R. A., Efficient assembly of very short oligonucleotides using T4 DNA Ligase. *BMC Research Notes* 2010, 3, 291, DOI: 10.1186/1756-0500-3-291.
- [291] Kámán-Tóth, E., Pogány, M., Dankó, T., Szatmári, Á. et al., A simplified and efficient *Agrobacterium tumefaciens* electroporation method. *Three Biotech* 2018, 8, 148, DOI: 10.1007/s13205-018-1171-9.
- [292] Munro, T. P., Pilbrough, W., Hughes, B. S., Gray, P. P., Cell line isolation and design, in: Moo-Young, M. (Ed.). *Comprehensive biotechnology*, Elsevier 2011, pp. 144–153, DOI: 10.1016/B978-0-08-088504-9.00024-6.
- [293] Quiroz, J., Tsao, Y.-S., Statistical analysis of data from limiting dilution cloning to assess monoclonality in generating manufacturing cell lines. *Biotechnology Progress* 2016, 32, 1061–1068, DOI: 10.1002/btpr.2290.
- [294] Collier, H. A., Collier, B. S., Poisson statistical analysis of repetitive subcloning by the limiting dilution technique as a way of assessing hybridoma monoclonality, in: *Methods in enzymology immunochemical techniques*, Academic Press, 1986, pp. 412–417, DOI: 10.1016/0076-6879(86)21039-3.
- [295] Langsdorf, E., Le Yu, Kanevskaia, L., Felkner, R. et al., Retrospective assessment of clonal origin of cell lines. *Biotechnology Progress* 2021, 37, e3157, DOI: 10.1002/btpr.3157.
- [296] Jansing, J., Buyel, J. F., The correlation between DsRed mRNA levels and transient DsRed protein expression in plants depends on leaf age and the 5' untranslated region. *Biotechnology Journal* 2019, 14, 1800075, DOI: 10.1002/biot.201800075.
- [297] Pejaver, V., Hsu, W.-L., Xin, F., Dunker, A. K. et al., The structural and functional signatures of proteins that undergo multiple events of post-translational modification. *Protein Science* 2014, 23, 1077–1093, DOI: 10.1002/pro.2494.
- [298] McFadden, G. I., Chloroplast origin and integration. *Plant Physiology* 2001, 125, 50–53, DOI: 10.1104/pp.125.1.50.
- [299] Dar, T. A., Singh, L. R., Protein modifocomics: From modifications to clinical perspectives, *Academic Press*, 2019.
- [300] Gomord, V., Faye, L., Posttranslational modification of therapeutic proteins in plants. *Current Opinion in Plant Biology* 2004, 7, 171–181, DOI: 10.1016/j.pbi.2004.01.015.
- [301] Audagnotto, M., Dal Peraro, M., Protein post-translational modifications: In silico prediction tools and molecular modeling. *Computational and Structural Biotechnology Journal* 2017, 15, 307–319, DOI: 10.1016/j.csbj.2017.03.004.

- [302] Yang, Y., Ding, X., Zhu, G., Niroula, A. et al., ProTstab – Predictor for cellular protein stability. *BMC Genomics* 2019, 20, 804, DOI: 10.1186/s12864-019-6138-7.
- [303] Menéndez, L., Argosf, P., Engineering protein thermal stability: Sequence statistics point to residue substitutions in α -helices. *Journal of Molecular Biology* 1989, 206, 397–406.
- [304] Guruprasad, K., Reddy, B. B., Pandit, M. W., Correlation between stability of a protein and its dipeptide composition: A novel approach for predicting in vivo stability of a protein from its primary sequence. *Protein Engineering, Design and Selection* 1990, 4, 155–161, DOI: 10.1093/protein/4.2.155.
- [305] Ikai, A., Thermostability and aliphatic index of globular proteins. *Journal of Biochemistry* 1980, 88, 1895–1898, DOI: 10.1093/oxfordjournals.jbchem.a133168.
- [306] Gamage, D. G., Gunaratne, A., Periyannan, G. R., Russell, T. G., Applicability of instability index for in vitro protein stability prediction. *Protein and Peptide Letters* 2019, 26, 339–347, DOI: 10.2174/0929866526666190228144219.
- [307] Fernandes, A., Vinga, S., Improving protein expression prediction using extra features and ensemble averaging. *Public Library of Science One* 2016, 11, e0150369, DOI: 10.1371/journal.pone.0150369.
- [308] Gengenbach, B. B., Rational and model-based characterization of heterologous gene expression in biological systems. Doctoral thesis, *RWTH Aachen University* 2021.
- [309] Circelli, P., Donini, M., Villani, M. E., Benvenuto, E. et al., Efficient *Agrobacterium*-based transient expression system for the production of biopharmaceuticals in plants. *Bioengineered Bugs* 2010, 1, 221–224, DOI: 10.4161/bbug.1.3.11722.
- [310] Jez, J., Castilho, A., Grass, J., Vorauer-Uhl, K. et al., Expression of functionally active sialylated human erythropoietin in plants. *Biotechnology Journal* 2013, 8, 371–382, DOI: 10.1002/biot.201200363.
- [311] Cosgrove, D. J., Plant cell growth and elongation. *Encyclopedia of Life Sciences* 2014, DOI: 10.1002/9780470015902.a0001688.pub2.
- [312] Ullisch, D. A., A fundamental research of growth, metabolism and product formation of tobacco suspension cells. Doctoral thesis, *RWTH Aachen University* 2012.
- [313] Winans S C, Kerstetter R A, Nester E W, Transcriptional regulation of the *virA* and *virG* genes of *Agrobacterium tumefaciens*. *Journal of Bacteriology* 1988, 170, 4047–4054, DOI: 10.1128/jb.170.9.4047-4054.1988.
- [314] Kubek, D. J., Shuler, M. L., The effect of variations in carbon and nitrogen concentrations on phenolics formation in plant cell suspension cultures. *Journal of Natural Products* 1980, 43, 87–96, DOI: 10.1021/np50007a006.
- [315] Tyree, M. T., Richter, H., Alternative methods of analyzing water potential isotherms: Some cautions and clarifications. *Journal of Experimental Botany* 1981, 32, 643–653, DOI: 10.1093/jxb/32.3.643.
- [316] Yang, D., Pan, S., Tyree, M. T., The impact of xylem cavitation on water potential isotherms measured by the pressure chamber technique in *Metasequoia glyptostroboides*. *Journal of Experimental Botany* 2016, 67, 4571–4580, DOI: 10.1093/jxb/erw234.
- [317] Siefritz, F., Expression and function of the *Nicotiana tabacum* aquaporin NtAQP1. Doctoral thesis, *Julius-Maximilians-Universität Würzburg* 2002.
- [318] Roy, B., Krishnan, S. P., Chandrasekaran, N., Mukherjee, A., Chapter Five: Toxic effects of engineered nanoparticles on plants using *Allium cepa* as a model system, in: Verma, S. K., Das, A. K. (Ed.). *Comprehensive analytical chemistry analysis, fate, and toxicity*

- of engineered nanomaterials in plants, *Elsevier*, 2019, pp. 125–143, DOI: 10.1016/bs.coac.2019.04.009.
- [319] Nagata, T., Nemoto, Y., Hasezawa, S., Tobacco BY-2 cell line as the HeLa cell in the cell biology of higher plants, in: International review of cytology, *Elsevier*, 1992, pp. 1–30, DOI: 10.1016/S0074-7696(08)62452-3.
- [320] Zambre, M., Terryn, N., Clercq, J. de, Buck, S. de et al., Light strongly promotes gene transfer from *Agrobacterium tumefaciens* to plant cells. *Planta* 2003, 216, 580–586. DOI: 10.1007/s00425-002-0914-2.
- [321] Lytvyn, D. I., Yemets, A. I., Blume, Y. B., UV-B overexposure induces programmed cell death in a BY-2 tobacco cell line. *Environmental and Experimental Botany* 2010, 68, 51–57, DOI: 10.1016/j.envexpbot.2009.11.004.
- [322] Fasano, R., Gonzalez, N., Tosco, A., Dal Piaz, F. et al., Role of Arabidopsis UV resistance locus 8 in plant growth reduction under osmotic stress and low levels of UV-B. *Molecular Plant* 2014, 7, 773–791, DOI: 10.1093/mp/ssu002.
- [323] Yokawa, K., Fasano, R., Kagenishi, T., Baluška, F., Light as stress factor to plant roots. *Frontiers in Plant Science* 2014, 5, 718, DOI: 10.3389/fpls.2014.00718.
- [324] Hemm, M. R., Rider, S. D., Ogas, J., Murry, D. J. et al., Light induces phenylpropanoid metabolism in Arabidopsis roots. *The Plant Journal* 2004, 38, 765–778, DOI: 10.1111/j.1365-3113X.2004.02089.x.
- [325] Bashandy, H., Jalkanen, S., Teeri, T. H., Within leaf variation is the largest source of variation in agroinfiltration of *Nicotiana benthamiana*. *Plant Methods* 2015, 11, 47, DOI: 10.1186/s13007-015-0091-5.
- [326] Knödler, M., Rühl, C., Emonts, J., Buyel, J. F., Seasonal weather changes affect the yield and quality of recombinant proteins produced in transgenic tobacco plants in a greenhouse setting. *Frontiers in Plant Science* 2019, 10, 1245, DOI: 10.3389/fpls.2019.01245.
- [327] Matsuda, R., Inter-batch variability of hemagglutinin content transiently expressed in *Nicotiana benthamiana* plants grown under sole-source lighting and sunlight conditions before gene transfer. *Journal of Agricultural Meteorology* 2022, 78, 164–173, DOI: 10.2480/agrmet.D-22-00019.
- [328] Sainsbury, F., Sack, M., Stadlmann, J., Quendler, H. et al., Rapid transient production in plants by replicating and non-replicating vectors yields high quality functional anti-HIV antibody. *Public Library of Science One* 2010, 5, e13976, DOI: 10.1371/journal.pone.0013976.
- [329] Ober, R. J., Ward, E.S., The influence of signal noise on the accuracy of kinetic constants measured by surface plasmon resonance experiments. *Analytical Biochemistry* 1999, 273, 49–59, DOI: 10.1006/abio.1999.4185.
- [330] Holzmeister, C., Charakterisierung des Redoxsystems in Arabidopsis thaliana-Pflanzen mit gestörter NO-Homöostase. Doctoral thesis, *Technische Universität München* 2013.
- [331] Logemann, E., Birkenbihl, R. P., Ülker, B., Somssich, I. E., An improved method for preparing *Agrobacterium* cells that simplifies the Arabidopsis transformation protocol. *Plant Methods* 2006, 2, 16, DOI: 10.1186/1746-4811-2-16.
- [332] Sheludko, Y. V., Sindarovska, Y. R., Im Gerasymenko, Bannikova, M. A. et al., Comparison of several *Nicotiana* species as hosts for high-scale *Agrobacterium*-mediated transient expression. *Biotechnology Bioengineering* 2007, 96, 608–614.
- [333] Halfhill, M. D., Millwood, R. J., Rufty, T. W., Weissinger, A. K. et al., Spatial and temporal patterns of green fluorescent protein (GFP) fluorescence during leaf canopy

- development in transgenic oilseed rape, *Brassica napus*. *Plant Cell Reports* 2003, 22, 338–343, DOI: 10.1007/s00299-003-0696-4.
- [334] Wydro, M., Kozubek, E., Lehmann, P., Optimization of transient *Agrobacterium*-mediated gene expression system in leaves of *Nicotiana benthamiana*. *Acta Biochimica Polonica* 2006, 53, 289–298, DOI: 10.18388/abp.2006_3341.
- [335] Goto, N. K., Kay, L. E., New developments in isotope labeling strategies for protein solution NMR spectroscopy. *Current Opinion in Structural Biology* 2000, 10, 585–592, DOI: 10.1016/S0959-440X(00)00135-4.
- [336] Bindschedler, L. V., Palmblad, M., Cramer, R., Hydroponic isotope labelling of entire plants (HILEP) for quantitative plant proteomics; An oxidative stress case study. *Phytochemistry* 2008, 69, 1962–1972, DOI: 10.1016/j.phytochem.2008.04.00.
- [337] Bouvignies, G., Markwick, P., Brüschweiler, R., Blackledge, M., Simultaneous determination of protein backbone structure and dynamics from residual dipolar couplings. *American Chemical Society* 2006, 128, 15100–15101, DOI: 10.1021/ja066704b.
- [338] Mycroft-West, C., Su, D., Elli, S., Li, Y. et al., The 2019 coronavirus (SARS-CoV-2) surface protein (Spike) S1 receptor binding domain undergoes conformational change upon heparin binding. *BioRxiv* 2020, DOI: 10.1101/2020.02.29.971093.
- [339] Ohki, S., Dohi, K., Tamai, A., Takeuchi, M. et al., Stable-isotope labeling using an inducible viral infection system in suspension-cultured plant cells. *Journal of Biomolecular NMR* 2008, 42, 271–277, DOI: 10.1007/s10858-008-9283-x.
- [340] Li, Y. D., Lamour, G., Gsponer, J., Zheng, P. et al., The molecular mechanism underlying mechanical anisotropy of the protein GB1. *Biophysical Journal* 2012, 103, 2361–2368, DOI: 10.1016/j.bpj.2012.10.035.
- [341] Frank, M. K., Dyda, F., Dobrodumov, A., Gronenborn, A. M., Core mutations switch monomeric protein GB1 into an intertwined tetramer. *Nature Structural Biology* 2002, 9, 877–885, DOI: 10.1038/nsb854.
- [342] Cheng, Y., Patel, D. J., An efficient system for small protein expression and refolding. *Biochemical and Biophysical Research Communications* 2004, 317, 401–405, DOI: 10.1016/j.bbrc.2004.03.068.
- [343] Filiou, M. D., Varadarajulu, J., Teplytska, L., Reckow, S. et al., The ¹⁵N isotope effect in *Escherichia coli*: A neutron can make the difference. *Proteomics* 2012, 12, 3121–3128, DOI: 10.1002/pmic.201200209.
- [344] Sacchi, G. A., Cocucci, M., Effects of deuterium oxide on growth, proton extrusion, potassium influx, and in vitro plasma membrane activities in maize root segments. *Plant Physiology* 1992, 100, 1962–1967, DOI: 10.1104/pp.100.4.1962.
- [345] Kelman, Z., Isotope labeling of biomolecules: Labeling methods, *Academic Press*, 2015, DOI: 10.1007/978-94-007-4954-2.
- [346] Grzesiek, S., Bax, A. D., Improved 3D triple-resonance NMR techniques applied to a 31 kDa protein. *Journal of Magnetic Resonance (1969)* 1992, 96, 432–440, DOI: 10.1016/0022-2364(92)90099-S.
- [347] Sattler, M., Fesik, S. W., Use of deuterium labeling in NMR: Overcoming a sizeable problem. *Structure* 1996, 4, 1245–1249, DOI: 10.1016/s0969-2126(96)00133-5.
- [348] Klement, Z., Method of obtaining fluid from the intercellular spaces of foliage and the fluid's merit as substrate for phytochemical pathogens. *Phytopathology* 1965, 55, 1033–1034.

- [349] Lohaus, G., Pennewiss, K., Sattelmacher, B., Hussmann, M. et al., Is the infiltration-centrifugation technique appropriate for the isolation of apoplastic fluid? *Physiologia Plantarum* 2001, 111, 457–465, DOI: 10.1034/j.1399-3054.2001.1110405.x.
- [350] Kingsbury, N. J., McDonald, K. A., Selective recovery from the interstitial spaces of *Nicotiana* species. Doctoral thesis, *University of California Davis* 2014.
- [351] Figueiredo, J., Cavaco, A. R., Guerra-Guimarães, L., Leclercq, C. et al., An apoplastic fluid extraction method for the characterization of grapevine leaves proteome and metabolome from a single sample. *Physiologia Plantarum* 2021, 171, 343–357, DOI: 10.1111/ppl.13198.
- [352] Gaberc-Porekar, V., Menart, V., Perspectives of immobilized-metal affinity chromatography. *Journal of Biochemical and Biophysical Methods* 2001, 49, 335–360, DOI: 10.1016/S0165-022X(01)00207-X.
- [353] Firer, M. A., Efficient elution of functional proteins in affinity chromatography. *Journal of Biochemical and Biophysical Methods* 2001, 49, 433–442, DOI: 10.1016/S0165-022X(01)00211-1.
- [354] Block, H., Maertens, B., Spriestersbach, A., Brinker, N. et al., Chapter 27: Immobilized-metal affinity chromatography (IMAC): A review, in: Burgess, R. R., Deutscher, M. P. (Ed.). *Methods in enzymology guide to protein purification*, Academic Press, 2009, pp. 439–473, DOI: 10.1016/S0076-6879(09)63027-5.
- [355] Wong, J. W., Albright, R. L., Wang, N.-H. L., Immobilized metal ion affinity chromatography (IMAC) chemistry and bioseparation applications. *Separation and Purification Methods* 1991, 20, 49–106, DOI: 10.1080/03602549108021408.
- [356] Lee, J., Kim, S. H., High-throughput T7 LIC vector for introducing C-terminal poly-histidine tags with variable lengths without extra sequences. *Protein Expression and Purification* 2009, 63, 58–61, DOI: 10.1016/j.pep.2008.09.005.
- [357] Buyel, J. F., Twyman, R. M., Fischer, R., Very-large-scale production of antibodies in plants: The biologization of manufacturing. *Biotechnology Advances* 2017, 35, 458–465, DOI: 10.1016/j.biotechadv.2017.03.011.
- [358] Buyel, J. F., Gruchow, H. M., Fischer, R., Depth filters containing diatomite achieve more efficient particle retention than filters solely containing cellulose fibers. *Frontiers in Plant Science* 2015, 6, DOI: 10.3389/fpls.2015.01134.
- [359] Landry, N., Pillet, S., Favre, D., Poulin, J. F. et al., Influenza virus-like particle vaccines made in *Nicotiana benthamiana* elicit durable, poly-functional and cross-reactive T-cell responses to influenza HA antigens. *Clinical Immunology* 2014, 154, 164–177, DOI: 10.1016/j.clim.2014.08.003.
- [360] Khanal, O., Singh, N., Traylor, S. J., Xu, X. et al., Contributions of depth filter components to protein adsorption in bioprocessing. *Biotechnology and Bioengineering* 2018, 115, 1938–1948, DOI: 10.1002/bit.26707.
- [361] Wiendahl, M., Schulze Wierling, P., Nielsen, J., Fomsgaard Christensen, D. et al., High-throughput screening for the design and optimization of chromatographic processes: Miniaturization, automation and parallelization of breakthrough and elution studies. *Chemical Engineering & Technology* 2008, 31, 893–903, DOI: 10.1002/ceat.200800167.
- [362] Ishihara, T., Kadoya, T., Endo, N., Yamamoto, S., Optimization of elution salt concentration in stepwise elution of protein chromatography using linear gradient elution data: Reducing residual protein A by cation-exchange chromatography in monoclonal antibody purification. *Journal of Chromatography A* 2006, 1114, 97–101, DOI: 10.1016/j.chroma.2006.02.042.

- [363] Konstantinidis, S., Goh, H. Y., Martin Bufájer, J. M., Galbert, P. de et al., Flexible and accessible automated operation of miniature chromatography columns on a liquid handling station. *Biotechnology Journal* 2018, 13, 1700390, DOI: 10.1002/biot.201700390.
- [364] Pogue, G. P., Vojdani, F., Palmer, K. E., Hiatt, E. et al., Production of pharmaceutical-grade recombinant aprotinin and a monoclonal antibody product using plant-based transient expression systems. *Plant Biotechnology Journal* 2010, 8, 638–654, DOI: 10.1111/j.1467-7652.2009.00495.x.
- [365] Cromwell, M. E. M., Hilario, E., Jacobson, F., Protein aggregation and bioprocessing. *The AAPS Journal* 2006, 8, E572-E579, DOI: 10.1208/aapsj080366.
- [366] Kumar, R., Ismail, A. F., Fouling control on microfiltration/ultrafiltration membranes: Effects of morphology, hydrophilicity, and charge. *Journal of Applied Polymer Science* 2015, 132, DOI: 10.1002/app.42042.
- [367] van Loghem, E., Frangione, B., Recht, B., Franklin, E. C., Staphylococcal protein A and human IgG subclasses and allotypes. *Scandinavian Journal of Immunology* 1982, 15, 275–278, DOI: 10.1111/j.1365-3083.1982.tb00649.x.
- [368] Gorbatiuk, O. B., Application of immunoglobulin-binding proteins A, G and L in the affinity chromatography. *Biotechnologia Acta* 2014, 7, 34–45. DOI: DOI:10.15407/biotech7.02.034.
- [369] Bornhorst, J. A., Falke, J. J., Chapter 16: Purification of proteins using polyhistidine affinity tags, in: *Methods in enzymology*, Elsevier, 2000, pp. 245–254, DOI: 10.1016/S0076-6879(00)26058-8.
- [370] Scheffel, J., Hober, S., Highly selective protein A resin allows for mild sodium chloride-mediated elution of antibodies. *Journal of Chromatography A* 2021, 1637, 461843, DOI: 10.1016/j.chroma.2020.461843.
- [371] Myszka, D. G., Rich, R. L., Implementing surface plasmon resonance biosensors in drug discovery. *Pharmaceutical Science & Technology Today* 2000, 3, 310–317, DOI: 10.1016/S1461-5347(00)00288-1.
- [372] Arfi, Z. A., Hellwig, S., Drossard, J., Fischer, R. et al., Polyclonal antibodies for specific detection of tobacco host cell proteins can be efficiently generated following RuBisCO depletion and the removal of endotoxins. *Biotechnology Journal* 2016, 11, 507–518, DOI: 10.1002/biot.201500271.
- [373] Jung, Y., Kang, H. J., Lee, J. M., Jung, S. O. et al., Controlled antibody immobilization onto immunoanalytical platforms by synthetic peptide. *Analytical Biochemistry* 2008, 374, 99–105, DOI: 10.1016/j.ab.2007.10.022.
- [374] Chatelier, R. C., Gengenbach, T. R., Griesser, H. J., Brighamburke, M. et al., A general method to recondition and reuse BIAcore sensor chips fouled with covalently immobilized protein/peptide. *Analytical Biochemistry* 1995, 229, 112–118, DOI: 10.1006/abio.1995.1386.
- [375] Müller, K. M., Arndt, K. M., Bauer, K., Plückthun, A., Tandem immobilized metal-ion affinity chromatography/immunoaffinity purification of His-tagged proteins: Evaluation of two anti-His-tag monoclonal antibodies. *Analytical Biochemistry* 1998, 259, 54–61, DOI: 10.1006/abio.1998.2606.
- [376] Quinn, J. G., O'Neill, S., Doyle, A., McAtamney, C. et al., Development and application of surface plasmon resonance-based biosensors for the detection of cell-ligand interactions. *Analytical Biochemistry* 2000, 281, 135–143, DOI: 10.1006/abio.2000.4564.

- [377] Puttharugsa, C., Wangkam, T., Huangkamhang, N., Gajanandana, O. et al., Development of surface plasmon resonance imaging for detection of *Acidovorax avenae* subspecies citrulli (Aac) using specific monoclonal antibody. *Biosensors and Bioelectronics* 2011, 26, 2341–2346, DOI: 10.1016/j.bios.2010.10.007.
- [378] Quinn, J. G., O'Kennedy, R., Biosensor-based estimation of kinetic and equilibrium constants. *Analytical Biochemistry* 2001, 290, 36–46, DOI: 10.1006/abio.2000.4919.
- [379] Lindner, P., Bauer, K., Krebber, A., Nieba, L. et al., Specific detection of his-tagged proteins with recombinant anti-His tag scFv-phosphatase or scFv-phage fusions. *Biotechniques* 1997, 22, 140–149, DOI: 10.2144/97221rr01.
- [380] Kaufmann, M., Lindner, P., Honegger, A., Blank, K. et al., Crystal structure of the anti-His tag antibody 3D5 single-chain fragment complexed to its antigen. *Journal of Molecular Biology* 2002, 318, 135–147, DOI: 10.1016/S0022-2836(02)00038-4.
- [381] Dell, A., Galadari, A., Sastre, F., Hitchen, P., Similarities and differences in the glycosylation mechanisms in prokaryotes and eukaryotes. *International Journal of Microbiology* 2010, 2010, DOI: 10.1155/2010/148178.
- [382] Korn-Wendisch, F., Rainey, F., Kroppenstedt, R. M., Kempf, A. et al., *Thermocrisum* gen. nov., a new genus of the order Actinomycetales, and description of *Thermocrisum municipale* sp. nov. and *Thermocrisum agreste* sp. nov. *International Journal of Systematic and Evolutionary Microbiology* 1995, 45, 67–77, DOI: 10.1099/00207713-45-1-67.
- [383] Freydank, A.-C., Brandt, W., Dräger, B., Protein structure modeling indicates hexahistidine-tag interference with enzyme activity. *Proteins* 2008, 72, 173–183, DOI: 10.1002/prot.21905.
- [384] Navarre, C., Muynck, B. de, Alves, G., Vertommen, D. et al., Identification, gene cloning and expression of serine proteases in the extracellular medium of *Nicotiana tabacum* cells. *Plant Cell Reports* 2012, 31, 1959–1968, DOI: 10.1007/s00299-012-1308-y.
- [385] Saier, M. H., Simoni, R. D., Regulation of carbohydrate uptake in gram-positive bacteria. *Journal of Biological Chemistry* 1976, 251, 893–894, DOI: 10.1016/S0021-9258(17)33867-X.
- [386] Conrad, U., Fiedler, U., Compartment-specific accumulation of recombinant immunoglobulins in plant cells: An essential tool for antibody production and immunomodulation of physiological functions and pathogen activity. *Plant Molecular Biology* 1998, 38, 101–109., DOI: 10.1007/978-94-011-5298-3_5.
- [387] Tkaczyk, C., Hua, L., Varkey, R., Shi, Y. et al., Identification of anti-alpha toxin monoclonal antibodies that reduce the severity of *Staphylococcus aureus* dermonecrosis and exhibit a correlation between affinity and potency. *Clinical and Vaccine Immunology* 2012, 19, 377–385, DOI: 10.1128/CVI.05589-11.
- [388] Rattanapisit, K., Phakham, T., Buranapraditkun, S., Siri wattananon, K. et al., Structural and in vitro functional analyses of novel plant-produced anti-human PD1 antibody. *Scientific Reports* 2019, 9, 1–10, DOI: 10.1038/s41598-019-51656-1.
- [389] Sack, M., Paetz, A., Kunert, R., Bomble, M. et al., Functional analysis of the broadly neutralizing human anti-HIV-1 antibody 2F5 produced in transgenic BY-2 suspension cultures. *The FASEB Journal* 2007, 21, 1655–1664, DOI: 10.1096/fj.06-5863com.
- [390] Katsamba, P. S., Navratilova, I., Calderon-Cacia, M., Fan, L. et al., Kinetic analysis of a high-affinity antibody/antigen interaction performed by multiple Biacore users. *Analytical Biochemistry* 2006, 352, 208–221, DOI: 10.1016/j.ab.2006.01.034.

- [391] Yang, D., Singh, A., Wu, H., Kroe-Barrett, R., Comparison of biosensor platforms in the evaluation of high affinity antibody-antigen binding kinetics. *Analytical Biochemistry* 2016, 508, 78–96, DOI: 10.1016/j.ab.2016.06.024.
- [392] Schmelcher, M., Shen, Y., Nelson, D. C., Eugster, M. R. et al., Evolutionarily distinct bacteriophage endolysins featuring conserved peptidoglycan cleavage sites protect mice from MRSA infection. *The Journal of Antimicrobial Chemotherapy* 2015, 70, 1453–1465, DOI: 10.1093/jac/dku552.
- [393] Stiefel, P., Mauerhofer, S., Schneider, J., Maniura-Weber, K. et al., Enzymes enhance biofilm removal efficiency of cleaners. *Antimicrobial Agents and Chemotherapy* 2016, 60, 3647–3652, DOI: 10.1128/AAC.00400-16.
- [394] Dobrynina, O. Y., Bolshakova, T. N., am Umyarov, Boksha, I. S. et al., Disruption of bacterial biofilms using recombinant dispersin B. *Microbiology* 2015, 84, 498–501, DOI: 10.1134/S0026261715040062.
- [395] Lister, J. L., Horswill, A. R., Staphylococcus aureus biofilms: Recent developments in biofilm dispersal. *Frontiers in Cellular and Infection Microbiology* 2014, 4, DOI: 10.3389/fcimb.2014.00178.
- [396] Olsen, N. M. C., Thiran, E., Hasler, T., Vanzieleghe, T. et al., Synergistic removal of static and dynamic Staphylococcus aureus biofilms by combined treatment with a bacteriophage endolysin and a polysaccharide depolymerase. *Viruses* 2018, 10, DOI: 10.3390/v10080438.
- [397] Chaignon, P., Sadovskaya, I., Ragunah, C., Ramasubbu, N. et al., Susceptibility of staphylococcal biofilms to enzymatic treatments depends on their chemical composition. *Applied Microbiology and Biotechnology* 2007, 75, 125–132, DOI: 10.1007/s00253-006-0790-y.
- [398] Gökçen, A., Vilcinskas, A., Wiesner, J., Methods to identify enzymes that degrade the main extracellular polysaccharide component of Staphylococcus epidermidis biofilms. *Virulence* 2013, 4, 260–270, DOI: 10.4161/viru.23560.
- [399] Diamos, A. G., Mason, H. S., Chimeric 3' flanking regions strongly enhance gene expression in plants. *Plant Biotechnology Journal* 2018, 16, 1971–1982, DOI: 10.1111/pbi.12931.
- [400] Kazici, H. C., Bayraktar, E., Mehmetoglu, Ü., Optimization of the asymmetric synthesis of chiral aromatic alcohol using freeze-dried carrots as whole-cell biocatalysts. *Green Processing and Synthesis* 2016, 5, 131–137, DOI: 10.1515/gps-2015-0118.
- [401] Villa, R., Molinari, F., Reduction of carbonylic and carboxylic groups by plant cell cultures. *ACS Journal of Natural Products* 2008, 71.4, 693–696, DOI: 10.1021/np070386s.
- [402] Lingg, N., Kröß, C., Engele, P., Öhlknecht, C. et al., CASPON platform technology: Ultrafast circularly permuted caspase-2 cleaves tagged fusion proteins before all 20 natural amino acids at the N-terminus. *New Biotechnology* 2022, 71, 37–46, DOI: 10.1016/j.nbt.2022.07.002.
- [403] Puigbò, P., Guzmán, E., Romeu, A., Garcia-Vallvé, S., OPTIMIZER: A web server for optimizing the codon usage of DNA sequences. *Nucleic Acids Research* 2007, 35, W126–W131, DOI: 10.1093/nar/gkm219.
- [404] Tashiro, M., Tejero, R., Zimmerman, D. E., Celda, B. et al., High-resolution solution NMR structure of the Z domain of staphylococcal protein A. *Journal of Molecular Biology* 1997, 272, 573–590, DOI: 10.1006/jmbi.1997.1265.

- [405] Sellman, B., Tkaczyk, C., Hua, L., Chowdhury, P., and Varkey, R, Antibodies that specifically bind *Staphylococcus aureus* alpha toxin and methods of use (EP2673373B3), MedImmune LLC, 2018.
- [406] Bertoni, M., Kiefer, F., Biasini, M., Bordoli, L. et al., Modeling protein quaternary structure of homo-and hetero-oligomers beyond binary interactions by homology. *Scientific Reports* 2017, 7, 1–15, DOI: 10.1038/s41598-017-09654-8.
- [407] Waterhouse, A., Bertoni, M., Bienert, S., Studer, G. et al., SWISS-MODEL: Homology modelling of protein structures and complexes. *Nucleic Acids Research* 2018, 46, W296-W303, DOI: 10.1093/nar/gky427.
- [408] Bolduc, O. R., Lambert-Lanteigne, P., Colin, D. Y., Zhao, S. S. et al., Modified peptide monolayer binding His-tagged biomolecules for small ligand screening with SPR biosensors. *Analyst* 2011, 136, 3142–3148, DOI: 10.1039/c1an15235a.
- [409] Zenn, H. M., Hutschenreiter, S., Herberg, F. W., Anti-histidine antibodies as tools for reversible capturing of his-tagged fusion proteins for subsequent binding analysis, in: Antibody engineering, *Springer*, 2010, pp. 667–681. DOI: 10.1007/978-3-642-01144-3_42
- [410] Winzor, D. J., Specific allowance for antibody bivalence in the determination of dissociation constants by kinetic exclusion assay. *Analytical Biochemistry* 2011, 414, 273–277, DOI: 10.1016/j.ab.2011.03.025.

VII. Appendix

VII.1 Publications

1. Opdensteinen, P., Clodt, J. I., Müschen, C. R., Filiz, V., & Buyel, J. F., A combined ultrafiltration/diafiltration step facilitates the purification of cyanovirin-N from transgenic tobacco extracts. *Frontiers in Bioengineering and Biotechnology* 2019, 6, 206, DOI: 10.3389/fbioe.2018.00206.
2. Gengenbach, B. B., Keil, L. L., Opdensteinen, P., Müschen, C. R., Melmer, G., Lentzen, H., Bührmann J., & Buyel, J. F., Comparison of microbial and transient expression (tobacco plants and plant-cell packs) for the production and purification of the anticancer mistletoe lectin viscumin. *Biotechnology and Bioengineering* 2019, 116(9), 2236-2249, DOI: 10.1002/bit.27076.
3. Knödler, M., Rühl, C., Opdensteinen, P., & Buyel, J. F., Activated cross-linked agarose for the rapid development of affinity chromatography resins-antibody capture as a case study. *Journal of Visualized Experiments* 2019, (150), e59933, DOI: 10.3791/59933.
4. Gengenbach, B. B., Opdensteinen, P., & Buyel, J. F., Robot cookies–plant cell packs as an automated high-throughput screening platform based on transient expression. *Frontiers in Bioengineering and Biotechnology* 2020, 8, 393, DOI: 10.3389/fbioe.2020.00393.
5. Opdensteinen, P., Lobanov, A., & Buyel, J. F., A combined pH and temperature precipitation step facilitates the purification of tobacco-derived recombinant proteins that are sensitive to extremes of either parameter. *Biotechnology Journal* 2021, 16(4), 2000340, DOI: 10.1002/biot.202000340.
6. Bernau, C. R., Jäpel, R. C., Hübbers, J. W., Nölting, S., Opdensteinen, P., & Buyel, J. F., Precision analysis for the determination of steric mass action parameters using eight tobacco host cell proteins. *Journal of Chromatography A* 2021, 1652, 462379, DOI: 10.1016/j.chroma.2021.462379.
7. Opdensteinen, P., Dietz, S. J., Gengenbach, B. B., & Buyel, J. F., Expression of biofilm-degrading enzymes in plants and automated high-throughput activity screening using experimental *Bacillus subtilis* biofilms. *Frontiers in Bioengineering and Biotechnology* 2021, 714, DOI: 10.3389/fbioe.2021.708150.
8. Opdensteinen, P., Meyer, S., Buyel, J. F., *Nicotiana* spp. for the expression and purification of functional IgG3 antibodies directed against the *Staphylococcus aureus* alpha toxin. *Frontiers in Chemical Engineering* 2021, 3, 737010, DOI: 10.3389/fceng.2021.737010.
9. Opdensteinen, P., Sperl, L.E., Mohamadi, M., Kündgen-Redding, N., Hagn, F. and Buyel, J.F., The transient expression of recombinant proteins in plant cell packs facilitates stable isotope labeling for NMR spectroscopy. *Plant Biotechnology Journal* 2022, 20(10), 1928-1939, DOI: 10.1111/pbi.13873.
10. Opdensteinen, P., & Buyel, J. F., Reducing water uptake into BY-2 cells by systematically optimizing the cultivation parameters increases product yields achieved by transient expression in plant cell packs. *Biotechnology Journal* 2022, 17(10), 2200134, DOI: 10.1002/biot.202200134.

11. Knödler, M. & Opdensteinen, P., Sankaranarayanan, R., Morgenroth, A., Buhl, E., Mottaghy, F., Buyel J. F., Simple plant-based production and purification of the assembled human ferritin heavy chain as a nanocarrier for tumor-targeted drug delivery and bioimaging in cancer therapy. *Biotechnology and Bioengineering* 2023, 120(4), 1038-1054, DOI: 10.1002/bit.28312.

VII.2 Publications in preparation

1. Opdensteinen, P., & J. F. Buyel, Reliable protein quantification using surface plasmon resonance spectroscopy (submitted). *Springer*.
2. Opdensteinen, P., & J. F. Buyel, Optimizing interleukin-6 and 8 production in plant cell packs and plants for application in advanced therapy medicinal products and cellular agriculture (in preparation).

VII.3 Conference contributions

1. Opdensteinen, P., Clodt, J. I., Müschen, C. R., Filiz, V., & Buyel, J. F., A combined ultrafiltration/diafiltration step facilitates the purification of biopharmaceutical proteins from tobacco extracts; Oral presentation and poster session, *Plant-Based Vaccines, Antibodies & Biologics* 2019, Riga.
2. Opdensteinen, P., Lobanov, A., & Buyel, J. F., A combined temperature and pH precipitation step facilitates the purification of tobacco-derived recombinant proteins that are sensitive to both conditions; Poster session, *ProcessNet* 2020, digital conference.
3. Opdensteinen, P., Meyer, S., Buyel, J. F., Expression and purification of functional IgG3 antibodies directed against the *Staphylococcus aureus* alpha toxin in *Nicotiana* spp.; Oral presentation, *International Society for Plant Molecular Farming* 2021, digital conference.
4. Opdensteinen, P., & Buyel, J. F., Reducing the water uptake of BY-2 cells by systematically optimizing cultivation conditions increases productivity and reduces variation during transient expression in plant cell packs; Oral presentation, *International Society for Plant Molecular Farming* 2022, Rome.

VII.4 Register of equipment

Name	Type/Use	Manufacturer
2100P ISO.....	Turbidimeter.....	Hach
2712120.....	Cuvettes.....	Ratiolab
4itude PCR plate.....	PCR.....	Brooks Life Sciences
AcroPrep Advance 30-40 µm.....	PCP casting.....	Pall
ÄKTA pure 25 L/M.....	Chromatography System.....	GE Healthcare
Amersham Protran nitrocellulose.....	Blotting.....	Merck
Avanti J-26 XP.....	Centrifuge.....	Beckmann-Coulter
Biacore T200.....	SPR.....	Cytiva
Biometra Trio thermal cycler.....	PCR cycler.....	Analytik Jena
Biophotometer 6131.....	Photometer.....	Eppendorf
Biowizard.....	Sterile bank.....	Kojair
Black half-area 96-well plates.....	Assays.....	Greiner BioOne
BP-410.....	Bag Filter.....	Fuhr
Canon 5600 scanner.....	Scanner.....	Canon
Capacity sensor 12×320 mm.....	BY-2 cultivation.....	Aber instruments
Cellstar multi-well culture plates.....	Biofilm assays.....	Greiner Bio One
Chromabond collection tubes.....	PCP extraction.....	Macherey-Nagel
Chrome steal bead 3 mm.....	PCP extraction.....	Spherotech
ClarioStar.....	Plate reader.....	BMG Labtech
Climoshaker ISF1-X.....	BY-2 cultivation.....	Kuhner
CM5 sensors.....	SPR.....	Cytiva
Cond 314i.....	Conductometer.....	WTW
Cylinders.....	Measuring cylinder.....	Brand
Deep well plates 2.0 mL.....	<i>Agrobacterium</i> cultivation.....	Ritter
Dri Block DB3.....	Heat block.....	Techne
Dual UV transilluminator.....	UV illuminator.....	VWR
EnSpire.....	Plate reader.....	Perkin Elmer
Eppendorf 5810 R.....	Centrifuge.....	Eppendorf
Erlenmeyer flasks 0.25/0.10 L.....	BY-2 cultivation.....	Schott
ETHG-912.....	Thermometer.....	Oregon Scientific
EZ-Control Unit.....	BY-2 cultivation.....	Applikon
F9-R.....	GE Healthcare.....	Fraction collector
Falcon tubes.....	Reaction tubes.....	Greiner Bio-One
FL 9175.....	Multichannel pipette.....	Anachem
Flat-bottom 96-well plates.....	Assays.....	Sarstedt
Forma-86C ULT.....	Freezer -20°C.....	Thermo Scientific
Freezer.....	Freezer -20°C.....	Siemens
Gas permeable membrane.....	Bacterial cultivation.....	Macherey-Nagel
GenePulser X-cell.....	Electroporation.....	Bio-Rad
Glass bioreactor double-walled 5.0 L.....	BY-2 cultivation.....	Applikon
GreenPower LED modules.....	Plant cultivation.....	Philips
HiG5000.....	Centrifuge.....	GC biotech
High Capacity Amine sensors.....	SPR.....	Bruker
HiTrap Chelating Sepharose FF.....	Chromatography.....	Cytiva
HiTrap protein G.....	Chromatography.....	Cytiva
Hydrosart 10/30/100 kDa.....	UF/DF membranes.....	Sartorius
IceMatic D201.....	Ice machine.....	Castel Mac
Innova 4230.....	Incubator shaker.....	New Brunswick Scientific
Janus G3 liquid handling station.....	Automation.....	Perkin Elmer
KM02 basic.....	magnet stirrer.....	IKA

L/S Masterflex.....	Peristaltic pump.....	Masterflex
Liebherr premium.....	Freezer -20°C.....	Liebherr
Lumilux 58W/830 warm white	Plant incubation after infiltration	Osram
Lumilux 58W/840 cool white.....	Plant incubation after infiltration	Osram
Mikro 220 R	Centrifuge	Hettich
MiniSart 0.2 µm	Syringe filter	Sartorius
MK 035S	Spectrometer	UPRTek
MM 300.....	Bead-mill.....	Retsch
N816.....	Vacuum pump.....	Labport
Nalgene cryogenic vials	Glycerol stocks.....	Thermo Fisher Scientific
Nalgene Rapid Flow 0.2 µm.....	Bottle top filter.....	Thermo Fisher Scientific
NanoDrop 2000	Concentration measurement.....	Thermo Fisher Scientific
Omnifix, 1-20 mL.....	Syringes.....	Braun
Osmomat 3000	Osmometer	Gonotec
PDH4 depth filter (K700 + KS50).....	Clarification	Pall
PH 3110.....	pH meter.....	WTW
Pipetman.....	Pipettes.....	Gilson
PowerPac HC	Electrophoresis module.....	Bio-Rad
ProBlend 6.....	Blender.....	Philips
RCT basic.....	Magnet stirrer.....	IKA
RoboColumn Chelating Sepharose.....	Chromatography.....	Repligen
Rotina 380R.....	Centrifuge	Hettich
RZR1	Small scale homogenizer.....	Heidolph
SartoFlow Slice 200	Benchtop crossflow system.....	Sartorius
Sartopore 2 150 (0.45 + 0.2 µm)	Sterile filter	Sartorius
Sartopure GF Plus glass fiber filter	Clarification	Sartorius
SonoPuls MS73	Sonication	Bandelin
SSM3.....	Mini-gyro rocker	Stuart
Synergy H1.....	Plate reader.....	BioTek
TE6101	Precision scale.....	Sartorius
Thermomixer compact.....	Thermomixer.....	Eppendorf
Thomson Ultra Yield flassk.....	<i>Agrobacterium</i> cultivation	VWR
Trans-Blot Cell	Blotting	Bio-Rad
Trinocular microscope.....	BY-2 characterization	BMS
Tubes (1.5, 2.0 mL)	Reaction tubes	Sarstedt
Varioklav	Steam sterilizer.....	H&P
Vantage liquid handling station.....	Automation	Hamilton
VEKT400	Vacuum pump	Elektro-Waerme-Aachen
VelaPad	Depth filter housing	Pall
Vortex-Genie 2	Vortex	Scientific Industries
Whatman filter paper 11 µm	BY-2 characterization	Whatman
XCell II Blot Module	Blotting	Thermo Fisher Scientific
XCell SureLock Mini-Cell	Electrophoresis.....	Thermo Fisher Scientific
XK26/20 column	Chromatography.....	Kronlab
Z001023551 pH sensor 12×235 mm	BY-2 cultivation.....	Applikon
Z010023525 DOT sensor 12×235 mm.....	BY-2 cultivation.....	Applikon

VII.5 List of chemicals

Name	Type/Use	Manufacturer
2,4-dichlorophenoxyacetic acid	Medium component.....	Duchefa
5-bromo-4-chloro-3-indolyl phosphate.....	Assays	Merck
Acetic acid	Buffer component.....	Carl Roth
Acetosyringone 97%.....	Buffer component.....	Merck
Adenosine diphosphate	Assays	Merck
Agar-agar	Medium component.....	Carl Roth
Alpha toxin	Assays	Abcam
Ammonium nitrate (¹⁵ N) 98 atom%	Medium component.....	Merck
Ampicillin.....	Antibiotic.....	Carl Roth
Anhydrotetracycline hydrochloride	Antibiotic.....	Merck
Beef extract.....	Medium component.....	Carl Roth
Bovine serum albumin	Assays	Merck
Calcium chloride dihydrate.....	Medium component.....	Carl Roth
Carbenicillin	Antibiotic.....	Duchefa
CHAPS	Detergent	Merck
Coomassie Protein Assay reagent.....	Assays	Thermo Fisher
Crystal violet (Neisser's solution II)	Assays	Carl Roth
Deuterium oxide 99.9 atom%	Medium component.....	Merck
DMSO.....	Solvent.....	Merck
Disodium phosphate dihydrate	Buffer component.....	Carl Roth
EDTA	Buffer component.....	Carl Roth
Ethanol.....	Sanitization/pre-wetting	Carl Roth
Ethidium bromide solution	Cloning	Carl Roth
Ethyl-3-diaminopropyl-carbodiimide	Amine coupling	Merck
Evans blue dye.....	Plant cell characterization.....	Merck
Ferric chloride hexahydrate	Medium component.....	Carl Roth
Ferty 2 Mega.....	Fertilizer	Planta
Formaldehyde	Buffer component.....	Carl Roth
Fructose	Medium component.....	Carl Roth
Gibson Assembly Mastermix.....	Cloning	New England Biolabs
Glucose-6-phosphate dehydrogenase.....	Assays	Merck
Glucose monohydrate	Buffer/medium component.....	Carl Roth
Glycerol	Buffer/medium component.....	Carl Roth
Glycine	Buffer component.....	Carl Roth
Goat anti-human Ig λ AP mAb	Antibody.....	Merck
Goat anti-human IgG AP mAb	Antibody.....	Jackson Immuno
Goat anti-mCherry	Antibody.....	Thermo Fisher
Goat anti-rabbit IgG AP mAb.....	Antibody.....	Jackson Immuno
HEPES	Buffer component.....	Carl Roth
HEPES-KOH	Buffer component.....	Merck
Hexokinase	Assays	Merck
Hydrochloric acid 37%	Buffer component.....	Carl Roth
Imidazole	Buffer component.....	Carl Roth
Kanamycin.....	Antibiotic.....	Duchefa
Magnesium sulfate heptahydrate	Medium component.....	Carl Roth
Magnesium chloride hexahydrate	Buffer/medium component.....	Carl Roth
Mannit.....	Medium component.....	Carl Roth
Manganese chloride tetrahydrate	Medium component.....	Carl Roth
MES.....	Buffer component.....	Carl Roth
Methanol.....	Buffer component.....	Carl Roth

Milk powder	Buffer component	Carl Roth
Monosodium glutamate	Medium component	Carl Roth
MOPS	Buffer component	Carl Roth
Murashige & Skoog salts	Buffer component	Duchefa
Myo-inositol	Medium component	Duchefa
N-hydroxysuccinimide	Amine coupling	Merck
Nickel(II) sulfate hexahydrate	Buffer component	Carl Roth
Nicotinamide adenine dinucleotide	Assays	Merck
Nitro blue tetrazolium	Assays	Merck
Novex NuPAGE 4-12% Bis-Tris	Electrophoresis	Life Technologies
NucleoSpin Plasmid kit	DNA purification	Macherey-Nagel
NucleoSpin gel and PCR clean-up kit	DNA purification	Macherey-Nagel
Q5 DNA polymerase	Cloning	New England Biolabs
PEG-6000	Cloning	Merck
Phenylalanine	Medium component	Duchefa
Pluronic L61	Medium component	Merck
Potassium phosphate	Buffer/medium component	Carl Roth
Proteinase K	Enzyme inactivation	Carl Roth
Rabbit anti-goat IgG AP mAb	Antibody	Jackson Immuno
Rabbit anti-His ₆ mAb	Antibody	GeneScript
Restriction enzymes	Cloning	New England Biolabs
Rifampicin	Antibiotic	Duchefa
Sera-Mag-Select	Cloning	Cytiva
Silwet Gold	Infiltration	Spiess-Urania
SimplyBlue SafeStain	Coomassie staining	Life Technologies
Sodium chloride	Buffer component	Carl Roth
Sodium dihydrogen phosphate	Buffer component	Carl Roth
Sodium metabisulfite	Buffer component	Carl Roth
Sodium hydroxide	Buffer component	Carl Roth
Sodium metabisulfite	Assays	Merck
Soy peptone	Medium component	Carl Roth
Sucrose	Buffer component	Duchefa
T4 DNA ligase	Cloning	New England Biolabs
Taq DNA polymerase	Cloning	New England Biolabs
Technical buffer	Calibration	WTW
Thiamin hydrochloric acid	Medium component	Duchefa
Threonine	Medium component	Duchefa
TRIS-base	Buffer component	Carl Roth
TRIS-hydrochloride	Buffer component	Carl Roth
Tryptophane	Medium component	Duchefa
Tryptone	Medium component	Carl Roth
Triton X-100	Detergent	Merck
Tween-20	Detergent	Merck
Yeast extract	Medium component	Carl Roth
Zinc chloride	Medium component	Carl Roth

VII.6 List of buffers

Name	Component	Concentration mM (g L ⁻¹)	Comment
Infiltration buffer (PCPs)	Murashige and Skoog major and minor salts	n.a. (0.5)	Adjusted to pH 5.6 with HCl, acetosyringone was added immediately before infiltration
	Sucrose	146.0 (50.0)	
	Glucose monohydrate	10.1 (2.0)	
	MES	30.0 (5.9)	
	Acetosyringone	0.2 (4.0×10 ⁻²)	
Infiltration buffer (differentiated plants)	Murashige and Skoog major and minor salts	n.a. (0.5)	Adjusted to pH 5.6 with HCl, acetosyringone was added immediately before infiltration
	Acetosyringone	0.2 (4.0×10 ⁻²)	
Extraction Buffer (extraction of plants and PCPs)	Disodium phosphate dihydrate	50 (8.9)	Adjusted to pH 8.0 with NaOH, sodium metabisulfite was added immediately before extraction, optionally modified addition of Triton (without sodium chloride)
	Sodium chloride	500.0 (29.0)	
	Sodium metabisulfite	10.0 (1.9)	
	Triton X-100 (optional)	0.2, 90% CMC	
Extraction Buffer (extraction of bacteria)	TRIS-HCl	50.0 (7.8)	Adjusted to pH 7.5 with NaOH
	Sodium chloride	50.0 (2.9)	
Phosphate buffer (infiltration centrifugation)	Disodium phosphate dihydrate	50.0 (8.9)	Adjusted to pH 8.0 with NaOH, sodium metabisulfite was added immediately before extraction
	Sodium chloride	500.0 (29.0)	
	Sodium metabisulfite	10.0 (1.9)	
Detergent buffer (infiltration centrifugation)	TRIS-HCl	100.0 (15.6)	Adjusted to pH 8.0 with NaOH
	Potassium chloride	500.0 (37.3)	
	CHAPS	6.0 (3.7)	
	Sodium sulfite	160.0 (20.2)	
IMAC charging solution	Nickel II sulfate hexahydrate	100.0 (26.3)	
IMAC equilibration buffer	Disodium phosphate dihydrate	20.0 (3.6)	Adjusted to pH 7.5 with NaOH
	Sodium chloride	500.0 (29.0)	
IMAC washing buffer	Disodium phosphate dihydrate	20.0 (3.6)	Adjusted to pH 7.5 with NaOH
	Sodium chloride	500.0 (29.0)	
	Imidazole	30.0 (2.0)	
IMAC elution buffer	Disodium phosphate dihydrate	20.0 (3.6)	Adjusted to pH 7.5 with NaOH
	Sodium chloride	500.0 (29.0)	
	Imidazole	300.0 (20.4)	

List of buffers continued.

Name	Component	Concentration mM (g L⁻¹)	Comment
Protein G equilibration buffer	Disodium phosphate dihydrate	12.3 (2.2)	pH 7.2
	Sodium dihydrogen phosphate	7.7 (1.2)	
	Sodium chloride	150 (8.8)	
Protein G washing buffer	Disodium phosphate dihydrate	12.3 (2.2)	pH 8.0
	Sodium dihydrogen phosphate	7.7 (1.2)	
	Sodium chloride	5.0 (0.3)	
Protein G elution buffer	Glycine	100 (7.5)	Adjusted to pH 2.0 with HCl
	Sodium chloride	500.0 (29.0)	
Protein G neutralization buffer	TRIS-HCl	1000.0 (121.1)	Adjusted to pH 9.0 with NaOH
PBS-(T) buffer	Sodium chloride	137.0 (8.0)	pH 7.4, prepared as 10× stock, Tween was added to the 1× stock
	Potassium chloride	2.7 (0.2)	
	Disodium phosphate dihydrate	8.1 (1.4)	
	Potassium phosphate	1.0 (0.2)	
	Tween-20 (optional)	n.a. (0.5)	
TAE buffer	TRIS-HCl	50.0 (6.0)	pH 8.0, prepared as 50× stock
	Acetic acid	50.0 (3.0)	
	EDTA	1.0 (0.3)	
HBS-EP buffer	HEPES	10.0 (2.4)	pH 7.4, prepared as 10× stock, Tween was added to the 1× stock
	EDTA	3.0 (0.9)	
	Sodium chloride	150.9 (8.8)	
	Tween-20	n.a. (0.5)	
Regeneration buffer	Glycine	100 (7.5)	Adjusted to pH 4.0 with HCl
	Sodium chloride	500.0 (29.0)	
	Tween-20	n.a. (0.5)	
Silver staining solution I	Acetic acid	n.a. (126.0)	Prepared immediately before use
	Methanol	n.a. (396.0)	
Silver staining solution II	Methanol	n.a. (396.0)	Prepared immediately before use
Silver staining solution III	Sodium thiosulfate	1.3 (0.2)	Prepared immediately before use

List of buffers continued.

Name	Component	Concentration mM (g L⁻¹)	Comment
Silver staining solution IV	Silver nitrate	1.2 (0.2)	Prepared immediately before use
Silver staining solution V	Sodium carbonate Formaldehyde	188.7 (20.0)	Prepared immediately before use
Silver staining solution VI	Acetic acid	n.a. (10.5)	Prepared immediately before use
Milk powder solution	Milk powder	n.a. (50.0)	Prepared in PBS-T buffer
AP buffer	TRIS-HCl Sodium chloride Magnesium chloride hexahydrate	100.0 (12.1) 100.0 (5.8) 5.0 (1.0)	Adjusted to pH 9.6 with NaOH
Biofilm assay buffer	TRIS-HCl	20.0 (3.2)	pH 8.0
PPK assay solution I	HEPES-KOH Magnesium chloride hexahydrate Ammonium sulfate ADP Hexametaphosphate PPK	50.0 (13.8) 10.0 (2.0) 50.0 (6.6) 5.0 (2.1) 0.3 (0.2) (5.0×10 ⁻⁶)	pH 7.5, ADP and enzyme stocks were prepared same-day fresh
PPK assay solution II	HEPES-KOH Sodium chloride Magnesium chloride hexahydrate Glucose monohydrate Hexokinase Glucose-6-phosphate dehydrogenase NAD ⁺	50.0 (13.8) 10.0 (0.6) 1.5 (0.3) 5.0 (1.0) 4 U 1 U 1.0 (0.7)	pH 7.5, NAD and enzyme stocks were prepared same-day fresh

ADP – adenosine diphosphate, AP – alkaline phosphatase, CMC – critical micelle concentration, HCL – hydrochloric acid, NAD⁺ – Nicotinamide adenine dinucleotide, NaOH – sodium hydroxide, PBS – phosphate buffered saline, PPK – polyphosphate kinase.

VII.7 List of cultivation media

Name	Component	Concentration mM (g L ⁻¹)	Comment
LB medium	Tryptone	n.a. (10.0)	Adjusted to pH 7.0 with NaOH, sterilized by autoclaving, sodium chloride was omitted for SacB negative selection
	Yeast extract	n.a. (5.0)	
	Sodium chloride	171.0 (10.0)	
	Agar-agar (optional)	n.a. (15.0)	
YEB medium	Beef extract	n.a. (5.0)	Adjusted to pH 7.0 with NaOH, sterilized by autoclaving
	Yeast extract	n.a. (1.0)	
	Peptone	n.a. (5.0)	
	Sucrose	14.6 (5.0)	
	Magnesium sulfate heptahydrate	2.0 (0.5)	
	Agar-agar (optional)	n.a. (15.0)	
PAM4 medium	Soy peptone	n.a. (20.0)	Adjusted to pH 7.0 with NaOH, sterilized by autoclaving, PAM4 medium was stored no longer than 2 weeks
	Yeast extract	n.a. (0.5)	
	Fructose	27.8 (5.0)	
	Magnesium sulfate heptahydrate	4.0 (1.0)	
	Agar-agar (optional)	n.a. (15.0)	
TB medium	Tryptone	n.a. (12.0)	Adjusted to pH 7.0 with NaOH, sterilized by autoclaving
	Yeast extract	n.a. (24.0)	
	Glycerol	54.7 (5.0)	
	Dipotassium phosphate	72.0 (12.5)	
	Potassium phosphate	17.0 (2.3)	
MS medium	Murashige and Skoog major and minor salts	n.a. (4.3)	Default pH of 5.8, sterilized by 0.2 µm filtration, stored in the dark
	<i>myo</i> -inositol	0.6 (0.1)	
	Thiamine-HCl	3.0×10 ⁻³ (1.0×10 ⁻³)	
	2,4-dichlorophenoxyacetic acid	9.0×10 ⁻⁴ (2.0×10 ⁻⁴)	
	Potassium phosphate	1.5 (0.2)	
MS medium H (isotope labeling)	Murashige and Skoog major and minor salts	n.a. (4.3)	Default pH of 5.8, sterilized by 0.2 µm filtration, stored in the dark, values for ammonium nitrate correspond to the concentration included in Murashige and Skog major and minor salts
	MS macro salts	0	
	MS micro salts	0	
	<i>myo</i> -inositol	0.6 (0.1)	
	Thiamine-HCl	3.0×10 ⁻³ (1.0×10 ⁻³)	
	2,4-dichlorophenoxyacetic acid	9.0×10 ⁻⁴ (2.0×10 ⁻⁴)	
	Potassium phosphate	1.5 (0.2)	
	Ammonium nitrate (¹⁴ N, not labeled)	20.6 (1.7)	
	Ammonium nitrate (¹⁵ NH ₄ ¹⁵ NO ₃)	0	
	Deuterium oxide	0	

List of cultivation media continued.

Name	Component	Concentration mM (g L⁻¹)	Comment
MS medium D (isotope labeling)	Murashige and Skoog major and minor salts	n.a. (4.3)	Default pH of 5.8, sterilized by 0.2 µm filtration, stored in the dark, values for ammonium nitrate correspond to the concentration included in Murashige and Skog major and minor salts
	MS macro salts	0	
	MS micro salts	0	
	<i>myo</i> -inositol	0.6 (0.1)	
	Thiamine-HCl	3.0×10 ⁻³ (1.0×10 ⁻³)	
	2,4-dichlorophenoxyacetic acid	9.0×10 ⁻⁴ (2.0×10 ⁻⁴)	
	Potassium phosphate	1.5 (0.2)	
	Ammonium nitrate (¹⁴ N, not labeled)	20.6 (1.7)	
	Ammonium nitrate (¹⁵ NH ₄ ¹⁵ NO ₃)	0	
	Deuterium oxide	50% (v v ⁻¹)	
MS medium (D)N (isotope labeling)	Murashige and Skoog major and minor salts	0	Default pH of 5.8, sterilized by 0.2 µm filtration, stored in the dark, deuterium oxide was replaced with water to obtain medium N
	MS macro salts	n.a. (1.6)	
	MS micro salts	n.a. (1.0)	
	<i>myo</i> -inositol	0.6 (0.1)	
	Thiamine-HCl	3.0×10 ⁻³ (1.0×10 ⁻³)	
	2,4-dichlorophenoxyacetic acid	9.0×10 ⁻⁴ (2.0×10 ⁻⁴)	
	Potassium phosphate	1.5 (0.2)	
	Ammonium nitrate (¹⁴ N, not labeled)	0	
	Ammonium nitrate (¹⁵ NH ₄ ¹⁵ NO ₃)	20.6 (1.7)	
	Deuterium oxide (optional)	50% (v v ⁻¹)	
MSgg medium	Potassium phosphate	3.3 (0.70)	Adjusted to pH 7.0 with NaOH, sterilized by 0.2 µm filtration, stored in the dark at 4°C
	MOPS	100.0 (20.9)	
	Magnesium chloride hexahydrate	1.1 (0.2)	
	Calcium chloride dihydrate	0.5 (7.7×10 ⁻²)	
	Manganese chloride tetrahydrate	3.0×10 ⁻² (6.0×10 ⁻³)	
	Ferric chloride hexahydrate	3.0×10 ⁻² (8.0×10 ⁻³)	
	Zinc chloride	5.1×10 ⁻² (7.0×10 ⁻³)	
	Thiamine-HCl	2.9×10 ⁻³ (1.0×10 ⁻³)	
	Glycerol	54.7 (5.0)	
	Monosodium glutamate	29.6 (5.0)	
	Tryptophane	0.2 (5.0×10 ⁻²)	
	Phenylalanine	0.3 (5.0×10 ⁻²)	
	Threonine	0.4 (5.0×10 ⁻²)	

HCL – hydrochloric acid, MS – Murashige and Skoog major and minor salts, MSgg – minimal salts glutamate glycerol, NAOH – sodium hydroxide, PAM4 – plant peptone *Agrobacterium* medium 4, TB – terrific broth, YEB – yeast extract broth.

VII.8 Expression vectors and primers

Supporting Table 1: Overview of primers used for cloning modular expression vectors and multi-domain antibody constructs.

Primer name	Sequence	Length [bp]
Cloning of modular expression vectors		
GA_pTRAc_BB_frwd	AAGAGAATTATGCAGTGCTGCCATAAC	27
GA_pTRAc_BB_rev	GTTATGGCAGCACTGCATAATTCTCTTACTGT CATG	36
GA_pTRAc_BB_CHS_rev	TAGAATCCTCGCCAGGAGGTACCATGGTGTTT TTTTTTTTTTTATAAATCTCTCTATAAATCTGA TTTGTGTTGTG	76
GA_pTRAc_BB_omega_rev	TAGAATCCTCGCCAGGAGGTACCATGGTCCTT GTAAATAGTAATTGTAATGTTG	54
GA_pTRAc_BB_TL_rev	TAGAATCCTCGCCAGGAGGTACCATGGCTATC GTTCTGTAAATGGTG	46
GA_pTRAc_BB_tag_frwd	CTCTTTGAGGGCCCTTAGACAGATGGCGGCCG CTCATCA CCATC	44
GA_IL6_frwd	ATGGTACCTCCTGGCGAGGATTCTA	25
GA_IL6_rev	CATCTGTCTAAGGGCCCTCAAAGAG	25
LPH_IL6_frwd	tagctaTCATGATGGAGTGGAGCTGGATCTTC TTGTTCTTGCTCAGCGGCACTGCAGGTGTTCA CTCCATGGTACCTCCTGGCGAG	86
LPH_IL6_rev	agtctaGCGGCCGCCATCTGTCTAAGG	27
rbcS_frwd	ctactaTCATGATGGCTTCCTCTGTTATTTCT	31
rbcS_rev	catgtaCCATGGCCCTAACGCGTC	24
Cloning of IgG3 domain exchange variants		
GA_IgG1_CH2_CH3_frwd	GATACCCACCGCCGTGTCCAAGATGTCCTGC TCCTGAACTTCTTGGTGGTC	52
GA_IgG1_CH2_CH3_rev	TGTAAGTATCTCAGTTCGGAAGGACAAACAG	31
GA_IgG1_CH3_frwd	CCTATCGAAAAGACCATCTCTAAGACCAAGGG TCAGCCTAGAGAACCGCAAG	52
GA_IgG3_no_CH2_CH3_frwd	CTGTTTGTCTTCGGAAC	18
GA_IgG3_no_CH2_CH3_rev	AGGACATCTTGGACACG	17
GA_IgG3_no_CH3_rev	CTTGGTCTTAGAGATGGTCTTTTC	24
GA_IgG3_no_Ch3_rev_V2	CTTGGTCTTAGAGATGGTC	19
Cloning of expression vectors for targeting antibodies to the vacuole		
GA_KISIA_IgG1_frwd	TGTCCCCTGGCAAGAAGATTCTATTGCTTGTT TGTCCTTCGGAACCTG	48
GA_KISIA_IgG1_rev	AGCAATAGAAATCTTCTTGCCAGGGGACAGAG	32
GA_KISIA_IgG3_frwd	TTGAGCCCTGGCAAGAAGATTCTATTGCTTGTT TTGTCCTTCGGAACCTG	49
GA_KISIA_IgG3_rev	GCAATAGAAATCTTCTTGCCAGGGCTCAAGC	32

Supporting Table 1 continued.

Primer name	Sequence	Length [bp]
Cloning of expression vectors for targeting antibodies to plastids/chloroplast		
IgG1_3_no_LPH_frwd	acgtatCCATGGCCCAAGTTCAGCTTCAAGAA TC	34
IgG1_3_rev	ctatgaCTCGAGCTAAGAGCACTCG	25
LPH_del_LC_frwd	*TCTTACGTGTTGACCCAAGATCC	23
LPH_del_LC_rev	TGGCCCAGGGTTGGACTC	18
Cloning of expression vectors for targeting antibodies to the apoplast (deletion of SEKDEL)		
KDEL_del_frwd	*TGTTTGTCTTCGGAAGTCTGAG	21
KDEL_del_IgG3_rev	CTTGCCAGGGCTCAAGC	17
KDEL_del_IgG1_rev	CTTGCCAGGGGACAGAG	17
Colony PCR and sequencing		
IgG_sequencing	TTCAAGAACCTCCTGTTCTC	20
35SS_FI	TGACGCACAATCCCACTATC	20
35SS_PARI	CCCTTATCTGGGAAGTACTC	20

Lowercase letters indicate non-coding sequences that served as spacer for restriction enzymes (cleavage close to the end of a DNA fragment). Asterisks indicate phosphorylated primers for ligation of blunt ends. BB – backbone, frwd – forward primer, GA – Gibson assembly, rev – reverse primer.

Supporting Table 2: Overview of vectors that were used in this study.

ID	Vector	Protein	5' UTR	Signal sequences	Compartment
Vectors for <i>Agrobacterium</i> -mediated transient expression in plants					
000001	pTRAc	IL6 (50% GC)	CHS	None	Cytosol
000002	pTRAc	IL6 (50% GC)	CHS	LPH	Apoplast
000003	pTRAc	IL6 (50% GC)	CHS	rbcS	Chloroplast/Plastids
000004	pTRAc	IL6 (50% GC)	CHS	LPH, SEKDEL	ER
000005	pTRAc	IL6 (50% GC)	omega	None	Cytosol
000006	pTRAc	IL6 (50% GC)	omega	LPH	Apoplast
000007	pTRAc	IL6 (50% GC)	omega	rbcS	Chloroplast/Plastids
000008	pTRAc	IL6 (50% GC)	omega	LPH, SEKDEL	ER
000009	pTRAc	IL6 (50% GC)	TL	None	Cytosol
000010	pTRAc	IL6 (50% GC)	TL	LPH	Apoplast
000011	pTRAc	IL6 (50% GC)	TL	rbcS	Chloroplast/Plastids
000012	pTRAc	IL6 (50% GC)	TL	LPH, SEKDEL	ER
000013	pTRAc	IL6 (33% GC)	CHS	None	Cytosol
000014	pTRAc	IL6 (33% GC)	CHS	LPH	Apoplast
000015	pTRAc	IL6 (33% GC)	CHS	rbcS	Chloroplast/Plastids
000016	pTRAc	IL6 (33% GC)	CHS	LPH, SEKDEL	ER
000017	pTRAc	IL6 (33% GC)	omega	None	Cytosol

Supporting Table 2 continued.

ID	Vector	Protein	5' UTR	Signal sequences	Compartment
000018	pTRAc	IL6 (33% GC)	omega	LPH	Apoplast
000019	pTRAc	IL6 (33% GC)	omega	rbcS	Chloroplast/Plastids
000020	pTRAc	IL6 (33% GC)	omega	LPH, SEKDEL	ER
000021	pTRAc	IL6 (33% GC)	TL	None	Cytosol
000022	pTRAc	IL6 (33% GC)	TL	LPH	Apoplast
000023	pTRAc	IL6 (33% GC)	TL	rbcS	Chloroplast/Plastids
000024	pTRAc	IL6 (33% GC)	TL	LPH, SEKDEL	ER
000025	pTRAc	IL8 (50% GC)	CHS	None	Cytosol
000026	pTRAc	IL8 (50% GC)	CHS	LPH	Apoplast
000027	pTRAc	IL8 (50% GC)	CHS	rbcS	Chloroplast/Plastids
000028	pTRAc	IL8 (50% GC)	CHS	LPH, SEKDEL	ER
000029	pTRAc	IL8 (50% GC)	omega	None	Cytosol
000030	pTRAc	IL8 (50% GC)	omega	LPH	Apoplast
000031	pTRAc	IL8 (50% GC)	omega	rbcS	Chloroplast/Plastids
000032	pTRAc	IL8 (50% GC)	omega	LPH, SEKDEL	ER
000033	pTRAc	IL8 (50% GC)	TL	None	Cytosol
000034	pTRAc	IL8 (50% GC)	TL	LPH	Apoplast
000035	pTRAc	IL8 (50% GC)	TL	rbcS	Chloroplast/Plastids
000036	pTRAc	IL8 (50% GC)	TL	LPH, SEKDEL	ER
000037	pTRAc	IL8 (33% GC)	CHS	None	Cytosol
000038	pTRAc	IL8 (33% GC)	CHS	LPH	Apoplast
000039	pTRAc	IL8 (33% GC)	CHS	rbcS	Chloroplast/Plastids
000040	pTRAc	IL8 (33% GC)	CHS	LPH, SEKDEL	ER
000041	pTRAc	IL8 (33% GC)	omega	None	Cytosol
000042	pTRAc	IL8 (33% GC)	omega	LPH	Apoplast
000043	pTRAc	IL8 (33% GC)	omega	rbcS	Chloroplast/Plastids
000044	pTRAc	IL8 (33% GC)	omega	LPH, SEKDEL	ER
000045	pTRAc	IL8 (33% GC)	TL	None	Cytosol
000046	pTRAc	IL8 (33% GC)	TL	LPH	Apoplast
000047	pTRAc	IL8 (33% GC)	TL	rbcS	Chloroplast/Plastids
000048	pTRAc	IL8 (33% GC)	TL	LPH, SEKDEL	ER
000049	pTRAc	PPK-RO	CHS	None	Cytosol
000050	pTRAc	PPK-RO	CHS	LPH	Apoplast
000051	pTRAc	PPK-RO	CHS	rbcS	Chloroplast/Plastids
000052	pTRAc	PPK-RO	CHS	LPH, SEKDEL	ER
000053	pTRAc	PPK-RO	omega	None	Cytosol
000054	pTRAc	PPK-RO	omega	LPH	Apoplast

Supporting Table 2 continued.

ID	Vector	Protein	5' UTR	Signal sequences	Compartment
000055	pTRAc	PPK-RO	omega	rbcS	Chloroplast/Plastids
000056	pTRAc	PPK-RO	omega	LPH, SEKDEL	ER
000057	pTRAc	PPK-RO	TL	None	Cytosol
000058	pTRAc	PPK-RO	TL	LPH	Apoplast
000059	pTRAc	PPK-RO	TL	rbcS	Chloroplast/Plastids
000060	pTRAc	PPK-RO	TL	LPH, SEKDEL	ER
000061	pTRAc	PPK-RO	CHS	None	Cytosol
000062	pTRAc	PPK-RO	CHS	LPH	Apoplast
000063	pTRAc	PPK-RO	CHS	rbcS	Chloroplast/Plastids
000064	pTRAc	PPK-RO	CHS	LPH, SEKDEL	ER
000065	pTRAc	PPK-RO	omega	None	Cytosol
000066	pTRAc	PPK-RO	omega	LPH	Apoplast
000067	pTRAc	PPK-RO	omega	rbcS	Chloroplast/Plastids
000068	pTRAc	PPK-RO	omega	LPH, SEKDEL	ER
000069	pTRAc	PPK-RO	TL	None	Cytosol
000070	pTRAc	PPK-RO	TL	LPH	Apoplast
000071	pTRAc	PPK-RO	TL	rbcS	Chloroplast/Plastids
000072	pTRAc	PPK-RO	TL	LPH, SEKDEL	ER
000073	pTRAc	PPK-TA	CHS	None	Cytosol
000074	pTRAc	PPK-TA	CHS	LPH	Apoplast
000075	pTRAc	PPK-TA	CHS	rbcS	Chloroplast/Plastids
000076	pTRAc	PPK-TA	CHS	LPH, SEKDEL	ER
000077	pTRAc	PPK-TA	omega	None	Cytosol
000078	pTRAc	PPK-TA	omega	LPH	Apoplast
000079	pTRAc	PPK-TA	omega	rbcS	Chloroplast/Plastids
000080	pTRAc	PPK-TA	omega	LPH, SEKDEL	ER
000081	pTRAc	PPK-TA	TL	None	Cytosol
000082	pTRAc	PPK-TA	TL	LPH	Apoplast
000083	pTRAc	PPK-TA	TL	rbcS	Chloroplast/Plastids
000084	pTRAc	PPK-TA	TL	LPH, SEKDEL	ER
000085	pTRAc	PPK-TA	CHS	None	Cytosol
000086	pTRAc	PPK-TA	CHS	LPH	Apoplast
000087	pTRAc	PPK-TA	CHS	rbcS	Chloroplast/Plastids
000088	pTRAc	PPK-TA	CHS	LPH, SEKDEL	ER
000089	pTRAc	PPK-TA	omega	None	Cytosol
000090	pTRAc	PPK-TA	omega	LPH	Apoplast
000091	pTRAc	PPK-TA	omega	rbcS	Chloroplast/Plastids

Supporting Table 2 continued.

ID	Vector	Protein	5' UTR	Signal sequences	Compartment
000092	pTRAc	PPK-TA	omega	LPH, SEKDEL	ER
000093	pTRAc	PPK-TA	TL	None	Cytosol
000094	pTRAc	PPK-TA	TL	LPH	Apoplast
000095	pTRAc	PPK-TA	TL	rbcS	Chloroplast/Plastids
000096	pTRAc	PPK-TA	TL	LPH, SEKDEL	ER
000101	pTRAc	DsRed	CHS	None	Cytosol
000102	pTRAc	DsRed	CHS	LPH	Apoplast
000103	pTRAc	DsRed	CHS	rbcS	Chloroplast/Plastids
000104	pTRAc	DsRed	CHS	LPH, SEKDEL	ER
000190	pTRAc	GB1	CHS	None	Cytosol
000191	pTRAc	GB1	CHS	LPH	Apoplast
000192	pTRAc	GB1	CHS	rbcS	Chloroplast/Plastids
000193	pTRAc	GB1	CHS	LPH, SEKDEL	ER
000194	pTRAc	GB1	omega	None	Cytosol
000195	pTRAc	GB1	omega	rbcS	Chloroplast/Plastids
000196	pTRAc	GB1	TL	None	Cytosol
000197	pTRAc	GB1	TL	rbcS	Chloroplast/Plastids
000222	pTRAc	Ferritin	CHS	None	Cytosol
000223	pTRAc	Ferritin	CHS	LPH	Apoplast
000224	pTRAc	Ferritin	CHS	rbcS	Chloroplast/Plastids
000225	pTRAc	Ferritin	omega	None	Cytosol
000226	pTRAc	Ferritin	omega	LPH	Apoplast
000227	pTRAc	Ferritin	omega	rbcS	Chloroplast/Plastids
000228	pTRAc	Ferritin	TL	None	Cytosol
000229	pTRAc	Ferritin	TL	LPH	Apoplast
000230	pTRAc	Ferritin	TL	rbcS	Chloroplast/Plastids
000237	pTRAc	IgG1	omega	2×LPH, SEKDEL	ER
000238	pTRAc	IgG1	TL	2×LPH, SEKDEL	ER
000239	pTRAc	IgG1	CHS	2×LPH, SEKDEL	ER
000240	pTRAc	IgG3	omega	2×LPH, SEKDEL	ER
000241	pTRAc	IgG3	TL	2×LPH, SEKDEL	ER
000242	pTRAc	IgG3	CHS	2×LPH, SEKDEL	ER
000243	pTRAc	IgG1	omega	LPH, SEKDEL	ER
000244	pTRAc	IgG1	TL	LPH, SEKDEL	ER
000245	pTRAc	IgG1	CHS	LPH, SEKDEL	ER
000246	pTRAc	IgG3	omega	LPH, SEKDEL	ER
000247	pTRAc	IgG3	TL	LPH, SEKDEL	ER

Supporting Table 2 continued.

ID	Vector	Protein	5' UTR	Signal sequences	Compartment
000248	pTRAc	IgG3	CHS	LPH, SEKDEL	ER
000249	pTRAc	IgG1	omega	LPH, KISIA	Vacuole
000250	pTRAc	IgG1	TL	LPH, KISIA	Vacuole
000251	pTRAc	IgG1	CHS	LPH, KISIA	Vacuole
000252	pTRAc	IgG3	omega	LPH, KISIA	Vacuole
000253	pTRAc	IgG3	TL	LPH, KISIA	Vacuole
000254	pTRAc	IgG3	CHS	LPH, KISIA	Vacuole
000255	pTRAc	IgG1	omega	LPH	Apoplast
000256	pTRAc	IgG1	TL	LPH	Apoplast
000257	pTRAc	IgG1	CHS	LPH	Apoplast
000258	pTRAc	IgG3	omega	LPH	Apoplast
000259	pTRAc	IgG3	TL	LPH	Apoplast
000260	pTRAc	IgG3	CHS	LPH	Apoplast
000261	pTRAc	IgG1	omega	rbcS	Chloroplast/Plastids
000262	pTRAc	IgG1	TL	rbcS	Chloroplast/Plastids
000263	pTRAc	IgG1	CHS	rbcS	Chloroplast/Plastids
000264	pTRAc	IgG3	omega	rbcS	Chloroplast/Plastids
000265	pTRAc	IgG3	TL	rbcS	Chloroplast/Plastids
000266	pTRAc	IgG3	CHS	rbcS	Chloroplast/Plastids
000267	pTRAc	IgG3+IgG1CH3	omega	2×LPH, SEKDEL	ER
000268	pTRAc	IgG3+IgG1CH3	TL	2×LPH, SEKDEL	ER
000269	pTRAc	IgG3+IgG1CH3	CHS	2×LPH, SEKDEL	ER
000270	pTRAc	IgG3+IgG1CH2-3	omega	2×LPH, SEKDEL	ER
000271	pTRAc	IgG3+IgG1CH2-3	TL	2×LPH, SEKDEL	ER
000272	pTRAc	IgG3+IgG1CH2-3	CHS	2×LPH, SEKDEL	ER
000273	pTRAc	IgG3+IgG1CH3	omega	LPH, SEKDEL	ER
000274	pTRAc	IgG3+IgG1CH3	TL	LPH, SEKDEL	ER
000275	pTRAc	IgG3+IgG1CH3	CHS	LPH, SEKDEL	ER
000276	pTRAc	IgG3+IgG1CH2-3	omega	LPH, SEKDEL	ER
000277	pTRAc	IgG3+IgG1CH2-3	TL	LPH, SEKDEL	ER
000278	pTRAc	IgG3+IgG1CH2-3	CHS	LPH, SEKDEL	ER
000279	pTRAc	IgG3+IgG1CH3	omega	LPH, KISIA	Vacuole
000280	pTRAc	IgG3+IgG1CH3	TL	LPH, KISIA	Vacuole
000281	pTRAc	IgG3+IgG1CH3	CHS	LPH, KISIA	Vacuole
000282	pTRAc	IgG3+IgG1CH2-3	omega	LPH, KISIA	Vacuole
000283	pTRAc	IgG3+IgG1CH2-3	TL	LPH, KISIA	Vacuole
000284	pTRAc	IgG3+IgG1CH2-3	CHS	LPH, KISIA	Vacuole

Supporting Table 2 continued.

ID	Vector	Protein	5' UTR	Signal sequences	Compartment
000285	pTRAc	IgG3+IgG1CH3	omega	LPH	Apoplast
000286	pTRAc	IgG3+IgG1CH3	TL	LPH	Apoplast
000287	pTRAc	IgG3+IgG1CH3	CHS	LPH	Apoplast
000288	pTRAc	IgG3+IgG1CH2-3	omega	LPH	Apoplast
000289	pTRAc	IgG3+IgG1CH2-3	TL	LPH	Apoplast
000290	pTRAc	IgG3+IgG1CH2-3	CHS	LPH	Apoplast
000291	pTRAc	IgG3+IgG1CH3	omega	rbcS	Chloroplast/Plastids
000292	pTRAc	IgG3+IgG1CH3	TL	rbcS	Chloroplast/Plastids
000293	pTRAc	IgG3+IgG1CH3	CHS	rbcS	Chloroplast/Plastids
000294	pTRAc	IgG3+IgG1CH2-3	omega	rbcS	Chloroplast/Plastids
000295	pTRAc	IgG3+IgG1CH2-3	TL	rbcS	Chloroplast/Plastids
000296	pTRAc	IgG3+IgG1CH2-3	CHS	rbcS	Chloroplast/Plastids
000395	pTRAc	SpA Z	CHS	None	Cytosol
000396	pTRAc	SpA Z	CHS	LPH	Apoplast
000397	pTRAc	SpA Z	CHS	rbcS	Chloroplast/Plastids
000398	pTRAc	SpA Z	CHS	LPH, SEKDEL	ER
000403	pTRAc	DspB	CHS	None	Cytosol
000404	pTRAc	DspB	CHS	LPH	Apoplast
000405	pTRAc	DspB	CHS	rbcS	Chloroplast/Plastids
000406	pTRAc	DspB	CHS	LPH, SEKDEL	ER
000419	pTRAc	LysK-L	CHS	None	Cytosol
000420	pTRAc	LysK-L	CHS	LPH	Apoplast
000421	pTRAc	LysK-L	CHS	rbcS	Chloroplast/Plastids
000422	pTRAc	LysK-L	CHS	LPH, SEKDEL	ER
000423	pTRAc	LysK-L	omega	None	Cytosol
000424	pTRAc	LysK-L	omega	LPH	Apoplast
000425	pTRAc	LysK-L	omega	rbcS	Chloroplast/Plastids
000426	pTRAc	LysK-L	omega	LPH, SEKDEL	ER
000427	pTRAc	LysK-L	TL	None	Cytosol
000428	pTRAc	LysK-L	TL	LPH	Apoplast
000429	pTRAc	LysK-L	TL	rbcS	Chloroplast/Plastids
000430	pTRAc	LysK-L	TL	LPH, SEKDEL	ER
000431	pTRAc	SacB	CHS	None	Cytosol
000432	pTRAc	SacB	CHS	LPH	Apoplast
000433	pTRAc	SacB	CHS	rbcS	Chloroplast/Plastids
000434	pTRAc	SacB	CHS	LPH, SEKDEL	ER
000435	pTRAc	SacB	omega	None	Cytosol

Supporting Table 2 continued.

ID	Vector	Protein	5' UTR	Signal sequences	Compartment
000436	pTRAc	SacB	omega	LPH	Apoplast
000437	pTRAc	SacB	omega	rbcS	Chloroplast/Plastids
000438	pTRAc	SacB	omega	LPH, SEKDEL	ER
000439	pTRAc	SacB	TL	None	Cytosol
000440	pTRAc	SacB	TL	LPH	Apoplast
000441	pTRAc	SacB	TL	rbcS	Chloroplast/Plastids
000442	pTRAc	SacB	TL	LPH, SEKDEL	ER
Expression vectors for <i>E. coli</i>					
000001	pET16b	PPK-RO	None	None	Cytosol
000002	pET16b	PPK-TA	None	None	Cytosol
000003	pASK-IBA33plus	DspB	None	None	Cytosol
Gene synthesis					
000001	pMA	IL6 (50% GC)	None	None	None
000002	pMA	IL6 (33% GC)	None	None	None
000003	pMA	IL8 (50% GC)	None	None	None
000004	pMA	IL8 (33% GC)	None	None	None
000005	pMA	GB1	None	None	None
000006	pMA	Ferritin	None	None	None
000007	pMK	IgG1	None	None	None
000008	pMK	IgG3	None	None	None
000009	pMK	SpA Z	None	None	None
000010	pMA	DspB	None	None	None
000011	pMA	LysK-L	None	None	None
000012	pMA	ECMV-IRES	None	None	None

By default, target proteins were codon optimized for *N. benthamiana* using the GeneOptimizer tool [208]. Values in brackets denote the GC content, if different codon optimization tools were used (Codon optimization with the GeneOptimizer tool resulted in a GC content of ~50%, whereas codon optimization with the OPTIMIZER tool [403] resulted in a GC content of ~33%). DspB – glycoside hydrolase Dispersin B from *Actinobacillus actinomycetemcomitans* (Uniport ID Q840G9), DsRed – fluorescent protein from *Discosoma* sp. (Uniprot ID Q9U6Y8), ECMV – *Encephalomyocarditis virus*, Ferritin – human ferritin heavy chain (UniProt ID P02794), GB1 – B1 domain of *Streptococcus* sp. protein G (Uniprot ID P06654), IgG1 – IgG1 antibody M12 [209], IgG3 – human IgG3 antibody (Uniprot ID P01860), IgG3+IgG1CH3 – IgG3 domain exchange variant containing an IgG1 CH3 domain, IgG3+IgG1CH3-2 – IgG3 domain exchange variant containing IgG1 CH2 and CH3 domains, IL6 – human interleukin 6 (Uniprot ID P05231), IL8 – human interleukin 8 (Uniprot ID P10145), IRES – internal ribosome entry site, LysK-L – fusion protein of LysK and lysostaphin [254], PPK-RO – polyphosphate kinase from *R. opacus*, PPK-TA – polyphosphate kinase from *T. agreste*, Spa Z – Z domain of *S. aureus* protein A [404], CHS – *Petroselinum hortense* chalcone synthase 5' UTR, omega – *Tobacco mosaic virus* omega prime sequence, TL – *Tobacco etch virus* leader sequence, SEKDEL – ER retention signal from the chaperone protein Grp78, KISIA – vacuolar targeting signal from the *Amaranthus hypochondriacus* 11S globulin, LPH – leader peptide of the antibody mAb24 heavy chain, rbcS – transit peptide from the RuBisCO small subunit of *Solanum tuberosum*.

Supporting Table 3: Overview of signal sequences used to direct target proteins to different plant cell compartments.

Signal peptide	Amino acid sequence	Mass [kDa]	Removal of signal peptide during processing
rbcS	MASSVISSAAVATRTNVTQAGS MIAPFTGLKSAATFPVSRKQNL ITSIASNGGRVRA	5.8	Yes
KDEL	SEKDEL	0.7	No
KISIA	KISIA	0.5	Yes
LPH	MEWSWIFLFLSGTAGVHS	2.1	Yes

KDEL – ER retention signal from the chaperone protein Grp78, KISIA – vacuolar targeting signal from the *Amaranthus hypochondriacus* 11S globulin, LPH – leader peptide of the antibody mAb24 heavy chain, rbcS – transit peptide from the ribulose-1,5-bisphosphate carboxylase/oxygenase (RuBisCO) small subunit of *Solanum tuberosum*.

Supporting Table 4: Enzymes that generate NcoI-compatible overhangs for restriction at the 5' end of the target protein. Depending on the nucleotide sequence of the target protein, different restriction enzymes can be employed to generate compatible overhangs, omitting the need to alter the nucleotide or amino acid sequence.

Enzyme	Restriction site	New restriction site after ligation with NcoI
AflIII	A*C(A,G)(T,C)GT	None (no sub-cloning capability)
BspHI (PagI)	T*CATGA	None (no sub-cloning capability)
BtgI	C*C(A,G)(T,C)GG	NcoI, BtgI, StyI
NcoI	C*CATGG	NcoI
PciI (PscI)	A*CATGT	None (no sub-cloning capability)
StyI	C*C(A,T)(A,T)GG	NcoI, BtgI, StyI

Round brackets indicate degeneracy (i.e. multiple nucleotides are allowed). Asterisks indicate the cleaving position of the restriction enzyme. Only enzymes with 6 bp recognition sequences were listed.

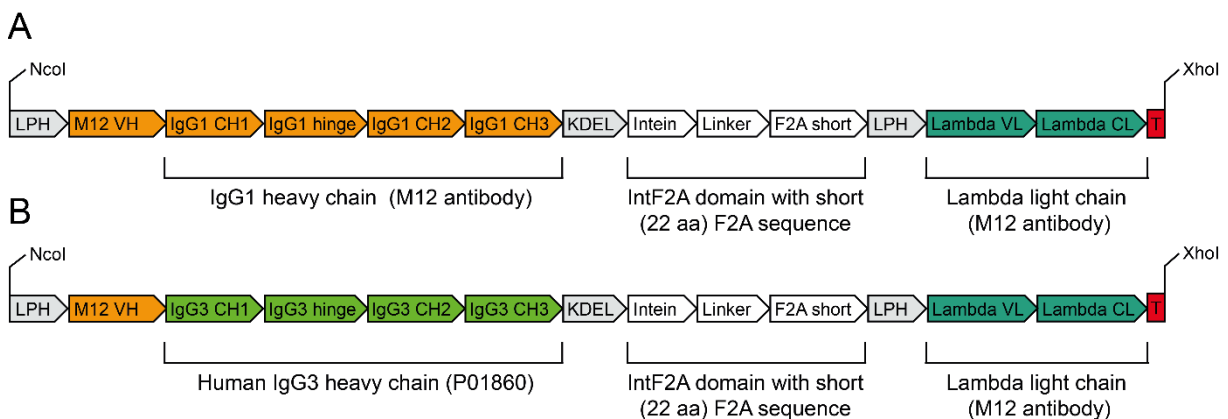


Figure S1: Construct design for cloning multi-subunit proteins into modular expression vectors. IgG1 (A) and IgG3 (B) constructs featured a self-cleaving linker composed of an intein and an F2A peptide [217] facilitating single-promotor transcription and stoichiometric translation of the antibody heavy and light chains. Deviating from the literature, a 22 amino acid F2A peptide was used instead of the 58 amino acid version. CDRs directed against *S. aureus* alpha toxin [405] were introduced into the variable domains of the M12 antibody [209]. Constructs for mAb expression were introduced into the modular vector system (Figure 3) by restriction cloning using NcoI and XhoI.

VII.9 Supplementary data

VII.9.1 SacB negative selection

Supporting Table 5: Emerging of sucrose resistant clones during SacB negative selection in liquid cultures. Exponential growth functions (Equation 9) were fitted to the growth curves of $\text{SacB}^{+/-}$ *E. coli* and $\text{SacB}^{+/-}$ *A. tumefaciens* cultivated in LB (*E. coli*) or PAM4 (*A. tumefaciens*) medium containing 100 g L⁻¹ sucrose (Figure 4G, H). Sucrose was omitted during regeneration.

Parameter	<i>E. coli</i> SacB^{+}		<i>E. coli</i> SacB^{-}		<i>A. tumefaciens</i> SacB^{-}	
	Value	Error	Value	Error	Value	Error
y_0	-0.09	0.08	-0.06	0.29	-0.04	0.05
A_l	0.01	0.01	0.14	0.08	0.01	0.01
t_l	2.32	0.51	4.24	0.61	8.97	1.94
k	0.43	0.09	0.24	0.03	0.11	0.02
τ	1.61	0.35	2.94	0.43	6.22	1.34

No growth of SacB^{+} *A. tumefaciens* was detectable through the OD_{600nm} in the presence of sucrose.

Supporting Table 6: Emerging of sucrose resistant *E. coli* clones during SacB negative selection in liquid cultures when regenerating cells in the presence and absence of sucrose. Exponential growth functions (Equation 9) were fitted to the growth curves of SacB^{+} *E. coli* cultivated in LB medium containing 100 g L⁻¹ sucrose (Figure S3). Cells were regenerated in the presence or absence of sucrose, using the same sucrose concentration as above (100 g L⁻¹).

Parameter	Regeneration in absence of sucrose		Regeneration in the presence of sucrose	
	Value	Error	Value	Error
y_0	-438393	460207	-131376	380362
A_l	3926	4062	1176	828
t_l	1.93	0.24	1.60	0.11
k	0.52	0.06	0.63	0.04
τ	1.34	0.17	1.11	0.08

When sucrose was omitted during regeneration, sucrose-resistant clones emerged after 7.5 ± 4.8 hours (Equation 10). When adding 100 g L⁻¹ sucrose during regeneration, sucrose-resistant clones emerged after 9.1 ± 3.1 hours (Equation 10). The parameters k and τ are derived parameters, where $k = 1/t_l$ and $\tau = t_l \times \ln(2)$. In relation to the axis scale (Figure S3), the y-intercept is reasonably close to zero.

```

1 aatcaggaag g gatggctga gggatatcgg atcgatcctt ttaacccat cacatatacc
61 tgccgttcac tattatttag tgaaatgaga tattatgata ttttctgaat tgtgattaaa
121 aaggcaactt tatgcccatg caacagaaac tataaaaaat acagagaatg aaaagaaaca
181 gatagatttt ttattctttt aggcccgtag tctgcaaate cttttatgat ttttatcaa
241 aaaaagagg aaaatagacc agttgcaatc caaacgagag tctaatagaa tgaggtcgaa
301 aagtaaatcg cgcgggttg ttactgataa agcaggcaag acctaaaatg tgtaaagggc
361 aaagtgtata ctttggcgtc accccttaca tatttaggt cttttttat tgtgcgtaac
421 taacttgcca tcttcaaaca ggagggtcgg aagaagcaga ccgctaacac agtacataaa
481 aaaggagaca tgaacgatga acatcaaaaa gtttgcaaaa caagcaacag tattaacctt
541 tactaccgca ctgctggcag gaggcgcaac tcaagcgttt gcgaaagaaa cgaacaaaaa
601 gccatataag gaaacatacg gcatttccca tattacagc catgatatgc tgcaaatccc
661 tgaacagcaa aaaaatgaaa aatatcaagt tctgagttc gattcgcca caattaaaaa
721 tatctctttt gcaaaaggcc tggacgtttg ggacagctgg ccattacaaa acgctgacgg
781 cactgtcgca aactatcacg gctaccacat cgtctttgca ttagccggag atcctaaaaa
841 tgcggatgac acatcgattt acatgttcta tcaaaaagtc ggcgaaactt ctattgacag
901 ctggaaaaac gctggccgcg tctttaaaga cagcgacaaa ttcgatgcaa atgattctat
961 cctaaaagac caaacacaag aatggtcagg ttcagccaca ttacatctg acggaaaaat
1021 ccgtttatc tacactgatt tctccggtaa acattacggc aaacaaacac tgacaactgc
1081 acaagttaac gtatcagcat cagacagctc ttgaacatc aacggtgtag aggattataa
1141 atcaatcttt gacggtgacg gaaaaacgta tcaaaatgta cagcagttca tcgatgaagg
1201 caactacagc tcaggcgaca accatacgct gagagatcct cactacgtag aagataaagg
1261 ccacaaatac ttagtatttg aagcaaacac tggaaactgaa gatggctacc aaggcgaaga
1321 atctttattt aacaagcat actatggcaa aagcacatca ttctccgctc aagaaagtca
1381 aaaactctg caaagcgata aaaaacgcac ggctgagtta gcaaacggcg ctctcggtat
1441 gattgagcta aacgatgatt acacactgaa aaaagtgatg aaaccgctga ttgcatctaa
1501 cacagtaaca gatgaaattg aacgcgcgaa cgtctttaa atgaacggca aatggtacct
1561 gttcactgac tcccgcggat caaaaatgac gattgacggc attacgtcta acgatattta
1621 catgcttggt tatgtttcta attctttaac tggcccatc aagccgctga acaaaactgg
1681 ccttggttta aaaatggatc ttgaccta c gatgtaacc ttacttact cacacttcgc
1741 tgtacctcaa gcgaaaggaa acaatgtcgt gattacaagc tatatgacaa acagaggatt
1801 ctacgcagac aaacaatcaa cgtttgcgcc aagcttctg ctgaacatca aaggcaagaa
1861 aacatctgtt gtcaaagaca gcatcctga acaaggacaa ttaacagtta acaataaga
1921 tatccaccg atatggccag tgtgc

```

Figure S2: SacB gene cassette for negative selection in *E. coli* and *A. tumefaciens*.

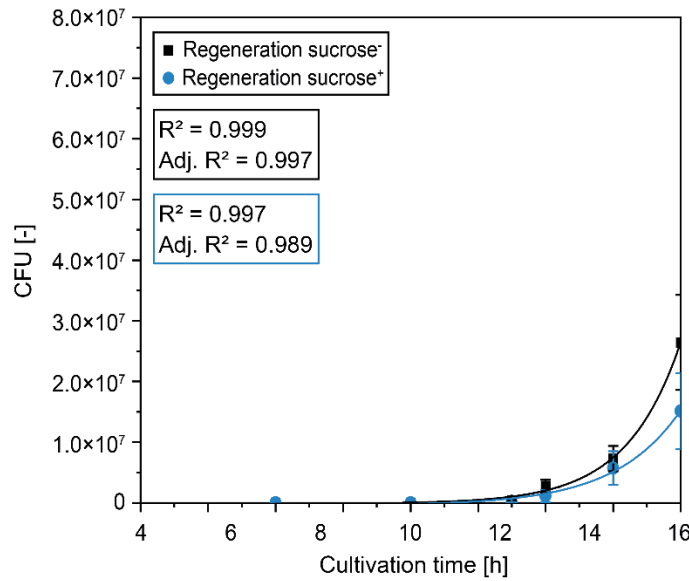


Figure S3: Growth curves of *SacB*⁺ *E. coli* in LB medium supplemented with sucrose depending on the regeneration procedure. A sucrose concentration of 100 g L⁻¹ was used for cultivation and optionally during regeneration. The OD_{600nm} was converted to CFU using a conversion factor of $7.94 \pm 2.00 \times 10^8$ CFU OD_{600nm}⁻¹ [267]. Growth curves were fitted to an exponential growth function (Equation 9, Supporting Table 6) using the software OriginPro.

Uncertainties for the time estimated for the emergence of sucrose-resistant clones during *SacB* negative selection (Figure S3) were calculated by Gaussian error propagation using the following equation.

$$s_F = \sqrt{s_t^2 \ln\left(\frac{y}{A_1} - \frac{y_0}{A_1}\right)^2 + \frac{s_{y_0}^2 t_1^2}{(y - y_0)^2} + \frac{s_{A_1}^2 t_1^2}{A_1^2}} \quad \text{Equation 22}$$

Where s_F is the uncertainty of the time estimated for the emergence of sucrose-resistant clones, y is the number of CFU at a given time of cultivation, y_0 is the y-offset, s_{y_0} is the standard error of the y-offset, A_1 is the amplitude, s_{A_1} is the standard error of the amplitude, t_1 is the growth constant and s_t is the standard error of the growth constant.

VII.9.2 Cloning automation

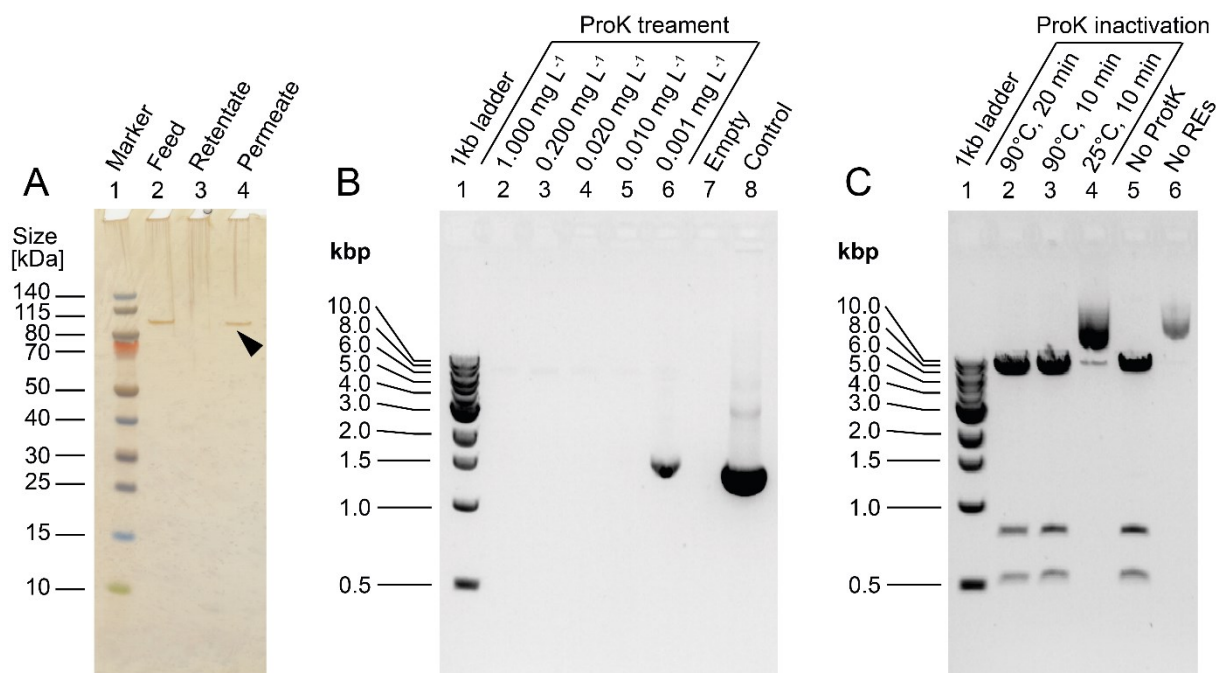


Figure S4: Polymerase inactivation during automated cloning. A. Q5 polymerase in Q5 reaction buffer was subjected to centrifugation with a 100 kDa membrane at $1000 \times g$ for 10 minutes at 22°C (II.2.9.1.1). The ~105 kDa polymerase (black arrow) passed the membrane. B. Polymerase inactivation with proteinase K. Q5 polymerase (in polymerase buffer) was incubated with 0.0001 – 1.000 mg L⁻¹ proteinase K for 20 minutes at 50°C. Residual Q5 polymerase activity was subsequently assessed in a PCR reaction (II.2.9.1.1). C. Inactivation of proteinase K before restriction cloning. Reaction mix containing vector pTRAc_000006 (Supporting Table 2) and proteinase K (in polymerase buffer) was subjected to a 90°C temperature treatment before adding restriction enzymes and CutSmart buffer to investigate residual proteinase activity (II.2.9.1.1). ProK – proteinase K, REs – restriction enzymes.

VII.9.3 Prediction of ideal expression cassettes

Supporting Table 7: Model factors with a significant influence on the accumulation of native IgG3 antibodies and IgG3-IgG1 domain exchange variants in differentiated *N. benthamiana* and *N. tabacum* plants as identified by analysis of variance (ANOVA). IgG3 accumulation levels were investigated in a 122-run historical response surface design (Figure 8A – D, Figure S5).

IgG3 accumulation in <i>N. benthamiana</i>			IgG3 accumulation in <i>N. tabacum</i>		
Source	F-value	p-value	Source	F-value	p-value
Model	27.13	< 0.0001	Model	7.81	< 0.0001
A (UTR)	5.44	0.0056	n.s.	n.s.	n.s.
B (cell compartment)	81.20	< 0.0001	B (cell compartment)	10.04	< 0.0001
C (antibody scaffold)	22.05	< 0.0001	C (antibody scaffold)	20.95	< 0.0001
BC	9.42	< 0.0001	BC	4.03	0.0004
Lack of fit	1.56	0.0883	Lack of fit	1.57	0.0862
Coefficients of determination	R ²	0.8052	Coefficients of determination	R ²	0.5514
	Adjusted R ²	0.7755		Adjusted R ²	0.4808
	Predicted R ²	0.7532		Predicted R ²	0.4345

Factors with a non-significant influence on the response ($p > 0.05$) were removed from the models. The values of R² and adjusted R² were in reasonable agreement (i.e. the differences were < 0.2). The low coefficients of determination observed for the *N. tabacum* model compared to the *N. benthamiana* model can be attributed to variation of the infiltrated leaf area (III.2.3.4). n.s. – the effect of the factor was not significant.

Supporting Table 8: Regression coefficients of models predicting the accumulation of native IgG3 antibodies and IgG3-IgG1 domain exchange variants *N. benthamiana* and *N. tabacum* plants. The regression coefficients describe the change of the response per unit change of an influence factor (Figure 8A – D, Figure S5, Supporting Table 7).

IgG3 accumulation in <i>N. benthamiana</i>			IgG3 accumulation in <i>N. tabacum</i>		
Factor	Term	Coefficient estimate	Factor	Term	Coefficient estimate
	Grand average (intercept)	25.24		Grand average (intercept)	10.82
5' UTR	CHS (A1)	-2.90	5' UTR	CHS (A1)	n.s.
	omega (A2)	3.31		omega (A2)	n.s.
	TL (A3)	-0.41*		TL (A3)	n.s.
Compartment	Apoplast (B1)	6.14	Compartment	Apoplast (B1)	8.98
	ER double LPH signal (B2)	17.82		ER double LPH signal (B2)	-2.50
	ER single LPH signal (B3)	6.88		ER single LPH signal (B3)	5.46
	Vacuole (B4)	-13.42		Vacuole (B4)	-2.34
	Plastid (B5)	-17.40*		Plastid (B5)	-9.60*
Antibody scaffold	Native IgG3 (C1)	-7.12	Antibody scaffold	Native IgG3 (C1)	
	IgG3 with IgG1 CH3 domain (C2)	0.74		IgG3 with IgG1 CH3 domain (C2)	-6.93
	IgG3 with IgG1 CH3/2 domain (C3)	6.38*		IgG3 with IgG1 CH3/2 domain (C3)	-0.63
Interaction of scaffold and compartment	B1 C1	-11.81	Interaction of scaffold and compartment	B1 C1	-8.10
	B2 C1	3.57		B2 C1	5.49
	B3 C1	1.21		B3 C1	-2.21
	B4 C1	5.14		B4 C1	-0.97
	B1 C2	-6.98		B1 C2	-5.34
	B2 C2	-8.52		B2 C2	0.54
	B3 C2	17.61		B3 C2	0.85
	B4 C2	-0.22		B4 C2	3.02

Asterisks indicate coefficients that were calculated manually, i.e. as the grand average across all factor levels (intercept) minus the difference between the grand average and the average at each level. The 5' UTR did not have a significant influence on IgG3 accumulation in *N. tabacum*, hence no regression coefficients are available for this expression system. n.s. – the effect of the factor was not significant.

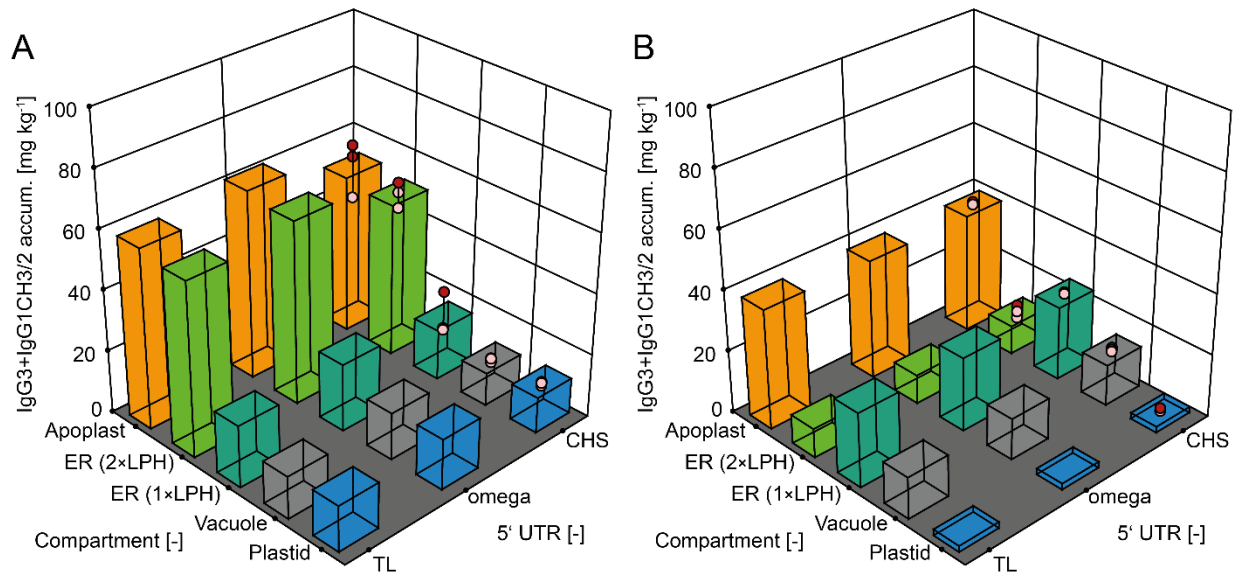


Figure S5: Models predicting the accumulation of IgG3 domain exchange variants in differentiated plants depending on the 5' UTR and expression compartment. A. Accumulation levels of IgG3 antibodies containing the CH2 and CH3 regions of the IgG1 antibody M12 (Figure S1) in *N. benthamiana* (Supporting Table 7). B. Accumulation levels of the same antibodies as in (A) in *N. tabacum* (Supporting Table 7). Whole plants were extracted 5 days after infiltration with *A. tumefaciens* (II.4.2.2) using a 3 v m⁻¹ ratio of extraction buffer (VII.6). The concentration of IgG3 antibodies in plant extracts was quantified by SPR (II.6.3.2).

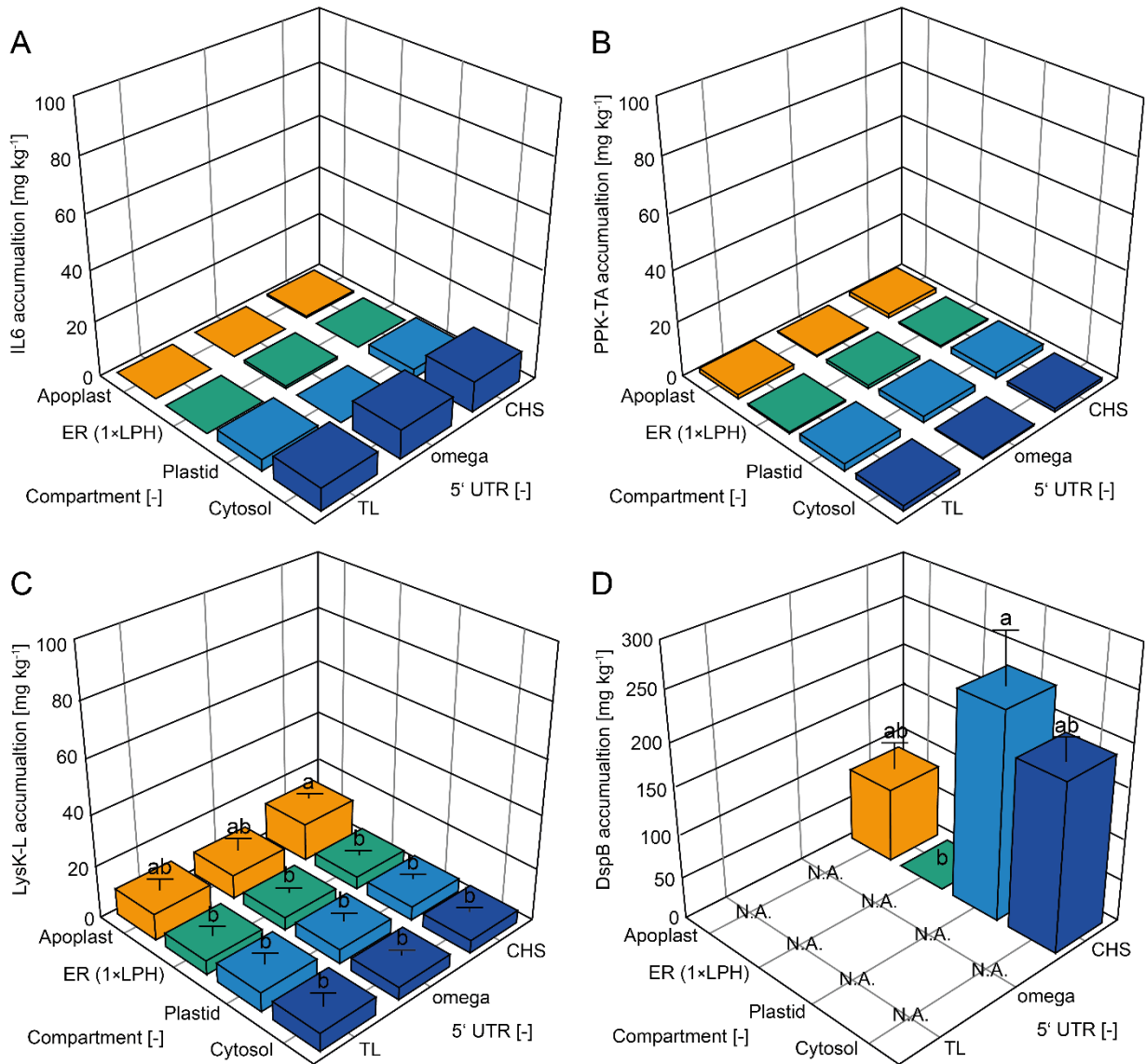


Figure S6: Accumulation of IL6, PPK-TA, LysK-L and DspB in BY-2 PCPs depending on the target compartment and 5' UTR. A. Accumulation of IL6 in BY-2 PCPs. B. Accumulation of PPK-TA in BY-2 PCPs. C. Accumulation of LysK-L in BY-2 PCPs. D. Accumulation of DspB in BY-2 PCPs. BY-2 cells were harvested from shake flasks after 168 hours of cultivation using sucrose (30 g L⁻¹) as a carbon source. PCPs were incubated for 72 hours after infiltration with *A. tumefaciens* (II.4.1.4) and extracted with a 3 v m⁻¹ ratio of extraction buffer (VII.6). Target proteins were quantified with a dot blot assay (II.6.5). If available, error bars represent the standard deviation from n = 3 PCPs. Conditions that share the same letter were not significant different (p > 0.05).

VII.9.4 Effect of intrinsic protein properties on accumulation

Supporting Table 9: Correlation between the protein instability index and recombinant accumulation levels in BY-2 PCPs. Data correspond to error weighted (Equation 18) linear fits (Figure S7A, C).

Protein subset	Sample n	Pearson's r	Adjusted R ²
IgG expression in the ER (single LPH)	4	-0.943	0.836
IgG expression in the ER (double LPH)	4	-0.989	0.966
IgG expression in the apoplast	4	-0.611	0.373
IgG expression in the vacuole	4	-0.949	0.852
IL6/8 expression in the cytosol ^a	2	-1.0	n.a.
IL6/8 expression in the apoplast ^a	2	-1.0	n.a.
IL6/8 expression in plastids ^a	2	-1.0	n.a.
IL6/8 expression in the ER ^a	2	-1.0	n.a.
PPK-RO/TA expression in the cytosol ^a	2	-1.0	n.a.
PPK-RO/TA expression in the apoplast ^a	2	-1.0	n.a.
PPK-RO/TA expression in plastids ^a	2	-1.0	n.a.
PPK-RO/TA expression in the ER ^a	2	1.0 ^c	n.a.
All target proteins ^b (pI 5.5 - 8.5)	6	-0.809	0.611
All target proteins ^b (pI < 5.5 or > 8.5)	4	-0.974	0.943

^a Only two interleukins (IL6 and IL8) and PPKs (PPK-RO, PPK-TA) were available for comparison.

^b Combined data from all proteins expressed in this work, namely PPK-RO, PPK-TA, IL6, IL8, DspB, IgG1, IgG3 (native and IgG1 domain exchange variants) and LysK-L. ^c PPK accumulation levels in the ER were close to the detection limit. n.a. – not available.

Supporting Table 10: Correlation between the protein aliphatic index and recombinant accumulation levels in BY-2 PCPs. Data correspond to error weighted (Equation 18) linear fits (Figure S7B, D).

Protein subset	Sample n	Pearson's r	Adjusted R ²
IgG expression in the ER (single LPH)	4	0.948	0.848
IgG expression in the ER (double LPH)	4	0.975	0.925
IgG expression in the apoplast	4	0.807	0.477
IgG expression in the vacuole	4	0.970	0.911
IL6/8 expression in the cytosol ^a	2	1.0	n.a.
IL6/8 expression in the apoplast ^a	2	1.0	n.a.
IL6/8 expression in plastids ^a	2	1.0	n.a.
IL6/8 expression in the ER ^a	2	1.0	n.a.
PPK-RO/TA expression in the cytosol ^a	2	1.0	n.a.
PPK-RO/TA expression in the apoplast ^a	2	1.0	n.a.
PPK-RO/TA expression in plastids ^a	2	1.0	n.a.
PPK-RO/TA expression in the ER ^a	2	-1.0 ^b	n.a.

^a Only two interleukins (IL6, IL8) and PPKs (PPK-RO, PPK-TA) were available for comparison.

^b PPK accumulation levels in the ER were close to the detection limit. n.a. – not available.

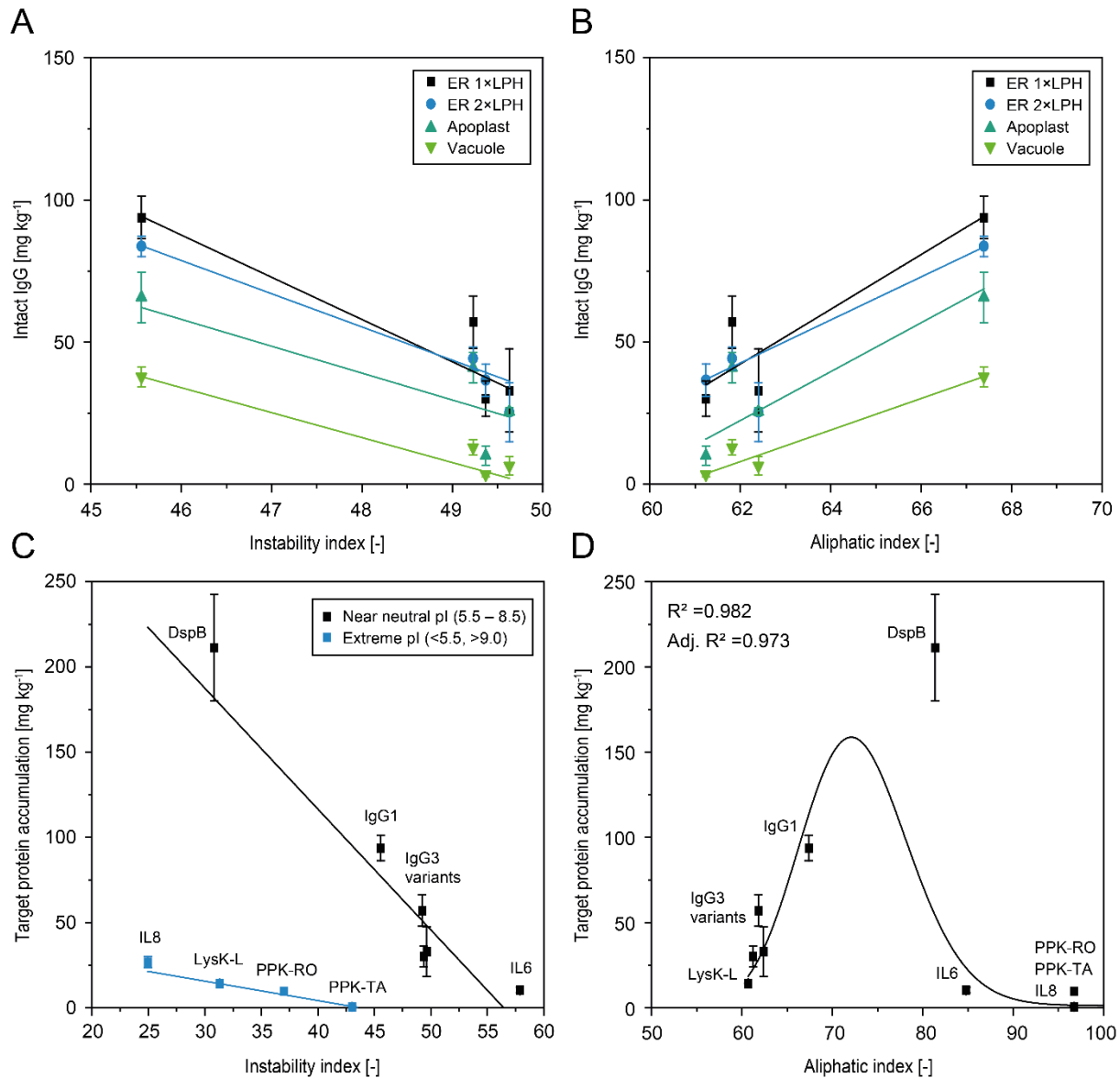


Figure S7: Correlation of transient protein accumulation levels with intrinsic protein properties.

A, C. The instability index was used as a measure for the *in vivo* half-life time of a protein. B, C. The aliphatic index was used as a measure for the thermal stability and flexibility of a protein (both are inversely related). Accumulation levels correspond to the optimal cell compartment for each model protein produced in BY-2 PCPs. A lognormal model was used to describe the preliminary relationship between the aliphatic index and recombinant protein accumulation levels (Equation 19).

VII.9.5 Origin of variability in BY-2 PCPs

Supporting Table 11: Comparison of intra and inter-batch variability during transient expression in BY-2 PCPs. Variability was calculated as the coefficient of variation of DsRed accumulation across all targeted compartments (cytosol, apoplast, plastids, ER). PCPs were cast from BY-2 cells cultivated in shake flasks (II.4.1.1) and stirred tank bioreactors (II.4.1.2) using sucrose or glucose as carbon source.

CV	Stirred-tank sucrose		Shake flasks sucrose		Shake flasks glucose	
Compartment	Intra-batch	Inter-batch	Intra-batch	Inter-batch	Intra-batch	Inter-batch
Average	21.6	85.1	14.4	54.2	9.9	31.4
SD	6.7	12.8	3.7	27.1	2.5	20.2

Data represent the average coefficient of variation calculated from $n = 3 - 7$ PCPs within each of 11 – 15 BY-2 batches (intra-batch variation) or the coefficients of variation (inter-batch variation) across 11 – 15 separate BY-2 batches. CV – coefficient of variation, SD – standard deviation.

Supporting Table 12: Model factors with a significant influence on DsRed accumulation in BY-2 PCPs as identified by analysis of variance (ANOVA). DsRed accumulation levels were investigated using a D-optimal response surface design with 92 runs, conducted in two blocks (Figure 11A).

Source	F-value	p-value
Model	424.73	< 0.0001
A (PCP incubation time)	2604.47	< 0.0001
B (BY-2 cell cultivation time)	54.03	< 0.0001
C (targeted sub-cellular compartment)	1317.86	< 0.0001
AB	19.26	< 0.0001
AC	18.14	< 0.0001
BC	157.02	< 0.0001
A ²	300.01	< 0.0001
B ²	130.14	< 0.0001
A ² B	32.55	< 0.0001
B ² C	8.57	< 0.0001
	R ²	0.9907
Coefficients of determination	Adjusted R ²	0.9883
	Predicted R ²	0.9807

Factors with a non-significant influence on the responses ($p > 0.05$) were removed from the model. With a difference < 0.2, the values of R², the adjusted R² and the predicted R² were in good agreement.

Supporting Table 13: Effect of the medium osmolality on BY-2 productivity. A lognormal model (Equation 19) used to describe the effect of the medium osmolality on BY-2 productivity (Figure 12B).

	Sucrose pH 5.6		Sucrose pH 7.5		Glucose pH 5.6	
Parameter	Value	Error	Value	Error	Value	Error
y_0	3.71	3.10	0.33	0.90	9.63	16.30
xc	143.63	2.20	141.15	2.18	185.39	10.7
w	0.09	0.01	0.13	0.02	0.22	0.06
A	5726.00	1150.85	4379.83	709.23	23509.47	10247.17

Supporting Table 14: Model factors with a significant influence on the productivity and cell wet mass of BY-2 PCPs as identified by analysis of variance (ANOVA). BY-2 growth and productivity were investigated in a D-optimal combined response surface-mixture design with 144 runs (Figure 13).

TSP-normalized DsRed accumulation			BY-2 cell wet mass		
Source	F-value	p-value	Source	F-value	p-value
Model	22.27	< 0.0001	Model	78.59	< 0.0001
Linear mixture	30.26	< 0.0001	Linear mixture	142.37	< 0.0001
AF	39.36	< 0.0001	AF	43.53	< 0.0001
AG	7.99	< 0.0001	n.s.	n.s.	n.s.
BF	16.68	< 0.0001	BF	57.92	< 0.0001
BG	22.54	< 0.0001	n.s.	n.s.	n.s.
CF	11.89	0.0008	CF	41.55	< 0.0001
CG	20.44	< 0.0001	n.s.	n.s.	n.s.
DF	6.53	0.0119	DF	34.88	< 0.0001
DG	21.2	< 0.0001	n.s.	n.s.	n.s.
EG	3.39	0.0203	EF	7.77	0.0061
BF ²	18.11	< 0.0001	CF ²	20.81	< 0.0001
DF ²	30.57	< 0.0001	n.s.	n.s.	n.s.
Coefficients of determination	R ²	0.8252	Coefficients of determination	R ²	0.8553
	Adjusted R ²	0.7881		Adjusted R ²	0.8444
	Predicted R ²	0.7338		Predicted R ²	0.8399

The sum of all light components in the mixture design corresponds to 100% (40 $\mu\text{mol m}^{-2} \text{s}^{-1}$). A – blue light, B – green light, C – red light, D – far-red light, E – light intensity, F – incubation time, G – target compartment, n.s. – not significant ($p > 0.05$).

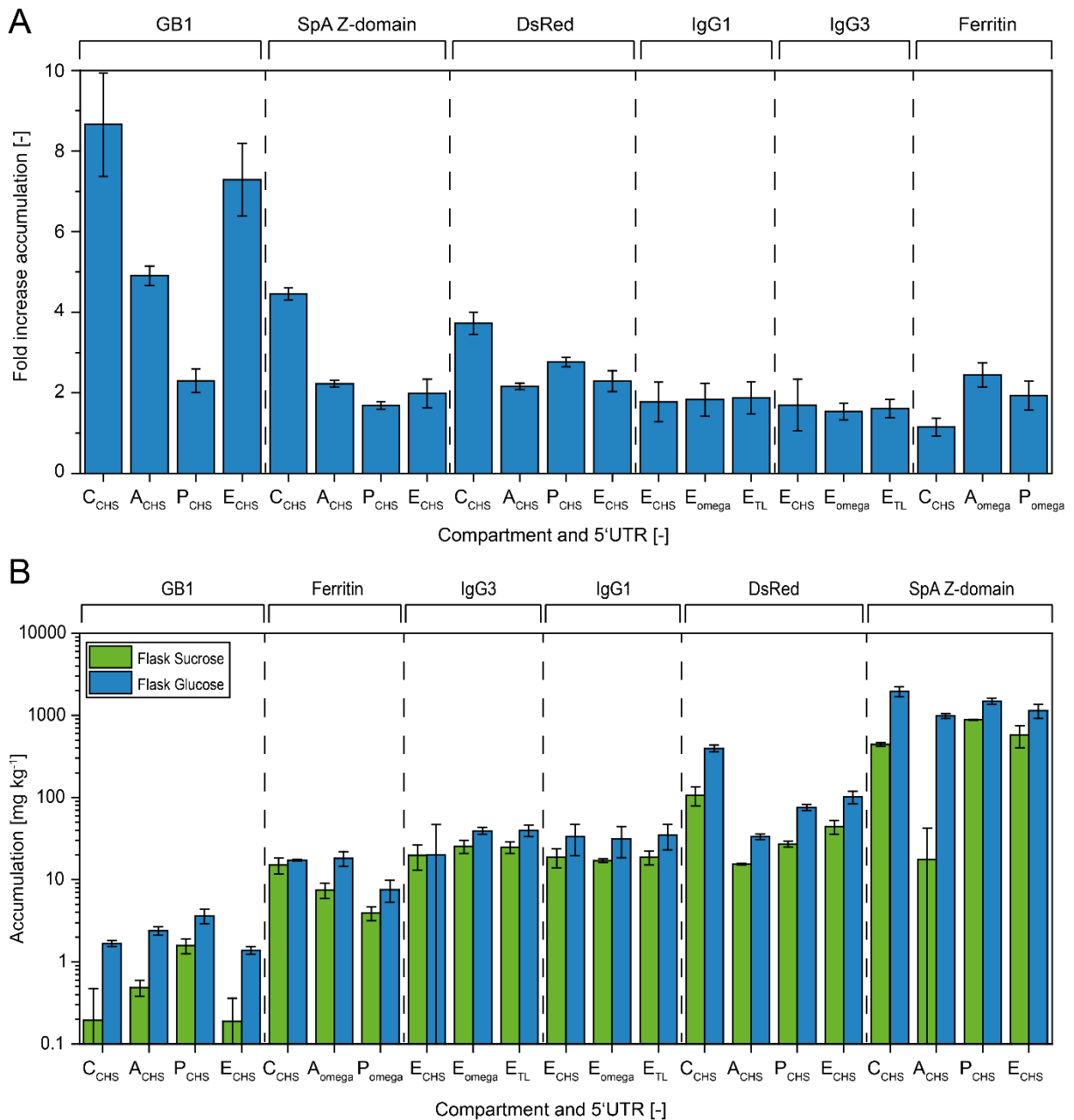


Figure S8: Productivity of BY-2 PCPs after infiltration with *A. tumefaciens* depending on the carbon source used for BY-2 cultivation. A. Increase in the accumulation of GB1, human ferritin (heavy chain), IgG1/3 antibodies, DsRed and SpA in BY-2 PCPs when replacing sucrose (30 g L⁻¹) with glucose (30 g L⁻¹) as carbon source for BY-2 cultivation. B. Absolute accumulation levels of the same target proteins in PCPs cast from BY-2s cultivated on sucrose or glucose. Accumulation levels of GB1, ferritin and SpA were quantified by dot blot (II.6.5), DsRed was quantified by fluorescence spectroscopy (II.6.2.1) and IgG1/3 antibodies were quantified by SPR (II.6.3.2). BY-2 cells were harvested after 168 hours and PCPs were incubated for 72 hours post infiltration. Error bars represent the standard deviation from n = 3 – 7 PCPs. Abbreviations refer to different subcellular compartments and subscript letters indicate the 5' UTR. C – cytosol, A – apoplast, P – plastids, E – endoplasmic reticulum, CHS – *Petroselinum hortense* chalcone synthase, omega – *tobacco mosaic virus* omega prime sequence, TL – *tobacco etch virus* leader sequence.

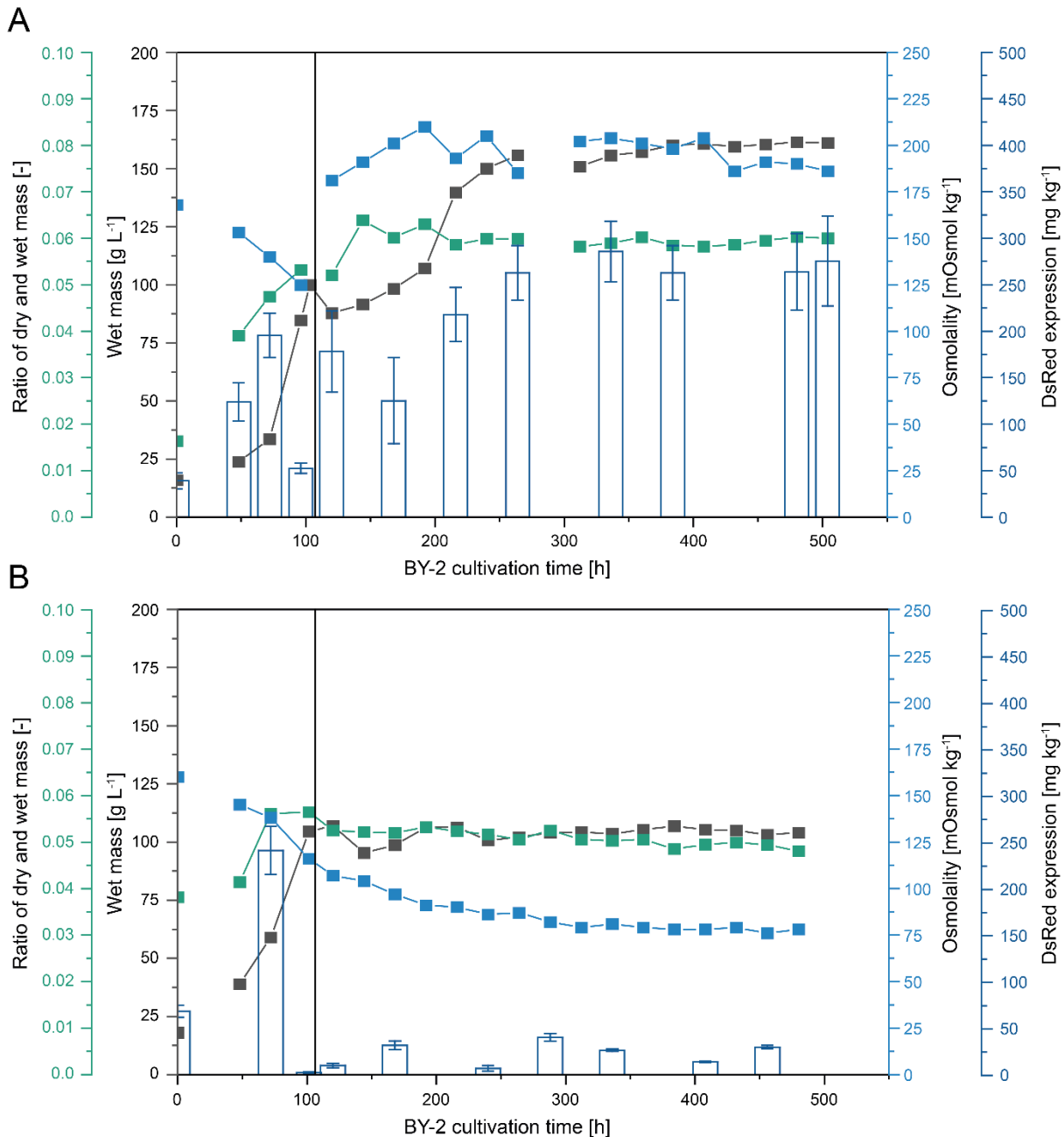


Figure S9: Effect of different feed compositions on the productivity of BY-2 PCs cultivated in 5 L stirred tanks. A. Fed-batch cultivation of BY-2 cells in a 5 L stirred tank (II.4.1.2) using twofold concentrated MS medium (VII.7) with 40 g L⁻¹ sucrose as feed. B. Fed-batch BY-2 cultivation in a 5 L stirred tank (II.4.1.2) using regular MS medium (VII.7) with 20 g L⁻¹ sucrose as feed. In all cultivations 30 g L⁻¹ sucrose was used as carbon source in the batch phase. A vertical black line denotes the end of the batch phase. During the fed-batch phase the BY-2 cell concentration was maintained at ~100 g L⁻¹ when feeding regular medium (B) and at ~150 g L⁻¹ when feeding twofold concentrated medium (A) using an RFIS probe (II.4.1.2). RFIS measures the volume of cells with an intact membrane and has been shown to correlate well with off-line parameters such as packed cell volume, wet cell mass and dry cell mass [224]. PCs were incubated for 72 hours after infiltration with *A. tumefaciens* and extracted with 3 v m⁻¹ extraction buffer (VII.6). The concentration of DsRed in PCP extracts was quantified by fluorescence spectroscopy (II.6.2.1). The osmolality of the cultivation supernatant was measured by freezing point osmometry (II.4.1.3). Error bars denote the standard deviation from n = 4 – 8 PCs.

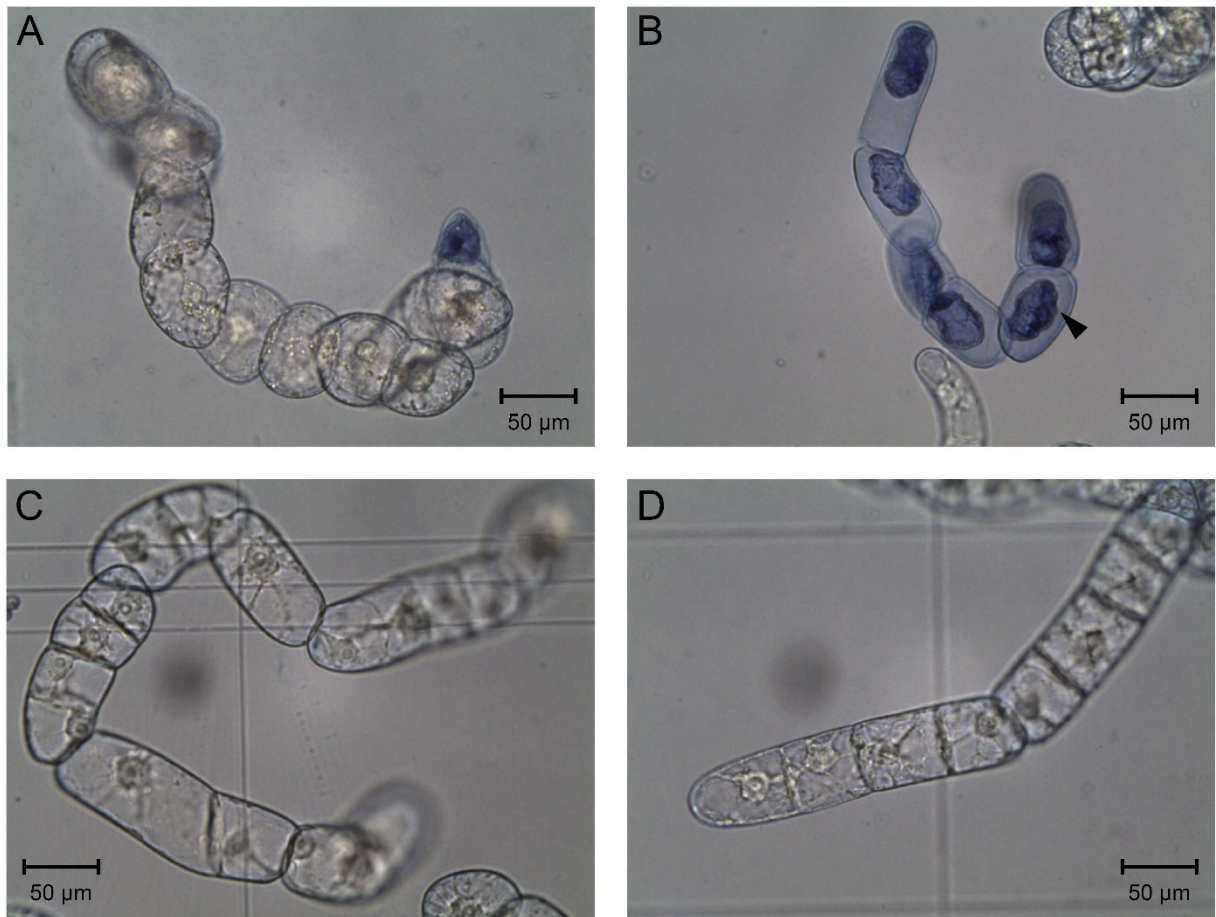


Figure S10: BY-2 cell morphology depending on the medium osmolality during cultivation in 5 L stirred tanks. A. Representative microscope picture of BY-2 cells after 7 days of batch cultivation in a stirred tank (II.4.1.2) with MS medium (VII.7) containing 30 g L^{-1} sucrose, corresponding to a medium osmolality of $56 \text{ mOsmol kg}^{-1}$. B. Detection of damaged cells in the same sample as in (A) using Evans blue staining (II.4.1.3). Cells with a damaged cell membrane appear blue (black arrows), while intact cells exclude the dye. C. Representative microscope picture of BY-2 cells after 7 days fed-batch cultivation using MS medium with 20 g L^{-1} sucrose as feed (VII.7), corresponding to a medium osmolality of $100 \text{ mOsmol kg}^{-1}$. D. Representative microscope picture of BY-2 cells after 14 days fed-batch cultivation using twofold concentrated MS medium with 40 g L^{-1} sucrose as feed (VII.7), corresponding to a medium osmolality of $190 \text{ mOsmol kg}^{-1}$. BY-2 cells exhibited a bloated morphology when the medium osmolality was $\leq 100 \text{ mOsmol kg}^{-1}$. Pictures were recorded with a trinocular microscope equipped with a $40 \times$ objective and a $10 \times$ eye piece (II.4.1.3).

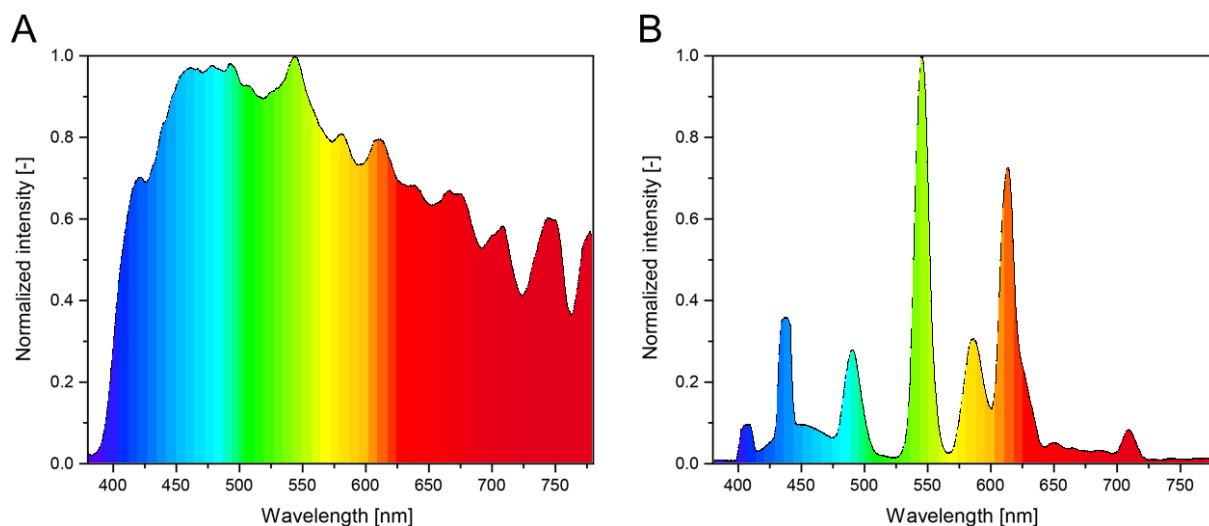


Figure S11: Light spectra recorded during cultivation of BY-2 cells in a 5.0-L glass stirred tank under two forms of illumination. A. Light spectrum measured under uncontrolled ambient conditions next to a window. B. Light spectrum measured under controlled conditions in a windowless room illuminated by artificial white light (Osram Lumilux Cool White, HO 49W/840). Light spectra were recorded with an UPRtek MK350S handheld spectrometer. Both settings correspond to a total photosynthetic photon flux density (PPFD) of $\sim 11 \mu\text{mol m}^{-2} \text{s}^{-1}$.

VII.9.6 Origin of variability in differentiated plants

Supporting Table 15: Effect of the plant morphology on the productivity during transient protein expression in *N. benthamiana*. A lognormal model (Equation 19) was used to describe the relationship of the plant biomass and the accumulation of IgG3 antibodies (Figure 15A).

Parameter	Value	Standard error
y_0	12.06	3.03
xc	90.27	12.03
w	0.46	0.11
A	2455.38	458.70

Supporting Table 16: Effect of the plant morphology on the productivity during transient protein expression in *N. tabacum*. An allometric model (Equation 21) was used to describe the effect of the plant morphology on the productivity during transient protein expression in *N. tabacum* (Figure 15B).

Parameter	Value	Standard error
a	28870.82	33484.36
b	-1.66	0.27

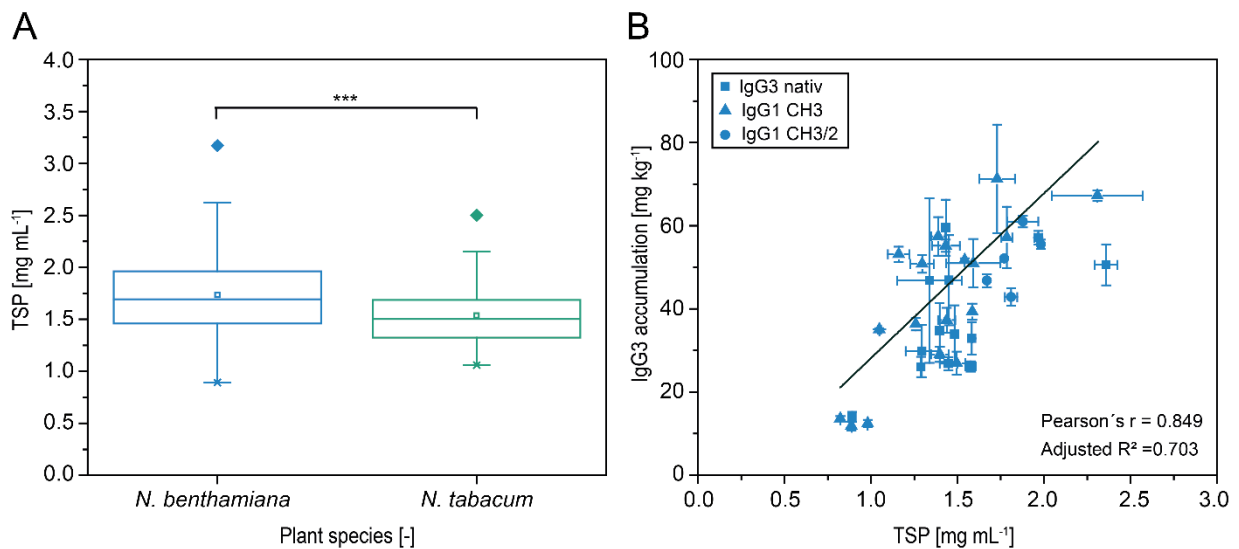


Figure S12: Comparison of TSP concentrations in extracts of *N. benthamiana* and *N. tabacum* plants and correlation of TSP and productivity. A. Concentration of TSP in extracts of 7 weeks old *N. benthamiana* and *N. tabacum* plants. The concentration of TSP in plant extracts was determined using the Bradford method (II.6.1). Error bars represent the standard deviation from $n = 84$ plants (* $p < 0.05$, ** $p < 0.01$, *** $p < 0.001$). B. Correlation of TSP and productivity during transient expression of IgG3 antibodies in 7 weeks old *N. benthamiana* plants. IgG3 concentrations were determined by SPR (II.6.3.2). B. Error bars represent the standard deviation from $n = 3$ plants. All plants were harvested 5 dpi and entire plants (including the stem) were extracted, using a 3 v m⁻¹ ratio of extraction buffer (VII.6).

VII.9.7 Isotope labeling in BY-2 PCPs

Supporting Table 17: Production and purification of isotope labeled GB1 in BY-2 PCPs. BY-2 cells were cultivated in MS medium containing 30 g L⁻¹ glucose and optionally 50% (v v⁻¹) deuterium oxide (medium D, VII.7), ¹⁵N-labelled ammonium nitrate (medium N, VII.7) or both isotopes (medium DN, VII.7). MS medium without isotopes was used as control (medium H, VII.7).

BY-2 cultivation medium					
Component	Unit	H	D	N	DN
Cell count at harvest	[10 ⁹ L ⁻¹]	2.38 ± 0.13	0.95 ± 0.26	2.05	1.12 ± 0.02
Cell viability at harvest ^a	[-]	0.97 ± 0.01	0.82 ± 0.06	0.97 ± 0.01	0.80 ± 0.04
BY-2 cell wet mass at harvest ^b	[g L ⁻¹]	244 ± 41	83 ± 11	286 ± 16	227 ± 60
BY-2 cell dry mass at harvest	[g L ⁻¹]	53	6	47	45
GB1 accumulation in PCPs ^c	[mg kg ⁻¹ wet cell biomass]	2.7 ± 2.8	56.4 ± 39.7	8.8 ± 6.6	23.8 ± 15.3
Theoretical volumetric GB1 yield ^d	[mg L ⁻¹]	0.66 ± 0.68	4.67 ± 3.29	2.51 ± 1.87	5.42 ± 3.48
Volume of BY-2 PCP extract used for IMAC	[mL]	10	5	15	15
GB1 purity after IMAC (densitometric evaluation) ^e	[% peak area of stained bands]	69	95	87	80
GB1 recovery after IMAC ^f	[% initial]	101	81	91	41

^a cell vitality was assessed after adapting BY-2 cells to deuterium oxide (50% v v⁻¹) for 30 days, using a passaging time of 7 – 11 days. ^b data correspond to n = 2 cultivations. ^c quantification by dot blot (II.6.5) using authentic His-tagged GB1 as standard. ^d values represent the theoretical yield in a stirred tank based on accumulation levels in PCPs. ^e GB1 purity after IMAC was estimated based on the densitometric evaluation of Coomassie-stained LDS gels (II.6.4.1) using the software AIDA Image Analyzer 5.0. ^f GB1 recoveries were estimated based on the densitometric evaluation of dot blots using standards with a known concentration and the software ImageJ [232]. Data values with variance indicate standard deviation. H – medium without isotopes, D – medium prepared with 50% (v v⁻¹) deuterium oxide, N – medium prepared with labeled ammonium nitrate, DN – medium prepared with 50% (v v⁻¹) deuterium oxide and labeled ammonium nitrate.

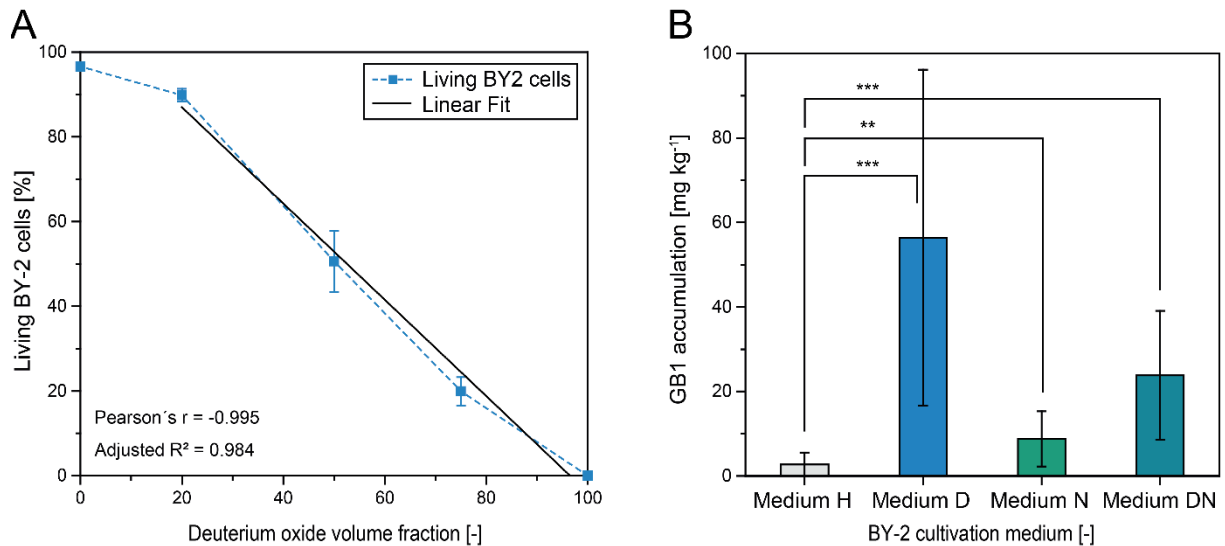


Figure S13: Effect of deuterium oxide on the vitality of BY-2 cell and expression of the model protein GB1 in BY-2 cells cultivated in the presence of isotopes. A. Correlation of the deuterium oxide volume fraction and BY-2 cell vitality prior adaption to deuterium oxide. Data correspond to BY-2 cells that have not been adapted to deuterium oxide. When excluding a control without deuterium, the BY-2 vitality correlated linearly with the deuterium oxide volume fraction. Error bars represent the standard deviation from $n = 2 - 3$ cultivations. B. Accumulation of GB1 in PCPs cast from BY-2 cells cultivated in media with isotopes (D, N, DN) and without (H) isotopes as estimated by dot blot (II.6.5) using His-tagged GB1 as a standard and a rabbit anti-His₆ and AP-labeled goat anti-rabbit antibodies. The carbon source for BY-2 cultivation was glucose (30 g L⁻¹) in all experiments. Error bars represent the standard deviation from $n = 12 - 14$ PCPs (*** $p < 0.0001$; ** $p < 0.01$). H – medium without isotopes, D – medium prepared with 50% (v v⁻¹) deuterium oxide, N – medium prepared with labeled ammonium nitrate, DN – medium prepared with 50% (v v⁻¹) deuterium oxide and labeled ammonium nitrate.

VII.9.8 Target protein purification

Supporting Table 18: Overview of chromatography columns used target protein purification.

Column type	Resin	Diameter [cm]	Bed height [cm]	Volume [mL]
OPUS RoboColumn	Chelating Sepharose FF	0.5	1.0	0.2
HiTrap	Chelating Sepharose FF	0.7	2.5	1.0
HiTrap	Protein G HP	0.7	2.5	1.0
XK2620	Chelating Sepharose FF	2.6	9.4	50.0

Supporting Table 19: Overview of HCPs that co-purified during IMAC. HCPs that co-purified with His-tagged PPKs during IMAC (Figure 18) were analyzed by mass spectrometry.

Protein [-]	Monomer size [kDa]	Oligomerization state [-]
Serine hydroxymethyltransferase (Uniprot ID A0A1J6HU64)	57.1	Tetramer
Glutamine synthetase (Uniprot ID Q69B32)	47.5	Homo-decamer
Xyloglucan endotransglucosylase_hydrolase (Uniprot ID O80431)	33.9	Monomer
Major latex protein (no Uniprot ID available)	16.5	n.a.

Bands corresponding to *Nicotiana* HCPs were cut out from Coomassie-stained LDS gels (**Figure 18**) and analyzed by tandem mass spectrometry with an AmaZon ETD MS ion trap spectrometer (Bruker). HCPs were identified by peptide mass fingerprinting using the software Mascot (Matrix Science, Boston, USA) and the SwissProt and Sol Genomics Network databases. Mass spectrometry was conducted by Michael Kupper (Fraunhofer IME, Aachen, Germany). The oligomerization state of HCPs was predicted based on homology models build with SWISS-MODEL [406, 407]. n.a. – not available.

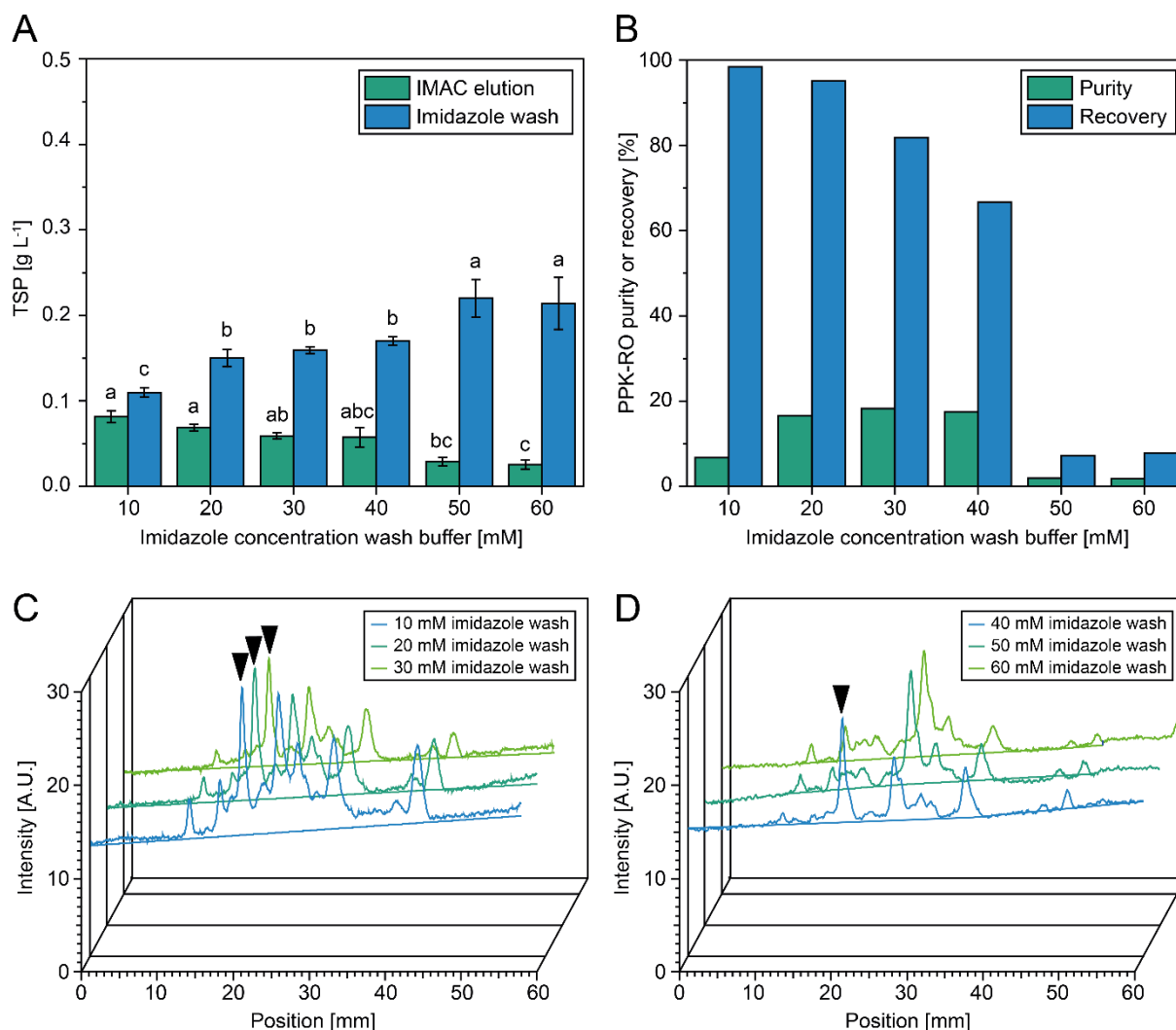


Figure S14: High-throughput chromatography screening. A, B. Analysis of IMAC wash and elution fractions from purification of PPK-RO on a liquid handling platform (Figure 18). C, D. Densitograms of IMAC elution fractions from the same experiment (Figure 18). Chromatography was performed with pre-packed Chelating Sepharose FF columns (0.2 mL column volume) on a Janus G3 liquid handling station, using 2 mL clarified *N. benthamiana* extract (II.5.3) as feed and 500 μ L buffer for washing (no imidazole, VII.6), removal of HCPs (10 – 60 mM imidazole, VII.6) and elution (300 mM imidazole, VII.6). The contact time was 2 minutes during all steps. The concentration of TSP in IMAC fractions was determined using the Bradford assay (II.6.1). PPK purities and recoveries were estimated by densitometry analysis of Coomassie-stained LDS gels (Figure 18) using the software AIDA 5.0. Black arrows in (C, D) denote the target protein peak. Error bars denote the standard deviation from $n = 3$ technical replicates.

VII.9.9 SPR quantification of His-tagged target proteins

Supporting Table 20: Assay specificity depending on the peptide design, buffer and flow rate. Peptides featured a His₆-tag and different spacers to improve accessibility of the tag and minimize non-specific binding [408]. Peptides were immobilized at similar molar concentrations (500 μ M) using an immobilization pH of 4.5 for peptide P1 and pH 4.0 for P2 and P3 (III.4.1.1). Clarified extracts of wildtype *N. benthamiana* plants (II.5.3) were diluted 1:20 in the respective buffer to investigate non-specific binding. The pH was 7.4 for all buffers. MonoRab anti-His antibody was used as ligand at a concentration of 10 nM.

Immobilized peptide [-]	Total binding [RU]	Unspecific binding [RU]	Specific binding [RU]	Ratio specific / unspecific binding
HBS-EP, flow rate 20 μ L min ⁻¹				
P1	430.96	275.86	155.10	0.56
P2	273.47	252.45	21.02	0.08
P3	244.39	235.67	8.72	0.04
PBS-T, flow rate 20 μ L min ⁻¹				
P1	334.08	143.07	191.01	1.34
P2	149.09	132.30	16.79	0.13
P3	155.20	144.59	10.61	0.07
PBS-T, flow rate 10 μ L min ⁻¹				
P1	339.57	133.04	206.53	1.55
P2	156.82	122.55	34.27	0.28
P3	147.17	127.42	19.75	0.15

P1 amino acid sequence – Ala₃His₆ (1.05 kDa), P2 amino acid sequence – (Leu-His-Asp)₂His₆ (1.57 kDa), P3 amino acid sequence – (Leu-His-Asp)₄His₆ (2.30 kDa).

Supporting Table 21: Experimentally derived dissociation rates (k_d) of commercial anti-His antibodies tested for the binding inhibition SPR assay.

Antibody	Experimental k_d [s ⁻¹]	Literature k_d [s ⁻¹]
THE His-tag antibody (GenScript)	$8.74 \times 10^{-5} \pm 9.22 \times 10^{-7}$	n.a.
MonoRab anti-His antibody (GenScript)	$1.22 \times 10^{-4} \pm 1.03 \times 10^{-6}$	n.a.
Anti-His ₆ antibody (Dianova)	$3.14 \times 10^{-3} \pm 7.07 \times 10^{-5}$	$9.70 \times 10^{-3} \pm 7.03 \times 10^{-3}$ [409]

The dissociation rate k_d was derived from three measurements with each antibody (Figure 21B). The normalized change in the response signal over time (Figure S15C) showed that the dissociation rate was independent of the amount of antibody captured on the chip surface. The signal decrease was > 5% compared to the initial response in all measurements, thus allowing a reliable estimation of the dissociation rate [390]. Data were recorded on a Sierra SPR4. n.a. – not available.

Supporting Table 22: Fitting of experimental binding inhibition data to different stoichiometries. Experimental binding inhibition data measured with 20 nM MonoRab anti-His antibody (Supporting Table 21) and 0.4 – 100.0 nM peptide P1 (Supporting Table 20) were fit to a 1:1 interaction model (Equation 23) or a 2:1 interaction model (Equation 24).

Parameter	1:1 interaction model		2:1 interaction model	
	Value	Standard error	Value	Standard error
P	20 (constant)	n.a.	20 (constant)	n.a.
K_D	1.76	1.00×10^{-3}	1.30	7.57×10^{-4}
Adj. R^2	0.998		0.883	

Data were fitted with OriginPro, using the total concentration of tagged peptide as independent variable, the concentration of free antibody as dependent variable and K_D and the total concentration of antibody, A_{total} (constant, 20 nM), as fitting parameters. n.a. – not available.

Supporting Table 23: Fitting of binding inhibition SPR assays. A Boltzmann fit (Equation 4) was used to describe binding inhibition SPR assays (Figure 21C).

Parameter	Value	Standard error
A_1	-35.57	13.12
A_2	97.86	0.12
x_0 (IC_{50})	10.34	2.73
dx	9.90	0.98

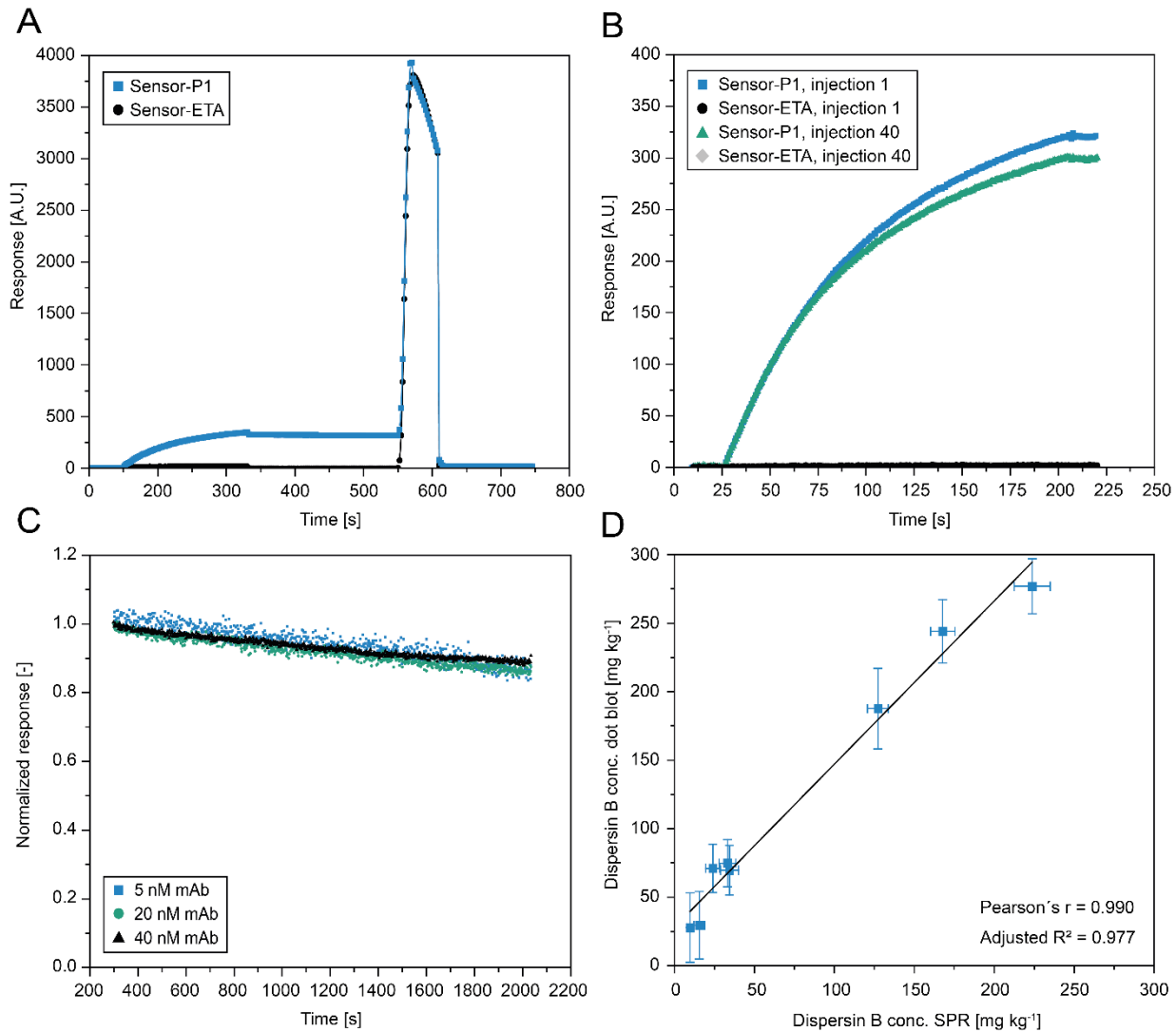


Figure S15: Assessment of binding stability, regeneration, capacity loss and accuracy in a binding inhibition SPR assay for detection of His-tagged target proteins. A. Sensor regeneration. A 30 s injection of regeneration buffer (VII.6) was used to remove captured antibody from the peptide-coated sensor. B. Sensor capacity loss after multiple cycles of injection and regeneration. A capacity loss of ~6% was observed after 40 injections. Antibody concentrations of 30 nM (MonoRab anti-His) were used to assess regeneration and capacity loss. C. Stability of the interaction between antibody and antigen. MonoRab anti-His antibody was captured on sensors coated with peptide P1 (Supporting Table 20) followed by a 30 min dissociation phase. Data are normalized (% initial) values calculated as the average from three injections. D. Quantification of DspB in *N. tabacum* extracts with a dot blot assay (II.6.5) and with a binding inhibition SPR assay (II.6.3.1). MonoRab anti-His antibody was used to detect DspB via a C-terminal His₆-tag in both assays. Error bars represent the standard deviation calculated from the 95% confidence interval of the DspB concentration measured in both assays (the 95% confidence interval is 3.92 standard errors wide). Data were recorded on a Sierra SPR2/4. OriginPro was used to plot and fit data. P1 – peptide P1 (Supporting Table 20), ETA – ethanolamine.

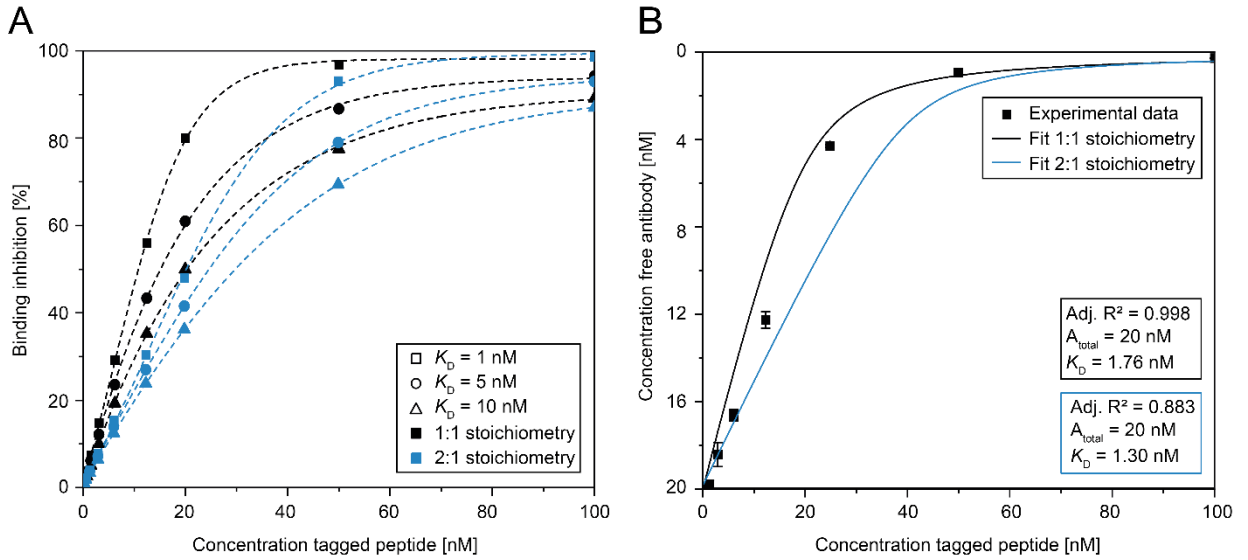


Figure S16: Simulated and experimental inhibition of anti-His antibody with His-tagged peptide in the binding inhibition SPR assay. A. Simulated binding inhibition of anti-His antibody depending on the binding stoichiometry, concentration of tagged peptide and the equilibrium dissociation constant, K_D . Equation 23 and Equation 24 were used to simulate a 2:1 or 1:1 binding stoichiometry, using a fix concentration of 20.0 nM anti-His antibody and 0.4 –100.0 nM His-tagged peptide. B. Fitting of experimental binding inhibition data (Figure 21C) to different models. Data were measured with 20 nM MonoRab anti-His antibody (Supporting Table 21) and 0.4 –100.0 nM peptide P1 (Supporting Table 20) and fitted to Equation 23 and Equation 24 with OriginPro, using the total concentration of tagged peptide as independent variable, the concentration of free antibody as dependent variable and K_D and the total concentration of antibody, A_{total} (constant, 20 nM), as fitting parameters (Supporting Table 22).

Calculation of the free antibody concentration in a mixture of antigen (His-tagged peptide) and antibody (anti-His), assuming a 1:1 binding stoichiometry (Figure S16):

$$A_{free} = \frac{A_{total} - P_{total} - K_D}{2} + \sqrt{\frac{(P_{total} + A_{total} + K_D)^2}{4} - P A} \quad \text{Equation 23 [378]}$$

Where A_{free} is the concentration of free antibody, A_{total} is the total concentration of antibody, P_{total} is the total concentration of tagged peptide and K_D is the equilibrium dissociation constant.

Calculation of the free antibody concentration in a mixture of antigen (His-tagged peptide) and antibody (anti-His), assuming a 2:1 binding stoichiometry (Figure S16):

$$A_{free} = \frac{-(K_D + P_{total} - 2A_{total}) + \sqrt{(K_D + P_{total} - 2A_{total})^2 + 8K_D A_{total}}}{4} \quad \text{Equation 24 [410]}$$

Where A_{free} is the concentration of free antibody, A_{total} is the total concentration of antibody, P_{total} is the total concentration of tagged peptide and K_D is the equilibrium dissociation constant.

VII.9.10 Target protein functionality

Supporting Table 24: Comparison of empirical kinetic parameters determined for plant-derived IgG3 antibodies directed against *S. aureus* alpha toxin with literature antibodies featuring the same CDRs. Kinetic parameters were calculated using the Biacore T200 evaluation software. K_D = equilibrium dissociation constant (Equation 6), k_a = association rate constant, k_d = dissociation rate constant.

	ER-derived IgG3	Apoplast-derived IgG3	Anti-alpha toxin 2A3.1 [44, 387]
K_D [nM]	3.09	3.43	0.60
k_a [$M^{-1} s^{-1}$]	2.11×10^5	1.97×10^5	13.7×10^5
k_d [s^{-1}]	6.51×10^{-4}	6.78×10^{-4}	8.21×10^{-4}

CDR – complementary determining region.

Supporting Table 25: Model factors with a significant influence on the integrity of IgG1 and IgG3 antibodies expressed in different plant cell compartments. The antibody integrity was investigated in an I-optimal split-plot design with 216 runs (Figure 23B).

Source	F-value	p-value
Whole plot	1.21	0.2733
A (PCP incubation time)	1.21	0.2733
Subplot	27.48	< 0.0001
B (BY-2 cultivation time)	12.19	0.0006
C (compartment)	126.00	< 0.0001
D (IgG scaffold)	21.96	< 0.0001
AC	3.36	0.0111
CD	4.76	< 0.0001
	R^2	0.7765
Coefficients of determination	Adjusted R^2	0.7444
	Predicted R^2	n.a.

Factors with a non-significant influence on the response ($p > 0.05$) were removed from the model unless required to maintain the model hierarchy. A predicted R^2 is not available for split-plot designs, because this metric cannot be calculated. With a difference > 0.2 , the values of R^2 and adjusted R^2 were in reasonable agreement.

Supporting Table 26: Treatment of experimental MRSA biofilms with recombinant DspB produced in BY-2 PCPs, *N. benthamiana* and *E. coli* (control). The relative IC_{50} (i.e the enzyme concentration required to reduce the biofilm to half the value between the top and bottom plateaus) was derived from dose response functions fitted to biofilm degradation data with DspB concentrations in the range of 0.0004 to 0.4 g L^{-1} (Figure 23D, Equation 8).

Fitting parameter	Dispersin B BY-2 PCPs	Dispersin B <i>N. benthamiana</i>	Dispersin B <i>E. coli</i>
A_1	65 ± 1	64 ± 2	64 ± 0
A_2	100	100	100
p	-1691 ± 567	-338 ± 130	-569 ± 53
$Span$	35 ± 2	36 ± 2	36 ± 0
$logx_0 (IC_{50})$	$5.0 \times 10^{-4} \pm 1.0 \times 10^{-4}$	$3.2 \times 10^{-3} \pm 6.0 \times 10^{-4}$	$3.1 \times 10^{-3} \pm 1.0 \times 10^{-4}$

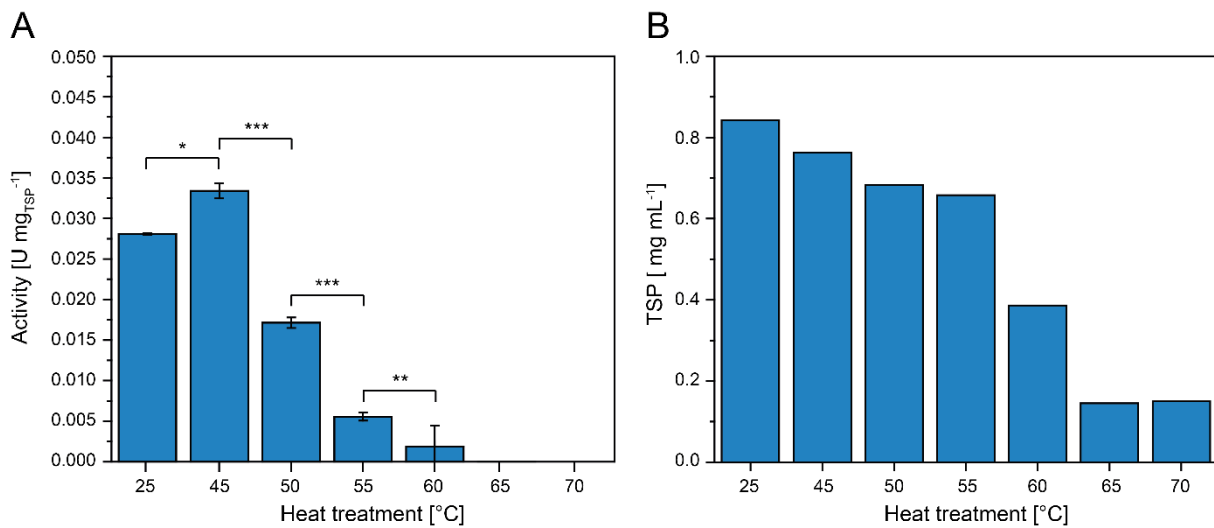


Figure S17: Effect of a heat treatment step on the activity of plant HCPs in the PPK activity assay. A, B. Wildtype *N. benthamiana* plants were extracted with a 3 v m⁻¹ ratio of extraction buffer (VII.6), clarified by depth filtration (II.5.3) and optionally subjected to heat treatment at 45 – 70°C in a 1 mL scale using a Zetasizer Nano [129]. Heat treatment consisted of a 1.5 min equilibration phase to reach the desired temperature and ensure temperature equilibrium [129], followed by incubation for additional 5 minutes. The supernatant with all HCPs that remained soluble after the heat treatment was tested for activity in the PPK activity assay (Figure 22B). Error bars represent the standard deviation from n = 3 reactions (*p < 0.05, **p < 0.01, ***p < 0.001).

VII.10 Curriculum vitae

Personal details

Name	Patrick Opdensteinen
Date of birth	05/18/1990
Place of birth	Nettetal
Nationality	German
ORCID	0000-0002-4068-0843
Email address	patrick.opdensteinen@rwth-aachen.de

Professional experience

01/2019 – present	Associated Doctoral Researcher in the DFG Research Training Group Tumor-Targeted Drug Delivery Manufacturing of biopharmaceuticals in the context of drug delivery
08/2017 – present	Scientist at the Fraunhofer Institute for Molecular Biology and Applied Ecology IME Manufacturing of biopharmaceuticals in plants, yeast and bacteria
05/2017 – 07/2017	Scientific Assistant at the Institute for Biology VI, RWTH Aachen University, Department of Biology Supervision of curricular internships in industrial biotechnology
10/2015 – 03/2016	Research Internship at the Sinskey Laboratory, Massachusetts Institute of Technology (MIT), Department of Biology Optimization of α -carotene production in <i>Corynebacterium glutamicum</i> by means of metabolic engineering and bioprocess optimization
11/2014 – 04/2015	Student Assistant at the Institute for Biology VII, RWTH Aachen University, Department of Biology Downstream processing of plant made biopharmaceuticals
09/2013 – 07/2014	Undergraduate Research Opportunities Program (UROP) Screening for a highly productive elite tobacco variety for the production of recombinant monoclonal anti-HIV antibody 2G12

Education

01/2018 – present	PhD Student Fraunhofer Institute for Molecular Biology and Applied Ecology IME, RWTH Aachen University
10/2014 – 03/2017	Master of Science in Molecular and Applied Biotechnology RWTH Aachen University Grade: 1.0 (with honors) Master Thesis (grade: 1.0) Strain development and process optimization for the production of the ZMapp anti-Ebola antibody cocktail components in glyco-engineered <i>Pichia pastoris</i>
10/2011 – 09/2014	Bachelor of Science in Molecular and Applied Biotechnology RWTH Aachen University Grade: 1.2

Bachelor Thesis (grade: 1.1)

Improved filtration methods for the clarification of tobacco extract and the purification of plant-derived biopharmaceuticals

08/2010 – 02/2011 **Community Service**

06/2010 **Abitur**
Werner-Jaeger-Gymnasium
Grade: 1.2 (valedictorian)

Stipends and awards

09/2018	DECHEMA student award
01/2018 – 10/2020	RWTH Doctorate Scholarship
09/2017	Springorum Commemorative Coin of the RWTH Aachen University
02/2012 – 03/2017	Scholarship of the German Academic Scholarship Foundation Foreign exchange scholarship from 10/2015 to 03/2016
10/2015 – 03/2016	RWTH Research Ambassador Scholarship
09/2015	International Genetically Engineered Machine (iGEM) competition Project awards: Best Manufacturing Project, Gold Medal
11/2014	Schöneborn Award of the Division for Biology
11/2014	International Genetically Engineered Machine (iGEM) competition Project awards: Best Measurement Project, Best Supporting Software, Gold Medal, Safety Commendation
06/2010	Karl-von-Frisch High School Graduate Award of the German Life Sciences Association
06/2010	High School Graduate Award of the German Chemical Society

Publications

03/2023	Knödler, M.*, Opdensteinen, P.* , Sankaranarayanan, R. A., Morgenroth, A., Buhl, E. M., Mottaghy, F. M., & Buyel, J. F. (2023). Simple plant-based production and purification of the assembled human ferritin heavy chain as a nanocarrier for tumor-targeted drug delivery and bioimaging in cancer therapy. <i>Biotechnology and Bioengineering</i> , 120(4), 1038-1054. *These authors contributed equally to the work
02/2023	Ridgley, L. A., Falci Finardi, N., Gengenbach, B., Opdensteinen, P. , Croxford, Z., Ma, J. K. C., ... & Teh, A. Y. H. (2023). Killer to cure: Expression and production costs calculation of tobacco plant-made cancer immune checkpoint inhibitors. <i>Plant Biotechnology Journal</i> .
06/2022	Opdensteinen, P. , Sperl, L. E., Mohamadi, M., Kündgen-Redding, N., Hagn, F., & Buyel, J. F. (2022). The transient expression of recombinant proteins in plant cell packs facilitates stable isotope labelling for NMR spectroscopy. <i>Plant Biotechnology Journal</i> .

- 06/2022 **Opdensteinen, P.**, & Buyel, J. F. (2022). Reducing water uptake into BY-2 cells by systematically optimizing the cultivation parameters increases product yields achieved by transient expression in plant cell packs. *Biotechnology Journal*, 2200134.
- 10/2021 **Opdensteinen, P.**, Meyer, S., & Buyel, J. F. (2021). *Nicotiana* spp. for the expression and purification of functional IgG3 antibodies directed against the *Staphylococcus aureus* Alpha toxin. *Frontiers in Chemical Engineering*, 50.
- 09/2021 **Opdensteinen, P.**, Dietz, S. J., Gengenbach, B. B., & Buyel, J. F. (2021). Expression of biofilm-degrading enzymes in plants and automated high-throughput activity screening using experimental *Bacillus subtilis* biofilms. *Frontiers in Bioengineering and Biotechnology*, 714.
- 08/2021 Li, C., Swofford, C. A., Rückert, C., Chatzivasileiou, A. O., Ou, R. W., **Opdensteinen, P.**, ... & Sinskey, A. J. (2021). Heterologous production of α -Carotene in *Corynebacterium glutamicum* using a multi-copy chromosomal integration method. *Bioresource Technology*, 341, 125782.
- 06/2021 Bernau, C. R., Jäpel, R. C., Hübbers, J. W., Nölting, S., **Opdensteinen, P.**, & Buyel, J. F. (2021). Precision analysis for the determination of steric mass action parameters using eight tobacco host cell proteins. *Journal of Chromatography A*, 1652, 462379
- 11/2020 **Opdensteinen, P.**, Lobanov, A., & Buyel, J. F. (2021). A combined pH and temperature precipitation step facilitates the purification of tobacco-derived recombinant proteins that are sensitive to extremes of either parameter. *Biotechnology Journal*, 16(4), 2000340.
- 05/2020 Gengenbach, B. B., **Opdensteinen, P.**, & Buyel, J. F. (2020). Robot cookies–plant cell packs as an automated high-throughput screening platform based on transient expression. *Frontiers in Bioengineering and Biotechnology*, 8, 393.
- 08/2019 Knödler, M., Rühl, C., **Opdensteinen, P.**, & Buyel, J. F. (2019). Activated cross-linked agarose for the rapid development of affinity chromatography resins-antibody capture as a case study. *Journal of Visualized Experiments*, (150), e59933.
- 05/2019 Gengenbach, B. B., Keil, L. L., **Opdensteinen, P.**, Müschen, C. R., Melmer, G., Lentzen, H., ... & Buyel, J. F. (2019). Comparison of microbial and transient expression for the production and purification of the anticancer mistletoe lectin viscumin. *Biotechnology and Bioengineering*, 116(9), 2236-2249.
- 01/2019 **Opdensteinen, P.**, Clodt, J. I., Müschen, C. R., Filiz, V., & Buyel, J. F. (2019). A combined ultrafiltration/diafiltration step facilitates the purification of cyanovirin-N from transgenic tobacco extracts. *Frontiers in Bioengineering and Biotechnology*, 6, 206.
- 08/2018 Rühl, C., Knödler, M., **Opdensteinen, P.**, & Buyel, J. F. (2018). A linear epitope coupled to DsRed provides an affinity ligand for the capture of monoclonal antibodies. *Journal of Chromatography A*, 1571, 55-64.

- 12/2017 Hanke R.*, Bailly N.*, Demling P.*, Gohr F. N.*, **Opdensteinen P.***, Osthege M. J.*, Joppich M., Sudarsan S., Schwaneberg U., Wiechert W., Blank L. M. (2017). Development of a modular biosensor system for rapid pathogen detection. Biosensing technologies for the detection of pathogens: A prospective way for rapid analysis, 89.
*These authors contributed equally to the work
- 08/2017 Purcell O.*, **Opdensteinen P.***, Chen W., Lowenhaupt K., Brown A., Hermann M., Cao J., Tenhaef N., Kallweit E., Kastillan R., Sinskey A. J., Perez-Pinera P., Buyel J. F., Lu T. K. (2017). Production of functional anti-Ebola antibodies in *Pichia pastoris*. ACS Synthetic Biology, 6(12), 2183-2190.
*These authors contributed equally to the work
- 01/2015 Buyel, J. F., **Opdensteinen, P.**, & Fischer, R. (2015). Cellulose-based filter aids increase the capacity of depth filters during the downstream processing of plant-derived biopharmaceutical proteins. Biotechnology Journal, 10(4), 584-591.

Language skills

German	Native language
English	Conversational proficiency (113/120 TOEFL iBT)
Latin	Qualification in Latin (Latinum)

EDP knowledge

Microsoft Office	Excel, PowerPoint, Word
Graphics software	Adobe Illustrator, Adobe Photoshop, Inkscape
Specialized software	AIDA, Design Expert, OriginLab, SnapGene, YASARA